Sérgio Manuel Campos da Silva

Strategies to improve transdermal drug delivery: hydrogel vehicles, permeation enhancers and iontophoresis

Faculdade de Farmácia da Universidade de Coimbra

Coimbra | 2013

Dissertation submitted to the University of Coimbra, in fulfillment of the requirements for the degree of Doctor of Philosophy in Pharmacy, specializing in Pharmaceutics.

Dissertação apresentada Universidade de Coimbra, para obtenção do grau de Doutor em Farmácia, na especialidade de Tecnologia Farmacêutica.

The work presented in this thesis was carried out at the Center of Pharmaceutical Studies (CEF), Department of Pharmaceutics, Faculty of Pharmacy, University of Coimbra (Portugal), at the Chemistry Center, Chemistry Department, University of Coimbra (Portugal) and at the Center for Dermal Research, New Jersey Center for Biomaterials / Ernest Mario School of Pharmacy, Rutgers University – The State University of New Jersey (United States of America), and funded by Fundação para a Ciência e Tecnologia (SFRH/BD/30537/2006), Lisboa, Portugal.

O trabalho apresentado nesta tese foi desenvolvido no Laboratório de Tecnologia Farmacêutica, Centro de Estudos Farmacêuticos (CEF) da Faculdade de Farmácia da Universidade de Coimbra (Portugal), no Centro de Química, Departamento de Química da Faculdade de Ciências e Tecnologia da Universidade de Coimbra (Portugal) e no Center for Dermal Research, New Jersey Center for Biomaterials / Ernest Mario School of Pharmacy, Rutgers University – The State University of New Jersey (Estados Unidos da América), e suportado financeiramente pela Fundação para a Ciência e Tecnologia (FCT), (SFRH/BD/30537/2006), Lisboa, Portugal.

Aos meus Pais, Avô, Padrinho e Irmã

Aos meus Familiares

Aos meus Amigos

“Life is not easy for any of us, but what of that? We must have perseverance and above all confidence in ourselves. We must believe that we are gifted for something and that this thing must be attained.”

Marie Curie

Acknowledgements

The completion of my dissertation and Ph.D. has been quite a long journey. It is true that *life is what happens while you are busy doing your Ph.D*. Life does not stand still, nor waits for you to be finished and have time to deal with it. Many things have happened and changed in the time I have been involved with this project. I have lost confidence many times, got writer's block just as many times, moved from place to place, dealt with computers crashing and with frustration in general, but I knew I would complete my Ph.D. I just feel I had to do it in my own time and my own terms.

My Ph.D. has always been a priority, but as most know, there are several priorities in a person's life at any time. Unfortunately due to life's challenges and the changes that followed, my dissertation could not always be the number one priority. At any rate, I have finished, but not alone. I surely could not have succeeded without the invaluable support of some very important people (VIP). Without them, especially those I am about to mention, I certainly wouldn't have gotten to where I am today, at least not sanely.

I would like to start by giving special thanks to my scientific advisors, Prof. João José Simões de Sousa from the Faculty of Pharmacy of the University of Coimbra, Prof. Alberto António Caria Canelas Pais from the Chemistry Department of the University of Coimbra and Prof. Bozena Michniak-Kohn from the Ernest Mario School of Pharmacy and New Jersey Center for Biomaterials / Center for Dermal Research of Rutgers University, the State University of New Jersey, USA. I would like to express my sincere gratitude to them for writing my research proposal, for having confidence in me, for hosting me, for creating the necessary conditions to work properly, for their continuous support, for the critical analysis and fruitful discussions, numerous papers and posters corrections throughout the entire period of my Ph.D.

My thesis is the product of an international collaboration established between my scientific advisors at Coimbra University and Rutgers University. Therefore, I am deeply grateful to Profs. Bozena Michniak-Kohn and Joachim Kohn for giving me the

opportunity to join The Laboratory for Drug Delivery (LDD), located at the New Jersey Center for Biomaterials at Rutgers University. Dr. Michniak-Kohn always made me feel like at home during my stays in the USA. That was one of the reasons that my initial 6-months stay turned into approximately 2 years. Her guidance and commitment to research excellence played an important role in the success of this international project. However, my various stays at Rutgers University would have been impossible without the precious contribution the staff members of the New Jersey Center for Biomaterials. Therefore, I would like to extend my gratitude to Carole Kantor, Debra Fenton, Don Lindorfer, Dr. Durgadas Bolikal, Kathy Piano, Marie Pavelchack, Melissa Aranzamendez, Milijana Djukovic, Dr. Sanjeeva Murthy and Shirley Maimone. I also would like to thank Prof. Ah-Ng Tony Kong, Director of Graduate Program in Pharmaceutical Sciences, from the Department of Pharmaceutics of the Ernest Mario School of Pharmacy for allowing me to use his microscopy facilities.

In Coimbra I must give special thanks to Prof. Maria da Graça Miguel and Prof. Filipe Antunes, from the Chemistry Department, University of Coimbra, for hosting me at Colloids Laboratory and for all the support given during the rheological studies. I am also deeply grateful to Prof. Artur Valente, from the Chemistry Department, University of Coimbra, for hosting me in his lab, for his academic support and input with the electrical conductivity studies. I equally would like to thank Dr. Telma Costa for her valuable help with fluorescence measurements, and Prof. Teresa Roseiro for her important assistance with PLTM studies. I also would like to extend my gratitude to Prof. Eduardo Marques, from the Chemistry Department, University of Porto, for providing the gemini surfactants that were tested as chemical penetration enhancers and for his valuable scientific contribution.

My great friend and labmate, Lawrence Hu, today working for Sanofi-Aventis in Shanghai, PRC, deserves a very special thanks from me. I have no words to describe how valuable his personal and professional contribution was during my stay in the USA, inside and outside the Laboratory for Drug Delivery. We spent countless hours together in the lab, helping each other running the permeation experiments, HPLC, cell culture work, cytotoxicity evaluations, etc. Lawrence was like an older brother that taught me many techniques in the lab, inspired me and helped keeping me motivated. I also would like to extend my gratitude to my labmate and friend, Vishwas Rai, from Ernest Mario School of Pharmacy, Rutgers University, for the help and assistance provided with the cell culture work. Very important was also the assistance of Mr. Valentin Starovoytov from the Division of Life Sciences, Electron Imaging Facility at Rutgers University for his valuable technical assistance in the SEM studies.

I would like to specially acknowledge my funding body, Fundação para a Ciência e Tecnologia (FCT, Lisboa, Portugal) for the PhD grant reference SFRH/BD/30537/2006. The grant was crucial for creating the necessary conditions to carry out the work in Coimbra, Portugal and in New Jersey, USA and gave me the opportunity to present it in numerous international meetings and conferences. I would like to express my great

appreciation to Dr. Olga Martinho, former head of the Human Resources at FCT that was always very kind and helpful assisting me obtaining the documentation needed for the VISA applications on time.

I have been fortunate to be surrounded by wonderful colleagues and friends, without whom life would be bleak. At some point, they were there for me, bearing the brunt of the frustrations and sharing the joy of the successes at work, during lunchtime, while having a snack or a coffee inside “Bar das Matemáticas” or outside at the yard of “Café do Botânico” or during our events. In Coimbra, I would like to give thanks to my colleagues and friends Ana Rita Figueiras, Ana Teresa Marques, Andreia Jorge, Andreza Ribeiro, Bruno Mendes, Bruno Medronho, Carla Vitorino, Luís Alves, Maria de Fátima Pinto, Maria del Carmen Móran, Mathew Davies, João Almeida, Rachel Evans, Raquel Teixeira, Rita Dias, Rui Pereira, Sandra Nunes and Sylwia Gaweda. In USA, I want to thank my colleagues and friends Brian Kilfoyle, Diksha Kaushik, Golshid Keyvan, Greg Simms, Jared Bushman, J. Peter Zhang, Matthew Laughland, Mindy Ezra, Petra Kleiner, Priya Batheja and Zheng Zhang.

I also want to specially express my gratitude to my great friend Bruno Mendes for the inestimable friendship and for putting his time and effort into the design this dissertation’s cover and João Laranjeiro (Criamagin) for the assistance provided with the graphical design of this dissertation.

Of course no acknowledgments would be complete without giving thanks to my family, especially my parents, my grandfather José, my sister Filipa, my uncle José, my aunt “China” and my cousins living in New Jersey, particularly Ana Cristina Lopes, Susie Lopes and Dora Marques. My parents have stimulated many worthy qualities in me, and given me a good basis to meet life. They have taught me about hard work and self-respect and have many times expressed their support in many different ways, how proud they are of me and how much they love me, particularly during those days in USA. I am proud of them too and love them very much. Another very important person in my life is my grandfather, José. His wise words, patience, genuine caring and concern, and faith in me during this journey, enabled me to attend life while also earning my Ph.D. I am deeply grateful to you, grandpa. My uncle José has been also an important person throughout my life in general and during this journey in particular. He has been my role model in many aspects, a great support since I moved to Coimbra. He has always encouraged me to be persistent, honest, and loyal, to think independently and of course, not less importantly, inspired in me his love for Académica. I would also like to thank my aunt “China”, for being such a good listener and for hosting me during the first two years in Cantanhede. Those breakfasts that you prepared were all I needed to start my days! Last but not least, I am very thankful to my cousins from New Jersey, Ana Cristina, Susie and Dora for the continuous support, love and for making my life in USA so much easier and better.

Acknowledgements

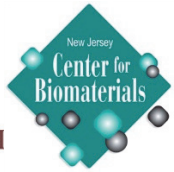

Contents

Abstract xv

Resumo xvii

1. General introduction 1

1.1. State of the art in transdermal drug delivery 1

1.1.1. Transdermal drug delivery – its origins 1

1.1.2. Advantages and limitations of the transdermal route 2

1.1.3. Drug delivery market and future perspectives 3

1.2. Background 5

1.2.1. The Skin 5

1.2.1.1. Functions 5

1.2.1.2. Anatomy and composition 6

1.2.2. Mechanisms of percutaneous absorption 10

1.2.2.1. Theoretical basis of percutaneous absorption 11

1.2.3. Skin permeation enhancement strategies – overcoming the barrier 12

1.2.3.1. Passive enhancement of skin permeation 13

1.2.3.2. Active enhancement of skin permeation – the use of electrical energy….. 17

1.2.4. Current experimental techniques used for in vitro percutaneous permeability testing 23

1.2.4.1. Franz diffusion cells 24

1.2.4.2. Membranes used for permeability testing 24

1.2.5. Transdermal drug delivery systems (TDDS) 25

1.2.5.1. Reservoir systems 26
1.2.5.2. Matrix systems 26
1.2.5.2.2. Matrix-dispersion system 26
1.2.5.3. Microreservoir systems 26
1.2.5.4. Hydrogels in transdermal drug delivery 27

1.3. Scope 29

2. Aggregation and gelation in hydroxypropylmethyl cellulose aqueous solutions... 31

2.1. Introduction 31

2.2. Experimental section 34
2.2.1. Materials and sample preparation 34
2.2.2. Rheological studies 34
2.2.3. Cloud point determination and polarized light thermal microscopy observations 34
2.2.4. Pyrene fluorescence measurements 35

2.3. Results 36
2.3.1. Rotational measurements at different shear rates 36
2.3.2. Oscillatory measurements 39
2.3.3. Optical transmittance measurements and polarized light thermal microscopy 41
2.3.4. Pyrene fluorescence measurements 42

2.4. Discussion 43
2.4.1. Aggregation and gelation 43
2.4.2. Assessment of active links 45
2.4.3. Shear rate effects 45

2.5. Conclusions 47

3. New insights on the interaction between hydroxypropylmethyl cellulose (HPMC) and sodium dodecyl sulfate (SDS) 49

3.1. Introduction 49

3.2. Experimental section 51
3.2.1. Materials and sample preparation 51

3.2.2. Electrical conductivity studies 51
3.2.3. Rheological studies 52
3.2.4. Optical transmittance measurements 53

3.3. Results and Discussion 53
3.3.1. Electrical conductivity studies to assess characteristic points and thermodynamics 54
3.3.1.1. Effect of HPMC on the electrical conductance of SDS 54
3.3.2. Viscoelastic properties of HPMC-SDS solutions 59
3.3.2.1. Monitoring the association between polymer and surfactant 60
3.3.2.2. Modulating the thermal gelation of HPMC 62
3.3.3. Characteristic points revisited with light transmittance studies 64
3.3.4. Rationale 65

3.4. Conclusions 66

4. Structure activity relationships in alkylammonium C_{12}-gemini surfactants used as dermal enhancers 69

4.1. Introduction 70
4.1.1. Drug information and background 73

4.2. Experimental section 74
4.2.1. Materials 74
4.2.2. Hydrogels composition and preparation 75
4.2.3. Porcine skin preparation 75
4.2.4. Composition and preparation of the enhancer solutions 75
4.2.5. Drug delivery studies 75
4.2.6. Drug quantification 76
4.2.7. Data analysis in the permeation studies 76
4.2.8. Skin integrity evaluation 77
4.2.8.1. Histology - light microscopy studies 77
4.2.8.2. Scanning Electron Microscopy studies 77
4.2.9. Cytotoxicity studies – MTT/MTS Assay 77

4.3. Results and Discussion 78
4.3.1. In vitro permeation studies 78
4.3.1.1. Effect of the penetration modifiers on the transdermal drug delivery of lidocaine hydrochloride 78

4.3.1.2. Effect of the penetration modifiers on the transdermal drug delivery of caffeine… 80

4.3.1.3. Effect of the penetration modifiers on the transdermal drug delivery of ketoprofen 81

4.3.2. Overview and comparison 82

4.3.3. Skin integrity evaluation 85

4.3.3.1. Histological studies 85

4.3.3.2. Scanning Electron Microscopy (SEM) studies 87

4.3.4. Cytotoxicity studies 88

4.4. Conclusions 91

5. A combination of nonionic surfactants and iontophoresis to enhance the transdermal drug delivery of ondansetron HCl and diltiazem HCl 93

5.1. Introduction 93

5.2. Experimental section 96

5.2.1. Materials and sample preparation 96

5.2.2. Hydrogel preparation 96

5.2.3. Porcine skin preparation 96

5.2.4. Preparation of Ag and AgCl electrodes 97

5.2.5. Preparation of enhancer solutions 97

5.2.6. Drug delivery studies 97

5.2.7. Drug delivery studies 97

5.2.8. Data analysis in the permeation studies 98

5.2.9. Skin integrity evaluation 98

5.2.9.1. Histology studies 98

5.2.9.2. Scanning Electron Microscopy studies 99

5.2.10. Cytotoxicity studies 99

5.3. Results 100

5.3.1. *In vitro* permeation studies 100

5.3.1.1. Effect of the penetration modifiers on the transdermal drug delivery of ondansetron HCl 100

5.3.1.2. Combined effect of the pre-treatment with penetration modifiers and iontophoresis on the transdermal drug delivery of ondansetron HCl 102

5.3.1.3. Effect of the penetration modifiers on the transdermal drug delivery of diltiazem HCl 103

5.3.1.4. Combined effect of the pre-treatment with penetration modifiers and iontophoresis on the transdermal drug delivery of diltiazem HCl 104
5.3.1.5. Overview and comparison 106
5.3.2. Skin integrity evaluation 109
5.3.2.1. Histological studies 109
5.3.2.2. Scanning Electron Microscopy studies 110
5.3.3. Cytotoxicity studies 111
5.4. Conclusions 113
Concluding remarks 115
References 119

List of Figures

Fig. 1.1 A diagrammatical illustration of the skin [32]. 6

Fig. 1.2 Structures and nomenclature of ceramides (CERs) in human SC [51]. The letters in parentheses present the ceramide classification as suggested by [54]. 8

Fig. 1.3 Representation of the epidermis, showing the process of cell differentiation and the establishment of the cornified envelope [32]. For terminal differentiation, epidermal cells move from the basal layer (stratum basale) through the spinous layer (stratum spinosum) and the granular layer (stratum granulosum) towards the stratum corneum. During this process, they develop from mitotically active cells into dead, flattened squames. At the various stages of this development, different proteins are expressed. Crosslinking of epidermal proteins eventually leads to the establishment of the cornified envelope, a thick peripheral protein envelope that stabilizes each corneocyte. Additionally, lipids are synthesized in lamellar granules which are subsequently extruded into the extracellular space where they surround the corneocytes and build the lipid envelope..... 9

Fig. 1.4 A schematic representation of the skin showing the different possible routes of penetration. The follicular area accounts for approximately 0.1% and the eccrine 10^{-3}% of the total surface area [60] 10

Fig. 1.5 Some methods for optimizing Transdermal drug delivery [75]. 13

Fig. 1.6 Structures of some chemical permeation enhancers (azone and oleic acid) and a schematic showing their interaction with a representative ceramide [60]. 16

Fig. 1.7 Diagram of iontophoretic technique: as current is applied the drug (D^+) are repelled into the skin and eventually absorbed in the systemic circulation. The anodal compartment contains an ionizable drug D^+ with its counter-ion A^- and Na^+Cl^-. The

application of an electric potential causes a current to flow through the circuit. At the electrode solution interface, the Ag^+ and Cl^-react to form insoluble AgCl, which is deposited on the electrode surface. Electromigration transports the cations, including the drug molecule, from the anodal compartment and into the skin. At the same time, endogenous anions, primarily Cl^-, move into the anodal compartment. In the cathodal chamber, Cl^- ions are released from the electrode and electroneutrality requires that either an anion is lost from the cathodal chamber or that a cation enters the chamber from the skin. Taken from ref. [120]. 19

Fig. 1.8 Schematic representation of a vertical Franz diffusion cell [158]. 24

Fig. 1.9 Schematic representation of transdermal drug delivery systems [181] 26

Fig. 1.10 Various delivery and release mechanism of hydrogels [182]..... 27

Fig. 2.1 Structure of natural cellulose. 32

Fig. 2.2 Structure of hydroxypropylmethyl cellulose (HPMC). 32

Fig. 2.3 Viscosity dependence on temperature for HPMC solutions of (a) 1%, (b) 2%, (c) 5% and (d) 10%, w/w. Curves are obtained at Newtonian shear rates (triangles), with imposed values respectively of 0.5, 0.05, 5.0×10^{-3} and 1.0×10–3 s^{-1}, and non-Newtonian shear rates (circles), of 50, 30, 5 and 1 s^{-1} respectively. 37

Fig. 2.4 Viscosity as a function of temperature for the indicated shear rates in the 2% HPMC solution. 38

Fig. 2.5 Viscosity as a function of shear rate in the 2% HPMC solution at the indicated temperatures. 38

Fig. 2.6 Storage (G', squares), loss (G'' , circles) and the complex viscosity (η^*, triangles) modulus, as a function of temperature, for HPMC solutions of (a) 1%, (b) 2%, (c) 5% and (d) 10%, w/w. Frequency is chosen so as to impose a value of G'' higher than G' at the initial conditions..... 40

Fig. 2.7 Optical transmittance measurements for the HPMC solution for the indicated concentrations. The 100% reference was taken as the transmittance at 25°C for each solution..... 41

Fig. 2.8 PLTM images for the 1% HPMC solution for the indicated temperatures (a) 25°C and (b) 90°C..... 42

Fig. 2.9 I_1/I_3 ratio of pyrene emission or micropolarity index (MI) progression with temperature for the 1% HPMC solution. 42

Fig. 2.10 Viscosity profiles at Newtonian (triangles) and non-Newtonian (circles) regimes, micropolarity index (stars) and optical transmittance (squares) measurements upon heating for the 1% HPMC aqueous solution. 46

Fig. 3.1 Dependence of the specific conductance of aqueous solutions of SDS, at 25.°C, in the presence of HPMC with a concentration of (a) 0.0% (w/v), (b) 0.25% (w/v), and (c) 0.75% (w/v). Arrows indicate the *cmc* (1), *cac* (2) and *psp* (3). 54

Fig. 3.2 Effect of HPMC concentration on the free energy of micellization of SDS, at 298.15 K, assuming that the polymer has only a spectator role on the equilibrium between SDS unimers and SDS micelles. The dashed horizontal line represents the free energy of micellization of SDS. 55

Fig. 3.3 Equilibrium scheme involving SDS unimers, SDS-HPMC aggregates and bulk SDS micelles. Solid black lines represent HPMC chains, blue and yellow spheres correspond to SDS micelles and counterions respectively. Surfactant unimer is represented as the small blue sphere connected to a red hydrophobic tail. While unimer-aggregate and unimer-bulk micelles can be regarded as independent equilibria, a large concentration of aggregates promotes a direct equilibrium of these aggregates with bulk micelles (indicated by the dashed double-arrow), without systematic disaggregation into unimers. 59

Fig. 3.4 Zero-shear viscosity as function of SDS concentration. Three different zones are visible. Before the first arrow is the pre-*cac* region. In the region between the two arrows, surfactant molecules start to form aggregates around hydrophobic moieties of the polymer, causing polymer swelling and leading to an increase in the viscosity. The second arrow indicates the maximum, which happens before the *psp*. After this concentration, surfactant molecules have saturated the polymer chains and start to form free micelles in solution, leading to screening of electrostatic repulsion and to an observable decrease in the viscosity. Solid lines are presented to guide the eye. 61

Fig. 3.5 Storage (*G'*, squares), loss (*G''*, circles) and the complex viscosity (η^*, triangles) modulus, as a function of temperature, for formulation S1.7 (on the left) and S17 (on the right). Frequency is chosen so as to impose a value of *G''* higher than *G'* at the initial conditions. Oscillation plots illustrate that gel formation occurs only for low concentration of SDS. For higher concentrations, the storage moduli *G'* does not intersect the loss moduli *G''* in the temperature range studied (25-90°C) indicating that gel formation is not detected. As the surfactant progressively ionizes the polymer inter-chain hydrophobic associations and thermal gelation become weaker or negligible. 63

Fig. 3.6 Dependence of the optical transmittance (800nm) at 25°C of HPMC-SDS solutions on SDS concentration. Solid lines are a guide for the eyes. 64

Fig. 3.7 Pictorial representation of the evolution of the SDS/HPMC/water system as a function of SDS and HPMC concentrations. Solid black lines represent HPMC chains, blue and yellow spheres correspond to SDS micelles and counterions respectively. The larger blue spheres indicate major hydrophobic association zones. 66

Fig. 4.1 Schematic representation of cationic gemini surfactant. These molecules are composed of two monomeric surfactant molecules linked by a spacer chain. 71

Fig. 4.2 Molecular structures of the chemical permeation enhancers used in this work (G12-2-12, G12-6-12, G12-10-12, DTAB and azone) 72

Fig. 4.3 Molecular structures of lidocaine hydrochloride monohydrate (on the left, a), Mw: 288.81; ACD/log*P*: 2.359; ACD/ log*D* (pH5.5): -0.13), caffeine (on the center, b), Mw: 194.19; ACD/log*P*: -0.628; ACD/ log*D* (pH5.5): -0.63) and ketoprofen (on the right, c), Mw: 254.28; ACD/log*P*: 2.911; ACD/ log*D* (pH5.5): 1.62) 73

Fig. 4.4 Cumulative amount of lidocaine HCl permeated across porcine skin as a function of time. Skin was pretreated for 1 hour with enhancer solutions in PG, prior the start of the permeation experiments. 79

Fig. 4.5 Cumulative amount of caffeine permeated across porcine skin as a function of time. Skin was pretreated for 1 hour with enhancer solutions in PG, prior the start of the permeation experiments. 80

Fig. 4.6 Cumulative amount of ketoprofen permeated across porcine skin as a function of time. Skin was pretreated for 1 hour with enhancer solutions in PG, prior the start of the permeation experiments. 82

Fig. 4.7 ER obtained pretreating the skin using the various CPE for lidocaine HCl (top), caffeine (center) and ketoprofen (bottom). 83

Fig. 4.8 Untreated (Control) porcine skin pictures were captured using an optical light microscope at 10x - a), 20x - b), 40x - c). The distinct skin layers can be observed: *stratum corneum* (SC), viable epidermis (VE), dermis (D) and hair follicles (HF) 86

Fig. 4.9 Porcine skin pictures were obtained from the skin samples used in the permeation experiments that were previously pretreated with the CPE. For simplicity only the pictures taken at 20x magnification are shown. The pictures refer to the samples pretreated with: PG (d), azone (e), DTAB (f), G12-2-12 (g), G12-6-12 (h), G12-10-12 (i) as penetration enhancer. 86

Fig. 4.10 SEM cross section of untreated porcine skin (control) at 100x (left top), 200x (right top), 400x (left bottom) and 600x (right bottom) magnification, revealing the skin

structures. This skin samples were not subjected to permeation studies and are presented for comparative purposes..... 87

Fig. 4.11 SEM cross-section pictures of porcine skin used in the permeation studies. These samples were pretreated with various permeation enhancers: PG (left top), azone (center top), DTAB (right top), G12-2-12 (left bottom), Gemini 12-6-12 (center bottom) and G12-10-12 (right bottom) at 400x magnification..... 88

Fig. 4.12 Pictures of cultured HEK (on the left) and HDF (on the right), seeded at 8.000 cells/well in appropriate culture medium, prior to the start of the MTS assay. 89

Fig. 4.13 MTS assay results for HEK. The bars represent the cell viability (%) for each permeation modifier and concentration tested. The error bars represent the standard deviation (N=6)..... 89

Fig. 4.14 MTS assay results for cultured HDF. The bars represent the cell viability (%) for each permeation modifier and concentration tested. The error bars stand for the standard deviation (N=6)..... 90

Fig. 5.1 Molecular structures of ondansetron hydrochloride dihydrate (on the left, Mw: 365.15; logP: 2.07; logD (pH5.5): 0.19) diltiazem hydrochloride (on the right, Mw: 450.14; logP: 3.63; logD (pH5.5): 0.76). 95

Fig. 5.2 Cumulative amount of ondansetron HCl permeated across porcine skin as a function of time. Skin was pretreated with various nonionic ether-monohydroxyl C_{12} surfactants 1 hour prior the start of *in vitro* experiments. Data is presented as means ± S.E.M. ($5 \leq N \leq 8$). 101

Fig. 5.3 Cumulative amount of ondansetron HCl permeated across porcine skin as a function of time. Skin was pretreated with various nonionic ether-monohydroxyl C_{12} surfactants 1 hour prior the start of in vitro experiments. Iontophoresis (0.3mA) was applied during the first 8 hours (stage 1), followed by a 16 h passive permeation. Data are presented as means ± S.E.M. (N=6). 103

Fig. 5.4 Cumulative amount of diltiazem HCl permeated across porcine skin as a function of time. Skin was pretreated with various nonionic ether-monohydroxyl C_{12} surfactants 1 hour prior the start of in vitro experiments. Data is presented as means ± S.E.M. ($3 \leq N \leq 7$)..... 104

Fig. 5.5 Cumulative amount of diltiazem HCl permeated across porcine skin as a function of time. Skin was pretreated with various nonionic ether-monohydroxyl C_{12} surfactants 1 hour prior the start of in vitro experiments. Iontophoresis (0.3mA) was applied during the first 8 hours (stage 1), followed by a 16 h passive permeation. Data are presented as means ± S.E.M. (N=6). 106

Fig. 5.6 Cumulative amount of ondansetron HCl permeated across porcine skin after 8h (stage 1) and 24h (stage 1 and 2). 107

Fig. 5.7 Cumulative amount of diltiazem HCl permeated after 8h (stage 1) and 24h (stages 1 and 2). 108

Fig. 5.8 Porcine skin pictures taken by an optical light microscope at a magnification of 20x after permeation experiments, except for the control (a), using $C_{12}E_5$ (b), $C_{12}E_5$ + iontophoresis (c), $C_{12}E_8$ + iontophoresis (d). The various skin layers and structures can be observed: stratum corneum (SC), viable epidermis (VE), dermis (D) and hair follicles (HF). 109

Fig. 5.9 SEM cross section of untreated porcine skin (control) at 100x and 400x magnification. This skin sample was not subjected to permeation studies. 110

Fig. 5.10 SEM cross-section pictures of porcine skin treated with nonionic surfactant $C_{12}E_8$ at 100x and 200x magnification taken after permeation studies. On the left picture, a hair filament in the dermis is visible. 111

Fig. 5.11 SEM cross-section pictures of porcine skin treated with nonionic surfactant $C_{12}E_5$ and iontophoresis (0.3mA, 8h) at 100x and 400x magnification..... 111

Fig. 5.12 MTS assay results for cultured HEK. The bars represent the cell viability (%) for each permeation modifier and concentration tested. The error bars stand for the standard deviation (N=6)..... 112

Fig. 5.13 MTS assay results for cultured HDF. The bars represent the cell viability (%) for each permeation modifier and concentration tested. The error bars stand for the standard deviation (N=6)..... 113

List of Tables

Table 1-1 Transdermal drugs approved by the FDA* updated from [25]. 4

Table 1-2 Companies with technologies for drug delivery by iontophoresis [26] 22

Table 2-1 Relaxation times, calculated by the intersection of G' and G'' in the frequency sweep tests at constant temperature, and storage modulus G' at 1 Hz. Data pertain to the 2% HPMC solution, and samples were in the steady-state 40

Table 2-2 The cloud point is described in Section 2.3. T_{c1} corresponds to the minimum before the sharp increase in viscosity at Newtonian shear rates and T_{c2} to the steep lowering in viscosity at high shear rate. Finally, T_{c3} is given by the intersection between the storage, G', and loss, G'', moduli. 44

Table 3-1 Effect of HPMC concentration on the association and micellization of SDS as seen by electrical conductivity at 25°C..... 56

Table 3-2 Effect of the temperature on the polymer (0.5%) induced association properties of sodium dodecyl sulfate..... 58

Table 3-3 List of formulations tested in the rheological and optical transmittance studies and corresponding composition. 60

Table 3-4 Gelation temperature for HPMC-SDS solutions. Gel formation requires higher temperature as SDS concentration increase, not being detected (n.d.) in our oscillation tests (1 Hz) for concentrations of SDS above 5.2mM. After a critical SDS concentration, gelation is totally inhibited, as can be seen in the oscillation tests..... 63

Table 3-5 Summary of *cac* and *psp* related values (mM) determined from conductivity, rheology and optical transmittance measurements are shown in the table above. These

were obtained by straight line interception at slope change (conductivity) and second degree polynomial fitting in the region of the minima (maxima) for rheological and optical transmittance measurements. The preceding inequality signs follow the considerations presented along the text. 65

Table 4-1 Effect of the chemical permeation enhancers on percutaneous permeation of lidocaine HCl across porcine skin. Data are presented as means ± S.D. (3≤N≤6). 79

Table 4-2 Effect of the chemical permeation enhancers on percutaneous permeation of caffeine across porcine skin. Data are presented as means ± S.D. (6≤N≤9). 80

Table 4-3 Effect of the chemical permeation enhancers on percutaneous permeation of ketoprofen across porcine skin. Data are presented as means ± S.D. (5≤N≤8)..... 81

Table 5-1 Effect of the chemical permeation enhancers on percutaneous permeation of ondansetron HCl across porcine skin. Data are presented as means ± S.D. (5≤N≤8). 101

Table 5-2 Combined effects of chemical permeation enhancers and iontophoresis (0.3mA, 8 h - stage 1) on the percutaneous permeation of ondansetron HCl across porcine skin. Data are presented as means ± S.D. (*N*=6). 102

Table 5-3 Combined effects of chemical permeation enhancers and iontophoresis on the percutaneous permeation of ondansetron HCl across porcine skin. Data pertain to post-iontophoresis period (0.0mA, 16h – stage 2), and are presented as means ± S.D. (*N*=6). 102

Table 5-4 Effect of the chemical permeation enhancers on percutaneous permeation of diltiazem HCl across porcine skin. Data are presented as means ± S.D. (3≤N≤7). 104

Table 5-5 Combined effects of chemical permeation enhancers and iontophoresis (0.3mA, 8 h - stage 1) on the percutaneous permeation of diltiazem HCl across porcine skin. Data are presented as means ± S.D. (*N*=6). 105

Table 5-6. Combined effects of chemical permeation enhancers and iontophoresis on the percutaneous permeation of diltiazem HCl across porcine skin. Data pertain to post-iontophoresis period (0.0mA, 16h – stage 2), and are presented as means ± S.D. (N=6). 105

Abstract

Transdermal delivery represents a good alternative to oral delivery of drugs and provides a convenient route of administration for a variety of clinical indications. It possesses some advantages over other ways of administration, being a non-invasive route, avoiding the first-pass metabolism in the GI tract, providing constant blood levels for drugs with a narrow therapeutic window, and minimizing side effects with a good patient compliance, since this dosage form is generally administered at most, once a day. The respective use is, however, limited by the poor penetration of drugs into the skin, caused by the major barrier to the transport within the skin, the stratum corneum, the outermost layer of the epidermis.

To overcome this limitation, passive and active penetration enhancement techniques have been developed over the years to improve the bioavailability and increase the range of drugs for which topical and transdermal delivery is a viable option. The use of chemical penetration enhancers aims at increasing skin permeability, by reversibly altering the physicochemical nature of the stratum corneum, reducing its diffusional resistance. Surfactants are a class of compounds that recognizably have effects on the permeability characteristics of several biological membranes, including the skin, and therefore are able to enhance the penetration of other compounds present in the formulation. Additionally, the use of methods involving external electrical energy sources, such as iontophoresis, are able to significantly increase the transdermal permeation of ionic drugs, and are capable of expanding the range of compounds that can be delivered transdermally. The combination of both approaches has been reported to produce synergistic effects in terms of permeation for various systems reported in the literature and is also investigated in this thesis.

Generally, the work presented in this dissertation focuses on the development of strategies to improve the delivery of drugs across the skin and comprises two distinct parts. Following a comprehensive introduction in Chapter 1, the work presented in

Chapter 2 and 3 is essentially centered on a HPMC-based hydrogel system that was selected to be the basis of the drug-carrier formulation in the in vitro permeation experiments addressed in Chapters 4 and 5.

Chapter 2 reports in detail the thermal behavior of the HPMC-based hydrogels. Polymer hydrophobicity upon heating evolution has been monitored using UV/vis and fluorescence spectroscopy and correlated with gel formation. This phenomenon has also been thoroughly investigated using rheological experiments with both large strain (rotational) tests at different shear rates and small strain (oscillatory) tests. The results obtained motivated a further, related, study on the interaction between the HPMC hydrogel and an ionic surfactant (SDS), which has been comprehensively investigated using conductivity, rheology and UV/vis transmittance methods, presented in Chapter 3. It was found that the addition of SDS to HPMC solutions affects both the behavior in terms of SDS micellization and that of the HPMC solution, but in a non-trivial way. A model for HPMC–SDS interaction has been proposed, rationalizing the evolution of the system at different SDS and HPMC concentrations.

Chapters 4 and 5 report in detail the use of several surfactants as chemical penetration enhancers, in the transdermal drug delivery of various drugs. The enhancement effects of this approach were assessed using in vitro studies that were carried out in Franz diffusion cells across dermatomed porcine skin. A series of dicationic (gemini) alkylammonium bromide surfactants with varying spacer lengths (G12-2-12, G12-6-12 and G12-10-12) were tested as chemical permeation enhancers (CPE) for lidocaine hydrochloride, caffeine and ketoprofen. Three nonionic ether-monohydroxyl surfactants ($C_{12}E_1$, $C_{12}E_5$ and $C_{12}E_8$) were also evaluated as CPE alone and in combination with iontophoresis in the transdermal drug delivery of two ionized drugs, namely ondansetron hydrochloride and diltiazem hydrochloride. The results obtained demonstrate that both approaches were successful and are able of significantly improve the transdermal delivery of drugs, especially when iontophoresis is employed. Moreover, skin integrity studies were performed to assess potential harmful effects on the tissues resulting from the compounds applied and/or from the methodology employed. Light microscopy and scanning electron microscopy (SEM) at different magnifications did not reveal noteworthy morphological or structural changes and gave positive indications for their safe use as skin permeation enhancers. Complementary, studies in human epidermal keratinocytes (HEK) and in human dermal fibroblasts (HDF) were performed to establish their relative cytotoxicity profiles and compare it with that of azone (laurocapram), one of the most studied permeation enhancers.

Resumo

A via transdérmica representa uma boa alternativa à administração oral de fármacos e constitui uma via de administração conveniente para um conjunto de indicações clínicas. Esta via apresenta algumas vantagens relativamente a outras vias de administração: é não-invasiva, evita o "efeito de primeira passagem" e permite a obtenção de um nível sanguíneo constante de fármacos com uma pequena janela terapêutica, minimizando a ocorrência de efeitos secundários. Habitualmente, a medicação administrada por esta via tem uma boa adesão terapêutica por parte dos pacientes, uma vez que estas formulações são administradas, no máximo, uma vez por dia. Contudo, a via transdérmica apresenta também algumas limitações devida à difícil penetração de fármacos na pele, particularmente através do *stratum corneum*, a camada mais superficial da epiderme e reconhecidamente a maior barreira à permeação de fármacos.

Para ultrapassar estas limitações, têm sido desenvolvidas ao longo dos anos diversas técnicas passivas e activas capazes de aumentar a biodisponibilidade e a gama de fármacos possíveis de administrar por via transdérmica. A utilização de promotores químicos da absorção tem como objectivo aumentar a permeabilidade da pele, por via da alteração transiente e reversível da organização lipídica que compõe o *stratum corneum*, reduzindo a sua barreira à difusão. Os tensioactivos são uma classe de compostos que, reconhecidamente têm efeitos na permeabilidade de diversas membranas biológicas, incluindo a pele, e por conseguinte, têm a capacidade de promover a permeação de outros compostos presentes numa formulação farmacêutica. Adicionalmente, a utilização de métodos que envolvam a utilização de fontes externas de energia eléctrica, de que é exemplo a iontoforese, são capazes de aumentar significativamente a permeação transdérmica de fármacos ionizados ou ionizáveis e permite expandir a gama de compostos que podem ser administrados por esta via. A combinação das duas estratégias é referida frequentemente por ter efeitos sinergísticos em termos da permeação em vários sistemas reportados na literatura, sendo também investigada nesta tese.

Em termos gerais, os trabalhos desenvolvidos e apresentados nesta dissertação abordam o desenvolvimento de métodos que melhorem a eficiência da entrega de fármacos por via transdérmica e é composto por duas partes distintas. Depois de uma introdução pormenorizada do tema feita no Capítulo 1, os trabalhos reportados nos Capítulos 2 e 3 abordam um sistema hidrogel de hidroxipropilmetil celulose (HPMC) que foi seleccionado como base da formulação para os fármacos, cujos estudos de permeação *in vitro* são reportados nos Capítulos 4 e 5.

No Capítulo 2 é abordado em pormenor o comportamento térmico de um hidrogel à base de um polímero de celulose modificado hidrofobicamente, HPMC. A evolução da hidrofobicidade das cadeias poliméricas com o aumento de temperatura foi monitorizada utilizando técnicas de espectroscopia de absorção UV-visível e de fluorescência e foi correlacionada com a formação de um sistema gel com a temperatura. Este fenómeno foi investigado através de técnicas reológicas, nomeadamente ensaios rotacionais com diferentes tensões de corte e a diferentes velocidades de corte e ensaios oscilatórios.

Os resultados obtidos anteriormente motivaram um estudo relacionado, descrito no Capítulo 3 desta dissertação, onde foi investigada a interacção entre o sistema hidrogel de HPMC e um tensioactivo iónico (SDS) recorrendo a técnicas de condutividade eléctrica, reologia e espectroscopia de absorção UV-visível. Verificou-se que a adição de SDS às soluções de HPMC afectou o processo de micelização do SDS, tendo também alterado, de um modo não trivial, as propriedades das soluções de HPMC. Foi proposto um modelo para a interacção entre o polímero HPMC e o tensioactivo SDS, racionalizando a evolução do sistema para diferentes concentrações de SDS e de HPMC.

Os Capítulos 4 e 5 desta dissertação relatam em pormenor a utilização de diferentes tensioactivos como promotores químicos da absorção de diversos fármacos por via transdérmica.

O efeito destes promotores foi investigado através de ensaios de permeação *in vitro* em células de difusão vertical de Franz. Nestes ensaios, foi usada pele de porco previamente cortada com um dermátomo, como modelo para a pele humana. Vários tensioactivos derivados de alquilamónio, com cadeias alquílicas de doze carbonos (C_{12}) e com variações estruturais no comprimento do espaçador (G12-2-12, G12-6-12, G12-10-12) foram testados como promotores químicos de absorção para três fármacos: hidrocloreto de lidocaína, cafeína e cetoprofeno. Três tensioactivos não iónicos alquil-oxietileno ($C_{12}E_1$, $C_{12}E_5$ and $C_{12}E_8$) foram também avaliados como promotores químicos de forma isolada ou em combinação com iontoforese na entrega transdérmica de dois fármacos: hidrocloreto de diltiazem e hidrocloreto de ondansetron. Os resultados obtidos demonstram que ambas as estratégias foram eficazes e capazes de aumentar significativamente a entrega transdérmica dos fármacos, especialmente quando a iontoforese foi utilizada. Adicionalmente foram efectuados estudos para averiguar a integridade da pele utilizada nos ensaios de permeação e potenciais efeitos tóxicos

causados pelos promotores de absorção ou pela metodologia utilizada. As imagens de microscopia óptica e de microscopia electrónica de varrimento (MEV), a diferentes níveis de ampliação, não revelaram alterações estruturais ou morfológicas significativas e deram indicações positivas quanto à utilização segura destes compostos como promotores da absorção transdérmica. Foram também efectuados estudos de citotoxicidade em linhas celulares de queratinócitos da epiderme humana (QEH) e em fibroblastos da derme humana (FDH), que permitiram estabelecer perfis de toxicidade relativa para os diferentes promotores e compará-los, por exemplo, com o da azona (laurocaprama), um dos mais estudados promotores da absorção transdérmica.

Chapter 1

General introduction

1.1. State of the art in transdermal drug delivery

1.1.1. Transdermal drug delivery – its origins

Transdermal drug delivery (TDD) refers for the transport of pharmaceutical actives to the human body through intact skin with the aim of a therapeutic effect. The application of substances to the skin for medicinal purposes has attracted considerable interest in recent years but as a concept is not new since many formulations have been used even in ancient times. Traditional preparations used include ointments, gels, creams and medicinal plasters containing natural herbs and compounds. Classical examples include the use of certain ointments and plasters. In the 16th century B.C. the Ebers Papyrus recommended that the husk of the castor oil plant be crushed in water and placed on an aching head and "the head will be cured at once, as though it had never ached" [1]. Another interesting story involves the mustard plaster. Mustard plant has been used both as a condiment and as an active ingredient with a therapeutic effect by the ancient Egyptians, Sumerians and Chinese. The mustard plaster, used in the management of severe chest pain congestion, was prepared by mixing the powered mustard seed (*Brassica nigra*) with warm water, and the resulting paste was spread on a strip of flannel and applied to the patient's chest with a cloth binding wrapped around the body to keep the plaster in the right position. The Greek physician Dioscorides, prescribed mustard for everything from tonsillitis to epilepsy, and the Romans combined ground mustard seed with vinegar to make an ointment for snakebites and scorpion stings and chewed the seed to relieve toothaches. In addition to mustard plasters, several other plasters were recognized in early 20th century editions of the United States

Pharmacopeia (USP) and National Formulary (NF). Belladonna Plaster, containing 0.25–0.30% of belladonna root alkaloids, was believed to act transdermally as an analgesic. Stronger Mercurial Ointment, a formulation containing 50% of elemental mercury, was reported to be an important precursor of the modern transdermal medication. It was used as a treatment for syphilis when Salvarsan and other arsenicals were in use, prior to the discovery of penicillin [2].

1.1.2. Advantages and limitations of the transdermal route

Like many alternative routes of delivery, the skin has both benefits and limitations when compared with more conventional methods such as the oral route. Drugs that are ingested orally must pass through the liver, where they undergo metabolism before entering the bloodstream. This often results in a reduced amount of active drug available to reach the site of action and means that drugs may have to be given in higher doses to compensate. Drugs administered via the skin are not subject to first-pass effect, and therefore may be administered in lower doses.

The main benefits associated with the transdermal route are thus the avoidance of first pass metabolism and other effects associated with the GI tract such as pH, chemical degradation, gastric emptying time or gastric irritation. The transdermal route can also provide a sustained and controlled delivery over a prolonged period of time which allows drugs with poor oral bioavailability and/or short biological half-lives to be administered at most, once a day [3, 4] and the maintenance of constant blood levels in the plasma for drugs with a narrow therapeutic window, thus minimizing the risk of toxic side effects or lack of efficacy caused by peaks and troughs in blood-drug concentration [5, 6]. This results in improved patient acceptance and compliance [7-9]. Transdermal delivery of drugs also provides direct access to target or diseased sites, e.g., the treatment of skin disorders such as psoriasis, eczema, and fungal infections [10]. In the event of any adverse reactions occurs that may occur, either systemic or local, the administration of the drug can be easily interrupted. In addition, the transdermal route offers an alternative in circumstances where oral dosing is not possible (in unconscious or vomiting patients) [6].

However transdermal delivery of drugs is also influenced and limited by some factors. Ideally the drugs suitable for transdermal use should meet certain requirements regarding their physicochemical properties such as a molecular weight below 500 Da since solute diffusivity across the SC is inversely related to its size [11]. The melting point should be ideally lower than 200°C [12] and should have an adequate aqueous and lipid solubility, as a Log P (octanol/water) ideally between 1–3 is required for systemic delivery to occur [13]. A predictive rule of thumb is that the maximum flux of drug through the skin should decrease by a factor of five for an increase of 100 Da in the molecular weight, while a decrease by a factor of ten is expected for an increase of 100°C in the melting point [14]. The transdermal route can only be applicable for potent

drugs that require only small plasma concentrations for a therapeutic effect (e.g. 10–30 ng/mL for nicotine) [15].The drugs, excipients, or other components of delivery devices applied topically should not cause an immune response or any kind of sensitization as the skin as an immunological barrier may be reactive by the exposure to certain stimuli, resulting in erythema, edema, etc. [16-19]. The transdermal delivery of drugs is also affected by intra-and inter-variability caused by differences in skin type, site of application, patient age, variation in adhesive effectiveness and it is associated with the permeability of intact and diseased skin. This implies that there are fast, slow and normal skin absorption profiles resulting in different biological responses [20-22]. Another issue that might affect the efficacy of the delivery of drugs administered topically is the presence of enzymes in the skin, mainly esterases and peptidases that can metabolize the drugs into therapeutically inactive forms. This is known as pre systemic metabolism [23].

1.1.3. Drug delivery market and future perspectives

Markets for transdermal drug delivery products are difficult to define because they overlap with the overall pharmaceutical markets of the drugs delivered by this route. Estimation can be made of the share of transdermal technologies in the overall market for drug delivery technologies. The transdermal delivery market was valued at $21.5 billion in 2010 and is predicted to reach $31.5 billion by 2015. The annual U.S. market for transdermal patches is estimated at more than $3 billion. Transdermal drugs account for more than 12% of the global drug delivery market [24].

The first transdermal patch (scopolamine) was approved in 1979 by the governmental agency Food Drug and Administration (FDA) for the relief of the symptoms of motion sickness, nausea, and vomiting. However, the real expansion of the transdermal market occurred with the introduction of the nicotine patches indicated for smoking cessation, in the early 1990’s.

The success of the transdermal approach is confirmed by the fact that there are currently more than 35 TDD products approved in the USA for the treatment of a wide variety of medical conditions including hypertension, angina, motion sickness, female menopause, male hypogonadism, severe pain, local pain control, nicotine dependence, and more recently, contraception and urinary incontinence. Some of the products are listed in Table 1-1.

As expected, the US market is the largest individual market. Currently, Novartis is the leading company, with a market share of 20%, mainly due to their branded products such as the Exelon® patch (a rivastigmine transdermal system which is the first transdermal therapy for Alzheimer's Disease) and some generic drugs from its Sandoz subsidiary (e.g. generic fentanyl, scopolamine, and nicotine patches.) Data indicates that

the transdermal market is still under expansion, but at a slower rate than the overall pharmaceutical market [26].

Table 1-1 Transdermal drugs approved by the FDA* updated from [25].

Approval year	Drug	Indication	Product Name	Marketing company
1979	Scopolamine	Motion sickness	Transderm-Scop	Novartis Consumer Health (Parsippany, NJ)
1981	Nitroglycerin	Angina pectoris	Transderm-Nitro	Novartis (East Hannover, NJ)
1984	Clonidine	Hypertension	Catapres-TTS	Boehringer Ingelheim (Ridgefield, CT)
1986	Estradiol	Menopausal symptoms	Estraderm	Novartis (East Hannover, NJ)
1990	Fentanyl	Chronic pain	Duragesic	Janssen Pharmaceutica (Titusville, NJ)
1991	Nicotine	Smoking cessation	Nicoderm, Habitrol, ProStep	GlaxoSmithKline (Philadelphia, PA), Novartis Consumer Health (Parsippany, NJ) Elan (Gainesville, GA)
1993	Testosterone	Testosterone deficiency	Testoderm	Alza (Mountain View, CA)
1995	Lidocaine/epinephrine (iontophoresis)	Local dermal analgesia	Iontocaine	Iomed (Salt Lake City, UT)
1998	Estradiol/norethidrone	Menopausal symptoms	Combipatch	Novartis (East Hannover, NJ)
1999	Lidocaine	Post-herpetic neuralgia pain	Lidoderm	Endo Pharmaceuticals (Chadds Ford, PA)
2001	Ethinyl estradiol/norelgestromin	Contraception	Ortho Evra	Ortho-McNeil Pharmaceutical (Raritan, NJ)
2003	Estradiol/levonorgestrel	Menopausal symptoms	Climara Pro	Bayer Healthcare Pharmaceuticals (Wayne, NJ)
2003	Oxybutynin	Overactive bladder	Oxytrol	Watson Pharma (Corona, CA)
2004	Lidocaine (ultrasound)	Local dermal anesthesia	SonoPrep	Echo Therapeutics (Franklin, MA)
2005	Lidocaine/tetracaine	Local dermal analgesia	Synera	Endo Pharmaceuticals (Chadds Ford, PA)
2006	Fentanyl HCl (iontophoresis)	Acute postoperative pain	Ionsys	Alza (Mountain View, CA)
2006	Methylphenidate	Attention deficit hyperactivity disorder	Daytrana	Shire (Wayne, PA)
2006	Selegiline	Major depressive disorder	Emsam	Bristol-Myers Squibb (Princeton, NJ)
2007	Rotigotine	Parkinson's disease	Neupro	Schwarz Pharma (Mequon, WI)
2007	Rivastigmine	Dementia	Exelon	Novartis (East Hannover, NJ)
2010	Buprenorphine	Chronic pain	Butrans	Purdue Pharma L.P. (Stamford, CT)

*This list includes transdermal patches and delivery systems approved by the FDA. Only the first approved product for a given drug or drug combination administered by a given delivery method is shown. Topical creams, ointments, gels and sprays are not included.

Future developments of drug delivery will likely focus on the continuing expansion of drugs available for use. Transdermal drug delivery systems have been considered for

use in the development of antihistamines, anti-arthritics, anti-addictives, -blockers, anti-emetics, calcium channel antagonists, tranquillizers, anti-asthmatics, antiviral agents, hormones and centrally acting cholinergic agents.

To advance our knowledge on the mechanism of transport of substances in both passive and enhanced drug delivery, visualization studies are necessary for intelligently addressing the feasibility of optimization of current and future drug delivery methods. Alternative transdermal drug delivery systems may involve the use of iontophoresis and phonophoresis. The customization of drug vehicles and enhancers may turn out to be the most promising future direction in drug delivery since the continuous steady state delivery of the drug achieved by these systems may not always provide an optimal therapeutic response.

To optimize chronopharmacology, the transdermal systems must release the drug with a variable pulsatile profile, which can be achieved by the use of iontophoresis, biphasic systems or feedback loops. Iontophoretic drug delivery presents formidable challenges to the development of safe, effective, and commercialized delivery, not only for peptides but also for a wide variety of drugs. The enormous market potential and patient compliance in this area has generated much interest and activity. The prospects of creating a safe and marketable iontophoretic drug delivery system will depend on iontophoretic device design and the drugs applied. The Macroflux patch may provide expanded drug delivery opportunities for therapeutic peptides, proteins, and vaccines [26].

1.2. Background

1.2.1. The Skin

The skin is the largest organ of the body, accounting for more than 10% of the body mass of an average person, covering an average area of 1.7m^2 and the one that enables the body to interact most intimately with its environment.

1.2.1.1. Functions

Numerous functions have been attributed to skin. Skin can act as an environmental barrier protecting the organism from harmful environmental aggressions (physical, chemical, radiation, microbiological), and it is well-known that is crucial for the maintenance of temperature, electrolyte and fluid balance [27, 28]. Skin acts a diffusion barrier that minimizes water loss that would result in dehydration, and as a barrier that can metabolize compounds to more easily eliminate products after absorption has occurred. Skin also plays an important role in body temperature regulation, in which blood vessels constrict to preserve heat and dilate to dissipate heat. Hair helps insulation, whereas sweating facilitates heat loss by evaporation. The skin also serves as

an immunological affector axis by having Langerhans cells process antigens and as an effector axis by setting up an inflammatory response to an external aggression. It has a well-developed stroma, which supports all other organs. The skin has neurosensory activity by which receptors sense touch, pain, and heat. In addition, the skin functions as an endocrine organ by synthesizing vitamin D and is a target for androgens that regulate sebum production and for insulin, which regulates carbohydrate and lipid metabolism. Skin possesses several sebaceous glands that secrete sebum, a complex mixture of lipids that function as antibacterial agents or as a water-repellent shield in many animals. The integument plays a role in metabolizing keratin, collagen, melanin, lipid, carbohydrate, and vitamin D as well as in respiration and in biotransformation of xenobiotics [29]. Skin has many requirements to fulfill and is therefore a heterogeneous structure that contains many different cell types that will be further discussed.

1.2.1.2. Anatomy and composition

Skin's structure and composition is responsible for its multiple known functions: protective, sensorial and metabolic, which are essential to the survival of humans and other mammals in a relatively adverse environment [30, 31].

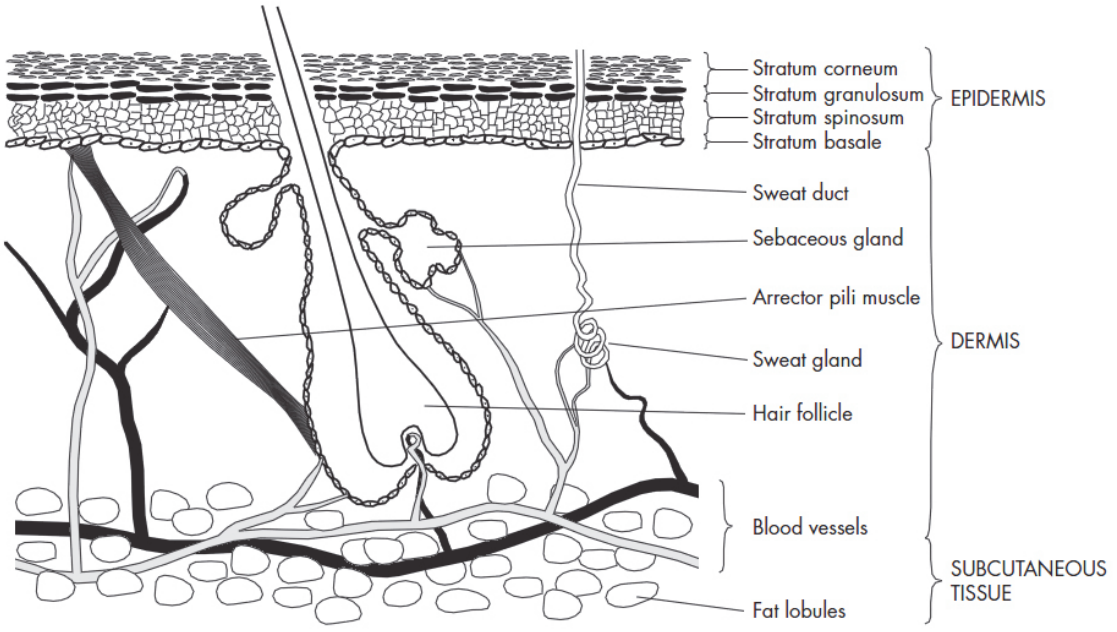

Fig. 1.1 A diagrammatical illustration of the skin [32].

The skin is a complex organ, anatomically consisting of four main layers: the stratum corneum (SC), the outermost layer of the tissue (a non-viable epidermal layer), the viable epidermis, the overlying dermis, and the hypodermis (the innermost subcutaneous fat layer).

A basement membrane separates the epidermis and dermis, whereas the dermis remains continuous with the subcutaneous and adipose tissues [33]. There are also several associated appendages such as hair follicles, sweat ducts, apocrine glands and nails.

1.2.1.2.1. Stratum Corneum

The *stratum corneum* (SC) is the skin's outermost layer and despite being only 10-20 μm thick it is largely responsible for the barrier properties of the skin due to its well organized structure, very high density and low hydration (10-30%) [28]. On most body sites the SC consists of 12-25 layers of cells (corneocytes) embedded in a complex matrix of stacked intercellular lipids arranged similarly to a "brick and mortar" model [33, 34], but it can vary as from 9 cell layers in the eyelids up to over 50 cell layers in the hand palms or feet soles [35]. The corneocytes are flattened, elongated, dead cells, lacking nuclei and other organelles, 1μm thick with a surface area of approximately 900 μm^2 [36] rich in insoluble keratins filaments (ca. 70%) and lipids (ca. 20%) bonded to a cornified cell envelope [27]. The corneocytes are the final product of the keratinocyte differentiation process that takes place along the epidermis and are continuously shed and renewed, in a process denoted as desquamation, completing a total turnover in 2-3 weeks. The corneocytes are linked by desmosomes (corneodesmosomes) and surrounded by a blend of intercellular lipids secreted from the lamellar granules of keratinocytes that define the tortuous pathways through which molecules can diffuse across the SC. Desmosomes are believed to responsible for the cohesion between SC cells, and their degradation is essential for desquamation [37]. Proteases have been demonstrated to degrade the desmosomal proteins [38-40], and it appears that hydrolysis of cholesterol sulfate also accompanies cell shedding [41]. These intercellular lipids are namely ceramides (CER) (45-50% by weight), cholesterol (CHOL) (25%), free fatty acids (FFA) (10-15%) and cholesterol sulfate (<5%) ordered in a bilayer arrangement [27]. It is also known that the exact composition of the stratum corneum lipid barrier strongly defines the performance of the skin properties [42-45] [24,27–29]. Pilgram et al. have shown that certain skin diseases such as atopic dermatitis and lamellar ichthyosis are associated to an abnormal SC lipid composition and organization [46]. This seems to indicate that specific CER species might be closely related to the regulation of keratinization from living epidermal cells to dead horny cells, together with other CER-related lipids. The lipid composition on the SC differs significantly from most other lipid membranes since it has longer and more saturated lipids and it has no phospholipids [47]. At least nine extractable ceramide subclasses [45, 48-50] were extracted from human SC and are classified as CER1 to CER9 according to their thin layer chromatographic mobility. More recently, two novel CER subclasses were reported recently [51], showing that the number of subclasses in human SC is still increasing [52]. Their respective molecular structures are illustrated in Fig. 1.2. All of the ceramides and the fatty acids found in SC are rod-like or cylindrical in shape, and these physical properties make these lipids suitable for the formation of highly ordered gel phase membrane domains. Gel phase domains will be less fluid, hence, less permeable than their liquid crystalline counterparts. Cholesterol is a

ubiquitous membrane lipid and is capable of either fluidizing membrane domains or of making them more rigid, depending on the physical properties of the other lipids and the proportion of cholesterol relative to the other components. The role of cholesterol in the epidermal barrier is probably to provide a degree of fluidity to what could otherwise be a rigid, possibly brittle membrane system. This may be necessary for the pliability of the skin [53].

Fatty acid / Sphingoid	Non-hydroxy fatty acid [N]	α-hydroxy fatty acid [A]	Esterified ω-hydroxy fatty acid [EO]
Dihydrosphingosine [DS]	CER[NDS]	CER[ADS]	CER[EODS]
Sphingosine [S]	CER[NS]	CER[AS]	CER[EOS]
Phytosphingosine [P]	CER[NP]	CER[AP]	CER[EOP]
6-hydroxy sphingosine [H]	CER[NH]	CER[AH]	CER[EOH]

Fig. 1.2 Structures and nomenclature of ceramides (CERs) in human SC [51]. The letters in parentheses present the ceramide classification as suggested by [54].

1.2.1.2.2. Viable Epidermis

The viable epidermis is a multilayered structure mainly composed of keratinocytes (95%) at different stages of differentiation and some other specialized cells such as melanocytes, Langerhans cells, Merkel cells, dendritic T cells [55]. The deepest layer of the epidermis is known as *stratum basale* (SB), a single layer of actively dividing epidermal stem cells linked to each other by desmosomes and connected to the basal membrane by hemidesmosomes [56] . The cells originated in the SB migrate then upwards to the next layer, the *Stratum Spinosum* (SS). The SS is the thickest layer of the epidermis and has a spiky appearance due to the abundance of desmosomes. Cells in this layer exhibit lipid-rich structures, the lamellar bodies (Odland bodies) and are richer in keratin filaments when compared to the cells in the SB. *Stratum Granulosum* (SG) corresponds to 3-5 layers of flattened keratinocytes showing clearly granules of keratohyalin, particularly significant due to its major role in the aggregation and alignment of keratin filaments. The Odland bodies are, at this stage, bigger and more

abundant. They enclose multiple lipidic lamellar units and hydrolytic enzymes (proteases, lipases and glycosidases). As the migration and differentiation takes place, Odland bodies migrate to the cell membrane, later releasing its content, a fundamental process in the formation of the SC extracellular lipid matrix. The *Stratum Lucidum* consists of some clear layers of flattened, compacted, anucleated cells, fully keratinized. It is only present in areas where the skin is particularly thick like the hand palms or the sole of the feet.

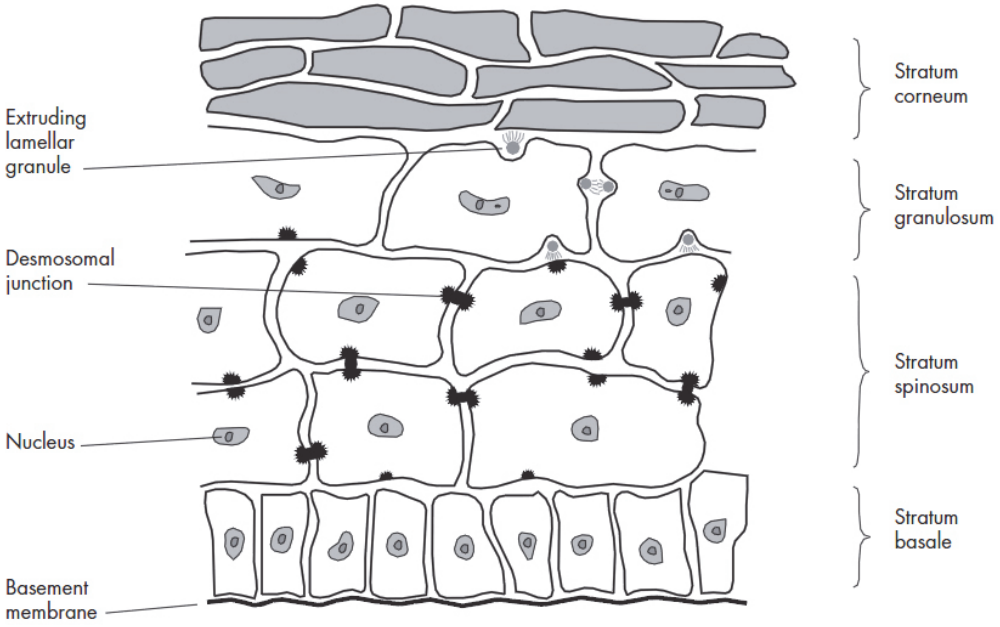

Fig. 1.3 Representation of the epidermis, showing the process of cell differentiation and the establishment of the cornified envelope [32]. For terminal differentiation, epidermal cells move from the basal layer (stratum basale) through the spinous layer (stratum spinosum) and the granular layer (stratum granulosum) towards the stratum corneum. During this process, they develop from mitotically active cells into dead, flattened squames. At the various stages of this development, different proteins are expressed. Crosslinking of epidermal proteins eventually leads to the establishment of the cornified envelope, a thick peripheral protein envelope that stabilizes each corneocyte. Additionally, lipids are synthesized in lamellar granules which are subsequently extruded into the extracellular space where they surround the corneocytes and build the lipid envelope.

1.2.1.2.3. Dermis

The dermis lies under the epidermis and is the principal mechanical support structure of the skin having also major roles in skin nutrition, thermal regulation and immune response. It is about 0.1– 0.5 cm thick and consists of dense connective tissue, rich in collagen, elastic and reticular fibers embedded in a mucopolysaccharide blend. The main cells found in the dermis are the fibroblasts, mast cells and macrophages. Other structures like blood and lymphatic vessels, sweat and sebaceous glands, sensory nerve endings and hair follicles are also found in this layer [57, 58].

1.2.1.2.4. Hypodermis

The hypodermis is the deepest skin structure. It is made of loose connective tissue and connects the dermis to the muscles and bones underneath. The predominant cells in this layer are the adipocytes, specialized in the storage of energy in the form of fat, but fibroblasts and macrophages are also present [57, 58].

In conclusion, it is very important to have a fundamental knowledge of skin microanatomy in order to identify the relevant compounds and structures that may interact with penetrating agents (such as drugs) so as to understand their ability to penetrate the *stratum corneum* and to develop strategies to efficiently and safely overcome that barrier.

1.2.2. Mechanisms of percutaneous absorption

The SC is a predominantly lipophilic barrier which minimizes transepidermal water loss (TEWL) and is at the same time the principal permeation barrier to percutaneous absorption. Due to the high organization level of the skin, drug molecules applied on its outer surface must follow tortuous paths, crossing all the skin cell layers and intercellular lipids, in order to reach the circulatory system in the dermis [59]. These routes are habitually classified as intercellular, transcellular and appendageal (via sweat glands and hair follicles). The relative contribution of these routes depends on the solubility, partition coefficient and diffusivity of the drug within these protein or lipid phases.

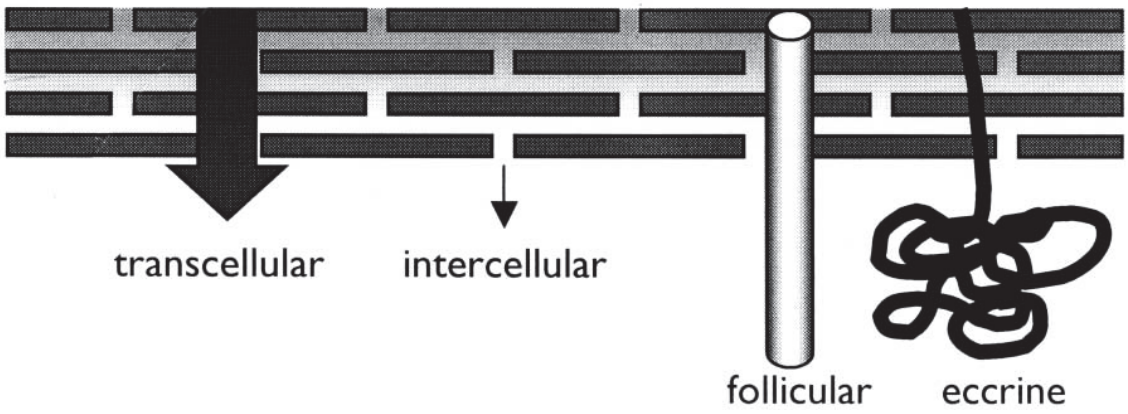

Fig. 1.4 A schematic representation of the skin showing the different possible routes of penetration. The follicular area accounts for approximately 0.1% and the eccrine 10^{-3}% of the total surface area [60] .

Since the appendageal area available for transport is only about 0.1% of the total skin surface area this route usually contributes negligibly to steady state drug flux, being is particularly relevant for ions and large polar molecules that struggle to cross intact SC. However, the intercellular route appears to be predominant, and therefore many enhancement techniques aim to disrupt or bypass the SC molecular architecture of bilayers of ceramides, fatty acids, cholesterol and cholesterol esters.

The transdermal delivery of small molecules has been considered as a process of interfacial partitioning and molecular diffusion through the SC. A typical mathematical model considers the SC as a two-phase protein-lipid heterogeneous membrane having the lipid matrix as the continuous phase [33, 61, 62]. Several theoretical skin-permeation models have been proposed which can predict the transdermal flux of a drug based on some of its physicochemical properties [63-67]. We often make assumptions in these models about the barrier properties of the skin and predict the transdermal flux of a drug from a saturated aqueous solution, given the water solubility and the molecular weight of the drug and its lipid-protein partition coefficient. Most of these theoretical expressions assume a two-compartment model of the SC based on a heterogeneous two-compartment system of protein-enriched cells embedded in lipid intercellular domains ("bricks and mortar model").

In the bricks and mortar model, the SC corneocytes are considered to be the bricks because of their resistant cell envelopes and keratin microfibrils, while the layers of lipids found between the cells are considered to be the mortar [34, 68]. The lipid ''mortar'' is the main barrier to water passing out through the SC [69]. The permeability of lipid soluble molecules is modeled by considering them to wind their way around the corneocyte bricks by diffusing through the lipid mortar [70]. Both the bricks and the mortar of the SC are produced by keratinocytes at the *stratum granulosum* (SG), at which keratinocytes release the lipids of the mortar into the space between the cells as they are being transformed into the corneocytes ''bricks.'' A major difference between the current and the earliest versions of the model is that we now know that the bricks are linked by desmosomes.

1.2.2.1. Theoretical basis of percutaneous absorption

Since there are little evidences suggesting that there are active processes accounting for the permeation of drug molecules across the skin, the transport process is controlled by a passive diffusion mechanism that can be described by the Fick's First Law of diffusion [71]. In permeation experiments Fick's first law is used to describe steady state diffusion and to analyze permeation data.

$$J = \frac{KD\Delta c}{h} \qquad (1.1)$$

where J stands for the steady-state flux per unit of area, D is the diffusion coefficient in the skin, K the partition coefficient between the skin and the formulation, Δc is the concentration difference across the skin and h corresponds to the diffusion path length. Since the drug concentration applied (c_{app}) to the skin is much larger than the concentration under the skin (infinite dosing) Eq. 1.1 can be simplified to

$$J = k_p \, c_{app} \qquad (1.2)$$

where k_p is a permeability coefficient (= KD / h) and is a heterogeneous rate constant having the units, for example, cm.h^{-1}. It is often difficult to separate K and D and their calculated magnitude will depend on h. The parameter h cannot be accurately estimated as it is related to the tortuosity of the intercellular channels, which is imprecise. The driving force for diffusion is often simplified as the concentration gradient. Strictly it should be the chemical potential gradient. This leads to confusion when concentrated solutions are used and often mention is made of the thermodynamic activity. Fick's laws of diffusion show that the flux (J) should increase linearly with concentration until c_{app} reaches the solubility limit [60, 72].

The concentration gradient of drug within the skin and the diffusivity, in accordance with Fick's Law, are therefore the two drug-related properties that influence flux across the skin. However, the concentration gradient, in turn, is influenced by the ability of the drug to partition into the skin and its ability to partition out of the skin into the underlying tissues.

The cumulative amount of drug permeating through the skin (Q_t) is given by

$$Q_t = \frac{KDC_s}{h}\left(t - \frac{h^2}{6D}\right) \qquad (1.3)$$

where C_s is the saturated reservoir concentration when a sink condition is maintained in the receptor solution. According to the definition on USP 32-NF27, sink conditions is defined as "*the volume of medium at least three times that required in order to form a saturated solution of drug substance*" when performing a dissolution procedure. When the steady-state line, calculated from the slope of the linear part of the permeation profile, is extrapolated to the time axis, the value of the lag time is obtained by the intercept at Q=0 i.e., corresponds to a cumulative amount of drug permeating through the skin equal to 0). The diffusion coefficient (D) can then be calculated from Eq. (1.1), by knowing the donor phase concentration and thickness of the barrier (h), and measuring the partition coefficient (K). The lag time method is commonly used for analysis of the permeation data from in vitro experiments with an infinite dosing technique, that is, where the skin separates an infinite reservoir of drug on the donor side and a perfect sink as receptor. However, the lag time method could be subjective as it requires an evaluation to determine the linearity of the permeation profile [73].

1.2.3. Skin permeation enhancement strategies – overcoming the barrier

In general, the SC is only permeable to small and moderately lipophilic molecules [74]. Therefore, in order to expand the range of molecules available for transdermal drug delivery, it is necessary to employ enhancement technologies to controllably, reversibly, and safely reduce the resistance of the outermost layer of the skin, the SC. A variety of

means have been studied in attempts to overcome this barrier. Such strategies include physical, biochemical, and chemical methods. The techniques that have emerged over the years can be generally categorized into passive or active (Fig. 1.5).

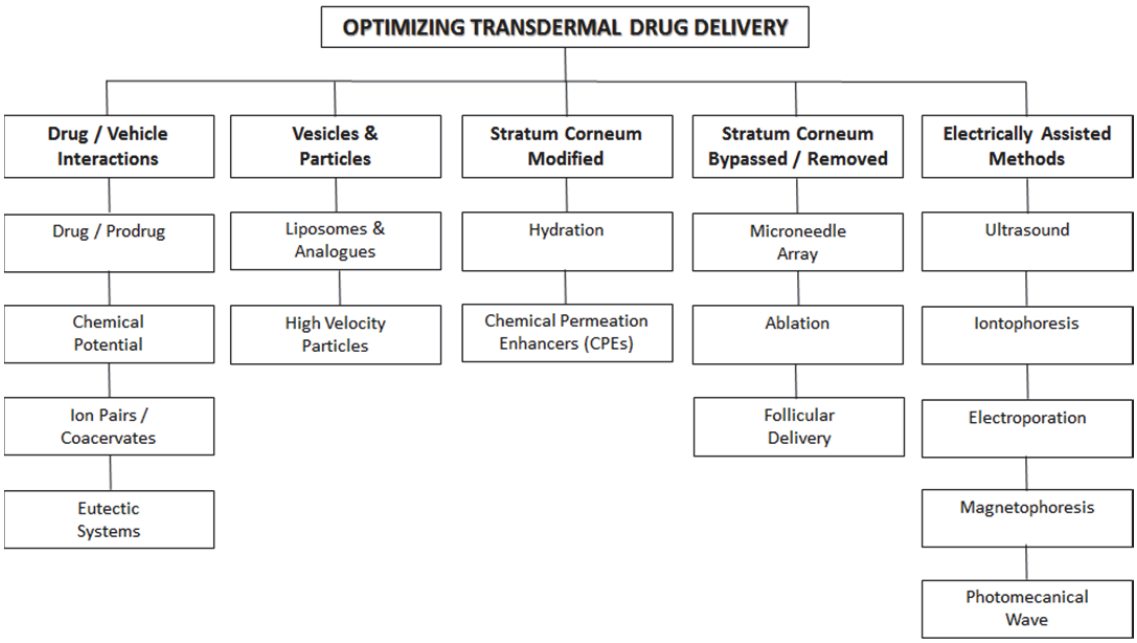

Fig. 1.5 Some methods for optimizing Transdermal drug delivery [75].

1.2.3.1. Passive enhancement of skin permeation

The conventional means of applying drugs to skin include vehicles such as ointments, creams, gels, and “passive” patch technology. However and based on Fick’s First law (Eq. 1.1), there are three permeation strategies that can increase the passive flux of a drug through the SC: by increasing the diffusion coefficient of the drug in the skin; by increasing the drug solubility in the skin and by increasing the degree of saturation of the drug in the vehicle, often referred as the super saturation approach. While the latter is based on the interaction between the drug and the vehicle, the two first strategies imply an effect of the vehicle on the barrier properties of the skin. Therefore, the most recent dosage forms have been developed in order to enhance the driving force of drug diffusion (thermodynamic activity) and/or to increase the permeability of the skin. Such approaches include the use of chemical permeation enhancers (CPE) [76-79], supersaturated systems [80], prodrugs or metabolic approach [81, 82], liposomes and other vesicles [83-93].

1.2.3.1.1. Chemical penetration enhancers (CPE)

CPE are compounds that facilitate the permeation of drugs transdermally by temporarily and reversibly diminishing the barrier resistance. An effective CPE may increase the diffusion coefficient of the drug in the SC (i.e. by disrupting the SC barrier), may increase the effective concentration of the drug in the vehicle, and may improve partitioning

between the formulation and the SC (usually by altering the solvent nature of the skin membrane to improve partitioning into the tissue) or, less likely, by decreasing the skin thickness (for example by providing a permeation “shortcut” as opposed to a tortuous pathway for a permeant). Ideally, these compounds should exhibit some desirable properties such as being non-toxic, non-irritating, non-allergenic, pharmacologically inert, but at the same time, chemically and physically compatible with the delivery system. They should provide a fast onset of action with a predictable and suitable duration of action for the drug used and must should work unidirectionally (i.e. should allow therapeutic agents into the body whilst preventing the loss of endogenous material). It is also important that when a CPE is removed from the skin the barrier properties should be restored rapidly and fully. In addition it should be cosmetically acceptable (odorless, tasteless, colorless), inexpensive and with good solvent properties [94]. Although many chemicals have been evaluated as penetration enhancers in human or animal skins, not surprisingly, no such material has yet been discovered that possesses the above listed ideal properties although some compounds demonstrate some or several of the above characteristics.

The mechanisms of action proposed for the CPE are diverse and complex. They can range from direct effects on the skin to alterations in the formulations. At biological concentrations, most of them interact with the intercellular lipid domains of the SC, causing fluidization, polarity alterations or lipid extraction and/or by affecting partitioning behavior. When acting directly on the skin CPEs can have effects on specific sites and structures such as the SC intracellular keratin, denaturing it or modifying its conformation causing swelling and increased hydration, the desmosomes that are responsible for the cohesion between corneocytes and on the intercellular lipid domains reducing the barrier resistance of the bilayer lipids. The disruption of the lipid bilayers could be homogeneous or heterogeneous depending if the enhancer distributes evenly along the bilayer lipids, or if it is concentrated within some domains. Such a phenomenon has been observed and reported for oleic acid and azone.

Due to the importance of chemical structure in the mechanism of action of these enhancers and the availability of a large amount of data, structure activity relationships have been developed for CPE. Factors such as the chain length, polarity, unsaturation and the presence of particular functional groups have been considered (e.g. [95-98]). Optimal penetration enhancement was obtained with saturated alkyl chain lengths of C_{10} to C_{12} attached to a polar head group, or C_{18} for unsaturated alkyl chains [99]. It should be noted that a direct relationship between drug and enhancer action for a specific permeation enhancer has also been reported in the literature. For example, the enhancement ratio promoted by nerolidol was found to decrease from 134.8 to 1.7 as the hydrophobicity of the drug is increased (from the relatively hydrophilic nicardipine hydrochloride to the hydrophobic tamoxifen) [100].

The term CPE includes a wide range of compounds such as water, sulphoxides (i.e. dimethylsuphoxide - DMSO), laurocapram (commercially known as azone), pyrrolidones,

fatty acids, alcohols, fatty alcohols, glycols, surfactants, urea, essential oils (i.e. terpenes and terpenoids), phospholipids and solvents. However and according to the work conducted for this thesis, special emphasis will only be given to surfactants, solvents (propylene glycol) and azone (used in this work for essentially for comparison).

1.2.3.1.1.1. Surfactants

Surfactants (surface active agents) comprise a class of compounds structurally consisting of a lipophilic alkyl or aryl fatty chain, linked to a hydrophilic head group, with amphiphilic properties which, therefore, can be employed as CPE. The hydrophilic portion can be nonionic, ionic or zwitterionic. Surfactants are present in many cosmetic and pharmaceutical formulations used as emulsifiers, wetting, suspending, solubilizing, and stabilizing agents. When applied to the skin, surfactants interact with the lipid molecules, intercalating into lipid bilayers. This results in interfacial defects and structure disruption causing the formation of diffusional paths for drugs molecules, being this the primordial mechanism of action. However, depending on the amphiphilic structure and concentration employed, local irritation of skin may be observed. Surfactants generally have low chronic toxicity and most have been shown to enhance the flux of materials permeating through biological membranes, such as the skin. Anionic surfactants are negatively charged compounds that include sodium lauryl sulphate (SLS). Cationic surfactants exhibit positive charges and include trimethylammonium bromide derivatives, such as some of the compounds used in this work (gemini surfactants). Ether-monohydroxyl surfactants (also used in this work as CPE) are examples of nonionic surfactants. Among the surfactant classes, non-ionic surfactants tend to be regarded as safe and therefore are less toxic and irritant than their charged counterparts. Charged surfactants have the potential to damage human skin, i.e. SLS has been reported to be a powerful irritant and caused an increase in the transepidermal water loss (TEWL) in human volunteers in vivo [101] and both anionic and cationic surfactants swell the stratum corneum and interact with intercellular keratin. The literature reports surfactant facilitated permeation of drugs such as diazepam, lorazepam, prazosin, piroxicam, hydrocortisone, lidocaine, etc. through various skin membranes, with significant flux enhancement [102-107].

1.2.3.1.1.2. Propylene glycol (PG)

PG has been reported to have penetration enhancement activity on its own [76, 108, 109] but it is mostly used as a vehicle for penetration enhancers and it has been shown to act synergistically when used concomitantly with other CPE such as oleic acid [110, 111]. PG permeates well through human SC and the respective mechanism of action is similar to those involved for ethanol and similar solvents. In this sense, PG can both alter the thermodynamic activity of the drug in the vehicle and therefore increasing the driving force for the diffusion process. At the same time, the interaction between PG and the SC can result in increased solubility of the drug in the SC, causing a facilitated

uptake of the drug into skin in addition some minor disturbance may occur due to intercellular lipid packing within the SC bilayers.

1.2.3.1.1.3. Azone

Azone (1-dodecylazacycloheptan-2-one or laurocapram) was the first molecule specifically designed as a skin penetration enhancer. Azone is a colorless, odorless liquid with a melting point of -7°C and it possesses a smooth, oily but yet nongreasy feel. As would be expected from its chemical structure, azone is a highly lipophilic material with a log P close to 6.2 and it is soluble in and is compatible with most organic solvents including alcohols and propylene glycol (PG). Azone has low irritancy, very low toxicity (oral LD_{50} in rat of 9 g/kg) and little pharmacological activity although some evidence exists for an antiviral effect.

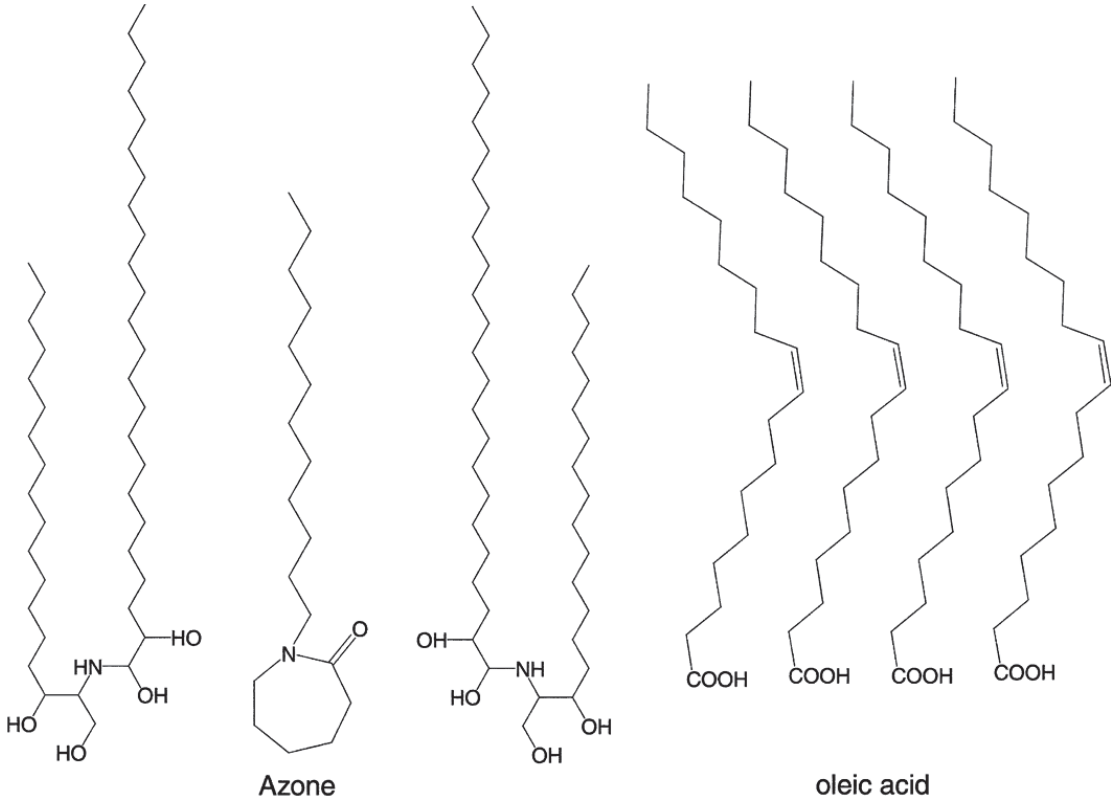

Fig. 1.6 Structures of some chemical permeation enhancers (azone and oleic acid) and a schematic showing their interaction with a representative ceramide [60].

Therefore, Azone appears to possess many of the desirable qualities listed above for a CPE. Azone has been reported to enhance skin delivery of a wide variety of drugs including steroids, antibiotics and antiviral agents [113-118]. Likewise other CPE's, the efficacy of azone appears to be concentration dependent and is also influenced by the choice of vehicle from which it is applied [119]. Although azone has been in use for so many years, its mechanism of action is still controversial and under study. Considering the chemical structure (possessing a large polar head group attached to a lipid alkyl

chain), azone probably exerts its penetration enhancing effects through interactions with the lipid domains of the SC, causing the disruption of the bilayer lipids arrangement.

However, the amount of drug that can be delivered using passive methods is still limited because the barrier properties of the skin are not fundamentally changed.

1.2.3.2. Active enhancement of skin permeation – the use of electrical energy

The advent of biotechnology in the latter half of the 20th century has led to the generation of therapeutically-active, large molecular weight (>500 Da), polar and hydrophilic molecules, such as peptides and proteins. These methods of permeation enhancement may involve the use of external electrical energy sources to act as a driving force and/or to reduce the barrier provided by the SC. The physical force involved can be iontophoresis, electro-osmosis or electroporation [112]. The increase in drug permeation as a result of this methodology can be attributed to either one or a combination of the following mechanisms: electrorepulsion (for charged solutes), electro-osmosis (for uncharged solutes), and electropertubation (for both charged and uncharged)[113].

Iontophoresis applies a small low voltage (typically 10 V or less) continuous constant current (typically 0.5 mA/cm^2 or less) to push a charged drug into skin or other tissue. In contrast, electroporation applies a high voltage (typically 50–500 V) pulse for a very short duration (less than 1 second) to permeabilize the skin. Electro-osmosis is a phenomenon that accompanies iontophoresis, where the electrical field creates a convective flow of water which allows hydrophilic compounds to be transported. Both electro-osmosis and electroporation, do not provide a driving force for delivery, but rather reduce the barrier to delivery [114].

1.2.3.2.1. Iontophoresis

Iontophoresis can be defined as a method of enhancing and controlling the penetration therapeutic agents in ionic form through the skin by the application of a low-level external electrical current across the skin [115, 116]. The drug is driven into the skin by electrostatic repulsion using an electrode of the same polarity as the charge of the drug.

1.2.3.2.1.1. Advantages and Disadvantages

Transdermal iontophoresis appears to be a promising technique for the delivery of a variety of compounds in a controlled and programmed manner. The technique has been observed to enhance the transdermal permeation of ionic drugs several-fold, and is capable of expanding the range of compounds that can be delivered transdermally.

Along with the benefits of bypassing hepatic first pass effect, and higher patient compliance, the additional advantages that the iontophoretic technique includes the delivery of both ionized and unionized drugs. An important advantage is that it also

improves the delivery of polar molecules (very limited on the passive approach) as well as high molecular weight compounds and, depending on the current applied, it is enables continuous or pulsatile delivery of drugs. If needed, it permits an easier termination of drug delivery, offering a better control over the amount of drug delivered, since the amount of compound delivered depends on applied current, duration of applied current, and area of skin exposed to the current. In addition, iontophoresis permits the restoration of the skin barrier functions without producing severe skin irritation and can be used for systemic or local (topical) delivery of drugs. Another important advantage is the reduction of inter and/ or intra subject variability in view of the fact that the rate of drug delivery is more dependent on applied current than on SC characteristics [117].

The reported limitations of iontophoretic systems include the amount of electric current that can be used in humans (regulatory limits currently are set at 0.5 mA cm^{-2}) and the irreversible damage such currents could do to the barrier properties of the skin. In addition, iontophoresis has failed to significantly improve the transdermal delivery of macromolecules of with molecular weight above 7000 Da [118]. The drugs delivered iontophoretically must be in aqueous solution and it must be ionized, which excludes some widely used drugs. The electrode and its content of drug applied to the skin act as a voltaic cell resulting in decreasing pH in the positive electrode and an increasing pH in the negative electrode, limiting the duration of treatment and there is usually a limit to the quantity of medication that can be delivered by this approach.

1.2.3.2.1.2. Principles of iontophoresis

The iontophoretic technique is based on the general principle that like charges repel each other. Thus during iontophoresis, if delivery of a positively charged drug (D^+) is desired, the charged drug is dissolved in the electrolyte surrounding the electrode of similar polarity, i.e. the anode in this example (Fig. 1.7). On application of an electromotive force, the drug is repelled and moves across the SC towards the cathode, which is placed elsewhere on the body. Communication between the electrodes along the surface of the skin has been shown to be negligible [119], meaning that the movement of the drug ions between the electrodes predominantly occurs through the skin and not on the surface. When the cathode is placed in the donor compartment of a Franz diffusion cell to enhance the flux of an anion, it is termed cathodal iontophoresis and for anodal iontophoresis, the situation would be reversed.

The skin, being negatively charged at physiological pH acts as a cation selective membrane and favors the motion of cations through anodal iontophoresis. Anodal iontophoresis also causes convective motion of the solvent occurring in response to the movement of counterions. This process is known as electro-osmosis and is involved in the motion of both neutral compounds and positively charged ions (Fig. 1.7).

In summary, the increase in drug permeation as a result of iontophoresis can be attributed to either one or to a combination of the following mechanisms: concentration

gradient (diffusive / passive transport component) and electrochemical potential gradient developed across the skin, increased skin permeability under applied electric current (electromigration / electrorepulsion) and a current-induced water transport effect (electro-osmosis / convective transport / iontohydrokinesis).

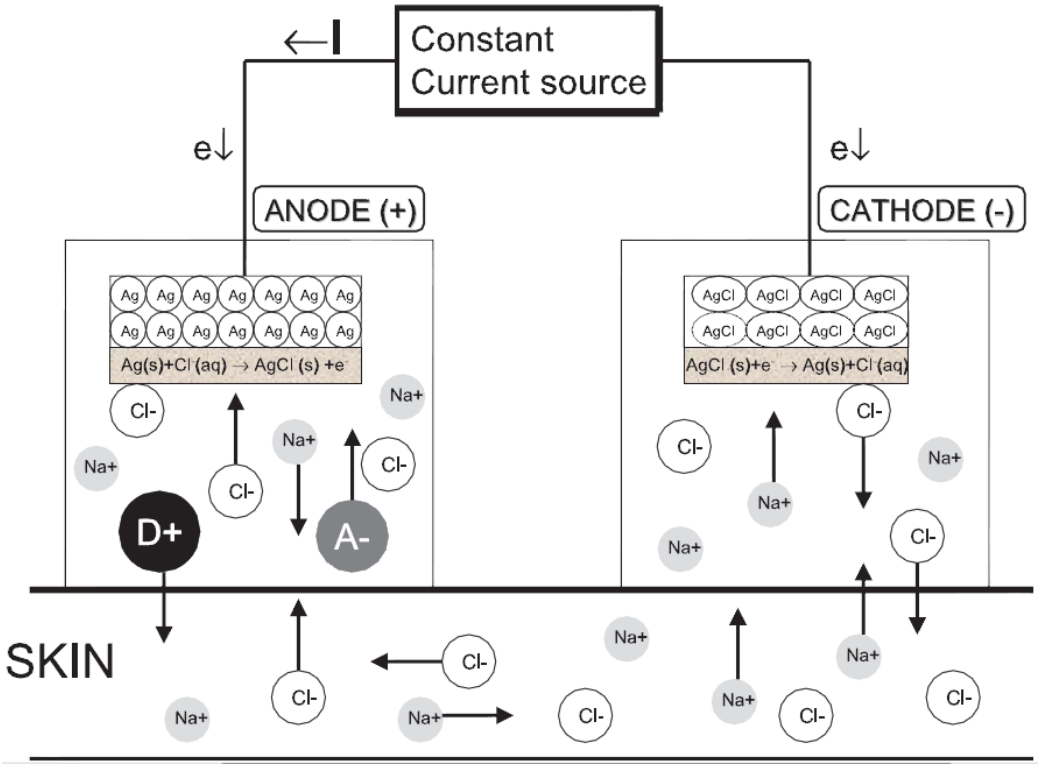

Fig. 1.7 Diagram of iontophoretic technique: as current is applied the drug (D^+) are repelled into the skin and eventually absorbed in the systemic circulation. The anodal compartment contains an ionizable drug D^+ with its counter-ion A^- and Na^+Cl^-. The application of an electric potential causes a current to flow through the circuit. At the electrode solution interface, the Ag^+ and Cl^-react to form insoluble AgCl, which is deposited on the electrode surface. Electromigration transports the cations, including the drug molecule, from the anodal compartment and into the skin. At the same time, endogenous anions, primarily Cl^-, move into the anodal compartment. In the cathodal chamber, Cl^- ions are released from the electrode and electroneutrality requires that either an anion is lost from the cathodal chamber or that a cation enters the chamber from the skin. Taken from ref. [120].

However, iontophoretic drug transport occurs mainly through electrorepulsion and electro-osmosis. The passive component contribution is negligible. Electrorepulsion refers to the drug transport across skin due to either the repulsion of cations into the skin from the anode (anodal iontophoresis) or the migration of anions into the skin from the cathode (cathodal iontophoresis). On the other hand, electro-osmosis is a phenomenon that occurs as a result of a net negative charge on the skin at physiological pH that subsequently leads to its cation permselectivity. This results in induced solvent flow that facilitates cation transport in anode-to-cathode direction, with inhibition of anion transport enabling enhanced transdermal delivery of neutral and polar solutes across the skin when an electric field is applied [121].

Due to the complex nature of iontophoretic delivery, a number of attempts have been made to define the respective delivery rate. The Nernst-Planck equation has been used with modifications to predict iontophoretic enhancement ratios (ratio of steady state flux in presence of electric potential and in absence of potential) as the original equation lacks a term for convective electroosmotic flow [122]. The contributions of osmotic flow have been studied and incorporated this fact into several equations [122-126].

Basically, the increased flux during iontophoresis (J_{ionto}) includes: 1) flux due to the electrochemical potential gradient across the skin; 2) change in the skin permeability due to the electric field applied; and 3) electroosmotic water flow and the resultant solvent drag [127].

$$J_{ionto} = J_{electric} + J_{passive} + J_{convective} \quad (1.4)$$

where $J_{electric}$ is the flux due to electric current application, $J_{passive}$ is the flux due to passive delivery through the skin and $J_{convective}$ is the flux due to convective transport due to electroosmosis.

1.2.3.2.1.3. Pathways of molecular transport in iontophoresis

Skin appendages which include sweat glands and hair follicles are postulated to be involved in the major pathways of drug transport during iontophoresis [128]. Other pathways which have been shown to be involved in iontophoretic delivery include paracellular transport especially for water and uncharged polar solutes[129], artificial shunts due to temporary disruption of the organized structure of the SC [130], potential-dependent pore formation has also been observed [127].

1.2.3.2.1.4. Factors affecting iontophoresis

The pH affects iontophoresis in two ways. The pH of the donor solution influences the pH of the skin and makes the skin a selective membrane especially if the pH of the skin rises above 4. This causes the carboxylic acid moieties in the skin to become ionized and then the anodal iontophoresis promotes the permeation of cationic drugs. The pH of the donor solution also affects the ionization of the drug itself. Therefore in most cases, a weakly basic drug will be ionized to a lower extent at pH higher than its pKa and will not permeate by electromigration in presence of iontophoresis. In this case the drug will be more dependent on electro-osmosis to travel across the skin. The type of electrodes used also affect the iontophoretic delivery. Electrodes Ag/AgCl are often selected as they resist to the changes in pH which are generally seen during the use of platinum or zinc/zinc chloride electrodes. The following reactions typically occur at the anode

$$Ag + Cl^- \rightarrow AgCl + e^- \quad (1.5)$$

The electron is released to the circuit and insoluble AgCl precipitates at the anode surface. In the case of other metals like platinum, the chloride ion at the anode will be converted to Cl_2 which will in turn react with water to generate hydronium ions. These would migrate to the donor solution and compete with similar-charged drug ions; being highly mobile it enters the skin thus reducing drug transport and simultaneously causing skin irritation.

Other important factors affecting iontophoretic delivery include concentration of co-ions (buffers), current intensity, type of current and skin used concentration of solute in the donor compartment, temperature of acceptor phase, charge on the drug and type of vehicle used. The presence of a co-ion (ion with the similar charge as the drug) results in competition between the drug and the co-ion, a reduction of the fraction of the current carried by the drug and thus a reduction in the transdermal iontophoretic flux of the drug. A most common source of co-ions is the buffer added to control the pH of the donor medium.

The pattern in which the current is applied also affects the permeation profile. The use of continuous direct current may cause skin polarization, which in turn reduces the efficiency of iontophoresis. To overcome this build-up, pulsed direct current is used which delivers direct current periodically allowing the skin to return in between to its original condition. The flux obtained by both methods is comparable and any polarization induced skin damage is also prevented [131].

1.2.3.2.1.5. Applications, current and future market perspectives

Transdermal iontophoretic systems have the potential to produce reproducible enhancement of transdermal delivery of molecules at levels that are therapeutically significant. These properties make the system suitable for the delivery of a wide range of molecules, including several macromolecules that demonstrate limited passive permeation. Therefore, iontophoresis has the potential to expand the range of compounds available for transdermal delivery to include proteins and peptides and enhance skin transport. Because the electrical current can be literally switched on and off and modified, iontophoretic delivery enables rapid onset and offset, and drug delivery is highly controllable and programmable.

The unique advantages of iontophoresis technology have led to successful commercial applications in the pharmaceutical, as well as physical therapy, industry. The key factors in commercialization are the net efficiency of the device, its portability and convenience of administration.

The PhoresorTM device (Iomed Inc.) was the first iontophoretic system to be approved by the Food and Drug Administration (FDA) in the late 1970s as a medical device. Iontophoretic systems are regulatory approved mainly for administering drugs into the body for medical purposes and specialized uses such as diagnosis of medical conditions

(e.g., cystic fibrosis) and glucose monitoring. To enhance patient compliance, the use of patient-friendly, portable and efficient iontophoretic systems have been under intense development over the years. Some of the best-known devices are the GlucoWatch® Biographer for monitoring glucose [132], the LidoSite® Patch (Vyteris, Inc.)[133, 134], the E-TRANS iontophoretic system with Fentanyl hydrochloride, IONSYS® for pain management [135] and IOMED's new Hybresis™ Iontophoresis Drug Delivery System [136].

Table 1-2 Companies with technologies for drug delivery by iontophoresis [26]

Company	Technology
3M	3M foam tapes, laminated with 3M proprietary acrylate adhesives, can be used in iontophoresis transdermal systems.
ALZA	IONSYS™ an iontophoretic system: composed of anodic (pH above 4) and cathodic reservoirs (pH below 4) with an electrical potential across both. The pH arrangement lowers skin resistance as well as skin irritation. Used for transdermal delivery of fentanyl-containing, analgesic.
Birch Point Medical	Wearable Electronic Disposable Drug delivery Technology (WEDD™) used for IontoPatch. A proprietary, ultra-thin, flexible and low cost battery technology provides an electric field to propel medication across the skin.
Empi	The Action Patch™ incorporates Empi's Dupel Iontophoresis System.
Dharma Therapeutics (subsidiary of Trascu Ltd)	Lecithin Organogel Assisted Delivery (LOAD): formulation of drugs in special mixtures of lecithins and combination of these with iontophoretic delivery. LOAD can be used to deliver bioactive peptides.
Genesis Medical Ltd	MiniPhysionizer is an iontophoresis method of delivering drugs to the affected site
Hisamitsu	Combination of iontophoresis with electrophoresis.
Iomed	Phoresor Iontophoretic Drug Delivery System uses a low level external power supply (DC, maximum output = 4.0 milliamps) to control the drug dose (dose controller). The low-level current from the dose controller speeds the transport of the positive or negatively charged ions from the drug solution into the patient's skin. Combination of iontophoresis with electrophoresis.
Life-Tech Inc.	Use of iontophoresis for pain relief and administration of other drugs.
NB Therapeutics Inc.	Iontophoresis for treatment of skin disorders: treatment of onychomycosis and nongenital warts caused by human papillomavirus are in phase II clinical trials.
Novartis	A patch with two electrodes in the form of electrically insulated juxtaposed medicament reservoir with current flowing through the reservoir.
OBJ Ltd	Dermaportation: combines the abilities of active iontophoresis to mobilize drug molecules with electroporation to control the behavior of the dermal barrier effect.
Transcu Ltd	Iontophoresis (for use in its lidocaine devices) and ionic passive devices.
Vyteris Inc.	Active, transdermal drug delivery platform employing an adhesive patch containing medication and a small electronic dose controller, which activates the electrode with a mild current, propelling the drug into the skin.

The incorporation of microprocessors into these devices by ALZA (now acquired by J&J) has resulted in a significant progress to ensure the safe and effective administration of potent drugs such as opioid analgesics [135]. These systems are capable of monitoring, recording, and displaying critical system functions to the caregiver and patient. The closed-loop use of information from biophysical or biochemical sensors to achieve individualized therapies, will likely drive future innovation in this field.

Currently, competition among the marketed iontophoretic systems is mainly between two brands: IONSYS™ (ALZA / Johnson & Johnson) and Phoresor (Iomed), which is a

combination of iontophoresis with electrophoresis. However, an extended comparative evaluation of iontophoretic technologies comprising 12 companies, has shown that passive controlled electrophoresis of Transcu Ltd has advantages over active electrophoresis and technologies that combine electroporation with electrophoresis for the following reasons: 1) Transcu's active delivery system requires lower current than competing technologies, which may produce some damage to the skin, and passive delivery system is even safer than active delivery system as it needs no external power source; (2) customized and controlled delivery would be suitable for personalized medicine approach, a trend that has already started in healthcare [26].

1.2.3.2.2. Iontophoresis in conjunction with chemical penetration enhancers

Although the use of iontophoresis results in much higher drug delivery if compared with conventional passive transdermal delivery, it still has limitations as a technique. CPEs can be used in combination with iontophoresis to achieve even higher drug penetration levels. In addition to increasing transdermal transport, a combination of chemical enhancers and electrically assisted delivery should also reduce the side effects such as irritation caused by high concentration of enhancers or stronger electric forces. The combined effects of enhancers and electrically assisted delivery depend on the physico-chemical properties of the penetrant, enhancer and their behavior under the influence of an electric field. Occasionally, the use of chemical enhancers has been reported to result in reduced flux compared with using iontophoresis alone [137, 138]. However, more often synergistic effects have been reported such as those with fatty acids [139-144] , and terpenes [145-149] , azone[143, 150-152], surfactants [153, 154], solvents, etc.

1.2.4. Current experimental techniques used for in vitro percutaneous permeability testing

Due to experimental and ethical difficulties, most of the transdermal drug delivery studies tend to use skin *ex-vivo* (*in vitro*) that inherently reduces some of the above complexity: regeneration stops, immune responses cease and metabolic activity is usually lost in these studies. However, it should always be kept in mind that data obtained from excised skin may not translate directly to the *in-vivo* situation.

In vitro permeation studies are widely used to investigate the permeability of drugs since excised skin maintains its barrier properties. Most of *in vitro* techniques are carried out using diffusion cells. These devices have in common the presence of a donor compartment (where the vehicle containing the drug is placed) and a receptor chamber (containing receptor medium) separated by a membrane (e.g. skin), under controlled temperature conditions. Nevertheless, diffusion cells can assume multiple aspects and different complexity levels, varying from two-compartment static diffusion cells (vertical or horizontal) [155] to multi-jacketed "flow-through" cells [156].

1.2.4.1. Franz diffusion cells

Vertical Franz diffusion cells (Fig. 1.8) are the most widely used *in vitro* percutaneous absorption studies. In these devices, a membrane is placed between the upper donor chamber (properly capped to avoid evaporation of the formulation), and the lower receptor chamber, kept together with a clamp. Such display allows the determination of a drug permeation profile across a specific membrane, to a receptor medium that is kept continuously stirring at a fixed temperature, after analysis with an appropriate analytical method (e.g. HPLC). Special attention must be taken while choosing the receptor medium. Ideally, it should simulate as accurately as possible the corresponding *in vivo* fluid (e.g. blood) and must ensure "sink conditions" for the drug under investigation [157]. Generally, *in vitro* methods allow a better control of the experimental conditions and are particularly useful during the earlier stages of research, limiting the number of expensive *in vivo* studies in humans and animals [57].

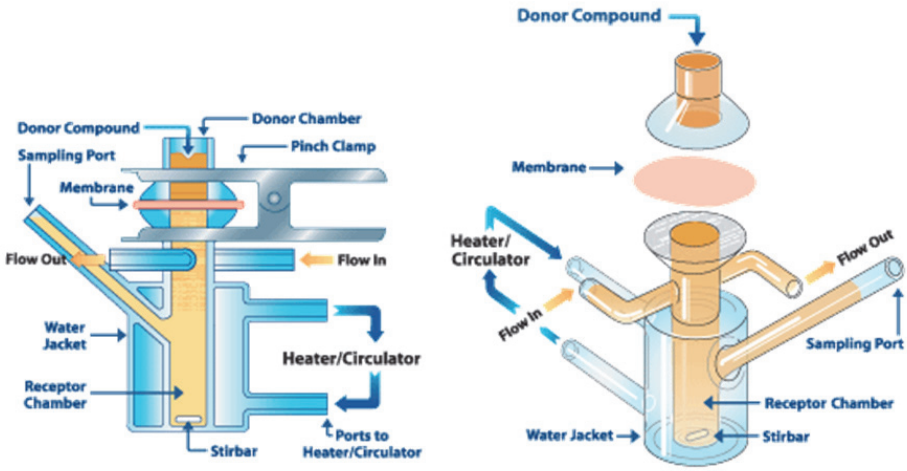

Fig. 1.8 Schematic representation of a vertical Franz diffusion cell [158].

1.2.4.2. Membranes used for permeability testing

Human skin is obviously the best membrane model to assess the transdermal absorption of a drug. However, due to its limited availability, alternative membranes models from animal sources or synthetic have been used with the same purpose.

1.2.4.2.1. Polymer membranes

A number of synthetic membranes have been tested as model membranes in permeability studies [159, 160]. Being a synthetic product, they exhibit less variability when compared other membranes from natural sources. Liquid membranes enclosing lipids as isopropyl myristate [161], dipalmitoyl phosphatidylcholine, linoleic acid and tetradecane [162] and others [163] or polymeric membranes based on polymers or combination of polymers such as polydimethylsiloxane (Silastic®) [164], poly-(2-

hydroxyethylmethacrylate), cellulose acetate [165, 166], silicone cellulose [167], silicone polycarbonate urethane (Carbosil®) [168] are examples of artificial membranes used with the objective of reproducing SC barrier properties.

1.2.4.2.2. Animal skin vs. human skin

Excised skin from different animal models has also been extensively used in studies assessing the transdermal absorption of drugs. Literature reports the use of skin from primates, pig, mouse, rabbit, rat, guinea pig and also snake models [169-176]. Its relevance as model depends on the similarity to human skin regarding physiological aspects such as blood perfusion, morphology and chemical composition. Considering this, and because the use of primates is restricted, the most significant and available model is porcine skin [177]. Furthermore it is well documented that porcine skin has similar physiological properties and anatomical features of human skin [172, 177-179]. Some studies designed to predict skin permeation in man reported that similar permeation values were obtained when porcine and human skin were tested under similar conditions *in vitro* [176, 177]. It has also been reported that both the morphology of the epidermis and upper dermis vasculature and functions of endothelial cells (e.g. plasminogen activator) in the pig were similar to that in man [180].The results of a study on the synthesis and turnover of membrane glycoconjugates in monolayer culture of pig and human epidermal cells reported identical values, concluding that pig cells can be used as a model for human cells [178]. Hence, in this work, porcine skin was selected to be used in substitution of human skin because it is functionally and structurally similar to the latter.

1.2.5. Transdermal drug delivery systems (TDDS)

Transdermal drug delivery technology represents one of the most rapidly advancing areas of novel drug delivery. This growth is catalyzed by developments in the field of polymer science. Polymers are the backbone of TDDS as they are often made of multilayered polymeric laminates in which a drug reservoir or a drug–polymer matrix is placed between two polymeric layers: an outer impermeable backing layer that prevents the loss of drug through the backing surface and an inner polymeric layer that acts as an adhesive and/or rate-controlling membrane.

Transdermal drug delivery systems are broadly classified into the following three types described below and represented on Fig. 1.9.

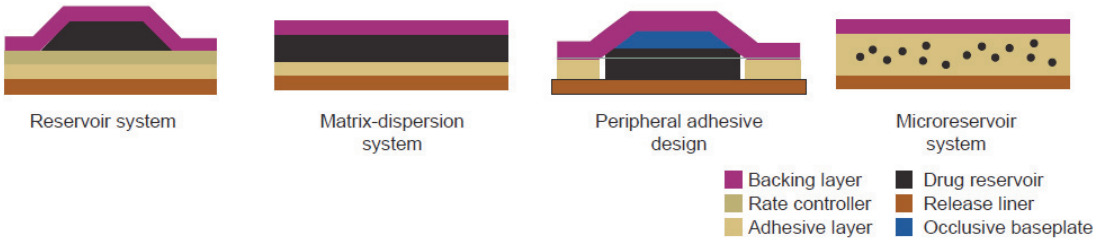

Fig. 1.9 Schematic representation of transdermal drug delivery systems [181]

1.2.5.1. Reservoir systems

In this system, the drug reservoir is embedded between an impermeable backing layer and a rate-controlling membrane. The drug releases only through the rate-controlling membrane, which can be microporous or nonporous. In the drug reservoir compartment, the drug can be in the form of a solution, suspension, or gel (very often a water-based gel, such as the ones used in this work) or dispersed in a solid polymer matrix. On the outer surface of the polymeric membrane, a thin layer of drug-compatible, hypoallergenic adhesive polymer can be applied.

1.2.5.2. Matrix systems

1.2.5.2.1. Drug-in-adhesive system

The drug reservoir is formed by dispersing the drug in an adhesive polymer and then spreading the drug-loaded polymer adhesive by solvent casting or by melting the adhesive (in the case of hot-melt adhesives) onto an impermeable backing layer. On top of the reservoir, layers of adhesive polymer are applied.

1.2.5.2.2. Matrix-dispersion system

The drug is dispersed homogeneously in a hydrophilic or lipophilic polymer matrix. This drug containing polymer disk is subsequently fixed onto an occlusive base plate in a compartment made from a drug-impermeable backing layer. Instead of applying the adhesive on the face of the drug reservoir, it is spread along the circumference to form an adhesive rim.

1.2.5.3. Microreservoir systems

This delivery system is a combination of reservoir and matrix-dispersion systems. The drug reservoir is formed by first suspending the drug in an aqueous solution of a water-soluble polymer and then dispersing the solution homogeneously in a lipophilic polymer to form thousands of microscopic spheres of drug reservoirs. The thermodynamically unstable dispersion is immediately stabilized by cross-linking the polymer *in situ* [181].

1.2.5.4. Hydrogels in transdermal drug delivery

According to the work conducted for this thesis, special emphasis will be given to gels, particularly water-based gels (or hydrogels) despite the various possibilities of vehicles used in transdermal drug delivery systems.

The widespread application of hydrogels is linked to the fact that they exhibit an intermediate behavior between solid and liquid materials. Hydrogels can be defined as three-dimensional, hydrophilic, polymeric networks capable of embedding large amounts of water. The networks are composed of polymers, which are insoluble due to the presence of chemical crosslinks (chemical gels), or physical crosslinks (physical gels), such as entanglements or crystallites which are responsible for its structure and physical integrity.

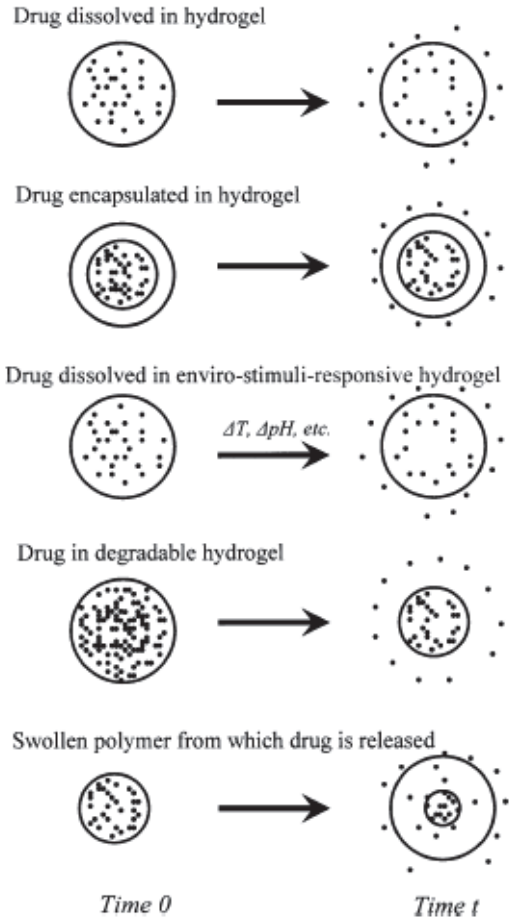

Fig. 1.10 Various delivery and release mechanism of hydrogels [182]

Because of their high water content and soft texture, hydrogels are biocompatible materials as they resemble natural living tissue more than any other class of synthetic biomaterials. The hydrated matrix results in good compatibility with proteins as well as living cells and body fluids [189, 190]. Therefore, hydrogels are nowadays widely used in

various therapeutic applications, e.g. tissue engineering, controlled drug delivery and diagnostic devices, e.g. medical and biological sensors, microarrays, diagnostic imaging [191].

Of the many applications of hydrogels, controlled drug delivery is one of the areas in which they have played a vital role as intelligent carriers. Due to the advances in polymer engineering, the physicochemical, mechanical, biological and functional properties can be easily modulated by manipulating the synthetic or processing methods. For example, hydrogels can be made to respond to environmental stimuli, such as temperature (e.g. poly(N-isopropylacrylamide) or PNIPAAm, PEO-PPO block copolymers and HPMC), pH (e.g. poly (acrylic acid) or PAA and Poly(N, N'-diethylaminoethyl methacrylate) or PDEAEM), light (copolymer of PNIPAAm and light sensitive chromophore, such as triphenylmethane and leuco derivatives), and specific molecules such as glucose (Poly(N-vinylpyrrolidone-co-phenyl boronic acid) or (Poly(NVP-co-PBA)) [192].

1.2.5.4.1. Matrix formers

Polymer selection and design must be considered when trying to meet the criteria for the creation of effective transdermal delivery systems. Polymers used in transdermal delivery systems should have biocompatibility and chemical compatibility with the drug and other components of the system, such as penetration enhancers and pressure-sensitive adhesives (PSAs). They should also be able to provide a consistent and effective delivery of a drug throughout the intended shelf life of the product and have generally-recognized-as-safe (GRAS) status.

In the case of matrix formers, the main challenge is in the design of a polymer matrix, followed by optimization of the drug-loaded matrix not only in terms of release properties, but also with respect to its adhesion–cohesion balance, physicochemical properties, and compatibility and stability with other components of the system as well as with the skin [181].

1.2.5.4.1.1. Hydroxypropylmethyl cellulose (HPMC)

HPMC is a versatile hydrophilic swellable polymer available in different grades, widely used in oral and topical formulations. It has also been tested as a matrix former in the design of patches of several drugs such as propranolol hydrochloride [183], flurbiprofen [184], tramadol [185], methotrexate [186], trimetazidine [187] and metformin [188]. In addition, HPMC has been shown to yield clear films because of the adequate solubility of the drug in the polymer. Matrices of HPMC without rate-controlling membranes have been observed to exhibit a burst effect during dissolution testing because the polymer was hydrated easily and swelled, leading to the fast release of the drug [183]. Moreover, HPMC is also chemically unreactive and therefore it is compatible with all active and non-active ingredients.

Because of the reasons listed above, HPMC was the polymer selected to be the matrix-former in the preparation of drug-loaded hydrogels in the permeation studies presented in later chapters of this thesis. Its temperature-induced behavior was thoroughly investigated, as well as the respective interaction with an ionic surfactant.

1.3. Scope

The work presented in this thesis aims at the development of strategies to improve the efficacy of the delivery of drugs across the skin. It comprises two distinct parts. The first one is addressed in Chapters 2 and 3, and consists of a detailed physicochemical characterization and study of the interaction with surfactants of the HPMC hydrogel. The latter is subsequently used as drug vehicle in the in vitro transdermal permeation studies, presented in Chapters 4 and 5.

Chapter 2

Aggregation and gelation in hydroxypropylmethyl cellulose aqueous solutions

This chapter focuses on the thermal behavior of hydroxypropylmethyl cellulose aqueous solutions, a hydrophobically modified cellulose derivative, from room temperature to higher temperatures, above gelation. Significant aspects essentially overlooked in the literature, such as the correlation between polymer hydrophobicity and rheological behavior, and the shear effect on thermal gelation are discussed here. The present observations allow composing a picture of the evolution of the system upon heating.

2.1. Introduction

Water soluble cellulose derivatives are mostly biocompatible polymers used in a wide range of applications, especially in food, pharmaceutical, and cosmetic industries [189, 190]. In particular, when dissolved in water, they can be used as thickeners, binding agents, emulsifiers, film formers, suspension aids, surfactants, lubricants and stabilizers [191]. The most common cellulose derivatives include methyl cellulose, hydroxypropyl cellulose, carboxymethyl cellulose and hydroxypropylmethyl cellulose (HPMC). Most of the applications of these cellulose derivatives solutions involve heating the polymer, and so it is crucial to understand the temperature dependence behavior of these solutions, which has been the object of various studies [192].

Cellulose is a natural polysaccharide, structurally consisting of a linear homopolymer backbone formed by D-glucopyranose units linked by β 1 - 4 glycosidic bonds [193, 194]. Pure cellulose, depicted in Fig. 2.1, is insoluble in water due to the existence of strong

intra-molecular interactions via hydrogen bonds, which represents a limitation in practical applications.

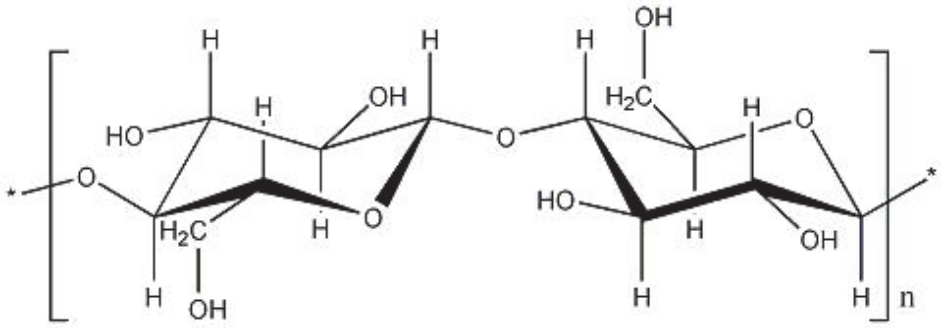

Fig. 2.1 Structure of natural cellulose.

This can be overcome by preparing water soluble cellulose derivatives. The derivatives result from the substitution of hydroxyl groups in each anhydroglucose ring by other functional groups that decrease the crystallinity of the substance [195].

In the case of HPMC, the hydroxyl groups are replaced by hydroxypropyl and methyl groups as seen in Fig. 2.2.

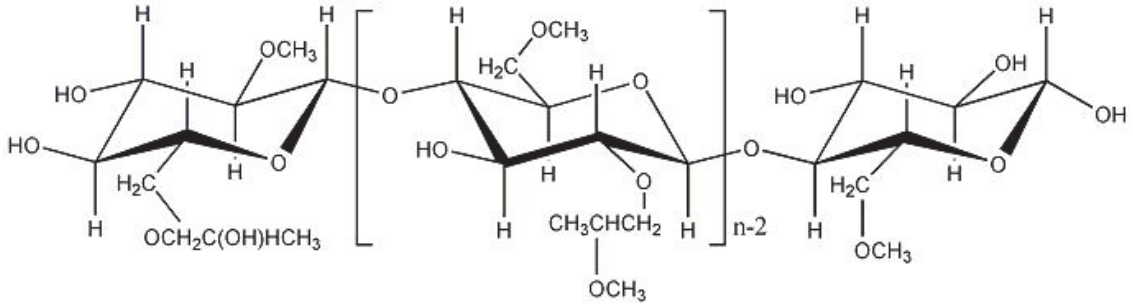

Fig. 2.2 Structure of hydroxypropylmethyl cellulose (HPMC).

There are three types of HPMC classified by the United States Pharmacopeia according to the chemical substitution of the ether: E (Hypromellose 2910), F (Hypromellose 2906) and K (Hypromellose 2208). The major chemical differences between these types of HPMC are in the degree of substitution, molar degree of substitution and degree of polymerization. The degree of substitution corresponds to the average number of substituted hydroxyl groups (maximum of 3), and the molar degree of substitution gives the number of substituents introduced into the anhydroglucose unit. Finally, the degree of polymerization is related to the average number of monomers in the chains [191].

HPMC aqueous solutions generally have the property of forming a reversible gel with temperature. Nevertheless, the study and understanding of this process is complex due the possibility of several different phenomena occurring during the heating cycle [196-198]. It is generally accepted that the thermoreversible gelation of HPMC solutions is due

to hydrophobic interactions, and it is sometimes indicated that clouding precedes gelation [199, 200].

Gelation can be detected by a sharp increase in viscosity [201]. The temperature at which this occurs is influenced by the type of cellulose ether (see e.g. ref. [192]). It has been observed that methylcellulose has a lower gelation temperature and forms firmer gels than HPMC with equivalent substitution and molecular weight, suggesting that hydroxypropyl substituents make the gelation process more difficult [202, 203]. Additionally, hydroxypropyl cellulose precipitates with increasing temperature but does not form a gel, which has been seen as evidence that the gelation of cellulose derivatives results from the exclusion of water (*syneresis*) from heavily methoxylated regions of the polymer [200, 204]. Conformational changes similar to those occurring in polyethylene-oxide have been presented as an explanation for the increasing hydrophobicity as temperature increases in substituted celluloses [205]. It is generally accepted that a polymer that provides such properties usually carries two different segments: one hydrophobic and one hydrophilic, distributed along the polymer chain. However, at higher temperatures the influence of the hydrophobic group is predominant [206]. Some authors also suggest that not only hydrophobic interaction but also hydrogen bonding may be involved in the gelation mechanism of cellulose derivatives [207].

The gelation phenomenon can be studied by a variety of techniques, which in turn provide different observables and different definitions for the gelation temperature. In this work, we use rheology to study the thermal behavior of a range of HPMC solutions. In particular, we investigate various factors that can be used to establish the gelation temperature. These include the “classical approach” in which a ramp is used to set an increasing temperature, where gelation is monitored through a sudden alteration in viscosity. We also look into how the viscosity varies (and gelation temperature) for different shear rates. Issues related to kinetic effects on gelation are discussed in conjunction with this approach. Oscillatory measurements give additional information on the system, and provide another estimate of the gelation temperature. UV-VIS spectroscopy measurements are used to determine the cloud point (CP). This technique, together with polarized light thermal microscopy (PLTM) is important to assess the formation and growth of polymer aggregates that will ultimately lead to a three dimensional gel network.

In this study, fluorescence spectroscopy using pyrene as a probe is performed in order to observe how the hydrophobic character of the polymer domains varies with temperature.

2.2. Experimental section

2.2.1. Materials and sample preparation

The cellulose derivative HPMC (METHOCEL® K15M Premium), 19%-24% methoxyl and 7-12% hydroxypropyl, M_w=4.3x10^5 Da was purchased from Dow Chemical Company and was used without further purification. Aqueous solutions of HPMC of different concentrations (1%, 2%, 5% and 10% w/w) were prepared by adding the desired amount of dry polymer to Millipore® water. The polymer solutions are above overlap concentration. Due to the long dissolution times, solutions were kept stirring for one week before use.

2.2.2. Rheological studies

The rheological measurements were conducted on a Reologica® Stresstech Rheometer equipped with automatic gap setting. A bob cup measurement system (CC 15) with a solvent trap was used to test all samples. The temperature control was achieved using a water bath system. All experiments based on a temperature ramp were performed from 25 to 90°C at a fixed heating rate of 1°C/min. A number of viscosity measurements were also conducted in steady-state conditions. Dynamic or shear viscosity was analyzed by rotational shear experiments. Prior to this, a viscometry test was carried out in order to determine both Newtonian and non-Newtonian regimes. Oscillation tests were performed to determine the storage modulus, G', and loss modulus, G". Oscillatory measurements can be used to study the structure of a material, in which the deformation in the oscillation has to be kept small. An important point is to check whether measurements are made in the linear viscoelastic regime, otherwise the results of the frequency experiments will depend not only on the frequency but also on the applied stress or deformation. A test of linearity, the oscillation stress sweep, was used to obtain the values of shear stress for which the viscoelastic functions are independent from the magnitude of the applied stress. The applied frequency was chosen ensuring that, at the initial conditions, G" is dominant. The complex viscosity modulus η^*, a mathematical representation of the viscosity in oscillatory tests [208], was also obtained. Finally, relaxation times were extracted from the moduli G' and G", represented as a function of the frequency (frequency sweep tests).

2.2.3. Cloud point determination and polarized light thermal microscopy observations

An ultraviolet-visible spectrophotometer (Shimadzu® UV - 2100) was used for the cloud point measurements. The sample was placed in a cell with a dimension of 1×1×5 cm. Millipore® water was used as reference. For temperature measurements, the cells were

placed in a cell-holder connected to a water bath system with temperature regulation (Julabo® F30-C). In addition to this regulator, an external temperature sensor (Pt 100) was placed in the sample cell. The absorption spectra (200-850 nm) confirmed that there were no UV-absorbing moieties in the solutions. The transmittance was measured at a wavelength of 800 nm as previously reported for a similar system [199]. The system was heated at a faster rate at lower temperatures. This was then reduced to a slower heating rate at the point where the transmittance started to decrease. The system was equilibrated for at least 30 minutes before each measurement.

The cloud point has been related to gelation, and different definitions were used to determine this point. In theory, the cloud point is defined as the temperature at which phase separation, in the form of turbidity, occurs for a 1% polymer concentration [209]. However, in practical applications the cloud point can be defined as the intersection of two straight lines drawn through the curves of absorbance at low and high temperatures, respectively [210], or as the 50% transmittance of the reference [199, 211] or as the maximum in the first derivative of absorbance in relation to temperature [212]. In this study the cloud point was considered to be the temperature at which the light transmittance was 50% of that obtained for the same sample at 25°C.

The microscopy analysis was performed using a Linkam system DSC 600® (Surrey, U.K.). The optical observations were conducted using a Leica® DMRB microscope and registered using a Sony CCD-IRIS/RGB video camera. The image analysis used Linkam system software with the Real Time Video Measurement System. The images were obtained combining the use of polarized light with wave compensators, at a 200× magnification.

The thermal behavior of the solutions was studied in heating/cooling cycles between 25°C and 90°C, at scanning rates of 5°C/min. The scans were made under a nitrogen atmosphere through the use of nitrogen flow.

2.2.4. Pyrene fluorescence measurements

The ratio of the first (I_1, λ=374 nm) and third (I_3, λ=388 nm) vibronic fluorescence emission intensities (I_1/I_3) of pyrene is known as the micropolarity index, and is a qualitative measurement of the polarity at the local environment of the probe [213]. This index is close to 2.0 in pure water and ca. 1.0 in hydrophobic solvents like toluene.

Being a hydrophobic probe, pyrene presents low solubility in water (approximately 10^{-6}M). Pyrene solutions were prepared by filtering pyrene-saturated Millipore® water. The samples were prepared *in situ* by adding 30 μL of the before mentioned solution to 3mL of 1% HPMC K15M solution and were left to equilibrate under stirring for 15 minutes inside of the measurement cell.

The fluorescence spectra were recorded with a Horiba-Jobin-Ivon SPEX Fluorolog® 3-22 spectrometer and were corrected for the instrumental response. The Fluorolog® consists of a modular spectrofluorimeter with a double grating excitation (range 200–950 nm, optimized in the UV and with a blazed angle at 330 nm) and emission (range 200–950 nm, optimized in the visible and with a blazed angle at 500 nm) monochromators. The bandpass for excitation and emission is 0–15 nm (values that are continuously adjustable from computer Datamax/32 software) and the wavelength accuracy is of 0.5 nm. The excitation source consists in an ozone-free 45O W Xenon lamp and the emission detector is Hamamatsu R928 Photomultiplier (200–900 nm range), cooled with a Products for Research thermoelectric refrigerated chamber (model PC177CE005) and a photodiode as the reference detector.

The system was equilibrated for at least 30 minutes before the measurement at each temperature.

2.3. Results

In this work we present four different strategies to investigate the thermal behavior of HPMC solutions: (i) the dependence of viscosity on temperature, at different shear rates through rotational tests; [214] (ii) the influence of temperature on the storage and loss moduli by oscillatory measurements, with inspection of relaxation times; (iii) clouding studies carried out via optical transmittance and PLTM measurements, and (iv) the evolution of the system polarity through fluorescence spectroscopy using pyrene as a probe.

2.3.1. Rotational measurements at different shear rates

Fig. 2.3 shows the viscosity-temperature behavior of the polymer solutions for the different concentrations of HPMC. For each solution, we have studied the viscosity upon heating for different values of the shear rate.

Let us first address the results at the lower, Newtonian, shear rates. As the temperature rises, the viscosity smoothly decreases up to a characteristic temperature, usually denoted as the gelation temperature [199]. A sharp increase in viscosity is seen after this temperature. This characteristic point is concentration dependent, with a tendency for a decrease with concentration from 2% onwards. For each temperature point the viscosity increases with HPMC content, as expected.

For the higher shear rates, corresponding to non-Newtonian regimes, viscosity suddenly drops close to the temperature at which gelation occurs for Newtonian shear rates. Then, this quantity reaches its lowest value and forms a plateau. The plateaus for higher and lower shear rates are observed for similar values of the temperature.

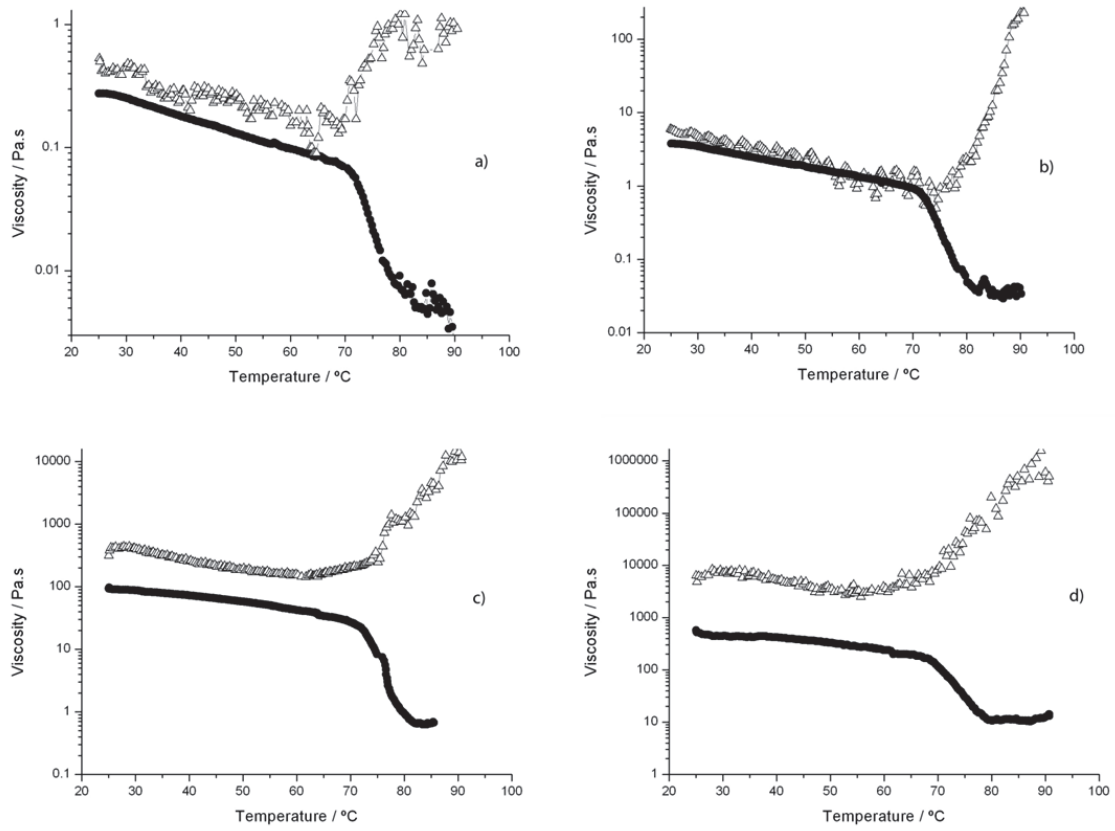

Fig. 2.3 Viscosity dependence on temperature for HPMC solutions of (a) 1%, (b) 2%, (c) 5% and (d) 10%, w/w. Curves are obtained at Newtonian shear rates (triangles), with imposed values respectively of 0.5, 0.05, 5.0×10^{-3} and 1.0×10–3 s^{-1}, and non-Newtonian shear rates (circles), of 50, 30, 5 and 1 s^{-1} respectively.

Viscosity vs. temperature plots for the 2% solution were also obtained with a systematic variation in the shear rate (Fig. 2.4). It is observed that, with increasing shear rate, the point at which viscosity starts to increase is moved towards higher temperatures. In our observations, shear rates of $8s^{-1}$, $10s^{-1}$and $30s^{-1}$ tend to prevent gelation, replacing the steep increase in viscosity by a not well defined plateau slightly above the global minimum.

This dependence is again highlighted in Fig. 2.5. For lower temperatures, below gelation, it is seen that the effect of shear rate upon viscosity, in this case shear thinning, is limited. As the temperature increases the viscosity diminishes as previously shown, but the Newtonian regime remains essentially unaffected. Above 70°C the behavior changes dramatically, and shear thinning amounts to several orders of magnitude. Basically, low shear rates correspond to very high viscosities (gel) but, when a sufficiently large shear rate is applied, viscosity sharply decreases. Note also the general good agreement between the values of viscosity depicted in the Newtonian regimes for each temperature, and those found in Fig. 2.3(b) for the lower shear rates. This indicates an appropriate choice of the shear rates used in the studies in which a temperature ramp is imposed, even for temperatures above gelation.

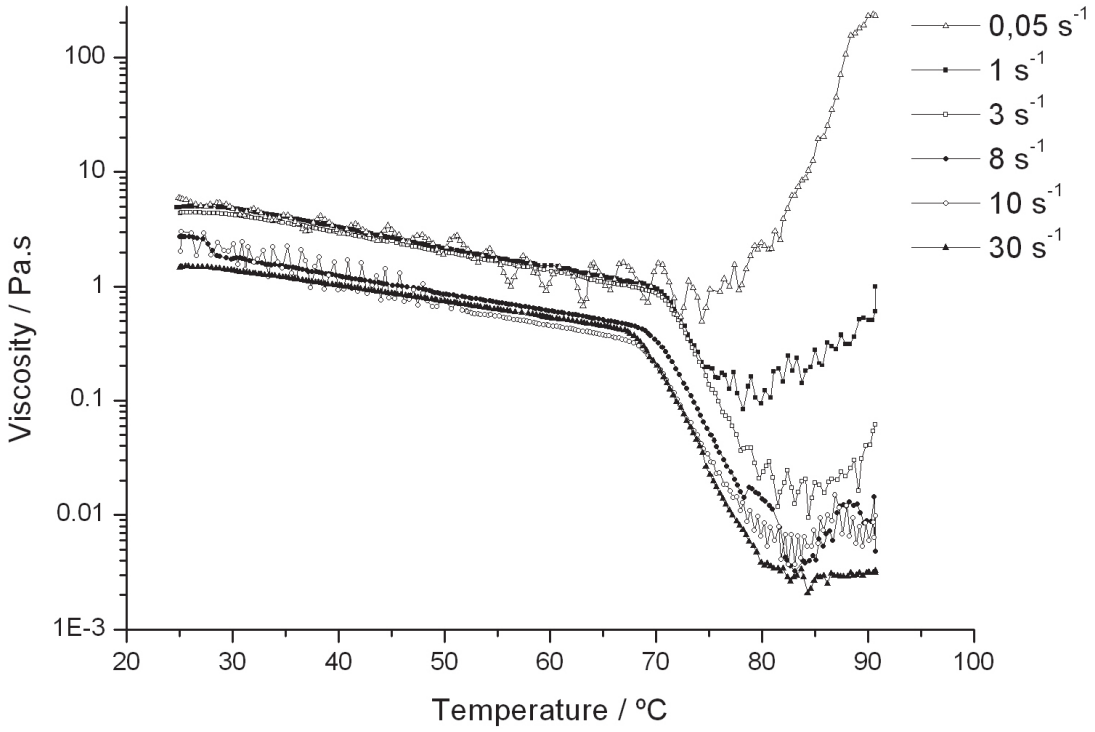

Fig. 2.4 Viscosity as a function of temperature for the indicated shear rates in the 2% HPMC solution.

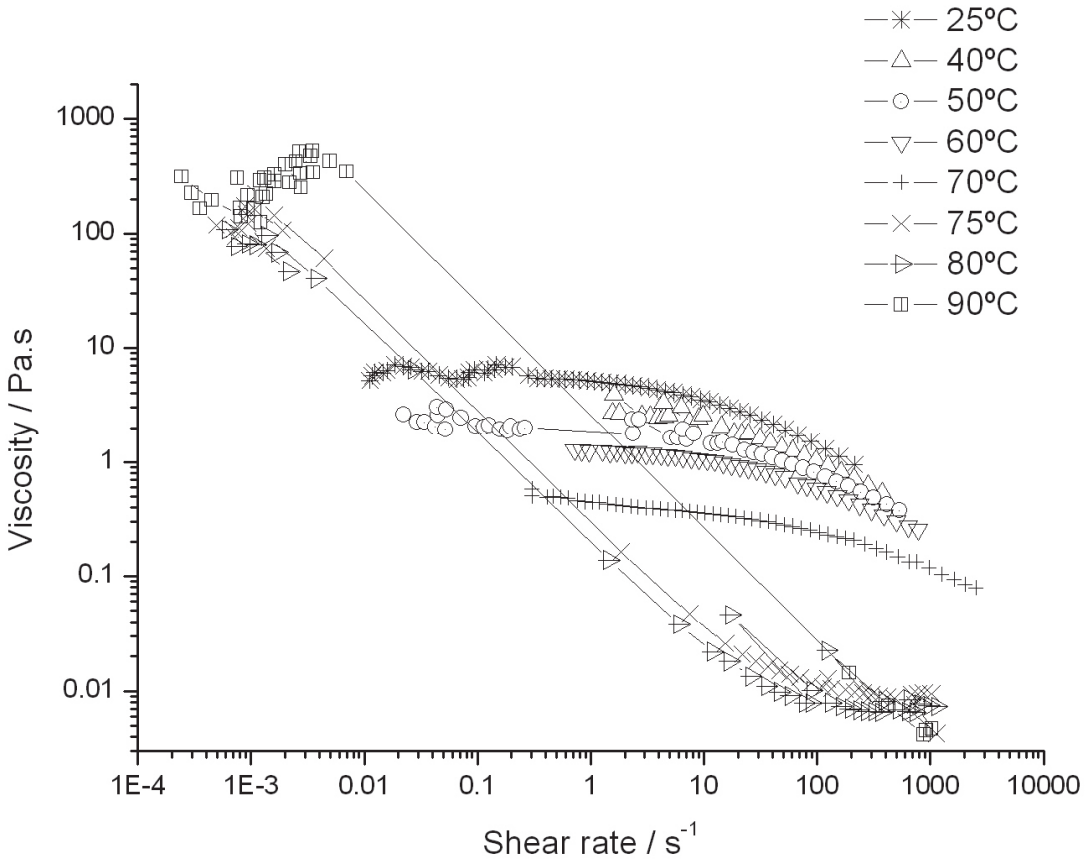

Fig. 2.5 Viscosity as a function of shear rate in the 2% HPMC solution at the indicated temperatures.

An issue that is not often addressed in these systems is the kinetic control over the gelation process. Tests conducted with the 2% HPMC solution show that gelation, with a viscosity close to 200 Pa.s, occurs at ca. 75°C if the system is left to evolve at this temperature for more than one hour, so as to reach the steady-state (data not shown). At lower temperatures, we have not been able to detect gelation.

It is thus likely that determinations such as those depicted in Fig. 2.3 corresponding to a rate of increase in temperature of 1°C/min (in which evaporation effects are minimized), may reflect some delay for establishing the actual value of the viscosity. However, the gelation temperature as extracted from the increase in viscosity is essentially accurate. It should be added that studies on the time evolution in methylcellulose systems have shown that significant equilibration occurs after ca. 5 minutes after temperature stabilization [197]. Thus, the studies based on light transmittance and pyrene fluorescence are performed on an essentially equilibrated system.

2.3.2. Oscillatory measurements

The temperature effect on gelation of the HPMC solutions was also studied by oscillatory tests and the results are shown in Fig. 2.6.

In general, as the temperature is increased, G” smoothly decreases until reaching a characteristic temperature after which a sharp decrease is observed. G’ shows a similar behavior, but the sharp decrease is less pronounced when compared to G”, and absent in the case of the 1% solution. It is interesting to note that this characteristic temperature is observed slightly above 70°C for all concentrations of this study, being independent of the concentration of HPMC.

Also observed is a final increase in both moduli with temperature, which is more significant for the storage modulus than for the loss modulus, at which G’ and G” curves intersect. At this point, the solution starts to gel as can be noticed by the sharp increase in the complex viscosity modulus. This is considered by a number of authors to be the gelation temperature [215, 216]. However, this crossing point depends both on the concentration of the polymer and on the frequency applied on oscillatory tests.

It should also be noted that G’ values at the end of the tests are always higher than at the initial conditions (25°C), but the same is not true for the G” measurements. It is seen that the absolute values of the moduli are higher with increasing HPMC content.

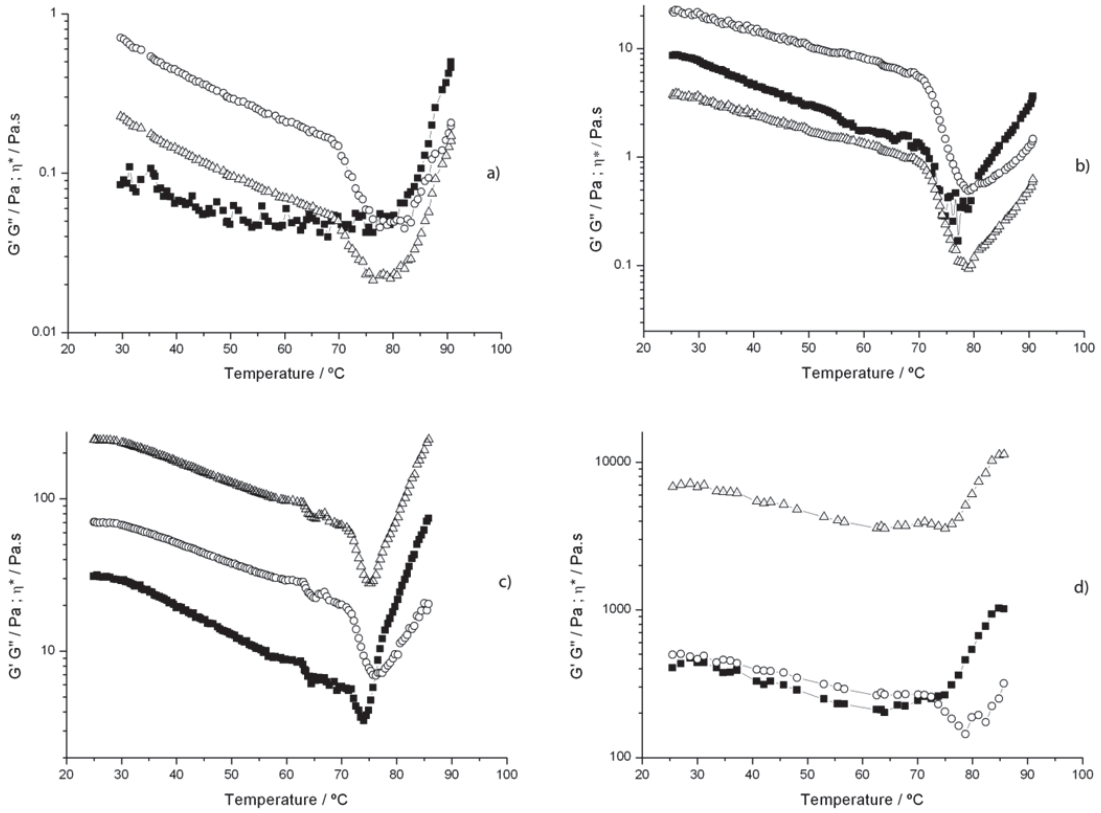

Fig. 2.6 Storage (G', squares), loss (G'' , circles) and the complex viscosity (*, triangles) modulus, as a function of temperature, for HPMC solutions of (a) 1%, (b) 2%, (c) 5% and (d) 10%, w/w. Frequency is chosen so as to impose a value of G'' higher than G' at the initial conditions.

Relaxation times, given by the intersection of G' and G" in the frequency sweep tests at constant temperature, and storage moduli at 1 Hz, with long equilibration times, are shown in Table 2-1 for the 2% solution. It is seen that, while the relaxation time always increases with temperature, the storage modulus G' shows a non-monotonic behavior.

Table 2-1 Relaxation times, calculated by the intersection of G' and G'' in the frequency sweep tests at constant temperature, and storage modulus G' at 1 Hz. Data pertain to the 2% HPMC solution, and samples were in the steady-state

Temperature (°C)	Relaxation time (s)	G' (Pa)
40	0.058	4.24
60	0.106	2.94
85	15.9	4.68

2.3.3. Optical transmittance measurements and polarized light thermal microscopy

The light transmittance of HPMC solutions at the wavelength of 800nm is plotted in Fig. 2.7 as a function of temperature. The highest concentration requires very high equilibration times, and was excluded. For HPMC concentrations between 1 and 5% it is seen that the transmittance curves have a very similar temperature profile. A long plateau in which the transmittance is hardly affected (100% relative to the value at 25°C) is followed by a sharp decrease at ca. 60°C, which reaches 0% at about 70°C. The cloud point, i.e. the reduction to 50% of the value at 25°C, is observed at ca. 68°C for every concentration.

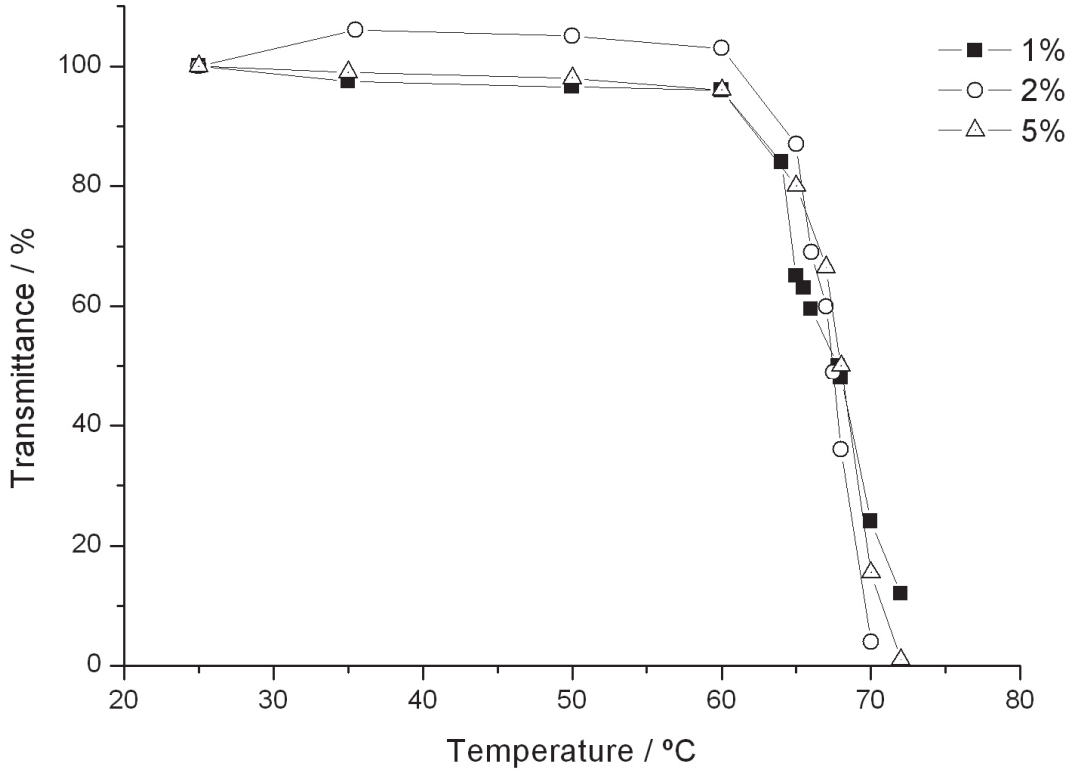

Fig. 2.7 Optical transmittance measurements for the HPMC solution for the indicated concentrations. The 100% reference was taken as the transmittance at 25°C for each solution.

Observations from PLTM confirm an isotropic liquid at lower temperatures as shown in Fig. 2.8(a), characteristic of the polymer sol. This behavior is seen up to temperatures close to gelation. As the temperature is increased above this point, the system exhibits some texture and, at the same time, light transmission is reduced as observed in Fig. 2.8(b).

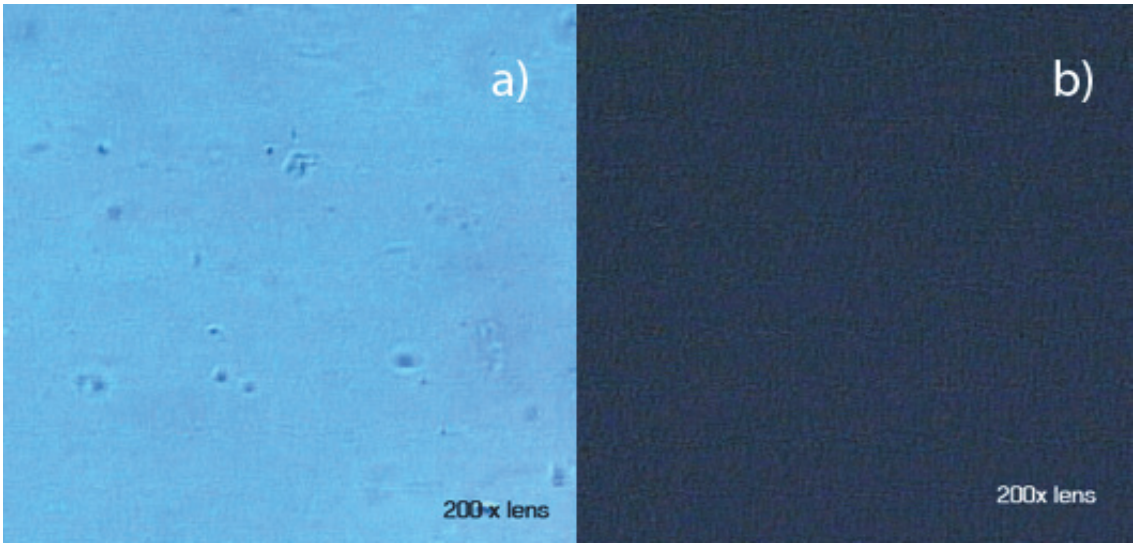

Fig. 2.8 PLTM images for the 1% HPMC solution for the indicated temperatures (a) 25°C and (b) 90°C.

2.3.4. Pyrene fluorescence measurements

The results on the evolution of the I_1/I_3 ratio are shown in Fig. 2.9

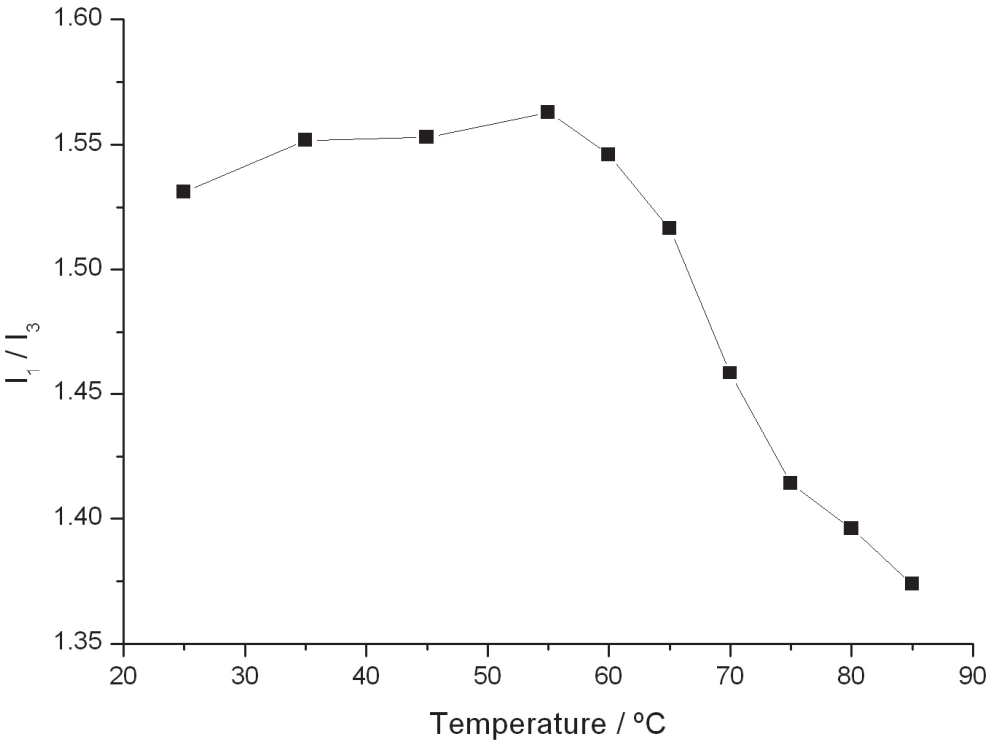

Fig. 2.9 I_1/I_3 ratio of pyrene emission or micropolarity index (MI) progression with temperature for the 1% HPMC solution.

We recall that a value slightly below 2 is expected for aqueous pyrene solutions, while values close to 1 are attained in apolar solvents. The 1% HPMC solution possesses

some hydrophobic character, which surpasses that of methylcellulose [217], probably due to the presence of the hydroxypropyl substituents. The value of I_1/I_3 does not significantly change until ca. 55°C. When the temperature is further increased, the emission intensity ratio decreases abruptly, after which the decrease becomes less pronounced (from 75°C onwards). This result is compatible with the optical light transmission measurements and PLTM observations.

2.4. Discussion

In what follows we will address different aspects of the thermal behavior of HPMC aqueous solutions. For a more systematic approach, these are divided in several relevant topics.

2.4.1. Aggregation and gelation

From the results, we can infer that gelation and aggregate formation upon heating are correlated. Between 25°C and 55°C, the fluorescence observations suggest that the character of the hydrophobic domains remains unchanged, and thus no significant aggregation of the polymer chains is expected. Within this temperature range, rheological data show a decrease in viscosity upon heating, following closely an Arrhenius behavior, with activation energies within 22-30 $kJmol^{-1}$ for the solutions under study. This is probably due to the weakening of intermolecular interactions because of the higher average speed of molecules and of the shorter times they spend in contact with the nearest neighbors.

However, from 55°C onwards, fluorescence results show an increase in the hydrophobic character of the system that is responsible for the polymer aggregation detected in the optical transmittance and PLTM studies. At a later stage, these aggregates are interconnected forming a three-dimensional network structure, and the shear viscosity increases. The variation in the hydrophobic character is relatively abrupt, contrasting to what happens in the case of methylcellulose [218].

Our rheological results indicate a delay between the onset of gelation, irrespective of the observable used for its definition, and full gelation, corresponding to the maximum in viscosity. The same picture was found by other authors using heat capacity at constant pressure to extract the gelation temperature in HPMC solutions [219]. These authors establish a degree of gelation, defined as the ratio between relative heat absorbed at any stage of gelation and the relative heat input required for complete gelation, suggesting a delay of ca. 10°C.

Table 2-2 The cloud point is described in Section 2.3. T_{c1} corresponds to the minimum before the sharp increase in viscosity at Newtonian shear rates and T_{c2} to the steep lowering in viscosity at high shear rate. Finally, T_{c3} is given by the intersection between the storage, G', and loss, G'', moduli.

% HPMC	Cloud point	T_{c1}	T_{c2}	T_{c3}
1	68	70	71	78
2	68	75	71	80
5	68	73	71	76
10	-	70	71	72

Table 2-2 gathers the cloud point values and, in order to further characterize the thermal rheological response of the polymer solutions, also includes a set of characteristic points. T_{c1} is defined, for Newtonian regimes, as the temperature corresponding to the viscosity minimum before the steep increase, T_{c2} represents the temperature at which viscosity sharply decreases for Non-Newtonian regimes, and T_{c3} is the temperature above which G' exceeds G´´. T_{c1} therefore reflects the sharp increase in viscosity when the gelation process is initiated; T_{c2} is compatible with a high hydrophobicity of the polymer chains and suggests strong chain aggregation with inhibited intercluster binding; T_{c3} shows the effect of hydrophobicity in the elastic behavior of the system.

The influence of concentration on these characteristic points can also be extracted from the same table. It is seen that the gelation temperature T_{c1} displays a non-monotonic behavior. The extreme values of T_{c1} in the concentration range under study differ by 5°C, which indicates some dependence on temperature. T_{c2} is, in our findings, almost independent of concentration. It reflects the behavior of the polymer in water that, unperturbed, would lead to gelation. We submit that this point gives also a good assessment of the gelation temperature. T_{c3} values are observed above T_{c1} and T_{c2} and show a similar trend as T_{c1}. This point presents, however, some dependence on the frequency applied in the oscillation test.

The cloud point is lower than T_{c1}, T_{c2} or T_{c3} and has also a negligible dependence on concentration. A similar situation is found for some cellulose systems [217], but it may be also close to [220] or clearly higher than the gelation temperature [218] for others. These discrepancies may be ascribed to different cellulose substituents, but it may also result from different definitions of both cloud point and gelation temperature.

We can schematically summarize the phenomena occurring while heating the polymer solution above 55°C as follows: firstly the polymer becomes more hydrophobic, then the solution clouds, and finally the physical gel based on hydrophobic associations is formed.

2.4.2. Assessment of active links

Relaxation times and storage moduli are displayed at different temperatures in Table 2-1. These parameters have a direct connection with the previous discussion [221]. While the physical meaning of G' is related to the density of the active links in the system, the relaxation time indicates the required time for the solid-liquid transition, which is related to the strength of the active links [222]. Table 2-1 exhibits three main regimes: at low temperatures (40°C), there are many weak active links, seen by high G' and low relaxation time. This is coherent with the entanglement picture, where many polymer chains touch each other due to overlapping, without any important physical interaction. At such temperatures the polymer is hydrophilic and can easily slide through the polymer matrix according to the reptation picture [223, 224]. This would lead to small relaxation times.

At intermediate temperatures (60°C), the active links are in lower amount but are considerably stronger than at lower temperatures. This is compatible with a partial dehydration of the polymer and consequent compaction. The bridging is less effective in this case but the contacts between the polymer chains are more effective.

At higher temperatures (85°C), above the cloud point, both storage moduli and relaxation times increase. At such temperatures, the polymer-based clusters interact hydrophobically and the strength of the active links is also clearly stronger than the ones at lower temperatures. The polymer association is based on its hydrophobicity and the energy penalty for hydration of the chain inhibits the chain detachment. By comparing the data in Table 2-1 with Fig. 2.3(b) (low shear rates), we can state that the thermal gelation is induced both by an increase of the number of active links, probably related to the increase of the dynamics with temperature, and also by an enhancement of the strength of the polymer associations.

2.4.3. Shear rate effects

Results obtained in this work show the influence of the shear rate in the formation of a gel in HPMC solutions for temperatures above 70°C. Studies have focused on the concentrations 1, 2, 5 and 10%, and have shown that for low shear rates there is a steep increase in viscosity when the gelation temperature is attained. These observations are consistent with those obtained in previous work on methyl cellulose solutions using rotational viscometry [201], and agree qualitatively with other previous data [199]. However, for higher shear rates, gel formation is inhibited. Initially the loss of hydration water of the polymer results in a smooth decrease of the viscosity, in a way similar to that observed for Newtonian regime. As the chains become more hydrophobic they tend to form clusters and the high shear rate applied disrupts the inter-cluster network and prevents gel formation. High shear rates destroy the inter-cluster bonds and viscosity

drops to very low values, even lower than those observed at 25°C. This behavior has not, to our knowledge, been documented before for HPMC gels.

Some of the above findings may tentatively be explained on the basis of characteristic reorganization times of the system [191]. For low temperatures, the viscosity results from random entanglements (too low values of viscosity for a gel, but too high for a typical liquid solution). The system is thus frequently reorganized, and high shear rates do not substantially disrupt the equilibrium behavior. As the temperature increases, clusters are formed as seen in cloud point studies and, after, gelation sets in. At this point, the system becomes more rigid, and reformation times concomitantly increase. If temperature is further increased, the number of collisions also increases, as does molecular motion, and reformation times decrease. The solid-like behavior of the system now becomes dominant in the measurements, and viscosity increases again as seen for intermediate shear rates (see Fig. 2.4).

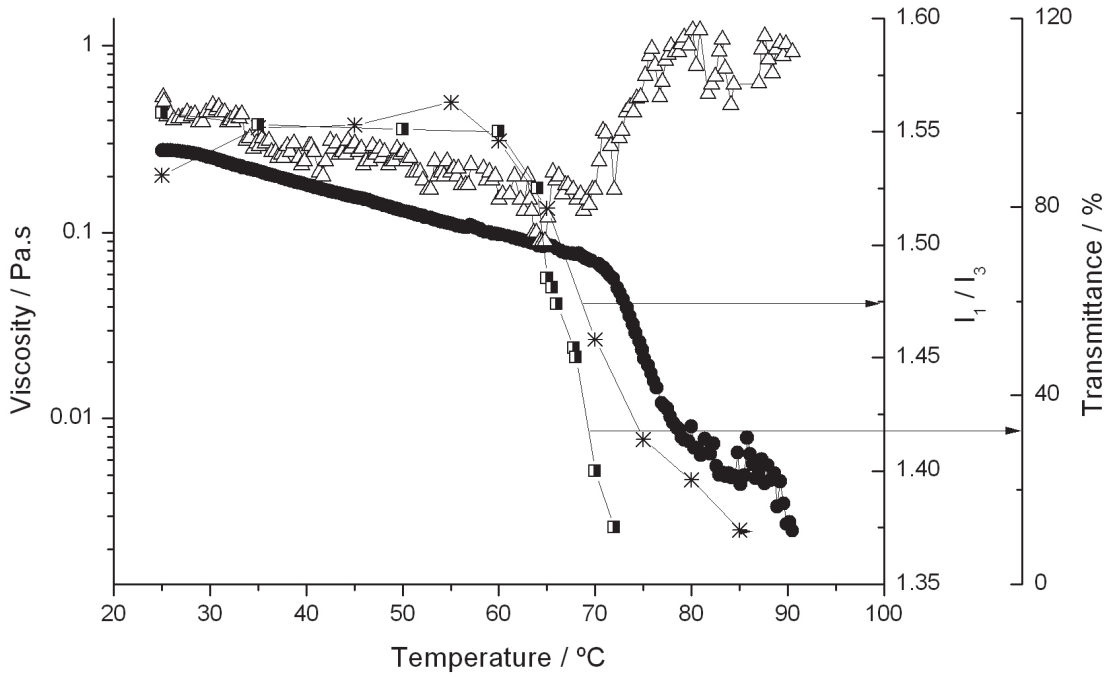

Fig. 2.10 Viscosity profiles at Newtonian (triangles) and non-Newtonian (circles) regimes, micropolarity index (stars) and optical transmittance (squares) measurements upon heating for the 1% HPMC aqueous solution.

In summary, we have inspected several observables (viscosity profiles at low and high shear rates, optical transmittance of the solution, micropolarity index) to assess the sequence of processes close to gelation. Additionally, we have looked into PLTM images at different temperatures. All this information is gathered in Fig. 2.10, in which several of these profiles are superimposed. This picture gives a unified view of the optical properties, viscosity profiles and hydrophobic behavior / aggregation, as previously discussed.

2.5. Conclusions

Results have allowed us to compose a picture of the evolution of HPMC aqueous solutions with temperature. Random entanglements, dominant at room temperature, are still present up to ca. 55°C. In this range, there is no evidence of association of the polymer in clusters or bundles, and no variation in the micropolarity index. Clouding sets in suddenly and is the first evidence of cluster formation, mainly due to hydrophobic interactions. At even higher temperatures, these clusters are further associated in a three-dimensional network, and gelation can be detected. The use of Non-Newtonian shear rates prevents gelation or causes its translation to higher temperatures.

Chapter 3

New insights on the interaction between hydroxypropylmethyl cellulose (HPMC) and sodium dodecyl sulfate (SDS)

In this chapter we address again studies on HPMC, now in more complex systems that include an anionic surfactant (sodium dodecyl sulfate, SDS) in aqueous solutions.

The effect of HPMC concentration on the critical association concentration (*cac*) of the surfactant and on the polymer saturation points (*psp*) was analyzed and allowed the establishment of association and micellization thermodynamic parameters at different polymer concentrations. The effect of temperature on these parameters was also investigated. Based on the findings, a model for HPMC–SDS interaction has been proposed, rationalizing the development of the system at different SDS and HPMC concentrations.

3.1. Introduction

Non-ionic cellulose derivatives comprise a broad group of biocompatible polymers. The respective aqueous solutions have gained a growing relevance in the last decades as a result of their interesting properties, which make them suitable to be used in several industrial applications such as cosmetics, drug formulations, detergents and food [190]. In many applications these aqueous solutions also contain ionic or non-ionic surfactants which are employed, among other reasons, to control the viscoelastic properties of these mixtures. The study of these systems is not only interesting from a perspective of industrial applications, but also for the fundamental understanding of polymer/ surfactant interaction.

Some water-soluble cellulose ethers have use in many applications as viscosity modifiers as a consequence of their capability to self-assemble via hydrophobic interactions. Another interesting feature of this class of water-soluble polymers is their ability to form, in aqueous solutions, reversible three-dimensional networks with temperature, a process known as thermal gelation. The sol-gel transition is a desirable occurrence with many uses such as material processing [225-229] and, particularly, a variety of bio-medical applications [230-234]. There are different common strategies to induce gel phases (or at least phases of higher viscosity) and they comprise increasing polymer concentration above the overlap concentration (the so-called *C**), and the addition of surfactants or other associative species to promote bridging and association [235, 236]. Gel formation can also be achieved by tuning the temperature, either by cooling or heating, depending on the physicochemical characteristics of the polymer. The gelation temperature can therefore be adjusted by changing polymer architecture and/or molecular weight. This has been addressed in many interesting contributions, mainly dealing with three types of systems, including nonionic polysaccharides such as ethyl (hydroxyethyl)cellulose (EHEC) [214, 237-241], poly(isopropylacrylamide) and its derivatives [242-246], and pluronics such as F127 [232, 247-249]. These systems exhibit an increase in viscosity above a critical temperature and are suitable for some biomedical applications, particularly for drug delivery systems [250-253]. Thermal gelation of polymers is ascribed to two different mechanisms: micellar-cubic phase transition, as observed in pluronics [254-256], or hydrophobization of some polymer segments, as in the case of hydroxypropylmethyl cellulose (HPMC) [257].

HPMC (see Fig. 2.2), in particular, can be seen as a hydrophobically modified cellulose derivative and it is frequently used in the food industry [258, 259], printing technology [260] and in many pharmaceutical applications [261] because it is biocompatible, non-toxic and exhibits good mechanical properties. The usefulness of HPMC is essentially based upon different key attributes: efficient thickening, film forming ability, and surface activity [262]. Furthermore, HPMC undergoes a reversible sol-gel transition which is today object of study of some research groups, using different approaches and techniques [263, 264]. This transition is due to the increased hydrophobicity of the respective chains upon heating, as it is shown on Chapter 2. Our findings clearly suggested that a polarity change occurs in some polymer segments, mostly composed of ethylene oxide groups. This is similar and compatible to what is observed for nonionic surfactants containing such groups: while they are miscible in water at low temperatures, clouding and phase separation occur at higher temperatures. A thorough discussion on this topic has been recently published [265].

In the process of self-association of polymers, the presence of surfactants has a noteworthy effect [266]. Surfactants are known to lower the interfacial tension between an aqueous solution and some other phase. In the case of ionic surfactants such as sodium dodecyl sulfate (SDS), the respective behavior is affected by the presence of a polymer in solution. The presence of surfactants may change the behavior of a polymer in solution. This can be exemplified by surfactant-induced thickening [209, 267-274],

surfactant-induced swelling [273] or compaction [274], surfactant –induced phase separation [209, 272], among other effects.

In an aqueous system containing both polymer and surfactant, there are clearly two important characteristic breakpoints in the interaction between these two entities. The first is known as the critical association concentration (*cac*) and represents the minimum surfactant concentration needed to start the polymer modulated surfactant association. The second breaking point is referred as the polymer saturation point (*psp*) and corresponds to the surfactant concentration at which the polymer chains become saturated of surfactant molecules. Subsequently, free micelles begin to form as further surfactant is added to the system. Various studies on this topic have been reported [275, 276].

In this Chapter, it is presented in detail the effect of the anionic surfactant (SDS) on the properties of aqueous solutions of HPMC. Sets of electrical conductivity, rheological and optical transmittance data are presented, helping to understand how polymer–surfactant interaction occurs at room temperature and upon heating, with emphasis on the thermal gelation. In addition, the effect of HPMC on the SDS association and micellization will also be addressed. The SDS-HPMC association is discussed not only based on the outcome of a thermodynamic analysis, but also supported by viscosity measurements and gel formation observables taken from rheological and optical transmittance tests. Models which allow the interpretation of SDS-HPMC interaction, at different concentrations of both components, are proposed from the experimental data.

3.2. Experimental section

3.2.1. Materials and sample preparation

Hydroxypropylmethyl cellulose (METHOCEL K15M Premium), 19%-24% methoxyl and 7-12% hydroxypropyl, M_w=4.3×10^{5}Da was a kind gift from Dow Chemical. Sodium dodecyl sulfate (SDS) was purchased from Fluka. Both reagents were used as received without further purification. Aqueous solutions of HPMC of different concentrations (0.1%, 0.25%, 0.50%, 0.75% and 1.0% w/w) were prepared by adding dry polymer powder to Millipore water. The polymer solutions were kept stirring for 48 hours before use.

3.2.2. Electrical conductivity studies

The electrical resistances of the solutions were measured using a Wayne–Kerr model 4265 Automatic LCR meter operating at 1 kHz. A dip-type conductance cell with a cell constant of 0.1002 cm^{-1}, with an uncertainty of 0.02%, was used [277]. Cell constants were determined from measurements with KCl (reagent grade, recrystallized, and dried)

using the procedure and data reported elsewhere [278]. Solutions were studied within 24 h of preparation. Measurements were taken at different temperatures, 25.0, 37.0 and 50.0 (± 0.1°C) using a Grant thermostat bath. In a typical experiment, 40 mL of HPMC aqueous solution was placed in the conductivity cell and subsequently, aliquots of the SDS solution were added in a stepwise manner using a Methrom 765 Dosimate micropipette. The conductance of the solution was measured and recorded after each addition once after the electrical resistance reached a stable value. House-made software was used both for programmed surfactant addition and acquisition of electrical resistance data after reaching equilibrium. The solution specific conductance value presented here, , was calculated from the experimental specific conductance and corrected for the experimental specific conductance of water or HPMC aqueous solution.

3.2.3. Rheological studies

All the rheological experiments were conducted using a controlled stress Reologica Stresstech rheometer (Lund, Sweden) equipped with automatic gap setting. All samples were allowed to equilibrate for 10 minutes before the measurements. A “bob and cup” geometry (CC 15) with solvent trap was used to prevent sample evaporation. Temperature control was achieved using a water bath system coupled to the rheometer measurement system. The studies with temperature ramps were performed from 25 to 90°C at a fixed heating rate of 1°C/min. Dynamic viscosity was analyzed by rotational shear experiments at 25°C. Flow curves were obtained by applying an increasing shear rate to the samples. Prior to this, a viscometry test was carried out for all samples in order to determine both Newtonian and non-Newtonian regimes and some useful parameters such as zero-shear viscosity (η_0) and infinite shear viscosity (η_∞).

In rheology, it is quite common to use equations that describe the shape of the general flow curves. These equations need at least four parameters. One of these examples and probably the most popular is the Cross equation (Eq. 3.1), used to extract some significant parameters from the viscosity vs. shear rate profile [279]

$$\frac{\eta - \eta_\infty}{\eta_0 - \eta_\infty} = \frac{1}{1 + (C\dot{\gamma})^m} \tag{3.1}$$

that is equivalent to

$$\eta = \eta_\infty + \frac{\eta_0 - \eta_\infty}{1 + (C\dot{\gamma})^m} \tag{3.2}$$

In the Cross equation, η is the viscosity at any shear rate, $\dot{\gamma}$, η_0 and η_∞ refer respectively to the asymptotic values of viscosity at very low shear rates (zero-shear viscosity) and at

very high shear rates (infinite-shear viscosity) respectively, *C* is known as the Cross rate constant parameter, with the dimension of time, and *m* is a dimensionless constant, indicating the degree of dependence of viscosity on the shear rate in the shear-thinning region. A value of zero for *m* indicates Newtonian behavior, while values of *m* close to 1 point to a shear-thinning behavior. The reciprocal of the time constant, 1/*C*, corresponds to a critical shear rate ($\dot{\gamma}^*$) signaling the end of the Newtonian plateau and the onset of shear-thinning region. The rheological curves obtained, in terms of viscosity vs. shear rate, corresponding to the different formulations tested, were mathematically fitted using the Eq. 3.2.

Oscillation tests (25-90°C) were conducted in order to determine both the storage modulus, (*G'*) and the loss modulus (*G''*). Oscillatory measurements are particularly useful to study the structure of some sensitive materials because the deformation magnitude in these tests is very small. A test of linearity, the oscillation stress sweep, was performed prior to all oscillatory tests to make sure that all measurements are within the linear viscoelastic region, otherwise the results would depend not only on the frequency selected but also on the applied stress of deformation. In turn, the applied frequency (1 Hz) was chosen ensuring that, at the initial conditions, *G''* is dominant. The complex viscosity modulus η^*, a mathematical representation of the viscosity in oscillatory tests, was also determined.

3.2.4. Optical transmittance measurements

A double-beam UV-VIS spectrophotometer (Shimadzu UV-2450) was used for the optical transmittance measurements. The samples were placed in a cell with a dimension of 1×1×5 cm. Millipore water was used as reference. For temperature measurements, the cells were placed in a cell-holder connected to a water bath system with temperature control (Haake Phoenix II – Thermo Scientific). In addition to this regulator, an external temperature sensor (Pt 100) was placed in the sample cell. The absorption spectra (200–850 nm) confirmed that there were no UV-absorbing moieties in the solutions. The transmittance of the samples was measured at a wavelength of 800 nm as previously reported for a similar system [199].

3.3. Results and Discussion

In what follows, it will be firstly presented the results obtained by the different techniques, starting with the conductivity measurements. All the results are thereafter subsequently integrated, discussed and rationalized.

3.3.1. Electrical conductivity studies to assess characteristic points and thermodynamics

3.3.1.1. Effect of HPMC on the electrical conductance of SDS

Electrical conductivity has been used to provide valuable information on the association between ionic surfactants and uncharged water-soluble cellulose derivatives, and several examples can be found in the literature [280, 281]. Fig. 3.1 shows the effect of the presence of hydroxypropylmethyl cellulose (HPMC) on the electrical conductance of aqueous SDS solutions. In the absence of HPMC, Fig. 3.1(a), the SDS electrical conductance shows two different linear regimes as a function of surfactant concentration, corresponding to the behavior below and above the critical micelle concentration (*cmc*). From these data, and by using the intersection of the data regression lines method [282], the *cmc* and the degree of counterion dissociation (α), have been calculated yielding 8.34 (±0.09) mM and 0.331 (±0.002), respectively, in close agreement with the values reported in literature [283, 284].

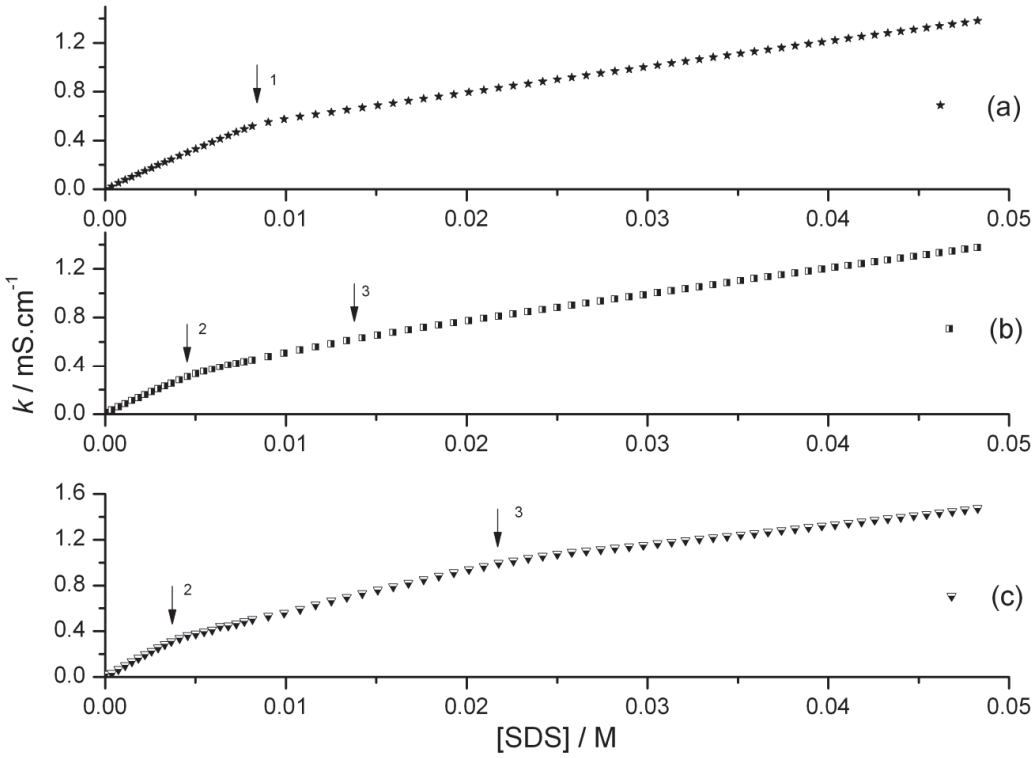

Fig. 3.1 Dependence of the specific conductance of aqueous solutions of SDS, at 25.°C, in the presence of HPMC with a concentration of (a) 0.0% (w/v), (b) 0.25% (w/v), and (c) 0.75% (w/v). Arrows indicate the *cmc* (1), *cac* (2) and *psp* (3).

In the presence of HPMC, a further transition point is observed on the conductivity of SDS/HPMC mixtures as a function of SDS concentration, Fig. 3.1(b) and Fig. 3.1(c). The

first point (2) in the presence of polymer corresponds to the critical association concentration (*cac*). The second transition point (3) corresponds to the onset of bulk micelle formation. This exceeds the polymer saturation point (*psp*), which represents the surfactant concentration needed to saturate the polymer. Up to the *psp*, it is likely to consider that SDS concentration in bulk is constant and equal to the *cac* value. After saturation of the polymer, bulk SDS concentration starts to increase and reaches the *cmc* value found in the absence of polymer, thus leading to the formation of micelles in the bulk. The *psp* and the onset of bulk micellization are, thus, in close proximity. In what follows, and for simplicity, transition point (3) will be denoted as *psp,* when extracted from conductivity measurements, but it constitutes in fact an upper limit (see below). It is worth noting that the slopes of κ=f ([SDS]) in the absence (above point (1)), and presence (above point (3)) of HPMC are very similar, which clearly confirms that for SDS concentrations above the *psp*, micellization takes place. For example, from data shown in Fig. 3.2, those slope values are $2.127(\pm0.008)\times10^{-2}$, $2.149(\pm0.005)\times10^{-2}$, $2.17(\pm0.04)\times10^{-2}$ $mS.cm^{-1}.M^{-1}$, for 0, 0.25 and 0.75% (w/v) HPMC concentration, respectively.

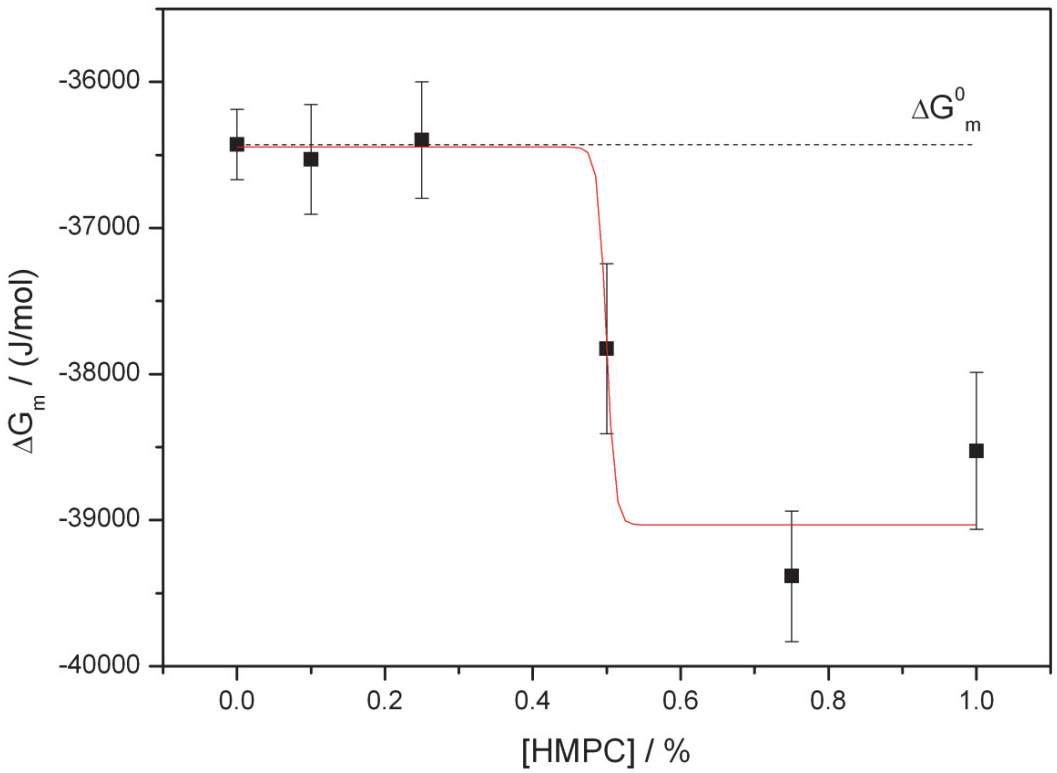

Fig. 3.2 Effect of HPMC concentration on the free energy of micellization of SDS, at 298.15 K, assuming that the polymer has only a spectator role on the equilibrium between SDS unimers and SDS micelles. The dashed horizontal line represents the free energy of micellization of SDS.

It is also worth noting that the *psp* increases linearly with HPMC concentration, following a straight line equation: (*psp*/ (%w/v)) = 10.9 (±0.9) + 15 (±1) × ([SDS]/mM). The

variation of *psp* with HPMC concentration is close to half of that has been reported elsewhere [275], which can probably be ascribed to different degrees of substitution in the modified cellulose polymers used.

We will now focus our discussion on the effect of HPMC on the association of SDS. The interaction between polymer and surfactant leads to an increase of the effective size of the ionic species and, consequently, the effect of the addition of SDS on the overall ionic mobility is smaller. The effect of HPMC concentration, at 25°C, in the *cac* of mixed SDS/HPMC solutions is shown in Table 3-1.

Table 3-1 Effect of HPMC concentration on the association and micellization of SDS as seen by electrical conductivity at 25°C.

[HPMC] / % (w/v)	cac / mM	$\Delta G°_a$ / (kJ/mol)	psp / mM	
0.0	8.34 (±0.09) [a]	–36.4 (±0.2) [b]		
0.1	5.4 (±0.3)	–33.1 (±0.8)	12.4 (±0.8)	11.6 [c]
0.25	5.3 (±0.2)	–34.8 (±0.6)	15.6 (±0.8)	
0.5	5.2 (±0.3)	–35.05 (±0.03)	16.9 (±1)	22.6 [c]
0.75	4.2 (±0.2)	–37.4 (±0.5)	22.7 (±0.3)	
1.0	2.6 (±0.4)	–37 (±1)	(±2)	

a) critical micelle concentration;
b) in the absence of HPMC the free energy of association corresponds to the free energy change for SDS micellization;
c) from [285]

As usual in these systems, the value of the *cac* is lower than the critical micelle concentration, indicating that the polymer-surfactant complex formation induces a more favorable SDS association. It is seen that the *cac* value remains approximately constant up to ca. 0.5% HPMC, in accordance with previous observations [275].However, for HPMC concentrations higher than 0.5%, the association between HPMC and SDS becomes significantly more favorable. This probably indicates that, above this concentration, the hydrophobic domains start to grow as the degree of overlap between different HPMC molecules increases and the respective hydrophobic patches associate.

The free energy of association can be calculated from [285, 286]:

$$\Delta G_a^{\circ} = (2-\alpha)RT \ln X \tag{3.3}$$

where *R* is the gas constant, *T* the absolute temperature, *X* is the critical association concentration, or the *cmc* in the absence of polymer, in mole fraction units (*cac*/ [H_2O]). α is the degree of counterion dissociation, calculated as the slope ratio $m_{2\text{-}3}/m_{0\text{-}2}$ [287], where the subscripts indicate the points that delimit the segment with each slope, with '0' for the axis origin (see Fig. 3.1). The degree of dissociation of SDS counterions in the presence of the polymer (ca. 0.55) is higher than that occurring for SDS micellization (ca.

0.33) and independent of the HPMC concentration. This can be justified by the occurrence of small (and less dense) aggregates [288, 289]. The calculated values of the free-energy indicate a SDS association process slightly less favorable for low polymer concentrations than SDS micellization. However, association and micellization values are very close, and conductivity focus on SDS association, probably only partially including the SDS-polymer interaction. The free-energy of association becomes more favorable at polymer concentrations higher than 0.5%.

To better understand the mechanism responsible for the association of SDS in the presence of HPMC, the effect of temperature on the thermodynamic association parameters of SDS was also studied. The dependence of the *cac* and α on the temperature (shown in Table 3-2), will allow us to compute the enthalpy of association (ΔH_a°), calculated by [286]

$$\Delta H_a^\circ = -RT^2\left[(2-\alpha)\frac{d\ln X}{dT} + \ln X\frac{d(1-\alpha)}{dT}\right] \tag{3.4}$$

Assuming a linear dependence of (ln *X*) and (1−α) on *T*, with slopes *m* and *m'*, respectively, Equation (3.4) can be re-written as

$$\Delta H_a^\circ = -RT^2\left[(2-\alpha)m + m'\ln X\right] \tag{3.5}$$

Finally, the entropy of association (ΔS_a°) was evaluated from

$$\Delta S_a^\circ = \frac{\Delta H_a^\circ - \Delta G_a^\circ}{T} \tag{3.6}$$

Table 3-2 shows the different thermodynamic association parameters for SDS in the presence of HPMC. We can conclude that the association of SDS in the presence of HPMC is enthalpy-dominated ($|\Delta H^o_a| > |T\Delta S^o_a|$), but the entropy component is also significant. This is easily justified by a predominantly hydrophobic interaction. However, this process can only be seen if a concomitant dehydration of the surfactant chain and polymer takes place. It is known that the micellization of SDS is only enthalpy driven in the presence of ionic solutes [290] and, consequently, the present results are in close agreement with both the presence of small SDS aggregates with low counterion condensation and also the amphiphilic character of HPMC [291]. Such behavior is also in agreement with the hypothesis that SDS aggregates are smaller than the corresponding micelles [292, 293].

A more comprehensive analysis of the data shown in Table 3-2 allows us to point out that association is slightly favored upon heating. Quantifying this effect as $\mathrm{d}\Delta G_a^\circ/\mathrm{d}T$, a

molar value of –80 JK^{-1} is obtained, which is very close to the value reported to the micellization of SDS in water (–82 JK^{-1}) [286]. A deeper analysis of the effect of temperature on the ΔG_a° shows that the hydrophobic effect due to the interaction between the hydrocarbon tail (and probably the hydrophobic part of polymer) and water plays an important role in the HPMC-SDS interaction as can be inferred from the enthalpy-entropy compensation, which can be quantified by [294]

$$\Delta H_a^\circ = \Delta H^* + T_c \Delta S_a^\circ \tag{3.7}$$

where the slope T_c is the compensation temperature, closely related with solute-solute and solute-solvent interactions and ΔH^* is the intercept of the compensation plots which gives the heat effect belonging to $\Delta S_a^0 = 0$, and can be interpreted as a measure of solute-solute interactions. By fitting the experimental data shown in Table 3-2 to Eq. (3.7), the following values for T_c and ΔH^* have been obtained: 368(±58) K and –38 (±2) $kJmol^{-1}$, respectively. Despite a rather low correlation coefficient (R^2 = 0.951), the T_c value is within the range (280-450 K) found for micellization processes [295] and ΔH^*, although more exothermic than what is observed for the SDS micellization: –29 $kJmol^{-1}$ [296], can be considered as indicative that hydrophobic interactions play a major role in the association process.

Table 3-2 Effect of the temperature on the polymer (0.5%) induced association properties of sodium dodecyl sulfate.

T / °C	ln X	$1-\alpha$	ΔG°a / kJ mol–1	ΔH°a / kJ mol–1	ΔS°a / J mol–1K–1
25	–9.26	0.547	–35.05 (±0.03)	–23.15 (±0.02)	39.9
37	–9.08	0.552	–35.44 (±0.04)	–26.22 (±0.03)	29.7
50	–8.93	0.559	–37.04 (0±.04)	–28.73 (±0.03)	25.7

Following further addition of SDS on aggregate-containing solution a second mechanism of association occurs, as pointed out before. The thermodynamic parameters for the micellization of SDS in the bulk, in the presence of different concentrations of HPMC at 298.15 K, were estimated assuming that the micellization of SDS can be treated also in the framework of the mass-law action model. The free energy of association is now calculated from an expression corresponding to Equation (3.3), but in which the estimate of the variation in ion condensation is given by the slopes after the *psp* and before the *cac* , the bulk concentration value of SDS is considered the *cmc* [209].

$$\Delta G_m = (2-\alpha) RT \ln\left(\frac{cmc}{[H_2O]}\right) \tag{3.8}$$

The use of Equation (3.8) in the terms described is based on the approximation that the equilibrium between bulk unimers and micelles is not affected by the presence of the surfactant saturated chains.

Fig. 3.2 summarizes the results obtained for the free energy of micellization in the bulk. This is independent of polymer concentration, up to a critical value. After this point (ca. 0.5%) micellization becomes more favorable. A possible interpretation of this data is that for saturated, scattered HPMC-SDS aggregates, the behavior is well described by the unimer-micelles equilibrium, being this equilibrium very similar to that observed in the absence of HPMC. However, for higher values of the HPMC concentration, partially formed micelles of a few unimers may be released from the HPMC-SDS aggregates, thus facilitating micelle formation. The analysis of Fig. 3.2 also highlights the importance of the degree of dissociation of counterions on the SDS micellization process, for HPMC concentration higher than 0.5% (w/v). The use of Eq. (3.8) in the conditions above would thus not be, strictum sensum, justifiable (see Fig. 3.3 for a pictorial description of these remarks).

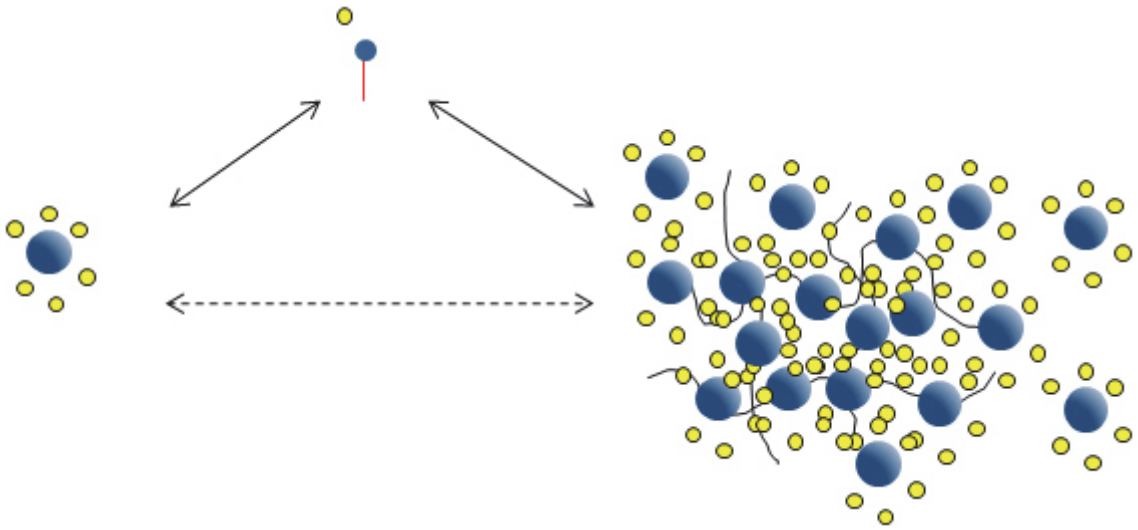

Fig. 3.3 Equilibrium scheme involving SDS unimers, SDS-HPMC aggregates and bulk SDS micelles. Solid black lines represent HPMC chains, blue and yellow spheres correspond to SDS micelles and counterions respectively. Surfactant unimer is represented as the small blue sphere connected to a red hydrophobic tail. While unimer-aggregate and unimer-bulk micelles can be regarded as independent equilibria, a large concentration of aggregates promotes a direct equilibrium of these aggregates with bulk micelles (indicated by the dashed double-arrow), without systematic disaggregation into unimers.

3.3.2. Viscoelastic properties of HPMC-SDS solutions

When discussing the association between a polymer such as HPMC and an ionic surfactant such as SDS that affects the polymer behavior in solution, it is relevant to study and discuss their rheological behavior. The insight obtained from rheological data is crucial to build up the picture of polymer-surfactant association at different conditions

and compositions. Table 3-3 shows the composition of the prepared polymer-surfactant solutions for a constant HPMC load of 1.0% (w/w).

Table 3-3 List of formulations tested in the rheological and optical transmittance studies and corresponding composition.

	HPMC K15M % (w/w)	SDS (g/100 mL)	SDS mM
S0.0	1.0	0.00	0.0
S1.7	1.0	0.05	1.7
S3.5	1.0	0.10	3.5
S5.2	1.0	0.15	5.2
S7.0	1.0	0.20	7.0
S8.7	1.0	0.25	8.7
S17	1.0	0.50	17
S26	1.0	0.75	26
S35	1.0	1.00	35
S43	1.0	1.25	43
S52	1.0	1.50	52

3.3.2.1. Monitoring the association between polymer and surfactant

Dynamic viscosity was determined by rotational shear experiments, at 25°C. Fig. 3.4 shows the dependence of zero-shear viscosity (η_0), mathematically obtained by fitting the viscosity vs. shear rate curves with the Cross model equation, on SDS concentration. Three different regions are visible, separated by two characteristic breakpoints, a local minimum and a local maximum, denoted as (1) and (2) on Fig. 3.4.

The rheological behavior of the mixed system is clearly sensitive to the association between HPMC and SDS. The profile obtained is in agreement with previous findings reported in the literature for cellulose ethers and SDS mixed systems [307, 308].

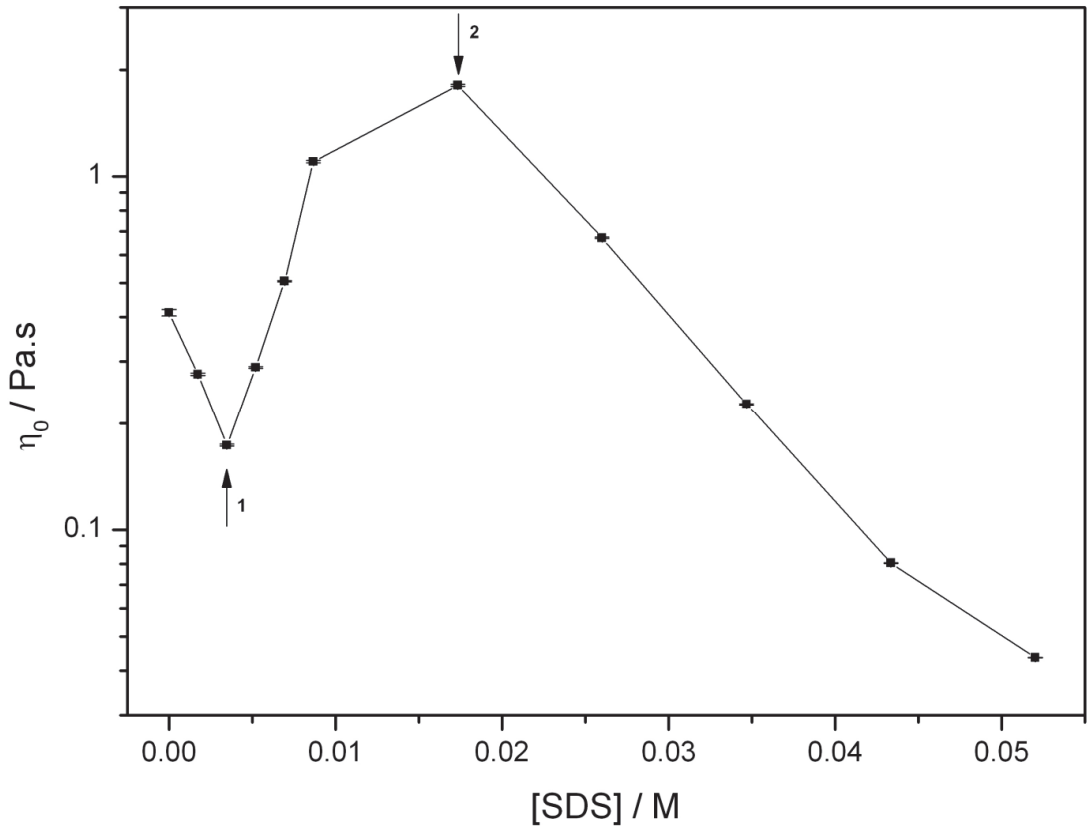

Fig. 3.4 Zero-shear viscosity as function of SDS concentration. Three different zones are visible. Before the first arrow is the pre-*cac* region. In the region between the two arrows, surfactant molecules start to form aggregates around hydrophobic moieties of the polymer, causing polymer swelling and leading to an increase in the viscosity. The second arrow indicates the maximum, which happens before the *psp*. After this concentration, surfactant molecules have saturated the polymer chains and start to form free micelles in solution, leading to screening of electrostatic repulsion and to an observable decrease in the viscosity. Solid lines are presented to guide the eye.

Below the first point, the surfactant is already interacting to the polymer, as seen in Fig. 3.4 by a relatively small decrease in the zero-shear viscosity (ca. 40%) up to a minimum close to the *cac*. Different explanations may be invoked to justify this observation. The most accepted one is that there is a chain contraction due to the intense intramolecular hydrophobic association junctions [297-299]. The binding of surfactant molecules to semi-flexible polymers such as EHEC or HPMC, may modify the respective stiffness and this may, in turn, induce a coil-to-globule transition. This phenomenon is ascribed to a balance between two forces: attractive hydrophobic association between the polymer and hydrocarbon tails of the surfactant, which bind to the polymer and make it less polar; and electrostatic repulsive forces between the polymer chains as the surfactant is added, therefore increasing the polarity of the polymer. Below the *cac*, electrostatic repulsion plays a minor role and a contraction of the polymer chains induced by the hydrophobic association inside the polymer is observed. For surfactant concentrations above the *cac* and below point (2), a significant increase in the viscosity upon surfactant addition is observed. At this stage micelle formation of SDS takes place along the HPMC chains and progressively converts the non-ionic polymer into a polyelectrolyte. Repulsion

among the negative charges of the polymer-surfactant complex causes the polymer to swell leading to a consequent increase in the shear viscosity. Polymer chains reach their maximum extension at point (2), resulting in a six fold enhancement in the viscosity from the minimum value read at *cac*. At this latter point, the polymer chains are virtually covered by surfactant micelles and further addition of the amphiphile causes an increase of free micelles in the bulk.

Above point (2), i.e., above the SDS concentration that promotes the maximal rigidity in the transient network, and with progressive addition of surfactant to the system, the viscosity starts to decrease and ultimately reaches values even lower than those obtained for the surfactant-free HPMC solution (S0.0). Within this region above the transition point (2), all the surfactant added will be placed in the bulk, firstly as unimers and, afterwards as free micelles (above the *cmc* value for bulk SDS concentration). Concomitantly, the presence of SDS in the medium increases the ionic strength and causes HPMC chains to shrink due to the screening of the electrostatic repulsion. At sufficiently high surfactant concentrations, the hydrophobic associations along HPMC chains are inhibited, the polymer contracts, and the viscosity reaches a global minimum, close to zero. In our view, the polymer saturation point, *psp*, is situated, in terms of SDS concentration, after transition point (2), but before the point where the viscosity in the presence of SDS equals that found in the absence of surfactant. The explanation is that (i) the destruction of the transient network provides additional room for surfactant associated upon the polymer, and (ii) HPMC chains associated with SDS are typically more extended than those in its absence, thus promoting a higher viscosity.

3.3.2.2. Modulating the thermal gelation of HPMC

Thermal gelation in cellulose based polymers requires a certain degree of insolubility of some polymer segments at sufficiently high temperatures. On the other hand, solubility can be enhanced by using a charged polymer instead, since the entropy of counterions favors the solubility. It would be interesting to check the dependence of the thermal gelation on the charge density of HPMC-SDS complex by using different concentrations of SDS and therefore be able to adjust it.

For each solution (S0.0-S52) we have conducted a number of viscosity measurements to investigate the influence of the presence of surfactant on the thermal gelation of HPMC. Oscillation tests were carried out to determine both the storage modulus *G'*, the loss modulus *G''* and the complex viscosity (γ^*).

Following the same strategy described in Chapter 2, gel formation was detected when the storage modulus *G'* intercepts the loss modulus *G''* in an ascending trend.

Experimental data presented in Table 3-4 shows that the addition of very low amounts of surfactant to the system shifts thermal gelation to higher temperatures. Another interesting fact is that thermal gelation is only observed for surfactant concentrations

lower than 7mM. For higher SDS concentration thermal gelation is inhibited, as seen in the oscillation plots (Fig. 3.5).

Table 3-4 Gelation temperature for HPMC-SDS solutions. Gel formation requires higher temperature as SDS concentration increase, not being detected (n.d.) in our oscillation tests (1 Hz) for concentrations of SDS above 5.2mM. After a critical SDS concentration, gelation is totally inhibited, as can be seen in the oscillation tests.

Formulation	Gelation temperature / °C
S0.0	74
S1.7	81
S3.5	83
S5.2	87
≥ S7.0	n.d.

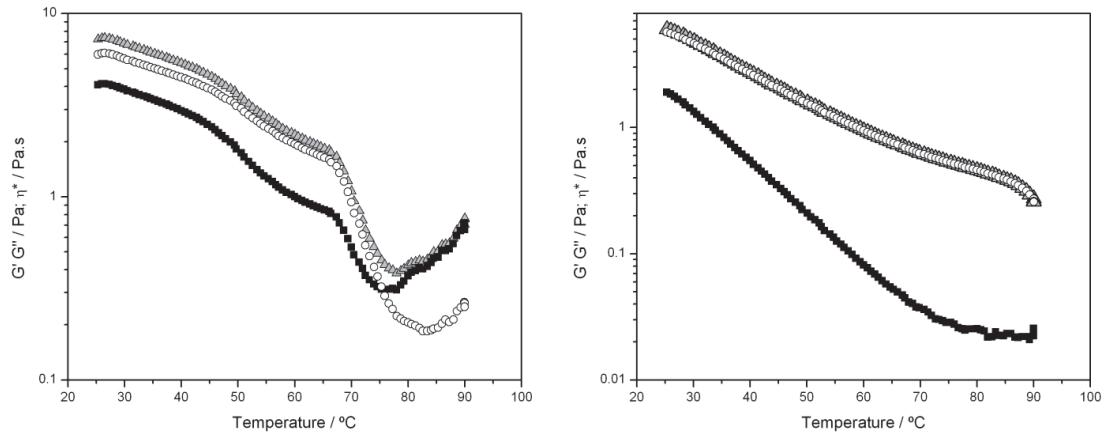

Fig. 3.5 Storage (*G'*, squares), loss (*G''*, circles) and the complex viscosity (*, triangles) modulus, as a function of temperature, for formulation S1.7 (on the left) and S17 (on the right). Frequency is chosen so as to impose a value of *G''* higher than *G'* at the initial conditions. Oscillation plots illustrate that gel formation occurs only for low concentration of SDS. For higher concentrations, the storage moduli *G'* does not intersect the loss moduli *G''* in the temperature range studied (25-90°C) indicating that gel formation is not detected. As the surfactant progressively ionizes the polymer inter-chain hydrophobic associations and thermal gelation become weaker or negligible.

The association of charged amphiphiles to HPMC brings a higher hydrophilic character to the polymer as result of a combined effect of the deactivation of polymer's hydrophobic regions and enhanced solubility due to the presence of charges along the chains. The hydrophobic association among polymer segments, which is the mechanism of thermal gelation of this type of polymers, is then inhibited. As the SDS concentration increases, thermal gelation is therefore shifted to higher temperatures and eventually

inhibited, which is in agreement with previous studies analyzing the effect of ionic surfactants on the thermal gelation of other cellulose ethers [300-303].

3.3.3. Characteristic points revisited with light transmittance studies

Optical transmittance studies were performed to gain additional insight on the mechanism of association between HPMC and SDS at room temperature. Changes in the optical properties of the system can be used to monitor how it evolves as more surfactant is present. To achieve that, optical transmittance tests were carried out for the solutions S0.0 – S52 (composition shown in Table 3-3). For sake of simplicity we considered the 1% HPMC hydrogel (S0.0) as reference i.e. 100% of transmittance at 800nm. Fig. 3.6 shows that in the formulations containing low amounts of SDS (in the pre-*cac* region) it is observed a progressive decrease in the transmittance until the minimum transmittance point ([SDS]=4.2×10^{-3}M).

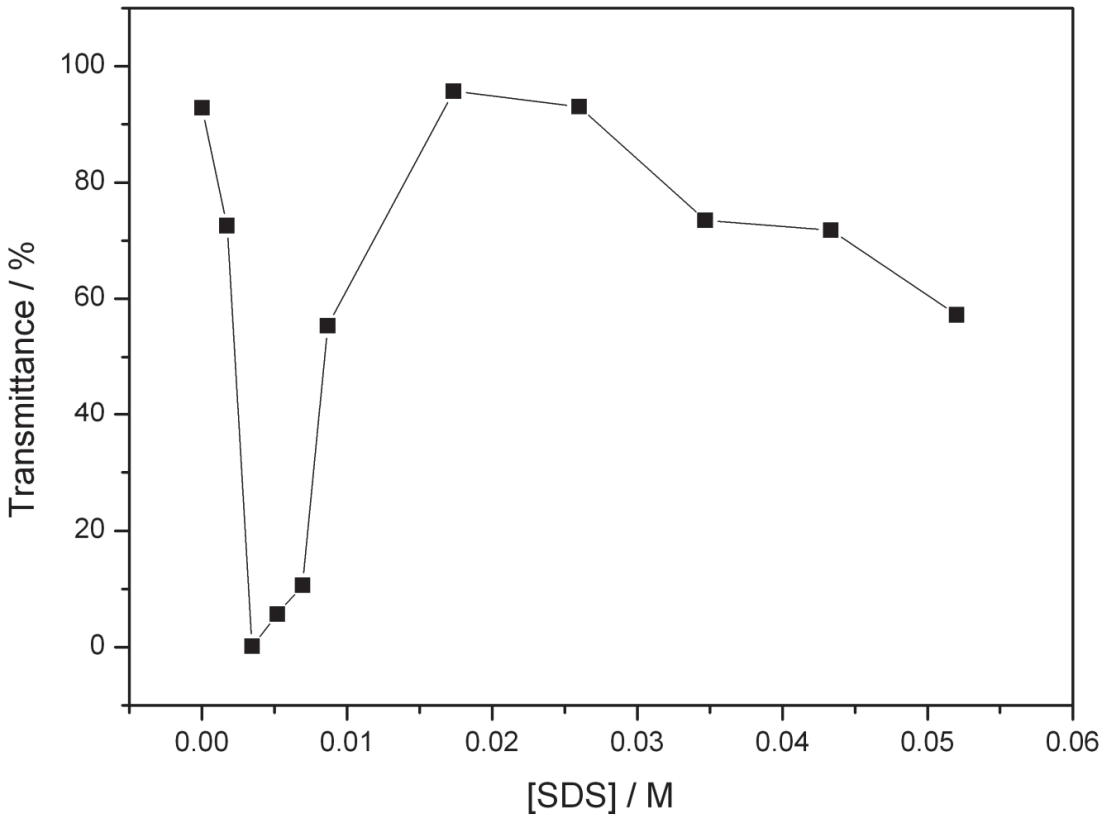

Fig. 3.6 Dependence of the optical transmittance (800nm) at 25°C of HPMC-SDS solutions on SDS concentration. Solid lines are a guide for the eyes.

This is in agreement with the mechanism we proposed above, explaining the decrease in the viscosity below the *cac* as a result of a salting-out-like effect. HPMC chains start to shrink leading to a lower entanglement level and consequently causing a decrease in the transmittance (Fig. 3.6) and in the viscosity (Fig. 3.4). The minimum in the optical transmittance is slightly above the values of *cac* determined by means of conductivity

(as is that of the rheological studies). These observations indicated that the shrinkage of polymer chains slightly extends above the *cac*. The analysis of Fig. 3.6 clearly indicates that after the minimum, the transmittance increases sharply until a local maximum, indicating that the polymer swells for concentrations of SDS above the *cac*. This is caused by the adsorption of negatively charged micelles onto the polymer chain. The polymer is therefore converted into a polyelectrolyte and, due to charge repulsion, HPMC chains extend and swelling occurs. The swelling of the polymer allows a higher light transmittance because of the low optical contrast of the system, and thus the transparency increases at this stage up to a maximum, close to the *psp* ([SDS]=2.1×10^{-2}M). For surfactant levels above this point, i.e. above the concentration at which all the polymer chains are covered by surfactant micelles, additional surfactant unimers will be located at the bulk, forming micelles. Charged micelles and counterions now act as salt and screen electrostatic repulsion among negative charges of the HPMC-SDS complex. Such screening leads to polymer compaction, which is responsible for the reduction in the optical transmittance of the system observed.

3.3.4. Rationale

Table 3-5 compiles the significant breakpoints found in the interaction between HPMC and SDS, and relates them with the phenomenological *cac* and *psp* values.

Table 3-5 Summary of *cac* and *psp* related values (mM) determined from conductivity, rheology and optical transmittance measurements are shown in the table above. These were obtained by straight line interception at slope change (conductivity) and second degree polynomial fitting in the region of the minima (maxima) for rheological and optical transmittance measurements. The preceding inequality signs follow the considerations presented along the text.

	Conductivity	Rheology	Optical transmittance
cac (mM)	2.6	<3.4	<4.2
psp (mM)	<26	>16	21

Fig. 3.7 is a graphical representation of the information gathered by the various techniques employed in this work. On the left panel, corresponding to a dilute regime, there is an initial decrease in the chain extension when SDS is first added (pre-*cac* region). After SDS association, the chains expand again due to electrostatic effects. Finally, at even higher surfactant concentration (above the *psp*), bulk micelles promote the compression of the SDS saturated HPMC backbone. On the right, we see a corresponding evolution for higher polymer concentration, now for a semi-dilute regime. The random entanglement in the absence of SDS is slightly perturbed by the compaction of the chains. Upon SDS association, the chains expand again and connecting nodes resulting from hydrophobic intra- and inter-chain association are formed. These, with excess SDS, are finally solubilized.

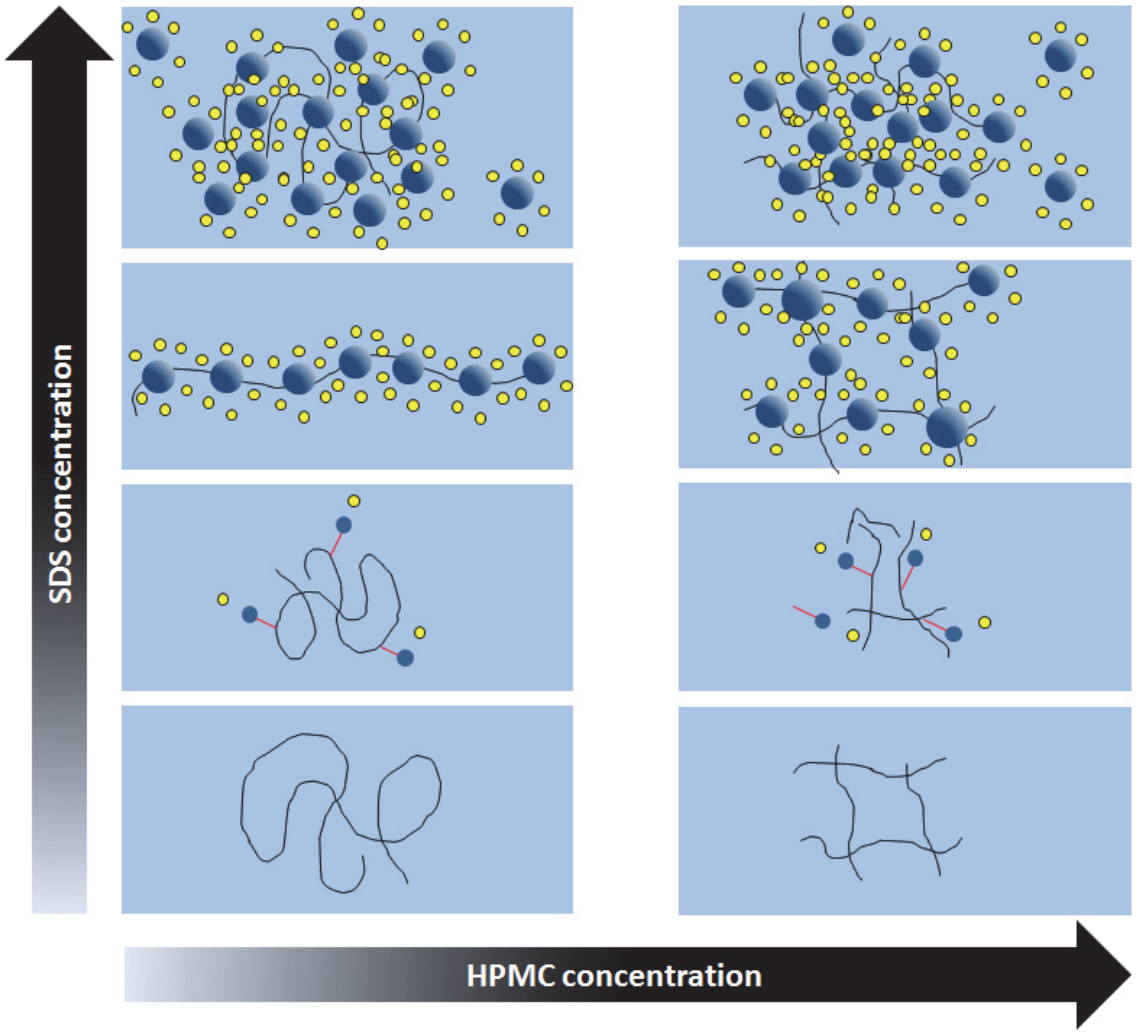

Fig. 3.7 Pictorial representation of the evolution of the SDS/HPMC/water system as a function of SDS and HPMC concentrations. Solid black lines represent HPMC chains, blue and yellow spheres correspond to SDS micelles and counterions respectively. The larger blue spheres indicate major hydrophobic association zones.

3.4. Conclusions

In the present chapter it was shown that the addition of SDS to HPMC solutions affects both the behavior in terms of SDS self-assembly and that of the HPMC solution, but in a non-trivial way. For diluted HPMC solutions, the *cmc* is reduced by ca. 60% of the *cac* value, which remains constant up to 0.5% HPMC solutions. The calculated free-energy of SDS association (which only partially includes the polymer-SDS interactions) also remains approximately constant, and indicates that the process is slightly less spontaneous than in the absence of HPMC. Again, for concentrations of HPMC above 0.5%, there is an increase in the absolute value of the free-energy surpassing the one found in the absence of HPMC. The polymer saturation point, in contrast, increases monotonically with HPMC concentration, as could be expected. After the saturation

point, the micellization process is very similar to that found in the absence of HPMC if the polymer solution is diluted, but becomes more favorable for higher concentrations.

For a constant (0.5%) concentration of HPMC, the SDS association process becomes more and more favorable as the temperature increases, in the range 25-50°C.

Rheological measurements at room temperature also indicate three regimes as a function of SDS concentration. The first is characterized by a decrease in viscosity, up to the *cac* value, followed by a drastic increase until the proximity of the *psp* where it starts to decrease again (these trends are in close agreement with those obtained with optical transmittance measurements). SDS also promotes an increase in the gelation temperature and, for high concentrations, may completely inhibit gel formation.

Chapter 4

Structure activity relationships in alkylammonium C_{12}-gemini surfactants used as dermal enhancers

The purpose of the study presented in this chapter was to determine the ability and the safety of a series of alkylammonium C_{12}-gemini surfactants to act as permeation enhancers for three model drugs, namely lidocaine HCl, caffeine and ketoprofen. In vitro permeation studies across dermatomed porcine skin were carried out over 24 hours, after pretreating the skin for 1 hour with an enhancer solution 0.16M dissolved in propylene glycol. The highest enhancement ratio (ER = 5.1) was obtained using G12-6-12, resulting in a cumulative amount of permeated lidocaine HCl of 156.54 $\mu g\ cm^{-2}$. The studies with caffeine and ketoprofen revealed that the most effective gemini surfactant was the one with the shorter spacer, G12-2-12. The use of the latter resulted in an ER of 2.4 and 2.2 in the passive permeation of caffeine and ketoprofen, respectively. However, azone was found to be the most effective permeation enhancer for ketoprofen, attaining a total of 138.36 $\mu g\ cm^{-2}$ permeated, 2.7-fold over controls.

This work demonstrates that this class of compounds is effective in terms of increasing the permeation of drugs, especially in the case of hydrophilic and ionized compounds, that do not easily cross the complex lipid barrier of the skin, the stratum corneum. Skin integrity evaluation studies did not indicate the existence of relevant changes in the skin structure after the use of the permeation enhancers, while the cytotoxicity studies allowed establishing a relative cytotoxicity profile including this class of compounds, single chain surfactants, and azone, a well-known permeation enhancer. A dependence of the toxicity to HEK and to HDF cell lines on the spacer length of the various gemini molecules was found.

4.1. Introduction

The stratum corneum (SC) is the skin outermost later and it is generally recognized to be the major barrier to the permeation of drugs applied topically. SC is composed of keratinocytes embedded in a complex extracellular lipid mixture, containing ceramides (45-50%), cholesterol (25%), free fatty acids (10-15%) and some other lipids such as cholesterol sulfate, highly organized as gel phase membrane domains [27].

Difficulties in obtaining and handling human skin have prompted researchers to employ alternative animal membranes for percutaneous studies. Among all, porcine skin is recognizably the closest model to human skin, since it has anatomical and morphological similarities with human skin [176, 304, 305], particularly in epidermis and upper dermis vasculature [180]. There are studies reporting similar *in-vitro* permeation values between human and porcine skin, and a significant positive correlation for the permeation of several drugs [172, 177].

The biggest challenge in transdermal drug delivery is to reversibly alter the barrier properties of the SC and, therefore, increase the transport of drugs across the skin. Such compounds are general known as chemical penetration enhancers (CPE) and have different mechanisms of action, which include increasing the partition of the drugs to the skin or their diffusion rates in the SC [12, 306, 307].

According to Fick's law of diffusion

$$J = \frac{D\, C_0 P}{h} \qquad (4.1)$$

where J is the steady-state flux, D is the diffusion coefficient of the drug in the SC, h is the diffusional path length or, in this case, the membrane thickness, P is the partition coefficient and C_0 is the drug concentration applied, a combination of enhancement effects on diffusivity and partitioning may result in an enhancement effect. Synergistic effects have been verified for many combinations, including azone and propylene glycol [308].

Surfactants comprise a broad class of compounds with surface-active properties, and consequently have a great potential to be used as permeation enhancers. Surfactants are often employed in transdermal formulations to increase the permeation of drug molecules across the skin. At concentrations below the critical micelle concentration (*cmc*), surfactants exist free in solution as unimers, and the effects of increasing skin permeability are generally ascribed to the ability of surfactant molecules to penetrate in the hydrophobic domains of the SC, therefore increasing the fluidity of the lipid structures [106].

The major concerns about the use of surfactants in TDD are associated with the possibility of local irritation, erythema, itching and the time required for adequate skin recovery, as well as problems related with the transport into the systemic circulation [2, 74, 309].

Despite the fact that cationic surfactants are reputedly at least as irritating as anionic ones, they are used in cosmetic formulations and have been reported to possess antibacterial properties [310, 311]. The potential of some alkyl surfactants to act as chemical permeation enhancers for various drugs have been studied and reported in the literature [106, 312-315]. Some studies have focused on the influence of the alkyl chain length on the potency of the surfactants as chemical permeation enhancers. The highest enhancer activity was found for surfactants with C_{12} alkyl chains [316].

Unlike conventional surfactants, which are composed by a single hydrophobic tail connected to a polar head group, gemini (or dimeric) surfactants structurally consist of at least two hydrophobic tails and two hydrophilic head groups covalently linked by a spacer group [317, 318]. The chemical structure of the spacer and head groups may vary, resulting in compounds with different physico-chemical properties. The spacer can be as short as 2 methylene groups or long (12 methylene groups), rigid (stylbene) or flexible (methylene chain), polar (polyether) or nonpolar (polyether sugar). Also, the polar head group can be positive (e.g. ammonium as in the compounds reported in this study), negative (phosphate, sulfate) or nonionic (aliphatic or aromatic) [318, 319].

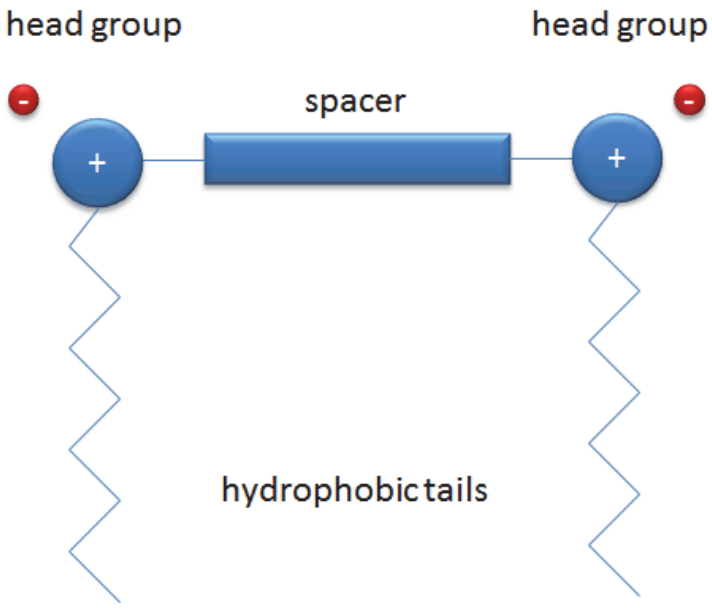

Fig. 4.1 Schematic representation of cationic gemini surfactant. These molecules are composed of two monomeric surfactant molecules linked by a spacer chain.

Gemini surfactants (Fig. 4.1) are typically micelle-forming surfactants that are reportedly more efficient in lowering the surface tension and have considerably lower critical micelle concentration (*cmc*) values than the corresponding single chain surfactants at the same

temperature, generally by one order of magnitude or more. These interfacial properties are attributed to the higher hydrophobicity of the gemini compared to their single chain homologues; furthermore, it is observed that for a series of *n-s-n* compounds, those properties are non-monotonically influenced by the spacer length, *s* [311, 320]. In what concerns to skin penetration enhancement of drugs, the enhanced interfacial properties may result in an efficient penetration enhancement using lower molar concentrations, therefore reducing the undesired irritancy or toxic effects on the skin. In addition, alkylammonium cationic gemini surfactants similar to those used in the present study have been reported to significantly interact with lipid membranes. It was reported that the presence of these compounds decreased the degree of organization of dipalmitoylphosphatidylcholine (DPPC) bilayers. The effect on the liposomes was found to be dependent on the spacer length, with the vertical positioning of gemini molecules inside the bilayer being governed by the hydrophobic effect upon the spacer [321].

The objective of this study is to evaluate the potential of a series of cationic C_{12}-alkylammonium gemini surfactants as CPE for various model drugs across porcine skin, following a methodology identical to that used in a previous work of the authors [322]. These compounds consist of dimethylene-1,2- bis (dodecyldimethylammonium bromide), hexamethylene-1,2- bis (dodecyldimethylammonium bromide) and decamethylene-1,2-bis (dodecyldimethylammonium bromide), respectively referred in this manuscript as G12-2-12, G12-6-12 and G12-10-12.

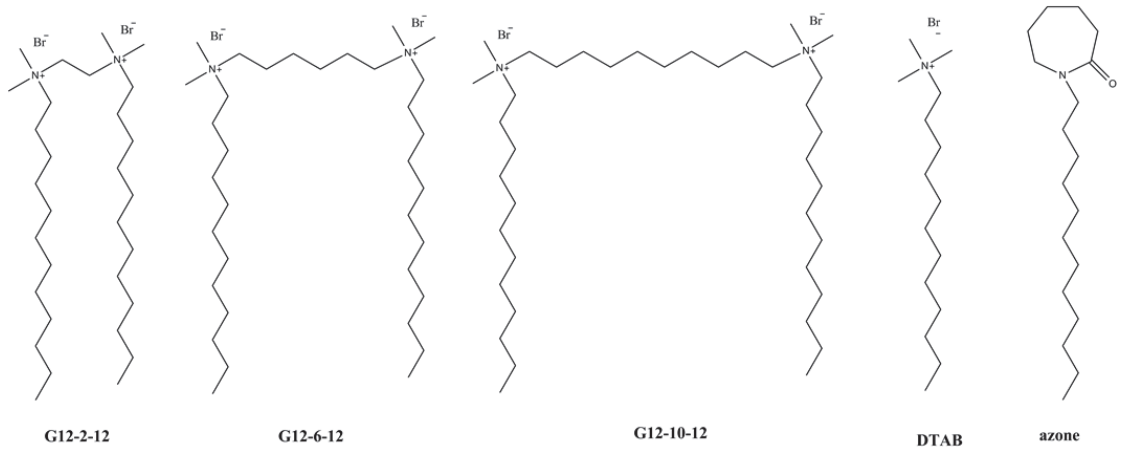

Fig. 4.2 Molecular structures of the chemical permeation enhancers used in this work (G12-2-12, G12-6-12, G12-10-12, DTAB and azone)

In spite of the fact that literature is abundant with studies that assess skin permeation enhancing by a variety of compounds, systematic approaches relating structure and enhancing efficiency are rare. In this work, different spacer lengths were chosen, implying different *cmc* values and different hydrophobicity of the compounds. Single chain alkylammonium surfactant dodecyltrimethylammonium bromide (DTAB) and azone, a well-known CPE [316, 323-328], both having C_{12}-akyl chains in their structures, were also used in this study, for comparative purposes (Fig. 4.2).

The variations imposed on the CPE are combined with the use of drugs with distinct physico-chemical properties: lidocaine HCl, positively charged; caffeine (non-ionized and hydrophilic) and ketoprofen (non-ionized and hydrophobic).

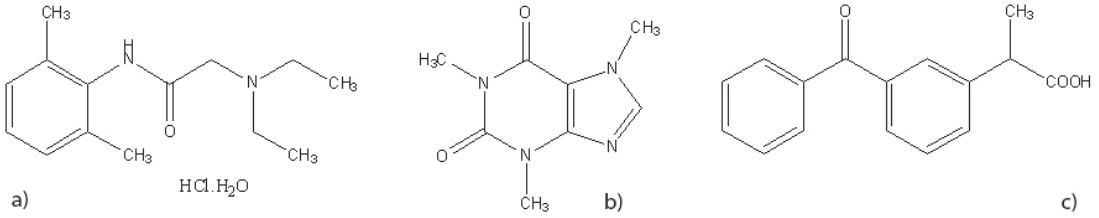

Fig. 4.3 Molecular structures of lidocaine hydrochloride monohydrate (on the left, a), Mw: 288.81; ACD/log*P*: 2.359; ACD/ log*D* (pH5.5): -0.13), caffeine (on the center, b), Mw: 194.19; ACD/log*P*: -0.628; ACD/ log*D* (pH5.5): -0.63) and ketoprofen (on the right, c), Mw: 254.28; ACD/log*P*: 2.911; ACD/ log*D* (pH5.5): 1.62)

4.1.1. Drug information and background

Lidocaine is a local anesthetic of the amide type. It is used for infiltration anesthesia and regional nerve blocks and is also classified as a Ib antiarrhythmic used in the treatment of ventricular arrhythmias, especially after myocardial infarction. It is generally administered as the hydrochloride form in pharmaceutical formulations. Lidocaine has a rapid onset of action and an intermediate duration, and it is readily absorbed from the GI tract, through mucous membranes and damaged skin, but is poorly absorbed through intact skin. Lidocaine undergoes a fast and extensive (about 90% of a given dose) first-pass metabolism, and the bioavailability is about 35% of an oral dose. The amount of lidocaine recommended for surface anesthesia varies in different countries, but normally doses are given as a 2% gels, ointments and topical solutions. The range can vary from 1 to 4% and, in some conditions lidocaine with a concentration of 10% has been formulated as a spray for application in mucous membranes.

Caffeine is a methylxanthine that inhibits the enzyme phosphodiesterase and has an antagonistic effect at central adenosine receptors. Pharmacologically, it is a stimulant of the CNS, especially the higher centers, producing a state of wakefulness and increased mental activity while its action on the respiratory center causes an increase in the rate and depth of respiration. Caffeine is also known for its bronchodilating properties, diuretic action and for improving the performance of muscular work. Caffeine is rapidly and completely absorbed after oral doses with negligible first-pass effect [329, 330] and it is also absorbed through the skin, quickly passing into the CNS. Caffeine oral doses range from 50 to 200 mg, despite unit doses of about 15-65 mg are present in oral analgesic formulations containing acetaminophen, aspirin or codeine.

Ketoprofen is a propionic acid derivative, pharmacologically considered a NSAID, used in the management of various musculoskeletal and joint disorders and dysmenorrhea, postoperative pain, acute gout or soft-tissues disorders. Ketoprofen is readily absorbed

from the gastrointestinal tract. It is also well absorbed from the intramuscular and rectal routes, but poorly absorbed through the skin. Topical application may cause contact and photoallergic dermatitis [331-334]. Daily use of ketoprofen usually ranges between 100 and 200 mg divided in several doses. 2.5% gel ketoprofen formulations are employed 2-3 times a day to treat local pain conditions.

Additionally, the effects on the skin structure of the CPE and methodology employed was studied using light microscopy and scanning electron microscopy (SEM). The cytotoxicity of all compounds was also assessed and discussed. These studies were performed in cultured human epidermal keratinocytes (HEK) and in human dermal fibroblasts (HDF).

4.2. Experimental section

4.2.1. Materials

Hydroxypropylmethyl cellulose (HPMC K15M) was a kind gift from Dow Chemical Company (USA). Lidocaine hydrochloride monohydrate, ketoprofen, caffeine and dodecyltrimethylammonium bromide (DTAB) (BioXtra, ≈ 99%), propylene glycol (PG) (Reagent Plus, 99%) were purchased from Sigma Aldrich (Saint Louis, MO, USA). Azone was synthesized at the New Jersey Center for Biomaterials, Rutgers, The State University of New Jersey (Piscataway, NJ, USA). The three cationic gemini surfactants used in this study (Fig. 4.2), alkylene bis(dodecyldimethylammonium bromide), 12-s-12 for s = 2, 6 and 10, namely dimethylene-1,2- bis (dodecyldimethylammonium bromide), hexamethylene-1,2- bis (dodecyldimethylammonium bromide) and decamethylene-1,2-bis (dodecyldimethylammonium bromide), were synthesized and purified in the Department of Chemistry and Biochemistry, University of Porto, according to the method of Menger [317, 335, 336]. The purity of the compounds was ascertained by NMR, differential scanning calorimetry and determination of critical micelle concentration (*cmc*) by surface tension. The values obtained for *cmc* were 0.85, 0.96 and 0.40 for G12-2-12, G12-6-12 and G12-10-12, respectively, all in good agreement with previously reported values [337]. Furthermore, no dips near the *cmc* break were found in the surface tension vs. concentration plots, further confirming that surface-active impurities are absent. Phosphate buffer saline tablets (PBS) were purchased from TIC Gums (Belcamp, MD, USA). Formalin 10% was purchased from Fisher Scientific, Inc. (Torrance, CA, USA). CellTiter 96® AQueous One Solution Cell Proliferation Assay (MTS) was purchased from Promega Corp (Madison, WI, USA). Tissue-Tek® O.C.T™ Compound was purchased from Sakura Finetek USA, Inc. (Agawam, MA, USA). Porcine skin tissue was obtained from young Yorkshire pigs (26.5–28 kg, UMDNJ, Newark, NJ). Human epidermal keratinocytes (HEK) and human dermal fibroblasts (HDF) were purchased from Invitrogen™ (Carlsbad, CA, USA).

4.2.2. Hydrogels composition and preparation

Drug-loaded HPMC hydrogels were prepared as follows. Lidocaine HCl hydrogel contained 2.5% (w/w) lidocaine HCl, 1% (w/w) HPMC K15M and deionized water. Caffeine hydrogel was composed of 1.5% caffeine, 1% (w/w) HPMC K15M and deionized water. Ketoprofen hydrogel contained 5% (w/w) ketoprofen, 1% (w/w) HPMC dissolved in a mixture of PG/water 80:20.

4.2.3. Porcine skin preparation

Porcine skin was excised and dermatomed using a Padgett® Model B Electric Dermatome (Integra LifeSciences, Plainsboro, NJ) with 650-750 μm thickness and stored at –80°C. Before the experiments, skin samples were thawed at room temperature, before immersion in PBS (pH=7.4) for 1 h, for equilibration.

4.2.4. Composition and preparation of the enhancer solutions

The enhancer solutions were prepared at a concentration of 0.16M in PG. All compounds were soluble in PG at the concentration used, and produced clear solutions.

4.2.5. Drug delivery studies

In vitro permeation studies were performed over 24 hours using vertical Franz diffusion cells (PermeGear, Inc., PA, USA) with a diffusion area of 0.64 cm^2 and a receptor compartment of 5.1mL filled with PBS solution (pH = 7.4). The receptor medium was maintained at 37°C ± 0.1 and stirred at 600 rpm during the permeation experiments. Drug loaded hydrogel (0.3 mL) was placed in each donor compartment and immediately covered with Parafilm®, preventing evaporation. Dermatomed porcine skin pieces with a thickness of 0.76 mm were used as a membrane. The skin was placed between the donor and receptor compartments, with the epidermal side facing up. At predetermined time points, namely 0, 4, 8, 12, 16, 20, 22 and 24 h, 300 μL samples were collected from the receptor compartment and immediately replaced with 300 μL of new PBS solution. The samples were kept in the refrigerator prior to HPLC analysis. Before initiating the *in-vitro* permeation experiments, all the skin samples, except the control, were pretreated with 60 μL of the various enhancer solutions, for 1 h. The origin, t=0, corresponds to the instant of application of the drug loaded hydrogel in the donor compartment. The sample concentrations were corrected to account for drug taken out at each sample point.

4.2.6. Drug quantification

All samples were analyzed using HPLC. The system consisted of an Agilent HP 1100 series with an autosampler, equipped with a quaternary pump and a VMD detector and an Agilent Chemstation. The quantification of lidocaine hydrochloride was carried out using a reverse phase Nova-Pak® C18 Column (4mm pore size, 3.9x300mm -Waters, Milford, MA, USA) with a guard column as the stationary phase. The mobile phase was prepared by mixing 50 mL of glacial acetic acid to 930 mL of water followed by adjusting the pH to 3.40 with a solution of 1M NaOH. Later, 4 volumes of the previous solution were mixed with 1 volume of Acetonitrile. The flow rate was set to 1.1 mL/min and the injection volume was 20μL. Lidocaine hydrochloride was detected at 254 nm and the retention time was ca. 4.5 minutes. The method showed a linear response in the 0.025-1.0 mg/mL (R^2 = 0.9998) with a daily RSD < ±3.0%. A reverse-phase C_{18} column (150 x 4.6mm C18 (2) 100 A Luna 5μm, Phenomenex®) with a guard column was the stationary phase for the caffeine assay, at 25°C. The mobile phase consisted of a mixture of 15% acetonitrile and 85% of a solution of 0.1% H_3PO_4 in water. The flow rate was set to 1.0 mL/min and the injection volume was 20 μL. Caffeine was detected at 273 nm and the retention time was ca. 4 minutes. The method showed a linear response in the 0.01-500 mg/mL range (R^2 = 0.9973) with a daily RSD < ± 3.0%. Ketoprofen was detected at 256 nm using a reverse-phase C_{18} column (150 x 4.6mm C18 (2) 100 A Luna 5μm, Phenomenex®) with a guard column as the stationary phase at 25°C. The mobile phase consisted of a mixture of 45% of a 0.1% solution of H_3PO_4 and 55% acetonitrile. The flow rate was set to 1.0 mL/min and the injection volume was 20 μL. In these conditions, the method exhibited a linear response between 0.01-100 mg/mL (R^2 = 1.0000), and the retention time was close to 4 minutes with a daily RSD < ±3.0%.

4.2.7. Data analysis in the permeation studies

The steady flux at time *t* (J, μg.cm^{-2}) was calculated from the slope of the linear portion of the plot of the cumulative drug amount permeated versus time. Q_{24} refers to the cumulative drug amount present in the receptor compartment solution after 24 h of permeation experiment. The enhancement ratio (ER) for flux was calculated using

$$ER = \frac{\text{flux for treated skin with enhancer}}{\text{flux for untreated skin (control)}} \quad (4.2)$$

Results are presented as mean ± standard deviation (SD) (*N*), where *N* is the number of replicates. Flux values were examined for significance using unpaired Student's *t*-test. The *p* value was set to 0.05, meaning that for $p < 0.05$, there was statistically significant difference between the control and the enhancers tested.

4.2.8. Skin integrity evaluation

Skin samples used in the permeation studies were subsequently rinsed with deionized water, dried and stored at -80°C. These samples were later investigated for the occurrence of morphological changes caused by the CPE and methodology employed.

4.2.8.1. Histology - light microscopy studies

Skin samples used in the permeation studies were sectioned and fixed using 10% buffered formalin for 24 hours at room temperature. Skin samples were subsequently dehydrated with 50%, 75%, 95% and 2 changes of 100% absolute ethanol for 1 hour each. Samples were embedded in Tissue-Tek® O.C.T. compound and frozen using dry ice [338]. Cross-section slices of 7μm thickness were obtained using a microtome (Leica Model CM 1850, Leica Microsystems, Inc. Bannockburn, IL, USA) and stained following the Ellis Hematoxylin and Eosin (H&E) staining protocol [339].

The stained slices were analyzed using a Nikon Eclipse E 800 light microscope (Micro Optics, Cedar Knolls, NJ, USA) at 10, 20 and 40 x. A Nikon Digital Camera (Model DXM 1200) was used to capture images. Images were processed using SPOT TM Imaging Software, Version 5.0 (Diagnostic Instrument, Inc., Sterling Heights, MI, USA).

4.2.8.2. Scanning Electron Microscopy studies

Skin samples were submerged in Tissue-Tek® O.C.T. Compound and frozen using dry ice. Cross-sectional slices of the frozen samples were prepared (10 μm thickness) using a microtome (Leica Model CM 1850, Leica Microsystems, Inc. Bannockburn, IL, USA). The samples were defrosted and fixed using 4% formaldehyde for 1.5 hours. Subsequently, skin samples were rinsed and placed in deionized water, at room temperature for 2 hours and dehydrated using solutions of 30%, 50%, 75%, and 95% ethanol in water for 25 minutes. Finally, they were placed in two changes of absolute ethanol (100%) for 2 hours at room temperature. The dehydrated samples were dried with a critical-point drier (model CPD 020) and coated with gold. Surface and cross-sections pictures of the samples were taken using Scanning Electron Microscopy (SEM - model AMARY-18301).

4.2.9. Cytotoxicity studies – MTT/MTS Assay

MTT / MTS assays are a colorimetric method used to determine the number of viable cells in cytotoxicity assays, widely reported in the literature for similar systems [340-343]. MTS reagent (CellTiter 96® AQueous One Solution Reagent) contains a tetrazolium compound [(3-(4,5-dimethylthiazol-2-yl)-5-(3-carboxymethoxyphenyl)-2-(4-sulfophenyl)-2H-tetrazolium, inner salt] which is converted by mitochondrial dehydrogenase enzymes of living cells into a colored formazan compound. The number of viable cells is directly

proportional to the quantity of formazan product formed as measured by the absorbance at 490nm (Promega Corp. Protocol, 2009). The levels of formazan formed were quantified using a Microplate Power Wave X Scanning Spectrophotometer (Bio-TEK Instruments, Inc. Winooski, VT, USA).

Cytotoxicity studies were carried out both in cultured HEK and in HDF seeded at 8000 cells/well in 96-well plates under sterile conditions. The objective was to evaluate the toxic effects of the CPE on these types of skin cells, establishing a concentration-toxicity response. HEK were seeded in 100μL/well of Epilife® (MEPI 500CA) medium supplemented with gentamycin (Gibco®), human keratinocyte growth supplement (Gibco®) and were incubating for 24 hours at 37°C, 5% CO_2 and 90% R.H. HDF were seeded in 100 μL/well of GIBCO®- Dulbecco's Modified Eagle Medium (DMEM) medium with 100 IU/mL penicillin, 100 IU/mL streptomycin and 10% fetal bovine serum. All the media and biological reagents were purchased directly from Invitrogen™, Inc. (Carlsbad, CA, USA).

After seeding, the culture medium was removed and cells were exposed to medium (control), propylene glycol (PG) and various concentrations (160, 16, 1.6, 0.16, 0.016 μM) of azone and cationic gemini surfactants solutions in PG, subsequently diluted in culture medium and placed in the incubator for an additional period of 24 hours in the same environmental conditions. After exposure, testing solutions were removed and replaced by a pre-mixed solution of MTS reagent (CellTiter 96® AQueous One Solution) and appropriate medium (Promega Corp. Protocol, 2009), and were returned to the incubator for 2 hours. The 96-well plates were read at 490nm using a plate reader (Microplate Power Wave X Scanning Spectrophotometer - Bio-TEK Instruments, Inc. Winooski, VT, USA).

Results are presented as % cell viability (mean ± standard deviation, N=6), *C.V.*, after background absorbance (abs), determined from “no cell” control wells was subtracted, according to

$$C.V. = \frac{\text{abs read in treated cells}}{\text{abs read in control (untreated) cells}} \quad (4.3)$$

4.3. Results and Discussion

4.3.1. In vitro permeation studies

4.3.1.1. Effect of the penetration modifiers on the transdermal drug delivery of lidocaine hydrochloride

As described in the experimental section, three gemini C_{12} surfactants, DTAB and azone were dissolved in PG at a concentration of 0.16M. The enhancer solutions were applied

to the epidermal side of dermatomed porcine skin placed between the donor and receptor compartments of Franz diffusion cells for 1 hour prior to the application of the lidocaine HCl loaded hydrogels. The results obtained are presented in Table 4-1 and the permeation profiles are shown in Fig. 4.4.

Table 4-1 Effect of the chemical permeation enhancers on percutaneous permeation of lidocaine HCl across porcine skin. Data are presented as means ± S.D. (3≤N≤6).

Penetration modifier	Flux (μg cm^{-2} h^{-1})	Q_{24} (μg cm^{-2})	ER
Control (drug-loaded hydrogel only)	2.43 ± 0.52	48.71 ± 11.00	-
Propylene glycol (PG)	3.23 ± 2.17	73.79 ± 48.10	2.2
0.16M G12-2-12 in PG*	3.96 ± 1.30	83.26 ± 27.66	2.7
0.16M G12-6-12 in PG*	7.60 ± 3.55	156.54 ± 80.08	5.1
0.16M G12-10-12 in PG*	5.75 ± 1.65	138.13 ± 31.18	3.9
0.16 M azone in PG*	5.08 ± 2.22	113.90 ± 52.72	3.4
0.16 M DTAB in PG*	5.53 ± 0.80	98.61 ± 15.08	3.7
* Statistically significant difference between enhancer and control, at $p < 0.05$ (Student's *t*-test)			

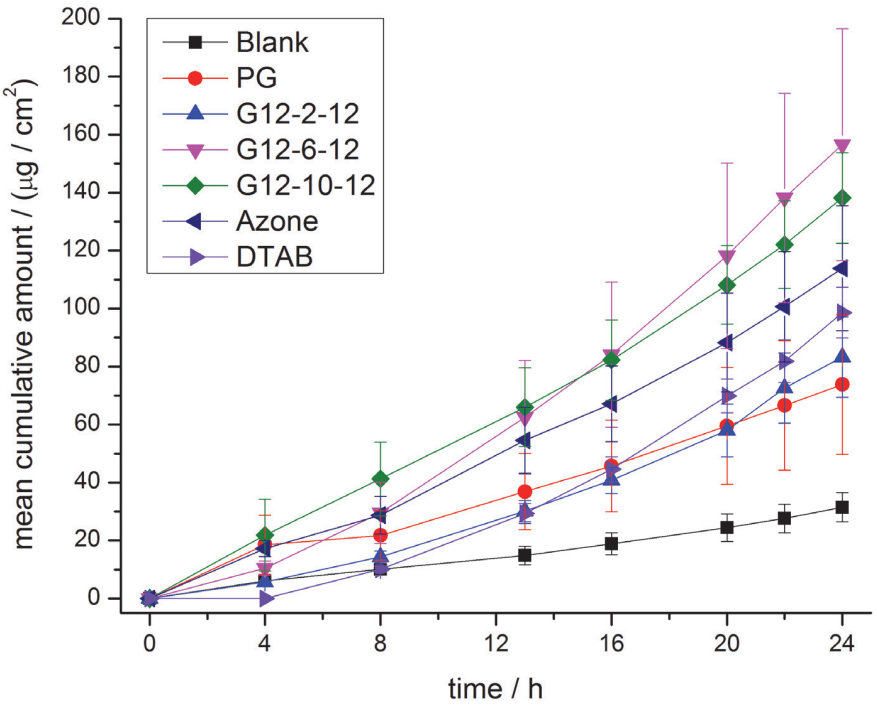

Fig. 4.4 Cumulative amount of lidocaine HCl permeated across porcine skin as a function of time. Skin was pretreated for 1 hour with enhancer solutions in PG, prior the start of the permeation experiments.

The use of all three gemini surfactants tested, DTAB and azone solutions resulted in a statistically significant increase ($p<0.05$) of lidocaine HCl permeation, when compared to control. G12-6-12 was shown to be the most effective permeation enhancer resulting in a 5-fold increase of the ER, followed by G12-10-12 (ER = 3.9), DTAB (ER = 3.7) and

azone (ER = 3.4). In contrast, PG and the gemini surfactant with the shorter spacer (G12-2-12) showed poor performance.

4.3.1.2. Effect of the penetration modifiers on the transdermal drug delivery of caffeine

Caffeine is a nonionic hydrophilic compound. The results obtained with this agent are presented in Table 4-2 and Fig. 4.5, and show that PG significantly decreased the amount of drug permeated, to approximately one half compared to the control.

Table 4-2 Effect of the chemical permeation enhancers on percutaneous permeation of caffeine across porcine skin. Data are presented as means ± S.D. (6≤N≤9).

Penetration modifier	Flux (μg cm^{-2} h^{-1})	Q_{24} (μg cm^{-2})	ER
Control (drug-loaded hydrogel only)	4.54 ± 0.96	99.72 ± 21.32	-
Propylene glycol (PG)*	1.87 ± 0.47	35.28 ± 7.49	0.4
0.16M G12-2-12 in PG*	10.93 ± 2.63	226.92 ± 58.75	2.4
0.16M G12-6-12 in PG*	8.15 ± 2.15	162.72 ± 35.40	1.8
0.16M G12-10-12 in PG	6.12 ± 2.11	127.91 ± 46.05	1.34
0.16 M azone in PG	5.70 ± 2.26	118.09 ± 45.74	1.3
0.16 M DTAB in PG*	10.52 ± 3.37	208.77 ± 62.07	2.32
* Statistically significant difference between enhancer and control at $p < 0.05$ (Student's *t*-test)			

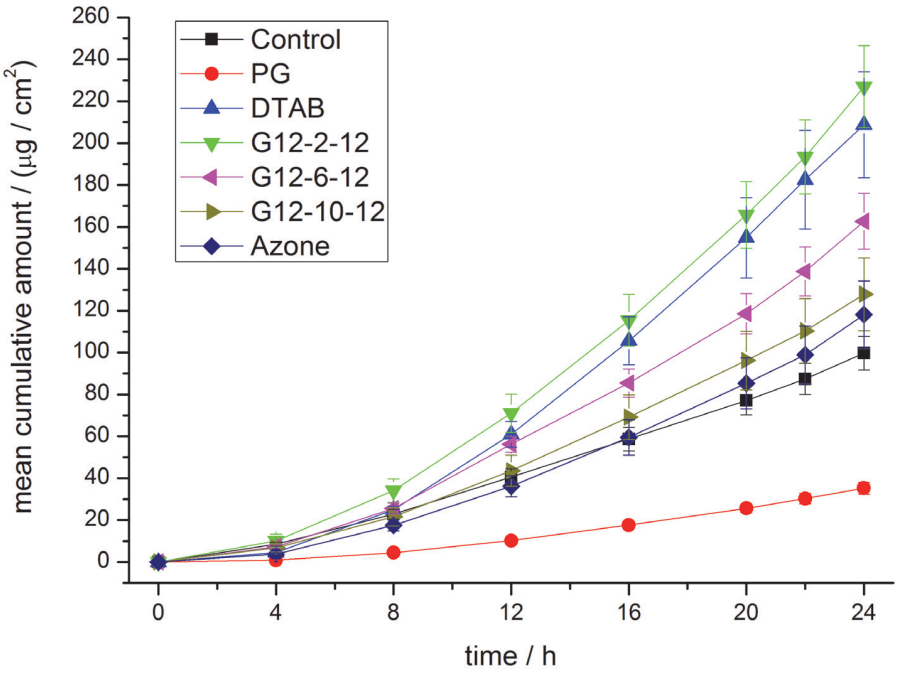

Fig. 4.5 Cumulative amount of caffeine permeated across porcine skin as a function of time. Skin was pretreated for 1 hour with enhancer solutions in PG, prior the start of the permeation experiments.

In contrast, gemini surfactants G12-2-12 and G12-6-12 and DTAB significantly increased the caffeine permeated after 24h by approximately 2-fold. Surprisingly, azone had a modest performance in terms of penetration enhancement, causing only a slight increase of caffeine permeated, with a value that is not statistically different from control.

4.3.1.3. Effect of the penetration modifiers on the transdermal drug delivery of ketoprofen

Permeation experiments using ketoprofen as model drug were slightly different from those of lidocaine HCl and caffeine. Unlike in the case of the previous drug-loaded hydrogels, PG was directly incorporated in the hydrogel formulation due to low solubility (51 mg/L) of ketoprofen in water-based vehicles and, for this reason, was not tested as CPE separately. Permeation data presented in Table 4-3 and in Fig. 4.6 shows that azone and Gemini G12-2-12 were the most effective CPE with respectively 2.7 and 2.2 enhancement ratios, and the only CPE tested that proved to be statistically different from the control.

Table 4-3 Effect of the chemical permeation enhancers on percutaneous permeation of ketoprofen across porcine skin. Data are presented as means ± S.D. (5≤N≤8).

Penetration modifier	Flux ($\mu g\ cm^{-2}\ h^{-1}$)	Q_{24} ($\mu g\ cm^{-2}$)	ER
Control (drug-loaded hydrogel only)	2.43 ± 0.52	48.71 ± 11.00	-
0.16M G12-2-12 in PG*	5.25 ± 2.19	110.15 ± 47.96	2.2
0.16M G12-6-12 in PG	2.44 ± 0.23	49.09 ± 5.56	1
0.16M G12-10-12 in PG	3.25 ± 0.97	65.53 ± 20.65	1.3
0.16 M azone in PG*	6.56 ± 1.02	138.36 ± 22.13	2.7
0.16 M DTAB in PG	3.39 ± 1.11	67.28 ± 21.93	1.4
* Statistically significant difference between enhancer and control at $p < 0.05$ (Student's *t*-test)			

Gemini G12-10-12 (ER = 1.3) and DTAB (ER = 1.4) caused a mild increase in the ketoprofen permeated, while the use of gemini G12-6-12 resulted in the same amount of ketoprofen permeated as control.

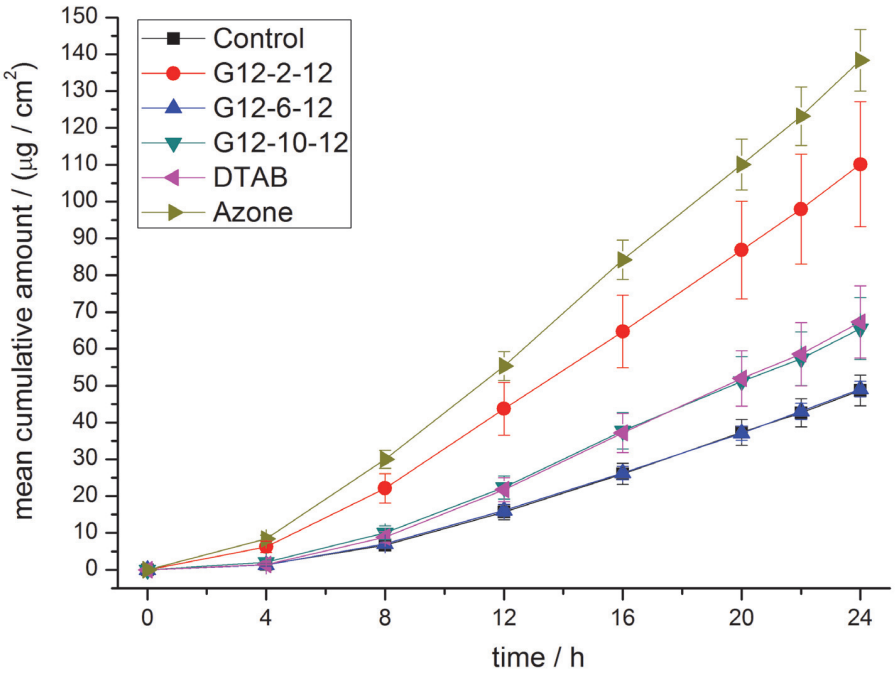

Fig. 4.6 Cumulative amount of ketoprofen permeated across porcine skin as a function of time. Skin was pretreated for 1 hour with enhancer solutions in PG, prior the start of the permeation experiments.

4.3.2. Overview and comparison

Fig. 4.7 summarizes the ER obtained using the CPE for the three drugs (lidocaine HCl, caffeine and ketoprofen). It is seen that the most effective CPE are those with shorter or intermediate spacer lengths. In the case of lidocaine HCl, the maximum ER was found with a spacer of 6 carbons (G12-6-12, ER=5.1), and the CPE with the shorter spacer (G12-2-12) was the least effective. However, as the hydrophobicity of the drug increases the trend changes. In the case of caffeine and ketoprofen, G12-2-12 was clearly the most effective CPE accounting for a 2.5-fold and 2.2-fold increase in the flux, respectively. In studies with caffeine, the effect of G12-6-12 was still significant (ER=1.8) while that of G12-10-12 was found negligible. Also negligible were the effects of both G12-6-12 and G12-10-12 in the case of ketoprofen.

It is also seen that in most cases steady-state permeation is attained after a period not exceeding 8h, and maintained for the full period of observation of 24h. Noting that the skin is pretreated with the CPE, and thus is not incorporated in the gel formulation, it is possible to infer that the enhancer effect is maintained in spite of phenomena such as permeation and dilution in the formulation. Otherwise, a decrease in the flux would be detected.

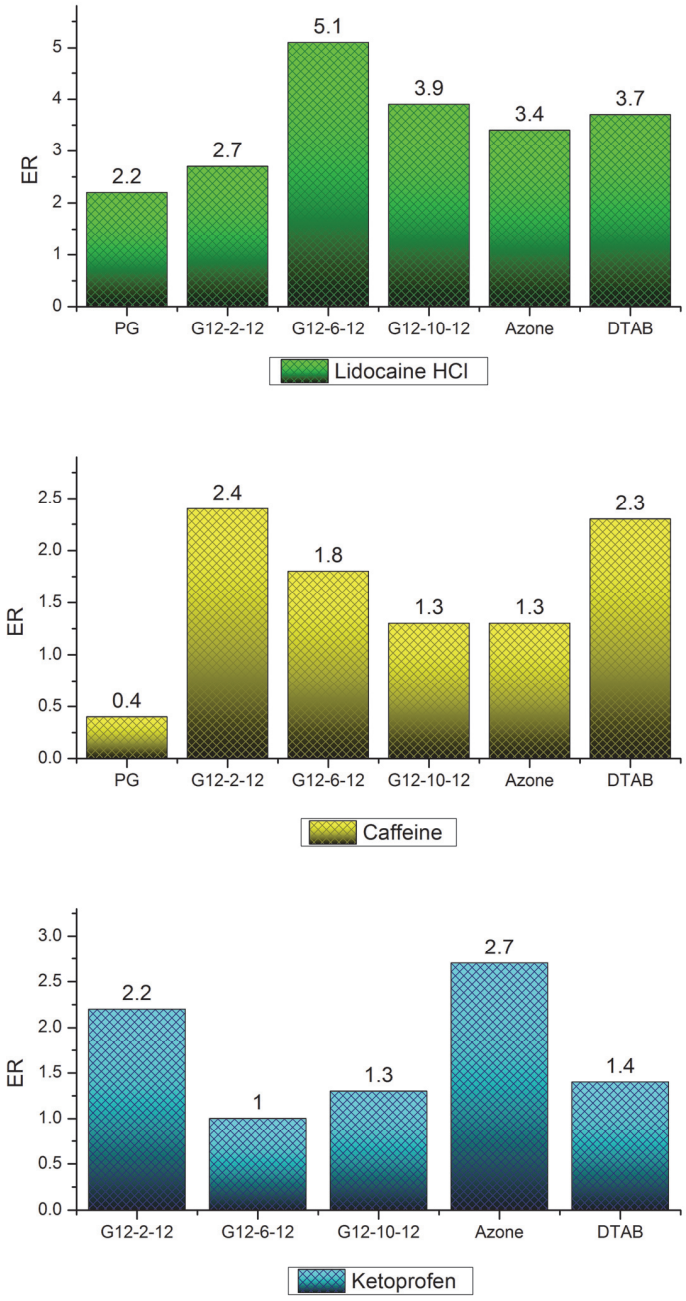

Fig. 4.7 ER obtained pretreating the skin using the various CPE for lidocaine HCl (top), caffeine (center) and ketoprofen (bottom).

The results obtained indicate that the effect of CPE is especially important in cases where the drug is clearly hydrophilic, decreasing as the hydrophobicity of the drug increases. This trend parallels with a previous work in which terpenes were used as CPE for drugs with different hydrophobicities [49].

Gemini molecules, owing to their amphiphilic nature and dicationic headgroup, will most certainly interact strongly with the intercellular lamellar lipid bilayers of SC. Moreover, due to the high gemini concentrations used in the formulations, one can presume that

ultimately there will be local compositional non-homogeneities in the lipid membranes, with the plausible formation of gemini-rich environments, through which the drugs will more easily permeate. It is well known that the interfacial and self-assembling properties of G12-s-12 gemini surfactants are determined by spacer length in a subtle way [344]. Due to its short 2-carbon spacer, G12-2-12 has a high positive charge density in the polar region of the molecule; moreover, its approximately cylindrical shape (critical packing parameter close to 1) dictates the formation of long cylindrical micelles already at low concentrations above the critical micelle concentration. G12-6-12, in turn, has a spacer that tends to lie “flat” at the interface, which implies an interfacial Gibbs energy penalty [344]. Thus, G12-6-12 has a higher cmc than G12-2-12 (0.96 and 0.85 mM, at 25°C, respectively) and forms micelles of higher curvature than G12-2-12: small spheroidal micelles that show limited growth with concentration. For G12-10-12, the long flexible spacer is able to more easily bend from the interface into the hydrophobic core of the aggregate, and hence this surfactant is characterized by a lower cmc (0.40 mM, at 25°C) than both G12-2-12 and G12-6-12, even despite the fact that the long spacer will create a unfavorable packing Gibbs energy term (higher chain conformational restrictions in the micellar core). G12-10-12 also forms small spheroidal micelles of limited concentration-induced growth.

Overall, it is reasonable to presume that these different gemini surfactants will induce different types of local bilayer perturbation in the SC, namely in terms of local curvature, surface charge density, and steric hindrance in the hydrophobic core of membranes. Recent studies on the effect of gemini surfactants on lipid bilayers show that gemini molecules with tails containing 12 carbons are effective in inducing a decrease in the overall order of the bilayers due to an interplay of effects [321, 345]. It was found that the longer spacers tend to bend towards the inside of the bilayers, just as in neat micelles and at air-water interface, which may explain, as a first approach, the similitude of action found in the present work between G12-6-12 and G12-10-12.

Furthermore, on the basis of the above considerations, the fact that G12-2-12 has the lowest ER for positively charged lidocaine can be reasonably understood because unfavorable electrostatic repulsions should be at stake in the interaction of G12-2-12-enriched bilayer domains with the drug. For G12-10-12, headgroup charge density may also be relatively high, due to inward bending of the spacer that will bring charges to closer distance, but previous studies on mixed gemini-lipid bilayers show that the molecule as whole tends to be vertically more indented into the bilayer, with the consequence that charge is less interfacially exposed [345]. Moreover higher steric hindrance (atom density) in the core may not facilitate drug permeation through the bilayer. The effect of G12-10-12 is hence comparable to that of DTAB. It appears that G12-6-12 has the most favorable spacer length for lidocaine permeation, having enough ability to perturb the bilayer but decreased headgroup charge density and spacer hindrance, compared to the other two gemini. The existence of an optimal spacer (and thus charge-to-charge) distance in the interaction of gemini with other molecules has been reported before, for example in gemini-polyelectrolyte mixtures [346].

In contrast, the short-spacer gemini seems to be the most efficient enhancer for caffeine and ketoprofen. Even though these drugs are uncharged, here we cannot discard the presence of electrostatic effects (albeit weak) promoting the enhancement, since caffeine is a relatively polar molecule and ketoprofen has an ionizable acidic group, and in both cases interaction with a cationic headgroup should be favorable. One slightly surprising result is the fact that G12-10-12, the most hydrophobic of the gemini, is not particularly effective as an enhancer for the most hydrophobic drug (ketoprofen), while G12-2-12 is significantly better. A possible explanation is the following: even though perturbation of the bilayer exists with G12-10-12 and a hydrophobic environment is "created", steric hindrance promoted by the relative long bent spacer in the hydrophobic core of the bilayer will not facilitate drug permeation. Azone was the most effective CPE in the case of ketoprofen, the most hydrophobic drug, while the single-chain surfactant DTAB, has shown an intermediate performance, ranking between the most and the least effective gemini surfactant, in each case. DTAB might have the same weak electrostatic effect as G12-2-12 but because of its single-chained structure (and higher curvature effects) it may not be as effective as the gemini in forming a local hydrophobic environment.

The present results indicate that the enhancing effects for the gemini molecules are a result of a combination of mechanisms, probably disturbing the SC lipid organization but also promoting the transport of the more hydrophilic, and charged drugs. Delipidization effects within the SC layer of the skin cannot also be discarded.

4.3.3. Skin integrity evaluation

Porcine skin samples used in the permeation experiments were carefully washed with water before storage at –80°C. Potential effects on the skin and morphological changes caused by the use of the chemical penetration enhancers and formulations were evaluated by means of histology-light microscopy and SEM.

4.3.3.1. Histological studies

Porcine skin samples used in the permeation experiments described above, pretreated with various permeation enhancers, were collected and later subject to histological procedures followed by observation, at different magnifications, using a light microscope.

Fig. 4.8 shows cross section pictures of untreated porcine skin obseved at three magnifications: 10x (a), 20x (b) and 40x (c), that were used as the negative control. The different layers of the skin can be identified based on the their morfological differences enhanced after the staining protocol employed. The outermost skin layer visible is the *stratum corneum* (SC). This is the the target struture for the chemical permeation enhancers. The viable epidermis (VE) is the dark colored struture underneath the SC

and above the dermis (D), the larger and lighter structure visible. Hair folicles are also visible in some of the pictures shown.

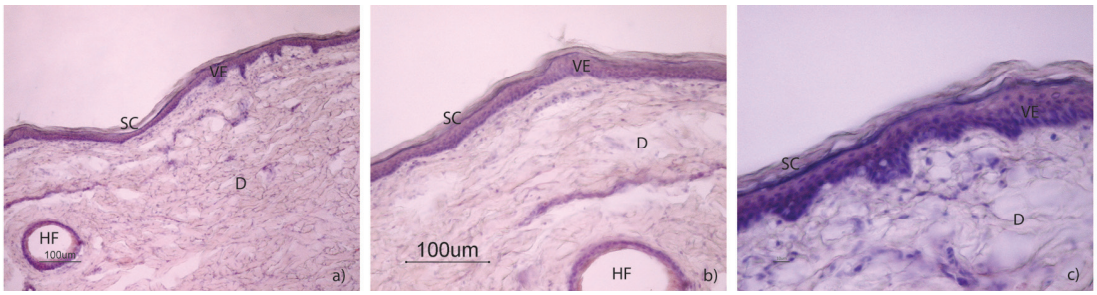

Fig. 4.8 Untreated (Control) porcine skin pictures were captured using an optical light microscope at 10x - a), 20x - b), 40x - c). The distinct skin layers can be observed: *stratum corneum* (SC), viable epidermis (VE), dermis (D) and hair follicles (HF).

The images presented in Fig. 4.9 were obtained from skin samples used in the permeation experiments treated with the different CPEs.

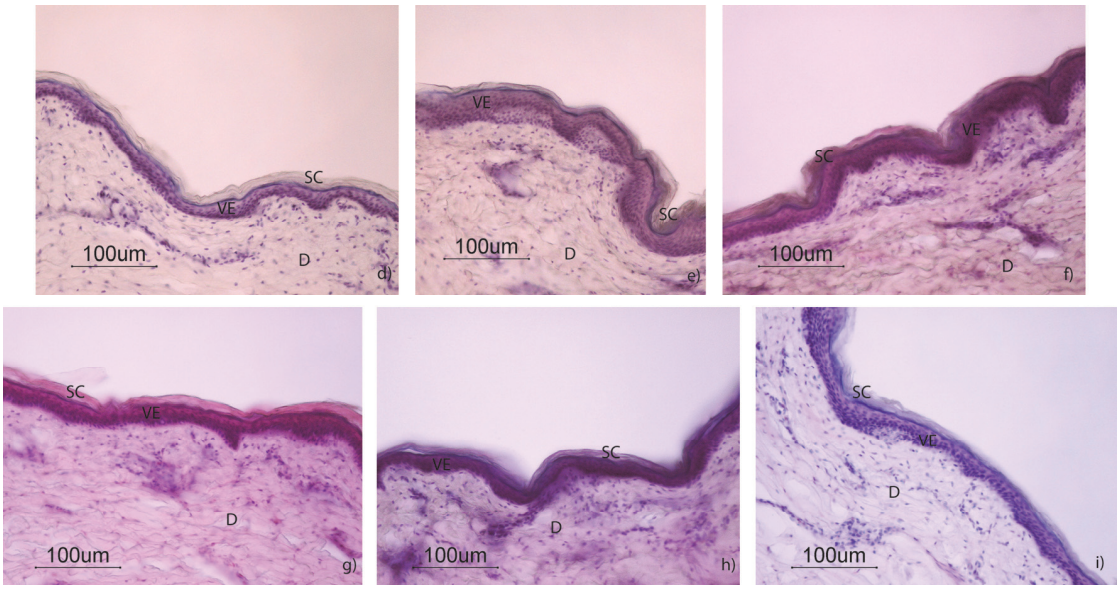

Fig. 4.9 Porcine skin pictures were obtained from the skin samples used in the permeation experiments that were previously pretreated with the CPE. For simplicity only the pictures taken at 20x magnification are shown. The pictures refer to the samples pretreated with: PG (d), azone (e), DTAB (f), G12-2-12 (g), G12-6-12 (h), G12-10-12 (i) as penetration enhancer.

These studies was performed in order to observe potential alterations and damages caused by the CPE to the skin structure, particularly on the outer layers, since the main target of the CPE is the intercellular lipid matrix of the SC. By comparing the images from the untreated skin samples (Fig. 4.8) and images of skin treated with the CPE (Fig. 4.9), it is observed that there are not relevant macroscopic differences concerning the integrity and cohesion between the skin layers. In both untreated and treated samples, the shedding of cells sheets from the SC is visible. The different shades are essentially due to the variability occurred during the staining protocol.

4.3.3.2. Scanning Electron Microscopy (SEM) studies

SEM studies were performed in order to observe the occurrence of potential harmful effects caused by the use of CPE on the skin that could not be perceived using conventional light microscopy. Since this technique has a large depth of field, the images obtained have a three-dimensional appearance, high-resolution even at high magnifications, revealing details of the surface of the skin.

Skin layers such as the SC (the outermost multi-layered structure), viable epidermis (the darker area) and dermis (the thickest structure mostly composed of connective tissue under the viable epidermis) are visible in detail in Fig. 4.10 and Fig. 4.11.

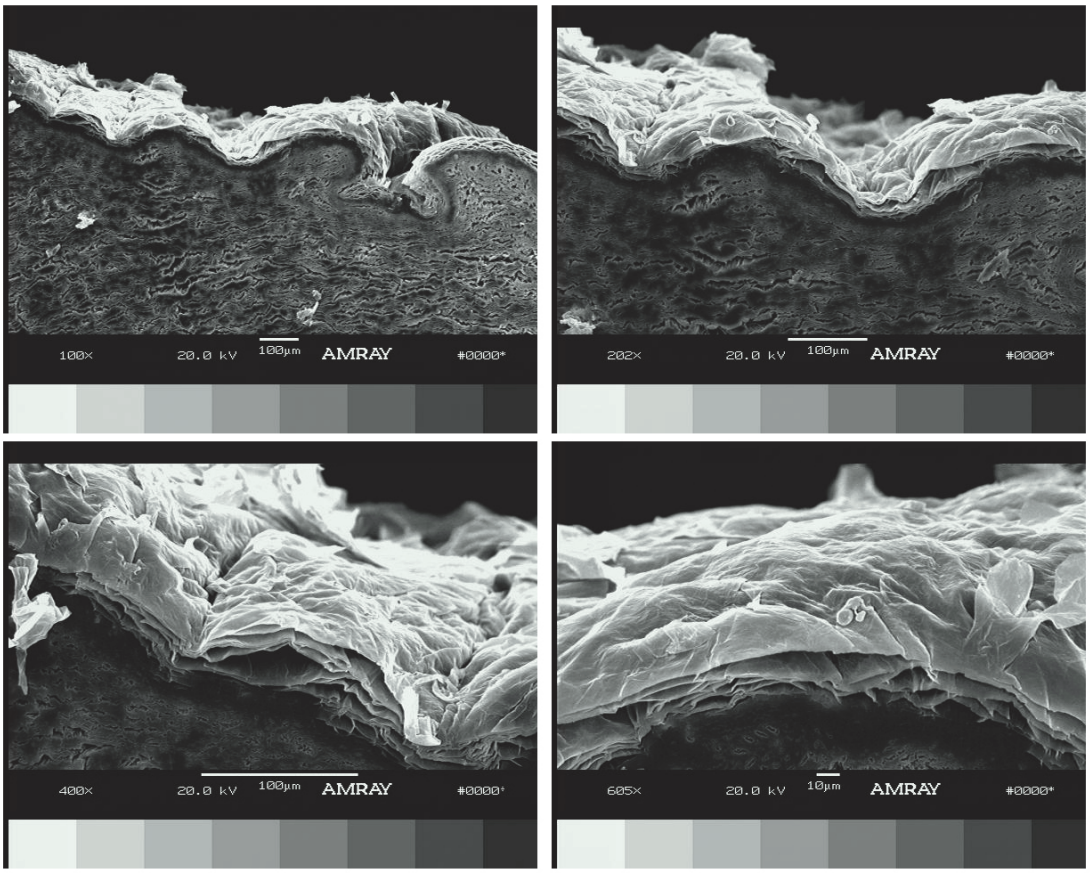

Fig. 4.10 SEM cross section of untreated porcine skin (control) at 100x (left top), 200x (right top), 400x (left bottom) and 600x (right bottom) magnification, revealing the skin structures. This skin samples were not subjected to permeation studies and are presented for comparative purposes.

Unlike the control samples shown in Fig. 4.10 presented for comparative purposes, the pictures presented in Fig. 4.11 were obtained from skin samples previously used in the permeation studies, reported in section 4.3.1. It can be observed some that some stratum corneum cells are naturally shedding, but it is seen both in the control and treated samples. Also noticed is some expected variability between the samples analyzed, mostly regarding the thickness of the stratum corneum, but changes or

damage to the skin structure caused by the CPE used that could result in permanent alterations or loss of integrity are not detected.

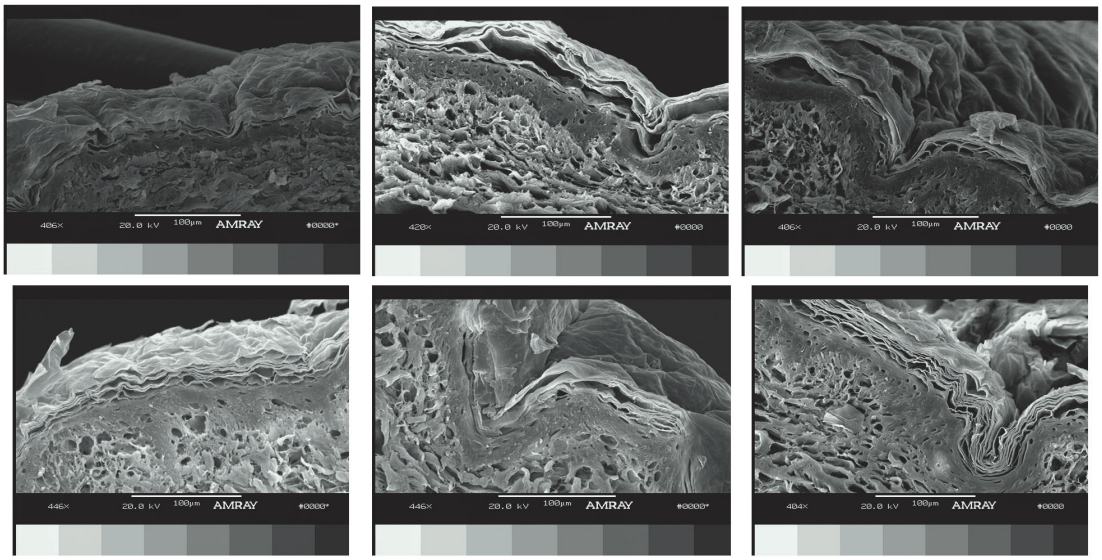

Fig. 4.11 SEM cross-section pictures of porcine skin used in the permeation studies. These samples were pretreated with various permeation enhancers: PG (left top), azone (center top), DTAB (right top), G12-2-12 (left bottom), Gemini 12-6-12 (center bottom) and G12-10-12 (right bottom) at 400x magnification.

4.3.4. Cytotoxicity studies

Skin irritation is commonly defined as a reversible inflammatory reaction produced by the arachidonic acid cascade and cytokines in the viable skin cells like keratinocytes and fibroblasts.

The determination of the cytotoxicity of the CPE used in this work was carried out by exposing cultured human epidermal keratinocytes (HEK) and human dermal fibroblasts (HDF) to various concentrations of the CPE, following the MTS assay protocol. MTT /MTS assay is generally regarded as a method that is able to provide a cost-effective, precise and reproducible index of viability for skin cells and an alternative for skin irritation assessment [347-349]. Unlike the skin tissue, the groups of cells cultured for the MTS assay is noticeably less complex in number and in cell types when compared to the skin tissue. Therefore the results should be regarded as an indication of potential and relative toxicity and irritation of the compounds to the skin cells.

Standard plots for HEK ($R^2 = 0.986$) and for HDF ($R^2 = 0.978$) were created based on the absorbance readings at 490 nm for 0, 2.000, 4.000, 6.000, 8.000 and 10.000 cells/well in order to ensure the linearity of the MTS assay method used (Fig. 4.12).

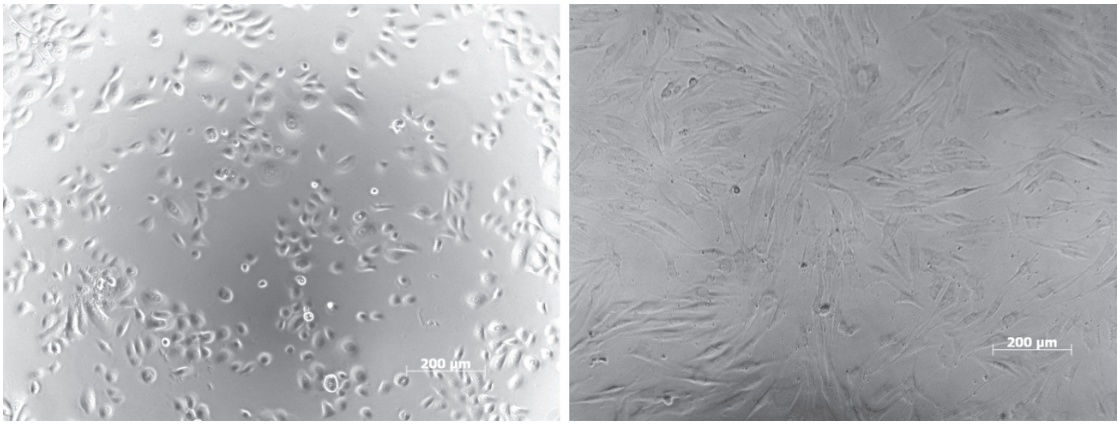

Fig. 4.12 Pictures of cultured HEK (on the left) and HDF (on the right), seeded at 8.000 cells/well in appropriate culture medium, prior to the start of the MTS assay.

The results obtained in the MTS assay are displayed in Fig. 4.13 (HEK) and in Fig. 4.14 (HDF).

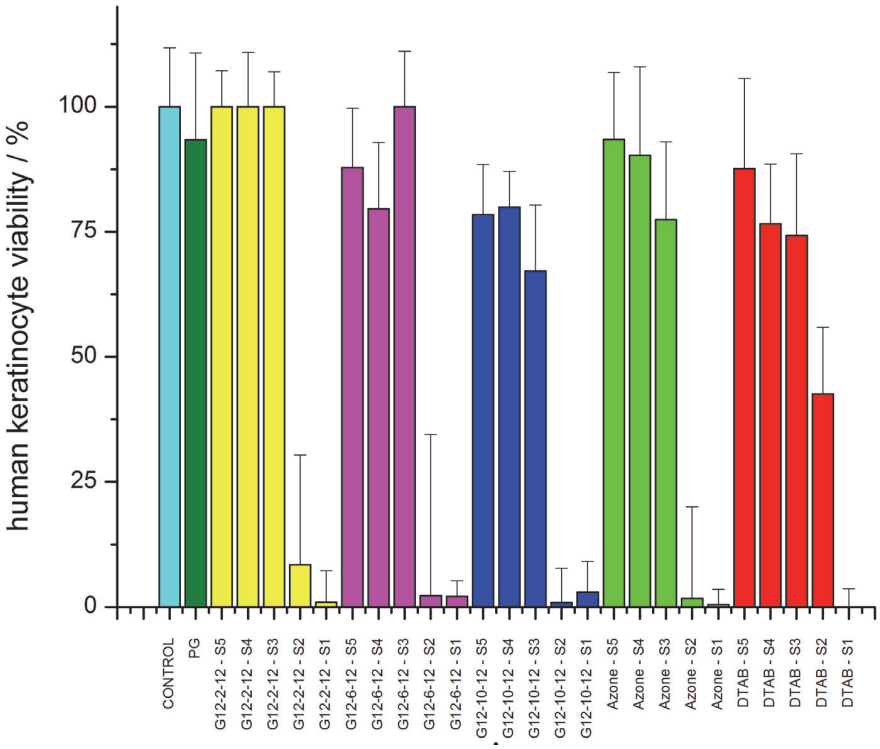

Fig. 4.13 MTS assay results for HEK. The bars represent the cell viability (%) for each permeation modifier and concentration tested. The error bars represent the standard deviation (N=6).

As shown on Fig. 4.13, PG did not significantly reduce the viability of HEK when compared to the control (cells not subjected to any CPE exposure). Therefore it can be assumed that the effect on the HEK viability is caused by the CPE and not by the vehicle where the CPE was incorporated. In opposite, when a concentration of 160 µM (S1) was applied to the cells it was observed that approximately 100% cell death occurred in all cases. The exposure to a concentration of 16 µM (S2) produced different results,

depending on the CPE used. HEK showed higher tolerance to the presence of DTAB, than for any gemini surfactants used or azone. It can also be concluded that concentrations of 1.6 μM or lower (S3, S4 and S5) are not considered harmful to the cells, as the cell viability is always close to 100%.

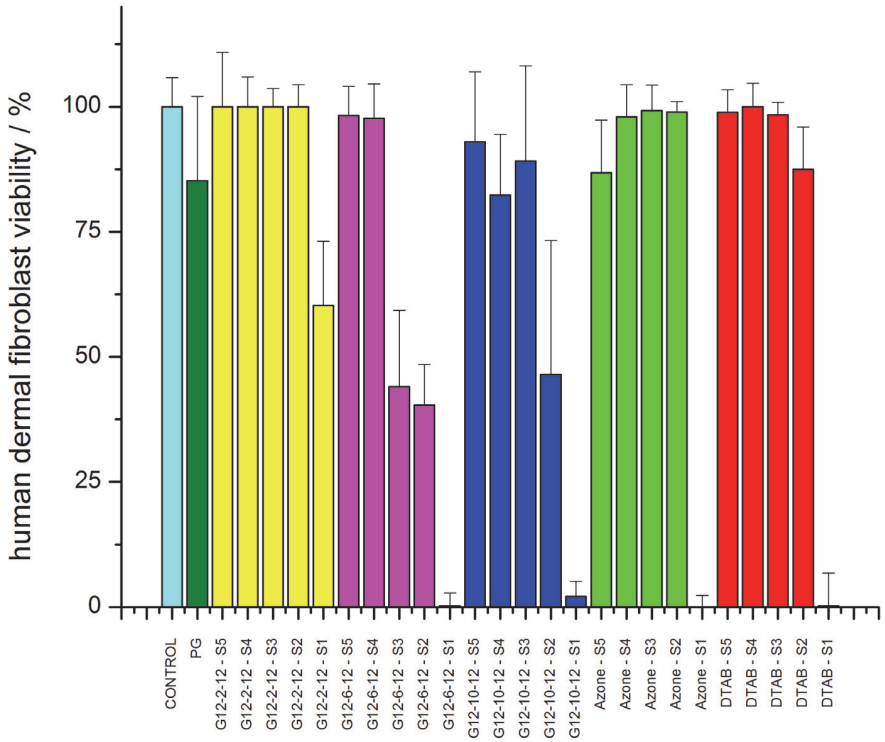

Fig. 4.14 MTS assay results for cultured HDF. The bars represent the cell viability (%) for each permeation modifier and concentration tested. The error bars stand for the standard deviation (N=6).

The results summarized in Fig. 4.14, demonstrate that HDF show higher tolerance to the presence of the CPE than HEK, as the cell viability is respectively higher for the first and lower for the later, for the same concentration of CPE employed.

PG exposure resulted in a slight reduction in HDF viability, yet not statistically significant from the control, as expected. CPE concentrations of 160 μM (S1) caused cell death in all cases except for gemini surfactant G12-2-12, where an approximately 60% of viability was observed. The presence of a concentration of 16 μM (S2) or lower of any penetration modifier did not cause a significant decrease in the HDF viability, except for enhancers G12-6-12 and G12-10-12. In both cases, cell viability was reduced in approximately 50% when HDF were exposed to a concentration of 16 μM (S2) and slightly less for a concentration of 1.6 μM (S3) only observed for G12-6-12.

A global analysis of the MTS assay results obtained with HDF suggests that the cytotoxicity of the gemini surfactants studied is dependent on spacer length. The compound with the shortest spacer, G12-2-12, was found to be less toxic to HDF when compared to the other gemini, and in fact to all CPE. We recall that both electrostatic

(headgroup charge density) and packing effects (spacer conformation and vertical positioning on the bilayer) may lie behind the structural perturbation of membranes that cause cytotoxic effects. A possible explanation for G12-2-12 effects in cultured HDF is that this gemini, as previously mentioned, may more easily fit into the lipid bilayer structure due to its cylindrical geometric shape (more akin to that of lipid molecules), thus causing less structural perturbation on the membrane. This effect, however, was not noticed in HEK, where DTAB was found to be the least destructive CPE, suggesting that for this cell line electrostatic effects (higher headgroup charge density for 12-2-12) may play a bigger role. Nevertheless, even for HEK, the shortest spacer gemini seems to be the least cytotoxic of all gemini, and even a little bit better than azone.

4.4. Conclusions

This work presents a systematic approach to the use of a series of gemini surfactants as permeation enhancers for drugs of varying hydrophobicity and belonging to different therapeutic groups. The gemini surfactant molecules differ only in the spacer length, comprising 2, 6 and 10 carbon atoms. It was observed that a maximal enhancing effect was achieved with the most hydrophilic and charged drug (lidocaine HCl). In this case, the gemini surfactant with the intermediate spacer length was the most effective. In contrast, for caffeine and ketoprofen, G12-2-12 was the most effective CPE. This suggests that this class of molecules promotes both SC perturbation and drug transport through the lipid barrier. It was also found that these compounds possess similar cytotoxic profiles to that of azone and their direct use in the skin tissue did not determine significant morphological changes. They are therefore, promising CPE candidates, essentially directed at permeation enhancing of hydrophilic drugs.

Chapter 5

A combination of nonionic surfactants and iontophoresis to enhance the transdermal drug delivery of ondansetron HCl and diltiazem HCl

The work presented in this Chapter reports the evaluation of three nonionic ether-monohydroxyl surfactants ($C_{12}E_1$, $C_{12}E_5$ and $C_{12}E_8$) as skin permeation enhancers in the transdermal drug delivery of two drugs: ondansetron hydrochloride and diltiazem hydrochloride, formulated as hydrogels. Passive and iontophoretic *in vitro* studies across dermatomed porcine skin were performed using vertical Franz diffusion cells during 24 hours. Skin integrity studies (light microscopy and SEM) were performed to assess potential harmful effects on the tissues resulting from the compounds applied and/or from the methodology employed. Complementary studies (MTT assay) were performed to gain information regarding the relative cytotoxicity of the penetration enhancers on skin cells.

5.1. Introduction

Historically, the biggest challenges in the development of transdermal drug delivery systems have focused in overcoming the skin barrier without causing harmful effects, principally local irritation.

Strategies to increase drug permeation across the skin include passive and active methods or the combination of both. The use of permeation modulators / enhancers is particularly useful since they have been reported to increase the diffusivity and/or the solubility of drugs in the skin by reversibly altering lipid organization of the SC, reducing the diffusional resistance [99, 350, 351]. Surface active agents (surfactants) comprise a

class of compounds with amphiphilic properties and, therefore, can be employed as permeation enhancers. When applied to the skin, surfactants interact with the lipid molecules, intercalating into lipid bilayers [321]. This results in interfacial defects and structure disruption causing the formation of diffusional paths for drugs molecules [60]. Depending on the amphiphilic structure and concentration employed, local irritation of skin may be observed. However, nonionic surfactants are commonly recognized to have the lowest irritating properties among all surfactant classes [309, 352].

As reported in Chapter 1, iontophoresis is a promising technique capable of extending the number of compounds that can be delivered transdermally, and is particularly useful for hydrophilic drugs and / or those with higher molecular weight. Based on the principle that like charges repel, iontophoresis consists of the application of an electrical current of low voltage to the skin, forcing the drug molecules to cross the SC. In the case of positively charged drugs such as those used in this work, drug molecules are repelled by the positive electrode (anode) into the skin, towards the negative electrode (cathode), reaching the systemic circulation. Negatively charged ions migrate in the opposite direction, closing the circuit [117, 120]. The use of chemical penetration enhancers with iontophoresis is regarded as one of the best strategies to enhance the permeation of drugs across the skin, combining the advantages of both approaches. It has been shown that in many cases the concentrations of enhancers can be reduced as well as the current levels without the loss of effectiveness of drug delivery. This approach has been extensively reported in the literature for different drugs, and in combination with different permeation enhancers [139-143, 146, 147, 353-358].

Ondansetron hydrochloride (Fig. 5.1-a) is a serotonin 5-HT3 receptor antagonist with antiemetic activity. It is used in the management of postoperative nausea and vomiting (PONV) and concomitantly with chemotherapy and radiotherapy. Despite that doses are normally expressed in terms of the base form it is also commonly administered as its hydrochloride form especially in injectable and oral dosage forms. Ondansetron undergoes a significant first-pass hepatic metabolism, which justifies the development of an alternative to the oral and injectable routes, such as the transdermal route, avoiding the gastrointestinal effects and associated pain , and promoting better patient compliance [359].

Diltiazem hydrochloride (Fig. 5.1-b) is a benzothiazepine calcium-channel blocker with peripheral and coronary vasodilator properties, used in the management of angina pectoris, cardiac arrhythmias and hypertension. Like ondansetron, it undergoes an extensive first-pass metabolism (bioavailability ca. 40%) and has been reported to cause GI disturbances, including nausea, vomiting and constipation. Therefore, the transdermal route also appears as a promising route of administration [359].

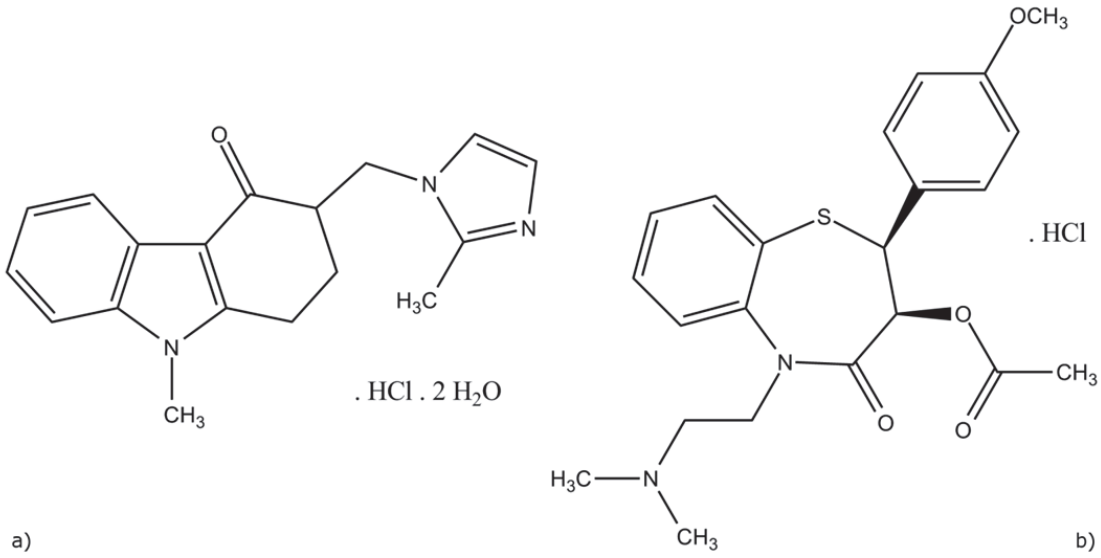

Fig. 5.1 Molecular structures of ondansetron hydrochloride dihydrate (on the left, Mw: 365.15; logP: 2.07; logD (pH5.5): 0.19) diltiazem hydrochloride (on the right, Mw: 450.14; logP: 3.63; logD (pH5.5): 0.76).

In addition, the work presented is of significant value since there are few studies in the literature reporting the transdermal use of ondansetron [360-362]. Diltiazem transdermal delivery has been the center of attention of some studies focusing on film, matrix or patch compositions alone [363-365] or concomitantly with iontophoresis [366]. Nolan and co-workers [140] studied the combined use of oleic acid as permeation enhancer and iontophoresis in the transdermal delivery of diltiazem hydrochloride and some other drugs, across human and murine skin. However, the use of various nonionic ether-monohydroxyl C_{12} surfactants, only differing from each other in the polar headgroups, as chemical permeation enhancers, or combined with iontophoresis has not been investigated to date.

The objective of the work reported here is the development of drug-loaded hydrogels suitable for transdermal drug delivery, and the evaluation of the efficacy of various nonionic ether-monohydroxyl C_{12} surfactants ($C_{12}E_1$, $C_{12}E_5$ and $C_{12}E_8$) as permeation enhancers, in the absence and presence of iontophoresis, for the drug delivery of ondansetron and diltiazem hydrochloride, across porcine skin. In addition, this work reports cytotoxicity studies (MTS assay) in human epidermal keratinocytes (HEK) and in human dermal fibroblasts (HDF), and histology and SEM studies were carried out on cells and skin tissue respectively, to evaluate potential harmful effects of the enhancers and of the methodology used.

5.2. Experimental section

5.2.1. Materials and sample preparation

Ondansetron HCl dihydrate (≥ 99%) and diltiazem HCl (≥ 99%) were purchased from Polymed Therapeutics, Inc. (Houston, TX, USA). Hydroxypropylmethyl cellulose (HPMC K15M) was a kind gift from Dow Chemical Company (USA). Propylene glycol (PG) (Reagent Plus, 99%), nonionic ether-monohydroxyl C_{12} surfactants, ethylene glycol monododecyl ether ($C12E_1$), pentaethylene glycol monododecyl ether ($C_{12}E_5$), octaethylene glycol monododecyl ether ($C_{12}E_8$), silver wire (Ag), silver chloride (AgCl) and citric acid monohydrate were purchased from Sigma Aldrich (Saint Louis, MO, USA). Indicative values of the logP and logD of the drugs and surfactants were obtained using suitable predicting software (ACD/LabsTM, Toronto, Canada). Azone was synthesized at the New Jersey Center for Biomaterials (Piscataway, NJ, USA). Phosphate buffer saline tablets (PBS) were purchased from TIC Gums (Belcamp, MD, USA). Formalin 10% was purchased from Fisher Scientific, Inc. (Torrance, CA, USA). CellTiter 96® AQueous One Solution Cell Proliferation Assay (MTS) was purchased from Promega Corp (Madison, WI, USA). Tissue-Tek® O.C.T™ Compound was purchased from Sakura Finetek USA, Inc. (Agawam, MA, USA). Porcine skin tissue was obtained from young Yorkshire pigs (26.5–28 kg, UMDNJ, Newark, NJ). Human epidermal keratinocytes (HEK) and human dermal fibroblasts (HDF) were purchased from Invitrogen™ (Carlsbad, CA, USA).

5.2.2. Hydrogel preparation

Ondansetron HCl hydrogel (pH 2.2) was composed of 2.0% (w/w) ondansetron HCl, 1.0% (w/w) HPMC K15M and deionized water. Citric acid 0.01% (w/w) was previously added to dissolve the ondansetron HCl. Diltiazem hydrogel (pH 4.4) contained 3.0% (w/w) diltiazem HCl, 1% (w/w) HPMC K15M and deionized water.

5.2.3. Porcine skin preparation

Porcine skin was obtained from young Yorkshire pigs. Prior to dermatoming, subcutaneous fat (hypodermis) was removed with a knife, avoiding contamination caused by contact with the outer layer of the skin. Porcine skin was excised and dermatomed into an approximate size of 1cm2, using a Padgett® Model B Electric Dermatome (Integra LifeSciences, Plainsboro, NJ) with 650-750 μm thickness and was stored at −80°C no more than 3 months prior to use. Immediately before the experiments, skin samples were defrosted, thawed and rinsed with water at room temperature, before immersion in PBS (pH=7.4) for 1 h to promote equilibration.

5.2.4. Preparation of Ag and AgCl electrodes

Pure silver (Ag) wire 0.5mm in diameter was used as the anode. AgCl electrode, the cathode was prepared by placing a pure silver wire and an AgCl powder coated wire in a beaker filled with 0.1 N HCl solution, both connected to a power source at 3.0 mA for 12 hours.

5.2.5. Preparation of enhancer solutions

All enhancer solutions were prepared at 0.16M in propylene glycol (PG). The enhancers tested were three nonionic ether-monohydroxyl C_{12} surfactants, ethylene glycol monododecyl ether ($C_{12}E_1$), pentaethylene glycol monododecyl ether ($C_{12}E_5$), octaethylene glycol monododecyl ether ($C_{12}E_8$) and Laurocapram / 1-dodecylazacycloheptan-2-one (azone). All enhancers were soluble in PG at the concentration used.

5.2.6. Drug delivery studies

In vitro permeation studies were carried out over a period of 24 hours in vertical Franz diffusion cells (PermeGear, Inc., PA, USA) with a diffusion area of 0.64cm^2 and a receptor compartment of 5.1 mL filled with PBS solution (pH=7.4), kept at 37°C ± 0.1 and stirred at 600 rpm. Drug loaded hydrogel (0.3 mL) was placed in each donor compartment and occluded with Parafilm® to prevent evaporation. Dermatomed porcine skin pieces (0.76 mm thickness) were placed between the donor and receptor compartments, with the epidermal side facing up. At predetermined time points (0.0, 1.0, 3.0, 5.0, 8.0, 12.0, 20.0 24.0 h), 300 μL samples were collected from the receptor compartment and immediately replaced with 300 μL of PBS solution. Samples were kept in the refrigerator prior to HPLC analysis. All the skin samples, except the control, were pretreated with 60 μL of the various enhancer solutions, for 1 h, prior to the application of the drug loaded hydrogel in the donor compartment (t = 0.0), both in passive and iontophoresis experiments. Iontophoresis experiments were carried out at 0.3mA for 8 hours (Stage 1) followed by 16 hours of passive diffusion (Stage 2), using a Phoresor II Auto (Model PM 850) as the power source. The anodal electrode (Ag) was in contact with the hydrogel formulation whereas the cathode (AgCl) was placed inside the receptor solution. Both electrodes were connected to the power source.

5.2.7. Drug delivery studies

All samples were analyzed using HPLC. The system consisted of an Agilent HP 1100 series with an autosampler, equipped with a quaternary pump and a VMD detector and an Agilent Chemstation. A reverse-phase C18 column (150 x 4.6mm C18 (2) 100 A Luna 5μm, Phenomenex®) with a guard column was the stationary phase for the Ondansetron

HCl assay, at 25°C. The mobile phase consisted of methanol and PBS (pH=7.4) at 65:35. The flow rate was set to 1.0mL/min and the injection volume was 20μL. Ondansetron HCl was detected at 310nm and the retention time was ca. 5 minutes. The method showed a linear response in the 0.1-500 μg range (R^2 = 1.0000) with a daily RSD < ±3.0%. Diltiazem HCl was detected at 240 nm using a reverse-phase C18 column (150 x 4.6mm C18 Luna 5μm, phenyl-hexyl, Phenomenex®) with a guard column as the stationary phase at 25°C. The mobile phase was prepared by mixing 4 volumes of methanol with 1 volume of water. The pH was then adjusted to 3.3 with glacial acetic acid. Final pH was adjusted to 6.6 using TEA. The flow rate was set to 1.2 mL/min and the injection volume was 20 μL. The retention time was ca. 3.3 minutes. The method showed a linear response in the 0.01-100 μg range (R^2 = 1.0000) with a daily RSD < ±3.0%.

5.2.8. Data analysis in the permeation studies

The steady flux at time *t* (J, μg.cm^{-2}) was calculated from the slope of the linear portion of the plot of cumulative drug amount permeated vs. time. Q_8 and Q_{24} refer respectively to the cumulative drug amount present in the receptor fluid after 8 and 24 hours. The enhancement ratio (ER) for flux was calculated using

$$ER = \frac{\text{flux for treated skin with enhancer or iontophoresis or their combination}}{\text{flux for untreated skin}} \qquad (5.1)$$

Results are presented as mean ± standard deviation (S.D.) (*N*), where *N* is the number of replicates. Flux values were examined for significance using unpaired Student's t test. The *p* value was set at 0.05, meaning that if $p < 0.05$, there was statistical significance between the control and the enhancers tested.

5.2.9. Skin integrity evaluation

Morphological changes and integrity evaluation was carried out by analyzing the structure of the skin by means of light microscopy and scanning electron microscopy of the samples used in the permeation studies. After permeation experiments, skin samples were immediately rinsed with deionized water, carefully dried and stored at –80°C until further use.

5.2.9.1. Histology studies

Skin samples used in the permeation studies were carefully sectioned and fixed using 10% buffered formalin for 24 hours at room temperature. Skin samples were subsequently dehydrated with 50%, 75%, 95% and 2 changes of 100% absolute ethanol for 1 hour each. Samples were embedded in Tissue-Tek® O.C.T. compound and frozen using carbon dioxide (dry ice) [338]. Cross-section slices of 7μm thickness were obtained

using a microtome (Leica Model CM 1850, Leica Microsystems, Inc. Bannockburn, IL, USA) and were stained following Ellis Hematoxylin and Eosin (H&E) staining protocol [339].

The stained slices were analyzed using a Nikon Eclipse E 800 light microscope (Micro Optics, Cedar Knolls, NJ, USA) at 10, 20 and 40 x. A Nikon Digital Camera (Model DXM 1200) was used to capture images. Images were processed using SPOT TM Imaging Software, Version 5.0 (Diagnostic Instrument, Inc., Sterling Heights, MI, USA).

5.2.9.2. Scanning Electron Microscopy studies

Skin samples were submerged in Tissue-Tek® O.C.T. Compound and frozen using dry ice. Cross-section slices of the frozen samples were cut with 10 μm thickness using a microtome (Leica Model CM 1850, Leica Microsystems, Inc. Bannockburn, IL, USA). The samples were defrosted and fixed using 4% formaldehyde for 1.5 hours. Following to this, skin samples were rinsed and placed in deionized water, at room temperature, for 2 hours. Samples were dehydrated using solutions of 30%, 50%, 75%, and 95% ethanol in water for 25 minutes and finally, skin samples were placed in two changes of absolute ethanol (100%) for 2 hours at room temperature. The dehydrated samples were dried with a critical-point drier (model CPD 020) and coated with gold. Surface and cross-sections pictures of the samples were taken using Scanning Electron Microscopy (SEM - model AMARY-18301).

5.2.10. Cytotoxicity studies

MTT / MTS assays are a colorimetric method used to determine the number of viable cells in cytotoxicity assays, widely reported in the literature for similar systems [340-343]. MTS reagent (CellTiter 96® AQueous One Solution Reagent) contains a tetrazolium compound [(3-(4,5-dimethylthiazol-2-yl)-5-(3-carboxymethoxyphenyl)-2-(4-sulfophenyl)-2H-tetrazolium, inner salt] which is converted by mitochondrial dehydrogenase enzymes of living cells into a colored formazan compound. The number of viable cells is directly proportional to the quantity of formazan product formed as measured by the absorbance at 490nm (Promega Corp. Protocol, 2009). The levels of formazan formed were quantified using a Microplate Power Wave X Scanning Spectrophotometer (Bio-TEK Instruments, Inc. Winooski, VT, USA).

Cytotoxicity studies were conducted both in cultured HEK and in HDF seeded at 8000 cells/well in 96-well plates under sterile conditions. The goal was to assess the toxic effects of the permeation enhancers on these types of cells. HEK were seeded in 100μL/well of Epilife® (MEPI 500CA) medium supplemented with gentamycin (Gibco®), human keratinocyte growth supplement (Gibco®) and were incubating for 24 hours at 37°C, 5% CO_2 and 90% R.H. HDF were seeded in 100μL/well of GIBCO®- Dulbecco's Modified Eagle Medium (DMEM) medium with 100IU/mL penicillin, 100 IU/mL

streptomycin and 10% fetal bovine serum. All the media and biological reagents were purchased directly from Invitrogen™, Inc. (Carlsbad, CA, USA).

After seeding, the culture medium was removed and cells were exposed to medium (control), propylene glycol (PG) and various concentrations (160, 16, 1.6, 0.16, 0.016 μM) of azone and nonionic ether-monohydroxyl C_{12}-surfactants ($C_{12}E_1$, $C_{12}E_5$ and $C_{12}E_8$) dissolved in PG and diluted in culture medium and were placed in the incubator for another 24 hours in the same environmental conditions. After the exposure, testing solutions were removed and replaced by a pre-mixed solution of MTS reagent (CellTiter 96® AQueous One Solution) and appropriate medium (Promega Corp. Protocol, 2009), and were returned to the incubator for 2 hours. After this the 96-well plates were read at 490nm using a plate reader (Microplate Power Wave X Scanning Spectrophotometer - Bio-TEK Instruments, Inc. Winooski, VT, USA).

Results are presented as % cell viability (mean ± standard deviation, N=6), *C.V.*, after background absorbance (abs), determined from "no cell" control wells, was subtracted, and was calculated according to

$$C.V. = \frac{\text{abs read in treated cells}}{\text{abs read in control (untreated) cells}} \qquad (5.2)$$

5.3. Results

5.3.1. *In vitro* permeation studies

The permeation studies were conducted essentially in two conditions, either by applying chemical permeation enhancer solutions alone or in combination with iontophoresis.

5.3.1.1. Effect of the penetration modifiers on the transdermal drug delivery of ondansetron HCl

Three nonionic ether-monohydroxyl C_{12} surfactants ($C_{12}E_1$, $C_{12}E_5$ and $C_{12}E_8$) and Azone were dissolved in PG (0.16 M) and applied to the skin (60 μL) one hour prior to the application to the skin of 0.3 ml of 2% ondansetron HCl loaded hydrogel.

The permeation parameters (Flux, Q_{24} and ER) are presented in Table 5-1.

Table 5-1 Effect of the chemical permeation enhancers on percutaneous permeation of ondansetron HCl across porcine skin. Data are presented as means ± S.D. (5≤N≤8).

Penetration modifier	Flux (μg cm^{-2} h^{-1})	Q_{24} (μg cm^{-2})	ER
Control (drug-loaded hydrogel only)	0.043 ± 0.14	0.8 ± 0.28	
Propylene glycol (PG)*	0.41 ± 0.27	8.68 ± 5.87	9.5
0.16M $C_{12}E_1$ in PG*	1.12 ± 0.21	23.32 ± 4.66	26
0.16M $C_{12}E_5$ in PG*	4.59 ± 0.78	93.41 ± 15.63	107
0.16M $C_{12}E_8$ in PG*	2.00 ± 0.69	38.53 ± 13.02	47
0.16 M Azone in PG	0.061 ± 0.020	0.98 ± 0.38	1.4
* Statistically significant difference between enhancer and control, at $p < 0.05$ (Student's *t*-test)			

All the permeation modifiers tested showed statistically significant enhancement ($p < 0.05$), except azone, and the nonionic surfactant $C_{12}E_5$ (ER=107) resulted in the highest permeation of ondansetron HCl of all the permeation modifiers.

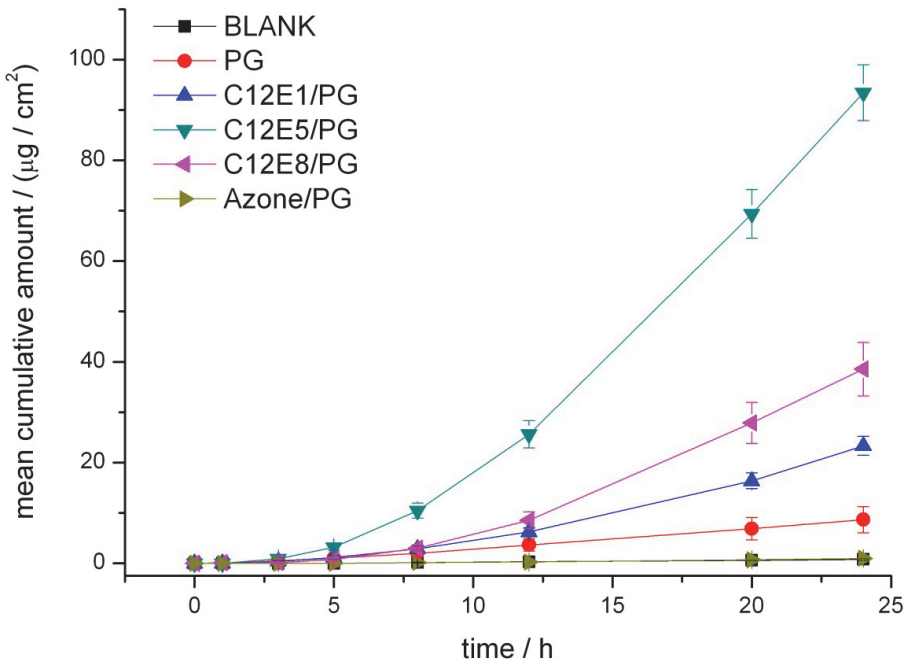

Fig. 5.2 Cumulative amount of ondansetron HCl permeated across porcine skin as a function of time. Skin was pretreated with various nonionic ether-monohydroxyl C_{12} surfactants 1 hour prior the start of *in vitro* experiments. Data is presented as means ± S.E.M. (5≤N≤8).

It is worth noting that the pretreatment with the vehicle (PG) caused an approximately 10 fold increase in the flux and 117 fold increase in the Q24, but this was clearly lower than the effect observed for the surfactants C12E1 (ER=26), C12E5 (ER=107) and C12E8 (ER=47). It should be recalled that these results have shown to be reproducible, with relative standard deviations typically between 25 and 33%.

Surprisingly, Azone had little effect and no statistical difference from the control was found. The permeation profile of the cumulative amounts of ondansetron HCl permeated across the skin over a period of 24 h is presented in Fig. 5.2.

5.3.1.2. Combined effect of the pre-treatment with penetration modifiers and iontophoresis on the transdermal drug delivery of ondansetron HCl

The combined effects of penetration modifiers and iontophoresis in the transdermal permeation of ondansetron HCl were also investigated. Similarly to the previous experiments, all the enhancers were dissolved in PG and applied to the skin 1 h prior the start of the experiment. Despite in vitro permeation experiments were carried out over a period of 24 hours, iontophoresis (0.3 mA) was only employed in the first 8 h (stage 1), followed by a post-iontophoresis passive diffusion period of 16 h (stage 2). Results are summarized in Table 5-2 (stage 1) and in Table 5-3 (stage 2).

Table 5-2 Combined effects of chemical permeation enhancers and iontophoresis (0.3mA, 8 h - stage 1) on the percutaneous permeation of ondansetron HCl across porcine skin. Data are presented as means ± S.D. (*N*=6).

Penetration modifier	Flux ($\mu g\ cm^{-2}\ h^{-1}$)	Q_8 ($\mu g\ cm^{-2}$)	ER
Control (only formulation)	16.35 ± 3.46	128.30 ± 25.83	
Propylene glycol (PG)	14.57 ± 2.78	112.31 ± 21.80	-
0.16M $C_{12}E_1$ in PG*	22.66 ± 3.76	173.48 ± 29.68	1.4
0.16M $C_{12}E_5$ in PG*	20.79 ± 3.20	159.63 ± 24.13	1.3
0.16M $C_{12}E_8$ in PG	15.24 ± 3.36	117.47 ± 26.84	-
0.16 M Azone in PG	12.12 ± 0.81	93.19 ± 5.73	-
* Statistically significant difference between enhancer and control at $p < 0.05$ (Student's *t*-test)			

Table 5-3 Combined effects of chemical permeation enhancers and iontophoresis on the percutaneous permeation of ondansetron HCl across porcine skin. Data pertain to post-iontophoresis period (0.0mA, 16h – stage 2), and are presented as means ± S.D. (*N*=6).

Penetration modifier	Flux ($\mu g\ cm^{-2}\ h^{-1}$)	Q_{24} ($\mu g\ cm^{-2}$)	ER
Control (only formulation)	5.50 ± 0.46	220.29 ± 24.99	
Propylene glycol (PG)	5.86 ± 1.12	208.91 ± 35.50	1.1
0.16M $C_{12}E_1$ in PG	6.99 ± 0.47	289.73 ± 37.22	1.3
0.16M $C_{12}E_5$ in PG*	10.74 ± 1.87	336.33 ± 48.03	2.0
0.16M $C_{12}E_8$ in PG*	11.84 ± 0.95	312.62 ± 25.34	2.15
0.16 M Azone in PG	5.29 ± 0.66	175.94 ± 6.88	-
* Statistically significant difference between enhancer and control at $p < 0.05$ (Student's *t*-test)			

Results showed that iontophoresis (0.3 mA, 8 h) caused a dramatic increase in the flux of ondansetron hydrochloride ranging between 5-fold for skin samples treated with $C_{12}E_5$

and 380 fold for the control samples (formulation only). The effect of the enhancers is barely noticed when iontophoresis is employed, because the contribution of the latter suppressed the contribution of the penetration modifiers, as expected. However, surfactants $C_{12}E_1$ and $C_{12}E_5$ still caused a noteworthy effect on the flux values, respectively 40% and 30%, which are statistically different from the control in stage 1 (Table 5-2). The increase is therefore substantial in absolute value, especially if compared with the permeated amounts obtained in the passive process. In stage 2 (Table 5-3), after iontophoresis was turned off, the flux values decreased as expected. However, skin samples treated with $C_{12}E_5$ and $C_{12}E_8$ showed statistically higher values than those observed for the control samples with an ER of 2. The analysis of Q_{24} values showed that the combined use of iontophoresis and nonionic surfactants $C_{12}E_5$ and $C_{12}E_8$ caused an approximately 400-fold increase in the cumulative amount of drug permeated in 24 h, in comparison with the passive diffusion in untreated skin (control), and an approximately 40-fold increase comparatively to the passive PG pretreated skin. The profiles obtained in these permeation experiments are summarized in Fig. 5.3.

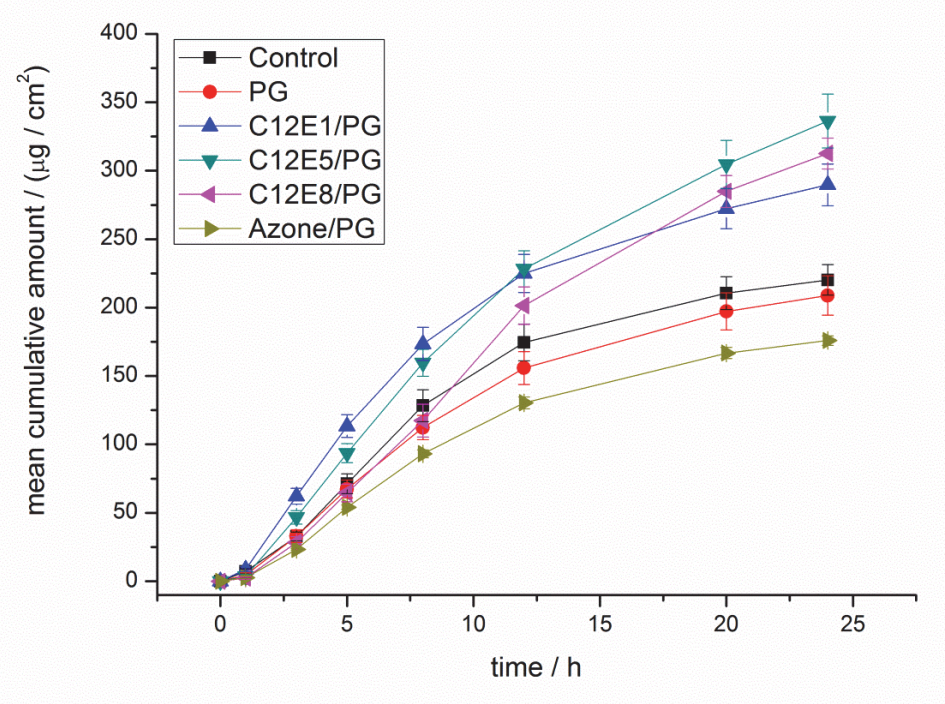

Fig. 5.3 Cumulative amount of ondansetron HCl permeated across porcine skin as a function of time. Skin was pretreated with various nonionic ether-monohydroxyl C_{12} surfactants 1 hour prior the start of in vitro experiments. Iontophoresis (0.3mA) was applied during the first 8 hours (stage 1), followed by a 16 h passive permeation. Data are presented as means ± S.E.M. (N=6).

5.3.1.3. Effect of the penetration modifiers on the transdermal drug delivery of diltiazem HCl

An identical study was carried out using diltiazem hydrochloride as the model drug. Passive diffusion experiments showed that all nonionic surfactants tested increased significantly the permeation of diltiazem HCl. The increase observed when azone was

employed was not statistically significant. $C_{12}E_5$ was found to be the most efficient penetration modifier tested, leading to a 9.4 fold increase in the flux values, as compared to control (Table 5-4). The profiles of the permeation experiments are summarized in Fig. 5.4.

Table 5-4 Effect of the chemical permeation enhancers on percutaneous permeation of diltiazem HCl across porcine skin. Data are presented as means ± S.D. (3≤N≤7).

Penetration modifier	Flux (μg cm^{-2} h^{-1})	Q_{24} (μg cm^{-2})	ER
Control (only formulation)	0.71 ± 0.26	13.53 ± 4.41	
Propylene glycol (PG)	0.55 ± 0.064	7.59 ± 1.34	-
0.16M $C_{12}E_1$ in PG*	3.98 ± 1.72	77.83 ± 37.07	5.6
0.16M $C_{12}E_5$ in PG*	6.68 ± 1.11	137.85 ± 29.40	9.4
0.16M $C_{12}E_8$ in PG*	3.57 ± 0.90	65.36 ± 19.27	5.0
0.16 M Azone in PG	2.52 ± 1.25	50.95 ± 26.67	3.5
* Statistically significant difference between enhancer and control at $p < 0.05$ (Student's *t*-test)			

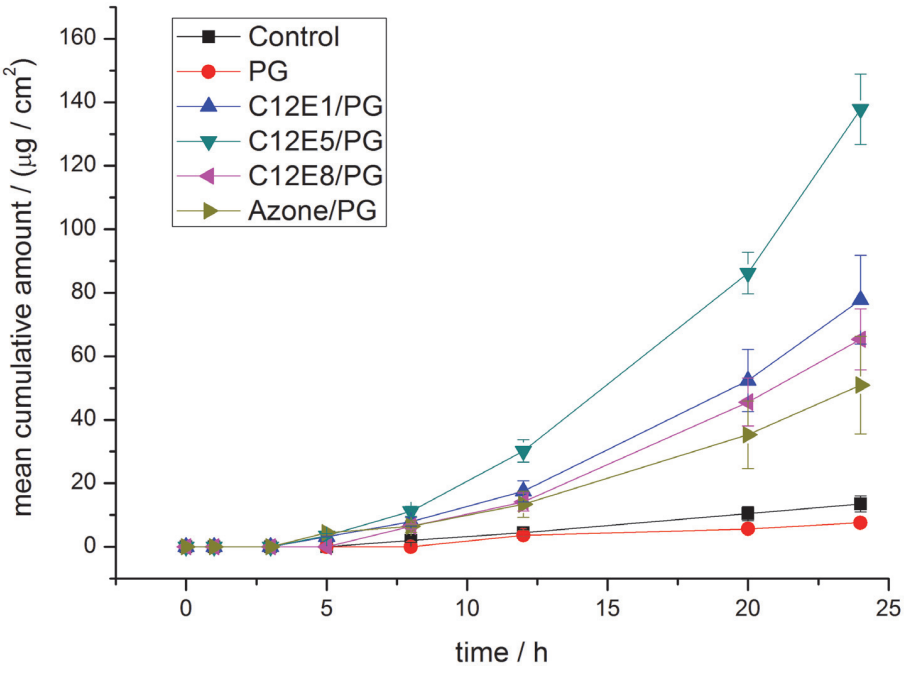

Fig. 5.4 Cumulative amount of diltiazem HCl permeated across porcine skin as a function of time. Skin was pretreated with various nonionic ether-monohydroxyl C_{12} surfactants 1 hour prior the start of in vitro experiments. Data is presented as means ± S.E.M. (3≤N≤7).

5.3.1.4. Combined effect of the pre-treatment with penetration modifiers and iontophoresis on the transdermal drug delivery of diltiazem HCl

Similarly to what was observed in the studies with ondansetron HCl, values of diltiazem flux, Q_8 and Q_{24} increased significantly following the use of iontophoresis (see the next

section). As presented in Table 5-5, in stage 1 (0-8 h), no statistically significant difference was observed between the three nonionic surfactants tested and azone. Despite the fact that the ER values are similar, $C_{12}E_8$ (1.6) and $C_{12}E_5$ (1.5) had higher activity compared to $C_{12}E_1$ (1.4) and Azone (1.3). Interestingly, PG pretreatment resulted in a significant decrease in the permeation parameters, in comparison to the control.

Table 5-5 Combined effects of chemical permeation enhancers and iontophoresis (0.3mA, 8 h - stage 1) on the percutaneous permeation of diltiazem HCl across porcine skin. Data are presented as means ± S.D. (*N*=6).

Penetration modifier	Flux ($\mu g\ cm^{-2}\ h^{-1}$)	Q_8 ($\mu g\ cm^{-2}$)	ER
Control (only formulation)	123.24 ± 12.78	964.64 ± 98.74	
Propylene glycol (PG)	102.09 ± 12.57	801.50 ± 95.49	-
0.16M $C_{12}E_1$ in PG*	166.25 ± 33.98	1289.30 ± 264.57	1.4
0.16M $C_{12}E_5$ in PG*	181.58 ± 24.74	1415.04 ± 190.55	1.5
0.16M $C_{12}E_8$ in PG*	199.00 ± 25.65	1547.02 ± 192.31	1.6
0.16 M Azone in PG*	163.07 ± 21.81	1267.69 ± 133.68	1.3
* Statistically significant difference between enhancer and control at $p < 0.05$ (Student's *t*-test)			

In stage 2 (8-16 h), the permeation parameters decreased comparatively to those for stage 1, but were clearly higher than those observed in the passive permeation study (Table 5-6). In this period, only enhancers $C_{12}E_5$ and $C_{12}E_8$ showed significantly higher permeation than the control. After 24 h of permeation, samples treated with a combination of iontophoresis (0.3mA, 8 h) and nonionic surfactants $C_{12}E_5$ and $C_{12}E_8$, reached 2530 and 2678 $\mu g/cm^2$ respectively, 1.5 and 1.6 times the amount of diltiazem HCl permeated in the control iontophoresis experiment.

Table 5-6. Combined effects of chemical permeation enhancers and iontophoresis on the percutaneous permeation of diltiazem HCl across porcine skin. Data pertain to post-iontophoresis period (0.0mA, 16h – stage 2), and are presented as means ± S.D. (N=6).

Penetration modifier	Flux ($\mu g\ cm^{-2}\ h^{-1}$)	Q_{24} ($\mu g\ cm^{-2}$)	ER
Control (only formulation)	43.78 ± 11.59	1689.87 ± 224.28	
Propylene glycol (PG)	36.49 ± 11.07	1409.43 ± 133.91	-
0.16M $C_{12}E_1$ in PG	47.76 ± 5.47	2092.71 ± 241.23	1.1
0.16M $C_{12}E_5$ in PG*	66.64 ± 13.38	2530.36 ± 286.97	1.5
0.16M $C_{12}E_8$ in PG*	66.81 ± 17.45	2678.15 ± 304.20	1.5
0.16 M Azone in PG	42.91 ± 7.48	1998.39 ± 133.68	-
* Statistically significant difference between enhancer and control at $p < 0.05$ (Student's *t*-test)			

By comparing Q_{24} values of iontophoresis (Table 5-6) against those in which this technique is absent (Table 5-4), it can be seen that the amount of drug permeated increased by ca. 200 fold when a combination of enhancer and iontophoresis was used.

The permeation profiles of diltiazem HCl across porcine skin, using a combination of iontophoresis and various enhancers are presented in Fig. 5.5.

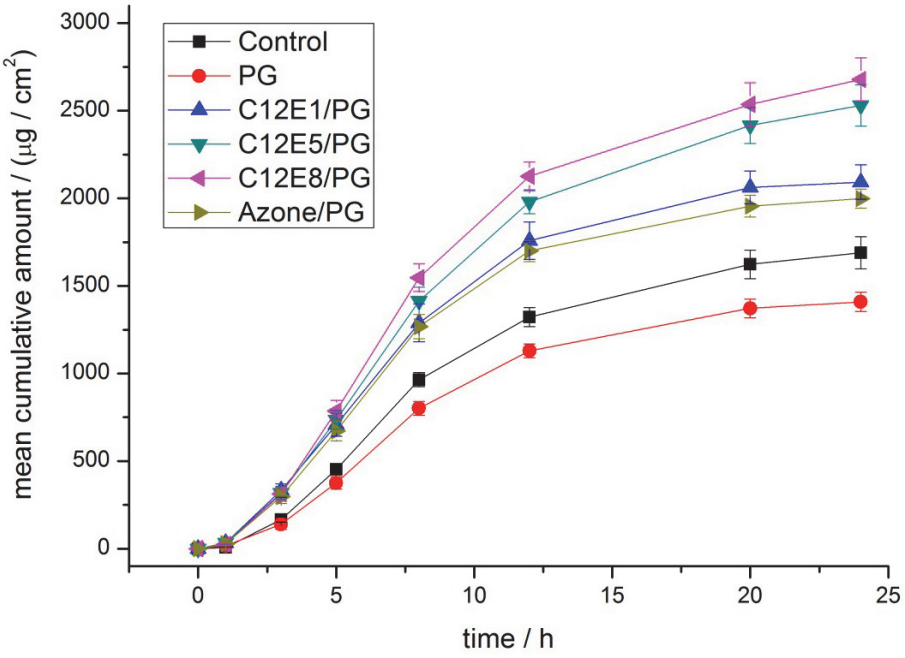

Fig. 5.5 Cumulative amount of diltiazem HCl permeated across porcine skin as a function of time. Skin was pretreated with various nonionic ether-monohydroxyl C_{12} surfactants 1 hour prior the start of in vitro experiments. Iontophoresis (0.3mA) was applied during the first 8 hours (stage 1), followed by a 16 h passive permeation. Data are presented as means ± S.E.M. (N=6).

5.3.1.5. Overview and comparison

Results show that in both in passive and post-iontophoresis stages, the enhancer with the best overall performance is $C_{12}E_5$. Despite the fact that it is very difficult to know the exact mechanism of permeation enhancement, a possible explanation for the observations will be given in what follows, based on some physico-chemical properties. The $C_{12}E_1$surfactant is the most hydrophobic compound (logP = 5.05) and is also the least effective both for passive and post-iontophoresis diffusion for both drugs. In passive diffusion, $C_{12}E_5$ (logP = 3.62) performs better for both drugs, in what seems a compromise between affinity for the lipid structures on the SC, higher for $C_{12}E_1$ and affinity for the drugs, higher for $C_{12}E_8$ (logP = 2.54). We note that, in a simple interpretation, affinity for the lipids correlates with disordering of the SC lipids, while affinity for the drug accounts for the facilitated transport of the drugs.

Also reported is the fact that $C_{12}E_5$ is more effective in association with diltiazem than ondansetron. It should be noted that in spite of the fact that the Mw of ondansetron HCl (Mw: 365.15; logP: 2.07; logD (pH5.5): 0.19) is lower than of the diltiazem HCl (Mw: 450.14; logP: 3.63; logD (pH5.5): 0.76), the former is a more hydrophilic drug, thus it permeates less in absolute values. Any increase caused by the enhancers is therefore

comparatively more significant than that for a more hydrophobic drug. This more pronounced effect occurs due to a facilitated transport of the hydrophilic drug through the lipid layers of the skin. This effect has been previously reported by A.F. El-Kattan et al.[367], where the ER of the chemical enhancers employed (terpenes) was much higher for the hydrophilic drugs and decreased with an increase in the hydrophobicity.

Fig. 5.6 and Fig. 5.7 summarize the results obtained in the permeation studies involving iontophoresis. We will first consider the data for ondansetron. Control and PG treated samples produced almost indistinguishable effects, both in stage 1, in which the electrical current was applied for 8 hours, and in the subsequent stage of 16 hours.

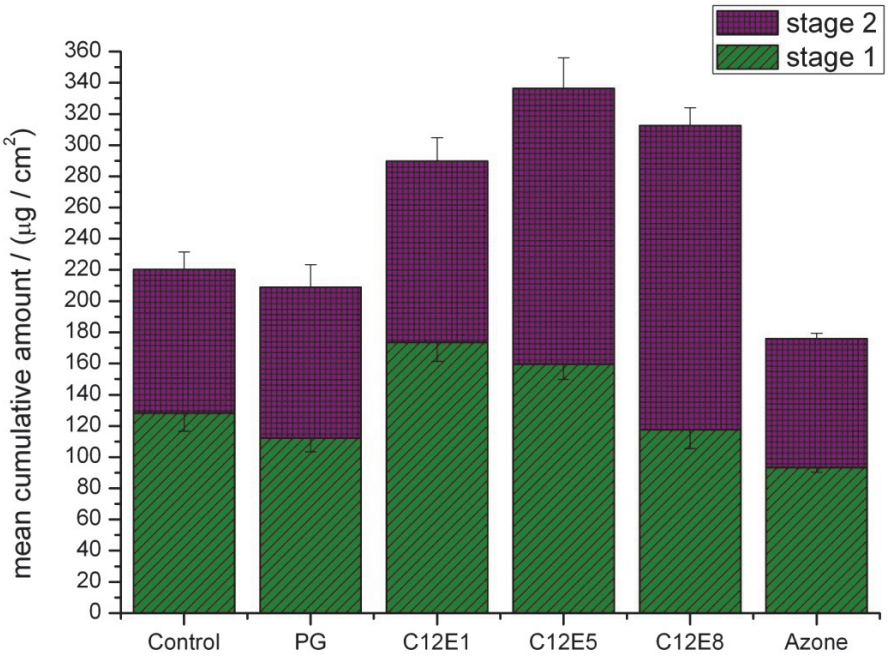

Fig. 5.6 Cumulative amount of ondansetron HCl permeated across porcine skin after 8h (stage 1) and 24h (stage 1 and 2).

Interestingly, azone treated skin displayed a slight reduction in the cumulative amount, compared to the iontophoresis control. The highest drug permeation was achieved with the surfactant treated samples. Relative to the control, the surfactants promoted drug delivery with an increase in flux between 30 and 40% in stage 1. This corresponded to a considerable amount, if we take in consideration the effect of iontophoresis and compare it to the passive process. It is seen that, also for stage 1, the samples treated with C12E1 showed the highest permeated amount of ondansetron, followed by skin samples treated with C12E5 and C12E8, respectively. Interestingly it was observed that this order was reversed in stage 2. Overall, during the 24 hours, the conjugation of the two opposite trends resulted in a maximum amount of drug permeated, when surfactant C12E5 was employed, with a slightly higher amount of drug permeated in stage 2 than during the iontophoretic stage. The latter effect was even more pronounced in samples treated with surfactant C12E8, while in the remaining samples drug permeation was higher for stage

1. For the most effective enhancer, C12E5, the enhancement ratio calculated on the basis of the total cumulative amount permeated, was 400-fold higher than that for passive control.

Data obtained with diltiazem hydrochloride showed that PG treatment caused a slight decrease in the permeated amount of drug compared to the control. However, all other enhancers tested had the opposite effect. The surfactants were again more effective than azone, and interestingly, the enhancing effect increased with increasing surfactant molecular weight. Generally, this increase was observed both in the iontophoresis and post-iontophoresis stages. It should be noted that, unlike what has been observed in studies with ondansetron, the iontophoresis stage corresponded to a permeated amount of drug which was always higher than that of stage 2. The use of $C_{12}E_8$ in combination with iontophoresis promoted the highest enhancement ratio.

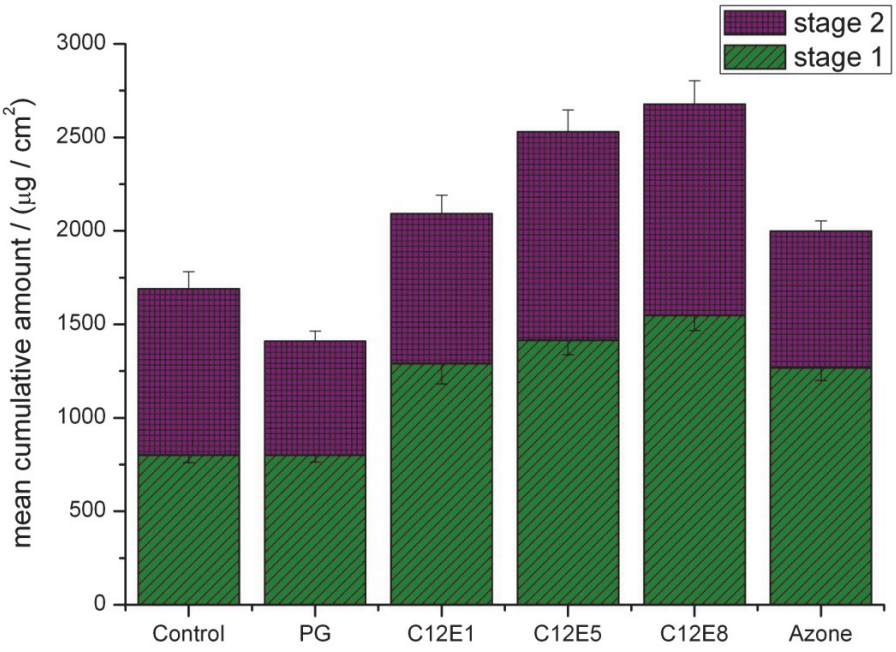

Fig. 5.7 Cumulative amount of diltiazem HCl permeated after 8h (stage 1) and 24h (stages 1 and 2).

A rough estimate based on the above results obtained with porcine skin, indicated that for the 24 hour period a total dose of ca. 8.4 mg and 67 mg would reach the blood stream for ondansetron and diltiazem, respectively, using a 5 x 5 cm^2 formulation patch. Therefore, these values show that the approaches described in this work may provide a promising strategy to obtain effective therapeutic levels for both drugs, taking into account that slightly higher values drug permeated are expected when using human skin [170, 172]. Moreover, higher blood concentrations can be reached with further formulation optimization and iontophoretic parameter adjustments (time and current intensity) applied to the skin.

5.3.2. Skin integrity evaluation

Skin samples used in permeation experiments were rinsed with water and kept frozen at −80°C until further use. Skin damage and morphological changes caused by the methodology employed (chemical penetration enhancers and iontophoresis) were assessed (light microscopy and SEM).

5.3.2.1. Histological studies

Histological procedures followed by light microscope observations at different magnifications (10, 20 and 40 x) were carried out in untreated (control) and treated skin samples. All the treated tissues were skin samples previously used as membranes in the *in vitro* permeation experiments, and subject to treatment with various penetration modifiers alone or in combination with iontophoresis.

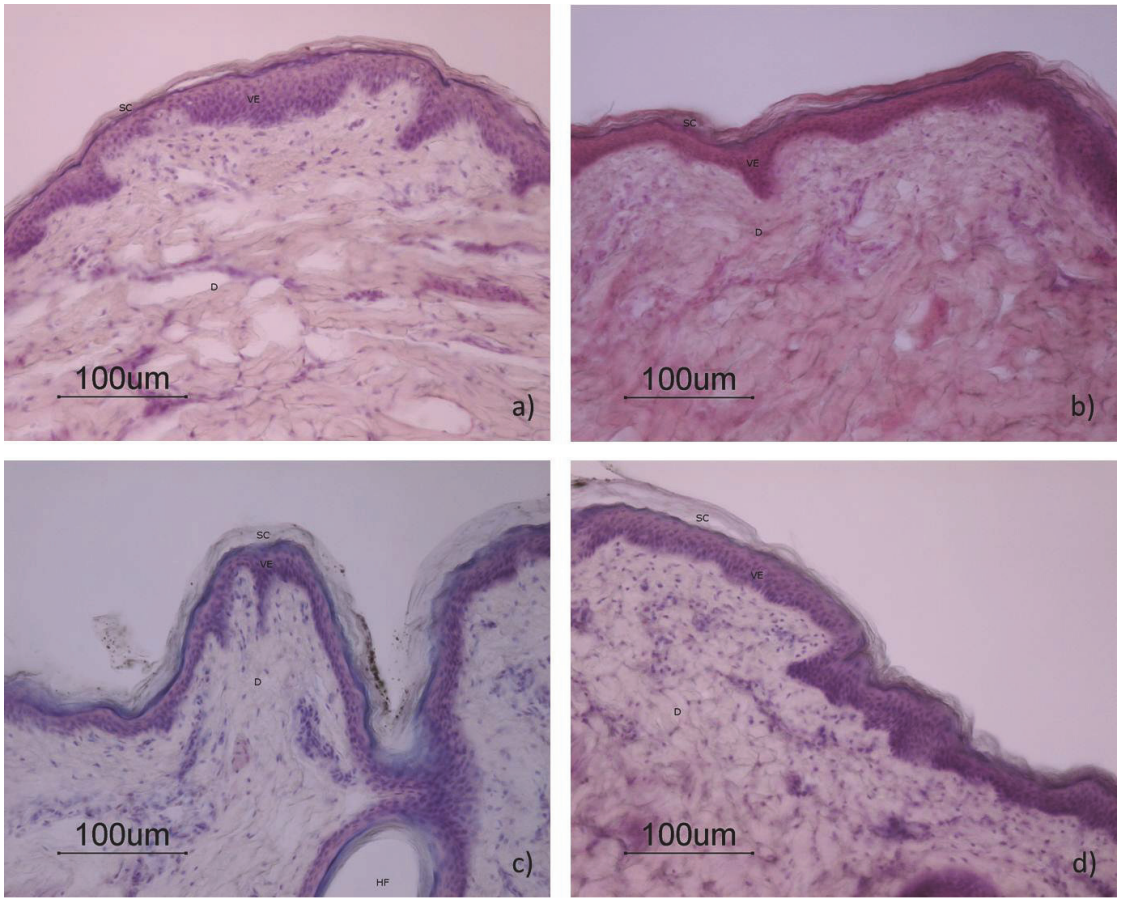

Fig. 5.8 Porcine skin pictures taken by an optical light microscope at a magnification of 20x after permeation experiments, except for the control (a), using $C_{12}E_5$ (b), $C_{12}E_5$ + iontophoresis (c), $C_{12}E_8$ + iontophoresis (d). The various skin layers and structures can be observed: stratum corneum (SC), viable epidermis (VE), dermis (D) and hair follicles (HF).

The histology work was performed on all skin samples treated with enhancers. However, we are presenting only skin samples treated with the enhancers that resulted in the most

efficient drug penetration. As can be observed in Fig. 5.8, no significant morphological or structural changes have been detected when comparing the control samples with those subjected to the combined treatment. No major changes were detected in cell morphology and cohesion, or in the level of organization of the tissues, but some areas of the SC were noted to be detaching or peeling off from the subsequent layer. However, this is also observed in the untreated samples and may be a result of sample handling. The variation observed in the properties related to the skin structure, such as the thickness of the SC, the density and depth of the rete pegs may be ascribed to inter-individual variability, and to the body area where the skin was obtained from. It is worth noting that skin samples subjected to iontophoresis exhibited small dark spots, consistent with residues of silver chloride, in the region of the SC.

5.3.2.2. Scanning Electron Microscopy studies

Scanning Electron Microscopy (SEM) studies were carried out to assess the skin integrity after the drug permeation experiments.

Skin layers such as the SC (the outermost multi-layered structure), viable epidermis (the darker area) and dermis (the thicker structure mostly composed of connective tissue under the viable epidermis) are visible in detail on the following figures (Fig. 5.9, Fig. 5.10 and Fig. 5.11).

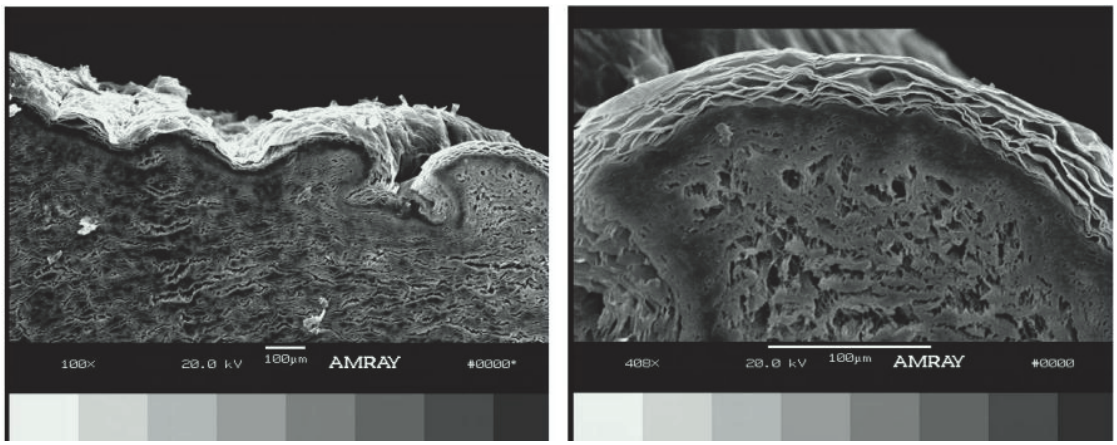

Fig. 5.9 SEM cross section of untreated porcine skin (control) at 100x and 400x magnification. This skin sample was not subjected to permeation studies.

It was observed that all the thirteen skin samples tested retained the cell-to-cell and layer-to-layer cohesion and their macroscopic structure after the cryo-SEM procedure. Despite all the treatments, the tissues remained compact, well stacked and with the same level of organization observed in untreated skin samples. By looking at the skin surface it can be seen that some corneocytes of the outermost layer of the SC were being shed, a normal process of skin cells renewal known as desquamation (as previously noted in the optical microscopy observations).

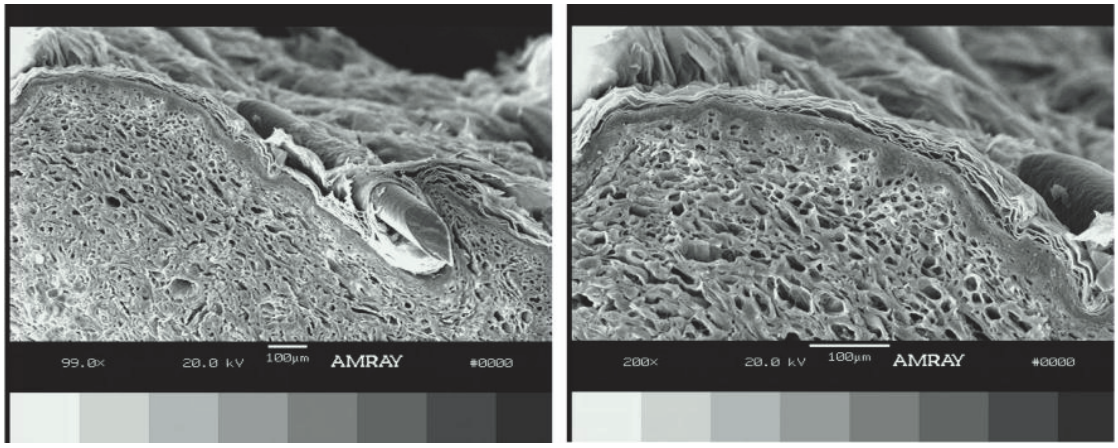

Fig. 5.10 SEM cross-section pictures of porcine skin treated with nonionic surfactant $C_{12}E_8$ at 100x and 200x magnification taken after permeation studies. On the left picture, a hair filament in the dermis is visible.

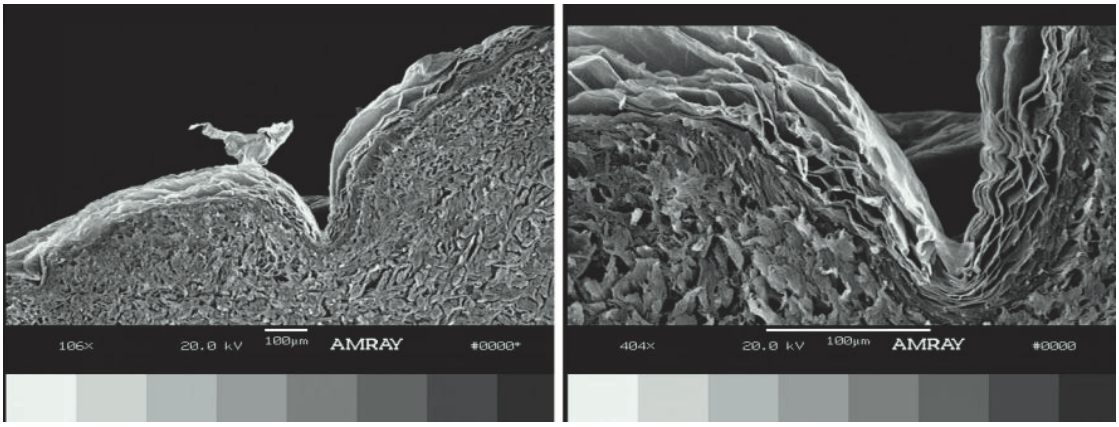

Fig. 5.11 SEM cross-section pictures of porcine skin treated with nonionic surfactant $C_{12}E_5$ and iontophoresis (0.3mA, 8h) at 100x and 400x magnification.

However, it can also be observed that, despite some swelling of the SC caused by the large amounts of water present in the drug-loaded hydrogels, the corneocytes of the SC are very well packed and in close contact with each other, providing the high organization needed for maintaining its barrier properties. Therefore, it can be concluded that no major differences were found between the control and the treated samples in terms of skin integrity.

5.3.3. Cytotoxicity studies

The potential cytotoxicity of the chemical penetration modifiers used was assessed by exposing cultured HEK and HDF to different concentrations of these compounds, and by evaluating and comparing the change in the mitochondrial metabolic activity of those cells using the MTS assay.

Standard plots for HEK ($R^2 = 0.986$) and for HDF ($R^2 = 0.978$) were constructed based on the absorbance readings at 490 nm for 0, 2.000, 4.000, 6.000, 8.000 and 10.000 cells/well to ensure the linearity of the MTS assay method used (see Fig. 4.12).

The results obtained in the MTS assays are presented in Fig. 5.12(HEK) and in Fig. 5.13(HDF).

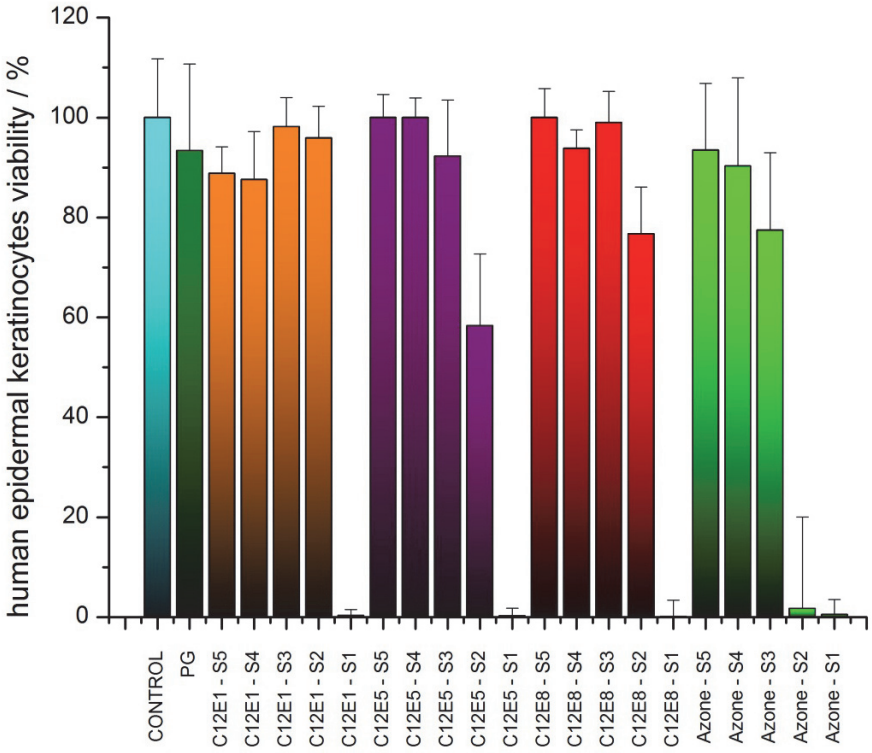

Fig. 5.12 MTS assay results for cultured HEK. The bars represent the cell viability (%) for each permeation modifier and concentration tested. The error bars stand for the standard deviation (N=6).

As can be seen on Fig. 5.12 PG did not significantly reduce the viability of HEK when compared to the control (untreated cells). However, 160 μM (S1) of all the compounds was lethal for all the HEK. Azone 16 μM (S2) use resulted in cell death at nearly 100%, however, compound $C_{12}E_1$ produced no harm to the cells. The same concentration of $C_{12}E_5$ and $C_{12}E_8$ caused, respectively, a cell viability reduction of 40% and 25%. Concentrations of 1.6 μM (S3) or lower (0.16 μM (S4) and 0.016 μM (S5)) of any of the enhancers did not cause significant cell viability reduction, except in the case of azone.

The MTS assay using HDF showed that the HDF exhibited higher tolerance to the permeation modifiers compared to the HEK. PG caused cell death to a higher extent than in the case of HEK, but this was not statistically significant. Concentrations of 16 M (S2) or lower of any penetration modifier did not cause a significant decrease in the HDF viability. A concentration of 160 M (S1) of any of the compounds tested was lethal to all the cells except in the case of the nonionic surfactant C12E1. Results obtained both in

HEK and in HDF suggest that the toxicity of the nonionic surfactants tested is molecular weight dependent.

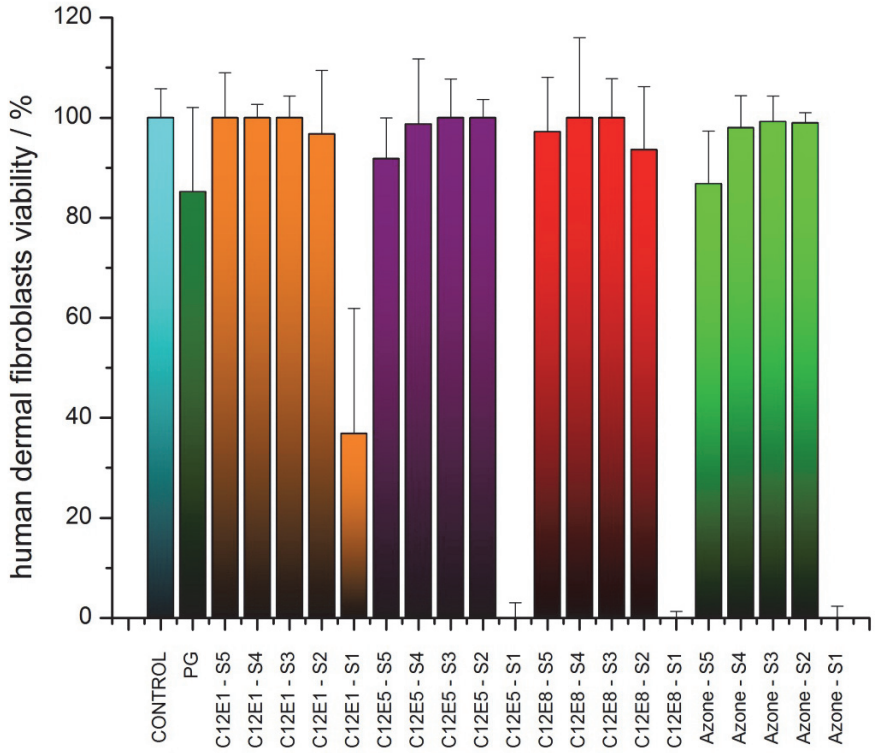

Fig. 5.13 MTS assay results for cultured HDF. The bars represent the cell viability (%) for each permeation modifier and concentration tested. The error bars stand for the standard deviation (N=6).

5.4. Conclusions

The results presented show that the nonionic ether-monohydroxyl surfactants tested were effective skin penetration enhancers for the transdermal drug delivery of ondansetron hydrochloride and diltiazem hydrochloride. The enhancement effects observed were dependent on the penetration modifier and on the drug used. Pentaethylene glycol monododecyl ether ($C_{12}E_5$), produced the highest flux values and cumulative amounts of drug permeated (Q_{24}) observed in the passive transdermal studies of both ondansetron hydrochloride (*ER* = 107) and diltiazem hydrochloride (*ER* = 9.4). The combined use of the chemical penetration enhancers and iontophoresis (0.3mA - 8h) significantly increased the amount of drugs permeated. Despite the fact that the major contribution in terms of drug permeation was derived from the iontophoresis transport, the various chemical penetration enhancers produced different levels of activity. The best results in terms of drug permeated were obtained with the combination of iontophoresis and the enhancer pentaethylene glycol monododecyl ether ($C_{12}E_5$) (*ER* = 420, compared to passive permeation without enhancer pretreatment) for ondansetron hydrochloride while octaethylene glycol monododecyl ether ($C_{12}E_8$) (*ER* = 200, compared to passive permeation without enhancer pretreatment) performed better with diltiazem

hydrochloride. Skin integrity evaluation studies did not show significant changes in the tissue morphology when compared to the untreated samples suggesting that these compounds are promising candidates for use in transdermal formulations. The present results suggest that both drugs can be successfully delivered through the skin using a combination of chemical enhancement and iontophoresis, attaining plasma levels comparable to those obtained with oral formulations

Concluding remarks

Transdermal drug delivery consists of the transport of pharmaceutical actives to the human body through intact skin aiming at a therapeutic effect. Overall, transdermal drug delivery offers interesting opportunities to address the low bioavailability of many oral drugs, the pain and inconvenience of injections, and the limited controlled-release options of both. However, the stratum corneum, the outer layer of the epidermis, is a formidable barrier to drug penetration, limiting transdermal bioavailability. For this reason, only a limited number of drugs have been successfully delivered via the transdermal route.

The work reported in this dissertation highlights the importance of combining different strategies to increase the permeation of drugs across the skin, without causing skin irritation or damage. It relies on fundamental approaches for the study of the formulation, based on HPMC hydrogels, including systems containing surfactants. Additionally, it contains a detailed assessment of the enhancing capabilities of various surfactants, including a series of cationic alkylammonium bromide gemini surfactants and nonionic ether-monohydroxyl surfactants for various drugs, with different physicochemical properties and therapeutic indications.

In what concerns the study of the thermal behavior of HPMC hydrogels, it was possible to establish various characteristic temperatures that were identified in the HPMC thermogelation process, based on different techniques. It was found that, as the system is heated, HPMC polymer chains become more hydrophobic and eventually start to aggregate in macroscopic clusters as confirmed by the clouding observed in the polymeric solutions. Random entanglements responsible for the viscosity at room temperature are progressively replaced by hydrophobic interactions. Upon further heating, these clusters associate in a three-dimensional network and gelation is detected.

In the study of the interaction between HPMC and SDS, the latter was chosen since anionic surfactants generally interact with different types of water-soluble polymers, in contrast to cationic ones in which a higher degree of counterion binding is observed. This made it simpler to analyze the interaction starting at minute concentrations of the surfactant, and allowed establishing an appropriate methodological approach which may be transposed to other systems containing different polymers and surfactants. Data obtained from electrical conductivity, rheological and optical transmittance techniques were crucial to understand the mechanism of polymer-surfactant interaction and how it affects the process of surfactant micellization and polymer thermal gelation. It was found that the presence of SDS causes an increase in the gelation temperature and that, for higher concentrations of SDS, gel formation is inhibited. Studies at room temperature showed that the interaction between HPMC and SDS occurs in three distinct stages: pre-*critical aggregation concentration (cac)*, between *cac* and *polymer saturation point (psp)* and after *psp*. Additionally, the free energy of micellization of SDS indicates that this phenomenon is independent of polymer concentration, up to 0.5% of polymer. For higher concentrations of the latter, SDS micellization becomes more favorable. It was also found that for a constant concentration of polymer (0.5%), SDS association becomes more favorable as the temperature increases in the range of 25-50°C. A rationale for the results has been proposed by a general model in which variations in both surfactant and HPMC concentration are included.

In the studies reporting the evaluation of a series of cationic alkylammonium bromide gemini surfactants as chemical permeation enhancers, it was found that the gemini G12-6-12 caused the highest increase in the permeation of the charged drug, lidocaine hydrochloride, attaining an approximately 5-fold enhancement, in comparison with the control. The enhancement effect observed was lower in the studies with caffeine and ketoprofen, but still statistically significant. The most effective gemini surfactant for caffeine and ketoprofen was the one with the shorter spacer, G12-2-12. However, in the case of the most hydrophobic drug, ketoprofen, azone (laurocapram) caused a slightly higher enhancement ratio, but not statistically different from that of the G12-2-12 surfactant. Results indicate that this class of compounds significantly increased the permeation of lidocaine hydrochloride, caffeine and ketoprofen and therefore are promising CPE candidates, essentially directed for enhancing permeation of hydrophilic and ionized drugs that do not easily cross the complex lipid barrier of the stratum corneum.

Additionally, a series of nonionic ether-monohydroxyl surfactants were evaluated as skin penetration enhancers for the passive and iontophoretic delivery of ondansetron hydrochloride and diltiazem hydrochloride. Not surprisingly, the enhancement effects observed were dependent on the penetration modifier and on the drug used. The highest flux values and cumulative amounts of drug permeated (Q_{24}) observed in the passive transdermal studies of both ondansetron hydrochloride (ER = 107) and diltiazem hydrochloride (ER = 9.4) was obtained using pentaethylene glycol monododecyl ether ($C_{12}E_5$). The combined use of CPEs and iontophoresis (0.3mA – 8h) considerably

increased the permeation of both drugs. The simultaneous use of $C_{12}E_5$ and iontophoresis resulted in an impressive 420-fold permeation enhancement of ondansetron hydrochloride. The combined use of octaethylene glycol monododecyl ether ($C_{12}E_8$) and iontophoresis resulted in a 200-fold flux enhancement ratio for diltiazem hydrochloride. The results obtained show that the compounds and methodology used are able to provide effective and safe therapeutic levels for both drugs. Supplementary formulation optimization and iontophoretic parameter tuning, such as time and current intensity applied to the skin, may be further adjusted in order to provide desired levels of drug permeated and, at the same time, minimize the occurrence of skin irritation problems.

Over the years, many potent enhancers have been discovered, but in most cases they are not free of toxicity / irritation issues, therefore limiting their clinical usefulness. For this reason, skin integrity evaluation studies and cytotoxicity studies in cultured human skin cells were performed in order to investigate if the surfactants investigated caused detrimental effects to the skin tissue. Despite of the fact that skin integrity evaluation studies did not reveal significant changes in the tissue morphology after the use of the several chemical enhancers, alone or in combination with iontophoresis, the long term local and systemic toxicity of the chemical enhancers in the final transdermal dosage form should be carefully assessed.

References

[1] L. Mez-Mangold, A history of drugs, F. Hoffmann-La. Roche, Basel, 1971.

[2] S. Scheindlin, Transdermal drug delivery: past, present, future, Mol Interv, 4 (2004) 308-312.

[3] J. Varvel, S. Shafer, S. Hwang, P. Coen, D. Stanski, Absorption characteristics of transdermally administered fentanyl, Anaesthesiology, 70 (1989) 928-934.

[4] S.I. Yang, H.Y. Park, W.S. Lee, H.Y. Shin, J.J. Kim, S.Y. Lee, Transdermal eperisone elicits more potent and longer-lasting muscle relaxation than oral operisone, Pharmacology, 71 (2004) 150-156.

[5] M. Cramer, S. Saks, Translating safety, efficacy and compliance into economic value for controlled release dosage forms, Pharmacoeconomics, 5 (1994) 482-504.

[6] C.A. Kormic, J. Santiago-Palma, N. Moryll, R. Payne, E.A. Obbens, Benefit-risk assessment of transdermal fentanyl for the treatment of chronic pain, Drug Saf, 26 (2003) 951–973.

[7] R. Payne, S.D. Mathias, D.J. Pasta, L.A. Wanke, W. R., M. R., Quality of life and cancer pain: satisfaction and side effects with transdermal fentanyl versus oral morphine, J Clin Oncol, 16 (1998) 1588-1593.

[8] T. Jarupanich, S. Lamlertkittikul, V. Chandeying, Efficacy, safety and acceptability of a seven-day, transdermal estradiol patch for estrogen replacement therapy, J Med Assoc Thai, 86 (2003) 836-845.

[9] D.F. Archer, V. Cullins, D.W. Creasy, A.C. Fisher, The impact of improved compliance with a weekly contraceptive transdermal system (Ortho Evra) on contraceptive efficacy, Contraception, 69 (2004) 189-195.

[10] C. Colin Long, Common skin disorders and their topical treatment,, in: K. Walters (Ed.) Dermatological and Transdermal Formulations, Marcel Dekker, New York, 2002, pp. 41-60.

[11] J.D. Bos, M.M.H.M. Meinardi, The 500 Dalton rule for the skin penetration of chemical compounds and drugs, Exp Dermatol, 9 (2000) 165-169.

[12] B.C. Finnin, Timothy M. Morgan, Transdermal penetration enhancers: Applications, limitations, and potential, J Pharm Sci, 88 (1999) 955-958.

[13] T. Yano, A. Nakagawa, M. Tsuji, K. Noda, Skin permeability of various non-steroidal antiinflammatory drugs in man, Life Sci, 39 (1986) 1043-1050.

[14] B. Berner, E.R. Cooper, Models of skin permeability, in: A.F.B. Kydonieus, B., Eds. (Ed.) Transdermal Delivery of Drugs, CRC, Boca Raton, FL, 1987, pp. 44.

[15] G.W. Cleary, Transdermal delivery systems; a medical rationale, in: V.P. Shah, H.I. Maibach (Eds.) In Topical Drug Bioavailability Bioequivalence and Penetration, Plenum Press, New York, 1993, pp. 17–68.

[16] D.J. Hogan, H.I. Maibach, Adverse dermatologic reactions to transdermal drug delivery systems, J Am Acad Dermatol, 22 (1990) 811–814.

[17] M. Murphy, A.J. Carmichael, Transdermal drug delivery systems and skin sensitivity reactions: incidence and management, Am J Clin Dermatol, 1 (2000) 361-368.

[18] A.J. Carmichael, Skin sensitivity and transdermal drug delivery: a review of the problem, Drug Safety, 10 (1994) 151-159.

[19] J. Toole, S. Silagy, A. Maric, B. Fath, E. Quebe-Fehling, P. Ibarra de Palacios, L. Laurin, M. Giguere, Evaluation of irritation and sensitisation of two 50 µg/day oestrogen patches, Maturitas, 43 (2002) 257-263.

[20] D. Southwell, B.W. Barry, R. Woodford, Variations in permeability of human skin within and between specimens, Int J Pharm, 18 (1984) 299-309.

[21] R.H. Larsen, F. Nielsen, J.A. Sørensen, J.B. Nielsen, Dermal penetration of fentanyl: Inter- and intraindividual variations, Pharmacol Toxicol, 93 (2003) 244-248.

[22] G.W. Cleary, E. Beskar, Transdermal and transdermal-like delivery system opportunities, in: Pharmatech (Ed.) Business Briefing, 2004.

[23] I. Steinsträsser, H.P. Merkle, Dermal metabolism of topically applied drugs: pathways and models reconsidered, Pharm Acta Helv, 70 (1995) 3–24.

[24] S. Baker, Transdermal Delivery Market Predicted to Reach $31.5 Billion by 2015, in: P.S. Report (Ed.), 2011.

[25] M.R. Prausnitz, R. Langer, Transdermal drug delivery, Nat Biotech, 26 (2008) 1261-1268.

[26] K.K. Jain, Transdermal Drug Delivery - Technologies, Companies & Markets, in, Jain PharmaBiotech, Basel, Switzerland, 2012.

[27] K.C. Madison, Barrier function of the skin: "La Raison d'Être" of the epidermis, J Invest Dermatol, 121 (2003) 231-241.

[28] P.M. Elias, Stratum corneum defensive functions: An integrated view, J Invest Dermatol, 125 (2005) 183-200.

[29] J.E. Riviere, Structure and function of skin, in: Dermal absorption models in toxicology and pharmacology, CRC Press, Boca Raton,, 2006.

[30] R. Wickett, M. Visscher, Structure and function of the epidermal barrier, American Journal of Infection Control, 34 (2006) S98-S110.

[31] D.N. Menton, A.Z. Eisen, Structure and organization of mammalian stratum corneum, J Ultra Mol Struct R, 35 (1971) 247-264.

[32] A.C. Williams, Structure and function of human skin, Pharmaceutical Press, London, 2003.

[33] P.M. Elias, Epidermal lipids, barrier function, and desquamation., J Invest Dermatol, 80 (1983) 44s-49s.

[34] Z. Nemes, P.M. Steinert, Bricks and mortar of the epidermal barrier, Exp Mol Med, 31 (1999) 5-19.

[35] Z. Ya-Xian, T. Suetake, H. Tagami, Number of cell layers of the stratum corneum in normal skin – relationship to the anatomical location on the body, age, sex and physical parameters, Arch Dermatol Res, 291 (1999) 555-559.

[36] R. Marks, The stratum corneum barrier: the final frontier, J Nutr, 134 (2004) 2017S-2021.

[37] M. Fartasch, I.D. Bassukas, T.L. Diepgkn, Structural relationship between epidermal lipid lamellae, lamellar bodies and desmosomes in human epidermis: an ultrastructural study, Brit J Dermatol, 128 (1993) 1-9.

[38] Y. Suzuki, J. Nomura, J. Koyama, I. Horii, The role of proteases in stratum corneum: involvement in stratum corneum desquamation, Arch Dermatol Res, 286 (1994) 249-253.

[39] T. Egelrud, A. Lundström, A chymotrypsin-like proteinase that may be involved in desquamation in plantar stratum corneum, Arch Dermatol Res, 283 (1991) 108-112.

[40] A. Lundström, T. Egelrud, Stratum corneum chymotryptic enzyme: a proteinase which may be generally present in the stratum corneum and with a possible involvement in desquamation., Acta Derm Venereol, 71 (1991) 471–474.

[41] S.A. Long, P.W. Wertz, J.S. Strauss, D.T. Downing, Human stratum corneum polar lipids and desquamation, Arch Dermatol Res, 277 (1985) 284-287.

[42] S. Motta, S. Sesana, R. Ghidoni, M. Monti, Content of the different lipid classes in psoriatic scale, Arch Dermatol Res, 287 (1995) 691-694.

[43] O. Bleck, D. Abeck, J. Ring, U. Hoppe, J.-P. Vietzke, R. Wolber, O. Brandt, V. Schreiner, Two ceramide subfractions detectable in Cer(AS) position by HPTLC in skin surface lipids of non-lesional skin of atopic eczema, J Invest Dermatol, 113 (1999) 894-900.

[44] M. Ponec, A. Weerheim, J. Kempenaar, A.M. Mommaas, D.H. Nugteren, Lipid composition of cultured human keratinocytes in relation to their differentiation, J Lipid Res, 29 (1988) 949-961.

[45] K.J. Robson, M.E. Stewart, S. Michelsen, N.D. Lazo, D.T. Downing, 6-Hydroxy-4-sphingenine in human epidermal ceramides, J Lipid Res, 35 (1994) 2060-2068.

[46] G.S.K. Pilgram, D.C.J. Vissers, H. van der Meulen, S. Pavel, S.P.M. Lavrijsen, J.A. Bouwstra, H.K. Koerten, Aberrant lipid organization in stratum corneum of patients with atopic dermatitis and lamellar ichthyosis, J Invest Dermatol, 117 (2001) 710-717.

[47] M. Lampe, A. Burlingame, J. Whitney, M. Williams, B. Brown, E. Roitman, P. Elias, Human stratum corneum lipids: characterization and regional variations, J Lipid Res, 24 (1983) 120-130.

[48] P.W. Wertz, M.C. Miethke, S.A. Long, J.S. Strauss, D.T. Downing, The composition of the ceramides from human stratum corneum and from comedones, J Invest Dermatol, 84 (1985) 410-412.

[49] M. Ponec, A. Weerheim, P. Lankhorst, P. Wertz, New acylceramide in native and reconstructed epidermis, J Invest Dermatol, 120 (2003) 581-588.

[50] M.E. Stewart, D.T. Downing, A new 6-hydroxy-4-sphingenine-containing ceramide in human skin, J Lipid Res, 40 (1999) 1434-1439.

[51] Y. Masukawa, H. Narita, E. Shimizu, N. Kondo, Y. Sugai, T. Oba, R. Homma, J. Ishikawa, Y. Takagi, T. Kitahara, Y. Takema, K. Kita, Characterization of overall ceramide species in human stratum corneum, J Lipid Res, 49 (2008) 1466-1476.

[52] J. van Smeden, L. Hoppel, R. van der Heijden, T. Hankemeier, R.J. Vreeken, J.A. Bouwstra, LC/MS analysis of stratum corneum lipids: ceramide profiling and discovery, J Lipid Res, 52 (2011) 1211-1221.

[53] P.W. Wertz, Lipids and barrier function of the skin, Acta Derm Venereol, Supp 208 (2000) 7-11.

[54] S. Motta, M. Monti, S. Sesana, R. Caputo, S. Carelli, R. Ghidoni, Ceramide composition of the psoriatic scale, BBA-Mol Basis Dis, 1182 (1993) 147-151.

[55] M. Foldvari, Non-invasive administration of drugs through the skin: challenges in delivery system design, Pharm Sci Technol To, 3 (2000) 417-425.

[56] D.T. Woodley, Importance of the dermal-epidermal junction and recent advances, Dermatology, 174 (1987) 1-10.

[57] K.A. Walters, Dermatological and Transdermal Formulations, Marcel Dekker, New York, 2002.

[58] J.E. Riviere, Dermal absorption models in toxicology and pharmacology, CRC Press, Boca Raton,, 2006.

[59] J. Hadgraft, K. Walters, Skin penetration enhancement, J Dermatol Treat, 5 (1994) 43 - 47.

[60] J. Hadgraft, Skin, the final frontier, Int J Pharm, 224 (2001) 1-18.

[61] A.S. Michaels, S.K. Chandrasekaran, J.E. Shaw, Drug permeation through human skin: Theory and invitro experimental measurement, Aiche J, 21 (1975) 985-996.

[62] P.M. Elias, Structure and function of the stratum corneum permeability barrier, Drug Dev Res, 13 (1988) 97-105.

[63] K. Tojo, Random brick model for drug transport across stratum corneum, J Pharm Sci, 76 (1987) 889-891.

[64] R.O. Potts, R.H. Guy, Predicting skin permeability, Pharm Res, 9 (1992) 663-669.

[65] W.J. Pugh, J. Hadgraft, Ab initio prediction of human skin permeability coefficients, Int J Pharm, 103 (1994) 163-178.

[66] L.A. Kirchner, R.P. Moody, E. Doyle, R. Bose, J. Jeffery, I. Chu, The prediction of skin permeability by using physicochemical data, Altern. Lab. Anim., 25 (1997) 359–370.

[67] A.J. Lee, J.R. King, D.A. Barrett, Percutaneous absorption: a multiple pathway model, J Control Release, 45 (1997) 141-151.

[68] P. Elias, S. Grayson, M. Lampe, M. Williams, B. Brown, The intercorneocyte space, in: G.P.E. R Marks (Ed.) Stratum corneum, Springer, Berlin Heidelberg New York, 1983, pp. 53-67.

[69] G. Grubauer, K. Feingold, R. Harris, P. Elias, Lipid content and lipid type as determinants of the epidermal permeability barrier, J Lipid Res, 30 (1989) 89-96.

[70] P. Elias, E. Cooper, A. Korc, B. Brown, Percutaneous transport in relation to stratum corneum structure and lipid composition, J Invest Dermatol, 76 (1981) 297-301.

[71] T. Higuchi, Physical chemical analysis of percutaneous absorption process from creams and ointments, J Soc Cosmet Chem, 11 (1960) 85-97.

[72] R.H. Guy, J. Hadgraft, Transdermal Drug Delivery - Second Edition, Revised and Expanded, Marcel Dekker, Inc., New York, Basel, 2003.

[73] A.K. Banga, Percutaneous absorption and its enhancement, in: T.F. Group (Ed.) Electrically Assisted Transdermal and Topical Drug Delivery, CRC Press, 1998.

[74] A. Naik, Y.N. Kalia, R.H. Guy, Transdermal drug delivery: overcoming the skin's barrier function, Pharm Sci Technol To, 3 (2000) 318-326.

[75] B.W. Barry, Novel mechanisms and devices to enable successful transdermal drug delivery, Eur J Pharm Sci, 14 (2001) 101-114.

[76] A.C. Williams, B.W. Barry, Penetration enhancers, Adv Drug Deliv Rev, 56 (2004) 603-618.

[77] B. Michniak, R. Thakur, Y. Wang, Essential oils and terpenes, in: Percutaneous Penetration Enhancers, Second Edition, Informa Healthcare, 2005, pp. 159-173.

[78] B.B. Michniak, M.R. Player, D.A. Godwin, C.A. Phillips, J.W. Sowell, In vitro evaluation of a series of azone analogs as dermal penetration enhancers: IV. Amines, Int J Pharm, 116 (1995) 201-209.

[79] B.B. Michniak, M.R. Player, D.A. Godwin, C.C. Lockhart, J.W. Sowell, In vitro evaluation of azone analogs as dermal penetration enhancers: V. Miscellaneous compounds, Int J Pharm, 161 (1998) 169-178.

[80] A. Davis, S.L. Raghavan, M. Pellett, J. Hadgraft, The application of supersaturated systems to percutaneous drug delivery, in: Transdermal Drug Delivery Systems, Informa Healthcare, 2002.

[81] J.C. Tsai, R.H. Guy, C.R. Thornfeldt, W.N. Gao, K.R. Feingold, P.M. Elias, Metabolic approaches to enhance transdermal drug delivery. 1. Effect of lipid synthesis inhibitors, J Pharm Sci, 85 (1996) 643-648.

[82] P.M. Elias, J. Tsai, G.K. Menon, W.M. Holleran, K.R. Feingold, The potential of metabolic interventions to enhance transdermal drug delivery, J Investig Dermatol Symp Proc, 7 (2002) 79-85.

[83] M. Mezei, Liposomes and the skin, in: G. Gregoriadis, A.T. Florence, H. Patel (Eds.) Liposomes in drug delivery, Harwood Academic, NewYork, 1993, pp. 125–137.

[84] G.M. El Maghraby, B.W. Barry, A.C. Williams, Liposomes and skin: From drug delivery to model membranes, Eur J Pharm Sci, 34 (2008) 203-222.

[85] E. Touitou, H.E. Junginger, N.D. Weiner, T. Nagai, M. Mezei, Liposomes as carriers for topical and transdermal delivery, J Pharm Sci, 83 (1994) 1189-1203.

[86] H. Schreier, J. Bouwstra, Liposomes and niosomes as topical drug carriers: dermal and transdermal drug delivery, J Control Release, 30 (1994) 1-15.

[87] G. Cevc, Transfersomes, in: Modified-Release Drug Delivery Technology, Informa Healthcare, 2002, pp. 533-546.

[88] G. Cevc, Lipid vesicles and other colloids as drug carriers on the skin, Adv Drug Deliv Rev, 56 (2004) 675-711.

[89] J.A. Bouwstra, P.L. Honeywell-Nguyen, G.S. Gooris, M. Ponec, Structure of the skin barrier and its modulation by vesicular formulations, Prog Lipid Res, 42 (2003) 1-36.

[90] B. Godin, E. Touitou, Ethosomes: new prospects in transdermal delivery, Crit Rev Ther Drug Carrier Syst, 20 (2003) 63-102.

[91] E. Touitou, N. Dayan, L. Bergelson, B. Godin, M. Eliaz, Ethosomes — novel vesicular carriers for enhanced delivery: characterization and skin penetration properties, J Control Release, 65 (2000) 403-418.

[92] L. Sheihet, P. Chandra, P. Batheja, D. Devore, J. Kohn, B. Michniak, Tyrosine-derived nanospheres for enhanced topical skin penetration, Int J Pharm, 350 (2008) 312-319.

[93] S. Heuschkel, A. Goebel, R.H.H. Neubert, Microemulsions - modern colloidal carrier for dermal and transdermal drug delivery, J Pharm Sci, 97 (2008) 603-631.

[94] B.W. Barry, Vehicle effect: what is an enhancer?, in: V.P.M. Shah, H. I., Eds. (Ed.) In Topical Drug Bioavailability, Bioequivalence, and Penetration, Plenum, New York, 1993, pp. 268-270.

[95] J.A. Bouwstra, L.J.C. Peschier, J. Brussee, H.E. Boddé, Effect of N-alkyl-azocycloheptan-2-ones including azone on the thermal behaviour of human stratum corneum, Int J Pharm, 52 (1989) 47-54.

[96] B.J. Aungst, Structure/effect studies of fatty acid isomers as skin penetration enhancers and skin irritants, Pharm Res, 6 (1989) 244-247.

[97] N. Kanikkannan, K. Kandimalla, S.S. Lamba, M. Singh, Structure-activity Relationship of Chemical Penetration Enhan-cers in Transdermal Drug Delivery, in: Curr Med Chem, Bentham Science Publishers Ltd., 2000, pp. 593.

[98] P.A. Cornwell, B.W. Barry, Sesquiterpene components of volatile oils as skin penetration enhancers for the hydrophilic permeant 5-fluorouracil, J Pharm Pharmacol, 46 (1994) 261-269.

[99] H.A.E. Benson, Transdermal Drug Delivery: Penetration Enhancement Techniques, Curr Drug Del, 2 (2005) 23-33.

[100] A.F. El-Kattan, C.S. Asbill, N. Kim, B.B. Michniak, The effects of terpene enhancers on the percutaneous permeation of drugs with different lipophilicities, Int J Pharm, 215 (2001) 229-240.

[101] R. Tupker, J. Pinnagoda, J. Nater, The transient and cumulative effect of sodium lauryl sulphate on the epidermal barrier assessed by transepidermal water loss: inter-individual

variation.The transient and cumulative effect of sodium lauryl sulphate on the epidermal barrier assessed by transepidermal water loss: inter-individual variation., Acta Derm Venereol, 70 (1990) 1-5.

[102] S.-C. Shin, C.-W. Cho, I.-J. Oh, Effects of non-ionic surfactants as permeation enhancers towards piroxicam from the poloxamer gel through rat skins, Int J Pharm, 222 (2001) 199-203.

[103] A. Nokhodchi, J. Shokri, A. Dashbolaghi, D. Hassan-Zadeh, T. Ghafourian, M. Barzegar-Jalali, The enhancement effect of surfactants on the penetration of lorazepam through rat skin, Int J Pharm, 250 (2003) 359-369.

[104] J. Shokri, A. Nokhodchi, A. Dashbolaghi, D. Hassan-Zadeh, T. Ghafourian, M. Barzegar Jalali, The effect of surfactants on the skin penetration of diazepam, Int J Pharm, 228 (2001) 99-107.

[105] M.J. Cappel, J. Kreuter, Effect of nonionic surfactants on transdermal drug delivery: I. Polysorbates, Int J Pharm, 69 (1991) 143-153.

[106] K.A. Walters, W. Bialik, K.R. Brain, The effects of surfactants on penetration across the skin, Int J Cosmetic Sci, 15 (1993) 260-271.

[107] B. Suresh, D. Rajendran, M. Sivabalan, S. Ponnusankar, S.A. Dhanaraj, S.R. Dube, Transdermal delivery of prazosin HCL with non-ionic surfactants, Indian J Pharm Sci, 59 (1997) 150-153.

[108] M. Goodman, B.W. Barry, Action of penetration enhancers on human skin as assessed by the permeation of model drugs 5-fluorouracil and estradiol. I. Infinite dose technique, J Invest Dermatol, 91 (1988) 323-327.

[109] C.M. Setty, Effect of chemical penetration enhancers on diclofenac diethylamine penetration through barrier from transdermal therapeutic system, J Pharmacy Research, (2009).

[110] H. Tanojo, H.E. Junginger, H.E. Boddé, In vivo human skin permeability enhancement by oleic acid: transepidermal water loss and fourier-transform infrared spectroscopy studies, J Control Release, 47 (1997) 31-39.

[111] E. Larrucea, A. Arellano, S. Santoyo, P. Ygartua, Combined effect of oleic acid and propylene glycol on the percutaneous penetration of tenoxicam and its retention in the skin, Eur J Pharm Biopharm, 52 (2001) 113-119.

[112] J.E. Riviere, M.C. Heit, Electrically-assisted transdermal drug delivery, Pharm Res, 14 (1997) 687-697.

[113] M.B. Brown, G.P. Martin, S.A. Jones, F.K. Akomeah, Dermal and transdermal drug delivery systems: current and future prospects, Drug Deliv, 13 (2006) 175 - 187.

[114] A.K. Banga, S. Bose, T.K. Ghosh, Iontophoresis and electroporation: comparisons and contrasts, Int J Pharm, 179 (1999) 1-19.

[115] A.K. Banga, Y.W. Chien, Iontophoretic delivery of drugs: Fundamentals, developments and biomedical applications, J Control Release, 7 (1988) 1-24.

[116] V. Srinivasan, W.I. Higuchi, M.-H. Su, Baseline studies with the four-electrode system: The effect of skin permeability increase and water transport on the flux of a model uncharged solute during iontophoresis, J Control Release, 10 (1989) 157-165.

[117] Y. Wang, R. Thakur, Q. Fan, B. Michniak, Transdermal iontophoresis: combination strategies to improve transdermal iontophoretic drug delivery, Eur J Pharm Biopharm, 60 (2005) 179-191.

[118] N. Kanikkannan, Iontophoresis-based transdermal delivery systems, Biodrugs, 16 (2002) 339-347.

[119] P. Glikfeld, C. Cullander, R.S. Hinz, R.H. Guy, A new system for *in vitro* studies of iontophoresis, Pharm Res, 5 (1988) 443-446.

[120] Y.N. Kalia, A. Naik, J. Garrison, R.H. Guy, Iontophoretic drug delivery, Adv Drug Deliv Rev, 56 (2004) 619-658.

[121] P. Batheja, D. Kaushik, L. Hu, B.B. Michniak-Kohn, Transdermal Iontophoresis, in: T. Briefings (Ed.), 2007.

[122] V. Srinivasan, W.I. Higuchi, A model for iontophoresis incroporating the effect of convective solvent flow, Int J Pharm, 60 (1990) 133-138.

[123] S.M. Sims, W.I. Higuchi, V. Srinivasan, Skin alteration and convective solvent flow effects during iontophoresis: I. Neutral solute transport across human skin, Int J Pharm, 69 (1991) 109-121.

[124] M.J. Pikal, Transport mechanisms in iontophoresis. I. A theoretical model for the effect of electroosmotic flow on flux enhancement in transdermal iontophoresis, Pharm Res, 7 (1990) 118-126.

[125] M.J. Pikal, S. Shah, Transport mechanisms in iontophoresis. II. electroosmotic flow and transference number measurements for hairless mouse skin, Pharm Res, 7 (1990) 213-221.

[126] M.J. Pikal, S. Shah, Transport mechanisms in iontophoresis. III. An experimental study of the contributions of electroosmotic flow and permeability change in transport of low and high molecular weight solutes, Pharm Res, 7 (1990) 222-229.

[127] P. Singh, H.I. Maibach, Iontophoresis in drug delivery: basic principles and applications, Crit Rev Ther Drug, 11 (1994) 161-213.

[128] Y.W. Chien, Transdermal route of peptide and protein drug delivery, Marcel Dekker Inc., New York, 1991.

[129] C. Cullander, What are the pathways of iontophoretic current flow through mammalian skin?, Adv Drug Deliv Rev, 9 (1992) 119-135.

[130] C. Cullander, R.H. Guy, Sites of iontophoretic current flow into the skin: Identification and characterization with the vibrating probe electrode, J Invest Dermatol, 97 (1991) 55-64.

[131] K. Okabe, H. Yamaguchi, Y. Kawai, New iontophoretic transdermal administration of the beta-blocker metoprolol, J Control Release, 4 (1986) 79-85.

[132] R.O. Potts, J. A. Tamada, M. J. Tierney, Glucose monitoring by reverse iontophoresis, Diabetes Metab Res Rev, 18 (2002) S49-S53.

[133] I. Vyteris, LidoSite® Patch in, 2010.

[134] W.T. Zempsky, J. Sullivan, D.M. Paulson, S.B. Hoath, Evaluation of a low-dose lidocaine Iontophoresis system for topical anesthesia in adults and children: A randomized, controlled trial, Clin Ther, 26 (2004) 1110-1119.

[135] K. Mystakidou, E-TRANS fentanyl. ALZA., Curr Opin Investig Drugs, 3 (2002) 463-469.

[136] T. Parkinson, M. Szlek, J. Isaacson, Hybresis™ - The hybridization of traditional with low-voltage iontophoresis, Drug Deliv Technol, 7 (2007) 54-60.

[137] E. Choi, S. Lee, S. Ahn, H. SM, The pretreatment effect of chemical skin penetration enhancers in transdermal drug delivery using iontophoresis, Skin Pharmacol Appl, 12 (1999) 326–335.

[138] S. Chesnoy, D. Durand, J. Doucet, G. Couarraze, Structural parameters involved in the permeation of propranolol HCl by iontophoresis and enhancers, J Control Release, 58 (1999) 163-175.

[139] K.S. Bhatia, S. Gao, J. Singh, Effect of penetration enhancers and iontophoresis on the FT-IR spectroscopy and LHRH permeability through porcine skin, J Control Release, 47 (1997) 81-89.

[140] L.M.A. Nolan, J. Corish, O.I. Corrigan, D. Fitzpatrick, Combined effects of iontophoretic and chemical enhancement on drug delivery: II. Transport across human and murine skin, Int J Pharm, 341 (2007) 114-124.

[141] Y. Wang, Q. Fan, Y. Song, B. Michniak, Effects of fatty acids and iontophoresis on the delivery of midodrine hydrochloride and the structure of human skin, Pharm Res, 20 (2003) 1612-1618.

[142] H.D.C. Smyth, G. Becket, S. Mehta, Effect of permeation enhancer pretreatment on the iontophoresis of luteinizing hormone releasing hormone (LHRH) through human epidermal membrane (HEM), J Pharm Sci, 91 (2002) 1296-1307.

[143] V.M. Meidan, M. Al-Khalili, B.B. Michniak, Enhanced iontophoretic delivery of buspirone hydrochloride across human skin using chemical enhancers, Int J Pharm, 264 (2003) 73-83.

[144] K.S. Bhatia, J. Singh, Synergistic effect of iontophoresis and a series of fatty acids on LHRH permeability through porcine skin, J Pharm Sci, 87 (1998) 462-469.

[145] K.S. Bhatia, J. Singh, Effect of linolenic acid/ethanol or limonene/ethanol and iontophoresis on the in vitro percutaneous absorption of LHRH and ultrastructure of human epidermis, Int J Pharm, 180 (1999) 235-250.

[146] V.B. Nair, R. Panchagnula, The effect of pretreatment with terpenes on transdermal iontophoretic delivery of arginine vasopressin, Il Farmaco, 59 (2004) 575-581.

[147] R. Prasad, V. Koul, S. Anand, R.K. Khar, Effect of DC/mDC iontophoresis and terpenes on transdermal permeation of methotrexate: In vitro study, Int J Pharm, 333 (2007) 70-78.

[148] O. Pillai, R. Panchagnula, Transdermal iontophoresis of insulin: V. Effect of terpenes, J Control Release, 88 (2003) 287-296.

[149] A. Doliwa, S. Santoyo, P. Ygartua, Effect of passive and iontophoretic skin pretreatments with terpenes on the in vitro skin transport of piroxicam, Int J Pharm, 229 (2001) 37-44.

[150] S. Ganga, P. Ramarao, J. Singh, Effect of Azone on the iontophoretic transdermal delivery of metoprolol tartrate through human epidermis in vitro, J Control Release, 42 (1996) 57-64.

[151] L. Hu, S.M.C. Silva, B.B. Damaj, R. Martin, B.B. Michniak-Kohn, Transdermal and transbuccal drug delivery systems: Enhancement using iontophoretic and chemical approaches, Int J Pharm, 421 (2011) 53-62.

[152] J. Hirvonen, K. Kontturi, L. Murtomäki, P. Paronen, A. Urtti, Transdermal iontophoresis of sotalol and salicylate; the effect of skin charge and penetration enhancers, J Control Release, 26 (1993) 109-117.

[153] Y. Wang, L.V. Allen, L.C. Li, Effect of sodium dodecyl sulfate on iontophoresis of hydrocortisone across hairless mouse skin, Pharm Dev Technol, 5 (2000) 533-542.

[154] G.L. Li, M. Danhof, P.M. Frederik, J.A. Bouwstra, Pretreatment with a water-based surfactant formulation affects transdermal iontophoretic delivery of R-apomorphine in vitro, Pharm Res, 20 (2003) 653-659.

[155] T.J. Franz, Percutaneous absorption. On the relevance of in vitro data, J Invest Dermatol, 64 (1975) 190-195.

[156] R.L. Bronaugh, R.F. Stewart, Methods for in vitro percutaneous absorption studies IV: The flow-through diffusion cell, J Pharm Sci, 74 (1985) 64-67.

[157] J.P. Skelly, A. Yacobi, V.P. Shah, G.L. Flynn, H.I. Maibach, R.C. Wester, R.H. Guy, FDA and AAPS report of the workshop on principles and practices of in vitro percutaneous penetration studies: relevance to bioavailability and bioequivalence., Pharm Res, 4 (1987) 265-267.

[158] I. PermeGear, Franz diffusion cells, in, 2012.

[159] J. Houk, R.H. Guy, Membrane models for skin penetration studies, Chem Rev, 88 (1988) 455-472.

[160] J. Hadgraft, R.H. Guy, Synthetic membranes as biological models, Adv Phar Sc, 6 (1992) 43-62.

[161] J. Hadgraft, G. Ridout, Development of model membranes for percutaneous absorption measurements. I. Isopropyl myristate, Int J Pharm, 39 (1987) 149-156.

[162] J. Hadgraft, G. Ridout, Development of model membranes for percutaneous absorption measurements. II. Dipalmitoyl phosphatidylcholine, linoleic acid and tetradecane, Int J Pharm, 42 (1988) 97–104.

[163] J. Hadgraft, K. Walters, P. Wotton, Facilitated transport of sodium salicylate across an artificial lipid membrane by Azone., J Pharm Pharmacol, 37 (1985) 725-727.

[164] M.A. Pellett, A.C. Watkinson, J. Hadgraft, R. Brain, An ATR-FTIR investigation of the interactions between vehicles and a synthetic membrane, in: Proceedings of the International Symposium of Controlled Released Bioactive Materials, 1994, pp. 439-440.

[165] R. Neubert, C. Bendas, W. Wolfgang, B. Gienau, F. W., A multilayer membrane system for modelling drug penetration into skin, Int J Pharm, 75 (1991) 89-94.

[166] R. Neubert, W. Wohlrab, C. Bendas, Modelling of drug penetration into human skin using a multilayer membrane system, Skin Pharmacol Physi, 8 (1995) 119-129.

[167] C. Nastruzzi, E. Esposito, C. Pastesini, R. Gambari, E. Menegatti, Comparative study on the release kinetics of methyl nicotinate from topical formulations., Int J Pharm, 90 (1993) 43-50.

[168] W. Russeau, J. Mitchell, J. Tetteh, M.E. Lane, J. Hadgraft, Investigation of the permeation of model formulations and a commercial ibuprofen formulation in Carbosil® and human skin using ATR-FTIR and multivariate spectral analysis, Int J Pharm, 374 (2009) 17-25.

[169] B. Godin, E. Touitou, Transdermal skin delivery: Predictions for humans from in vivo, ex vivo and animal models, Adv Drug Deliv Rev, 59 (2007) 1152-1161.

[170] W.G. Reifenrath, E.M. Chellquist, E.A. Shipwash, W.W. Jederberg, Evaluation of animal models for predicting skin penetration in man, Fund Appl Toxicol, 4 (1984) S224-S230.

[171] R.L. Bronaugh, R.F. Stewart, E.R. Congdon, Methods for in vitro percutaneous absorption studies II. Animal models for human skin, Toxicol Appl Pharm, 62 (1982) 481-488.

[172] A.M. Barbero, H.F. Frasch, Pig and guinea pig skin as surrogates for human in vitro penetration studies: A quantitative review, Toxicol In Vitro, 23 (2009) 1-13.

[173] S. Nicoli, C. Padula, V. Aversa, B. Vietti, P.W. Wertz, A. Millet, F. Falson, P. Govoni, P. Santi, Characterization of rabbit ear skin as a skin model for in vitro transdermal permeation experiments: histology, lipid composition and permeability, Skin Pharmacol Physi, 21 (2008) 218-226.

[174] R.D. Lee, H.S. White, E.R. Scott, Visualization of iontophoretic transport paths in cultured and animal skin models, J Pharm Sci, 85 (1996) 1186-1190.

[175] P.C. Rigg, B.W. Barry, Shed snake skin and hairless mouse skin as model membranes for human skin during permeation studies, J Invest Dermatol, 94 (1990) 235-240.

[176] M.J. Bartek, J.A. Labudde, H.I. Maibach, Skin permeability *in vivo*: comparison in rat, rabbit, pig and man, J Invest Dermatol, 58 (1972) 114-123.

[177] F.P. Schmook, J.G. Meingassner, A. Billich, Comparison of human skin or epidermis models with human and animal skin in in-vitro percutaneous absorption, Int J Pharm, 215 (2001) 51-56.

[178] H.W. Davies, M.D. Trotter, Synthesis and turnover of membrane glycoconjugates in monolayer culture of pig and human epidermal cells, Brit J Dermatol, 104 (1981) 649-658.

[179] M. Mowafy, R.G. Cassens, Microscopic structure of pig skin, J Anim Sci, 41 (1975) 1281-1290.

[180] P. Forbes, Vascular supply of the skin and hair in swine., Adv. Biol. Skin, 9 (1969) 419-432.

[181] S. Kandavilli, V. Nair, R. Panchagnula, Polymers in transdermal drug delivery systems, in: Pharmaceutical Technology, 2002, pp. 62-80.

[182] N.A. Peppas, J.Z. Hilt, A. Khademhosseini, R. Langer, Hydrogels in biology and medicine: from molecular principles to bionanotechnology, Adv Mater, 18 (2006) 1345-1360.

[183] M. Guyot, F. Fawaz, Design and in vitro evaluation of adhesive matrix for transdermal delivery of propranolol, Int J Pharm, 204 (2000) 171-182.

[184] P.R.P. Verma, T.E.G.K. Murthy, Transdermal flurbiprofen delivery using HPMC matrices: design, in vitro and in vivo evaluation, Drug Dev Ind Pharm, 23 (1997) 633-638.

[185] A.R. Chandak, P.R.P. Verma, Development and Evaluation of HPMC Based Matrices for Transdermal Patches of Tramadol, Clin Res Regul Aff, 25 (2008) 13-30.

[186] A. Chandak, P. Verma, Design and development of HPMC based polymeric films of methotrexate - physicochemical and pharmacokinetic evaluations, Yakugaku Zasshi: The Pharmaceutical Society of Japan, 128 (2008) 1057-1066.

[187] Y.S. Krishnaiah, S.M. Al-Saidan, Transdermal permeation of trimetazidine from nerodilol-based HPMC gel drug reservoir system across rat epidermis, Med Prin Pract, 17 (2008) 37-42.

[188] L. Jahan, R. Ferdaus, S.M. Shaheen, M.Z. Sultan, M.A. Mazid, In vitro transdermal delivery of metformin from a HPMC/ PVA based TDS-patch at different pH, J Sci Res, 3 (2011) 661-667.

[189] V. Kumar, G.S. Banker, Chemically-modified cellulosic polymers, Drug Dev Ind Pharm, 19 (1993) 1-31.

[190] J.F. Kennedy, G.O. Phillips, P.A. Williams, J.L. Picullel, Cellulose and cellulose derivatives: Physico-chemical aspects and industrial applications, Cellucon ’93 proceedings, Lund, 1993.

[191] C. Clasen, W.M. Kulicke, Determination of viscoelastic and rheo-optical material functions of water-soluble cellulose derivatives, Prog Polym Sci, 26 (2001) 1839-1919.

[192] J.L. Ford, Thermal analysis of hydroxypropylmethylcellulose and methylcellulose: powders, gels and matrix tablets, Int J Pharm, 179 (1999) 209-228.

[193] A. O'Sullivan, Cellulose: the structure slowly unravels, Cellulose, 4 (1997) 173-207.

[194] D. Klemm, B. Heublein, H.-P. Fink, A. Bohn, Cellulose: fascinating biopolymer and sustainable raw material, Angew Chem Int Edit, 44 (2005) 3358-3393.

[195] T. Funami, Y. Kataoka, M. Hiroe, I. Asai, R. Takahashi, K. Nishinari, Thermal aggregation of methylcellulose with different molecular weights, Food Hydrocolloid, 21 (2007) 46-58.

[196] S. Hussain, C. Keary, D.Q.M. Craig, A thermorheological investigation into the gelation and phase separation of hydroxypropyl methylcellulose aqueous systems, Polymer, 43 (2002) 5623-5628.

[197] N. Sarkar, Kinetics of thermal gelation of methylcellulose and hydroxypropylmethylcellulose in aqueous solutions, Carbohyd Polym, 26 (1995) 195-203.

[198] R. Kita, T. Kaku, K. Kubota, T. Dobashi, Pinning of phase separation of aqueous solution of hydroxypropylmethylcellulose by gelation, Phys Lett A, 259 (1999) 302-307.

[199] X.M. Xu, Y.M. Song, Q.N. Ping, Y. Wang, X.Y. Liu, Effect of ionic strength on the temperature-dependent behavior of hydroxypropyl methylcellulose solution and matrix tablet, J Appl Polym Sci, 102 (2006) 4066-4074.

[200] C. Sammon, G. Bajwa, P. Timmins, C.D. Melia, The application of attenuated total reflectance Fourier transform infrared spectroscopy to monitor the concentration and state of water in solutions of a thermally responsive cellulose ether during gelation, Polymer, 47 (2006) 577-584.

[201] N. Sarkar, Thermal gelation properties of methyl and hydroxypropyl methylcellulose, J Appl Polym Sci, 24 (1979) 1073-1087.

[202] A. Haque, E.R. Morris, Thermogelation of methylcellulose. Part I: molecular structures and processes, Carbohyd Polym, 22 (1993) 161-173.

[203] A. Haque, R.K. Richardson, E.R. Morris, M.J. Gidley, D.C. Caswell, Thermogelation of methylcellulose. Part II: effect of hydroxypropyl substituents, Carbohyd Polym, 22 (1993) 175-186.

[204] R.N. Ibbett, K. Philp, D.M. Price, ^{13}C n.m.r. studies of the thermal behaviour of aqueous solutions of cellulose ethers, Polymer, 33 (1992) 4087-4094.

[205] G. Karlström, A. Carlsson, B. Lindman, Phase diagrams of nonionic polymer-water systems: experimental and theoretical studies of the effects of surfactants and other cosolutes, J Phys Chem-US, 94 (1990) 5005-5015.

[206] M.R. Aguilar, C. Elvira, A. Gallardo, B. Vásquez, J.S. Róman, Smart polymers and their applications as biomaterials, in: Topics in Tissue Engineering, N Ashammakhi, R Reis & E Chiellini, 2007, pp. 1-27.

[207] Y. Sekiguchi, C. Sawatari, T. Kondo, A gelation mechanism depending on hydrogen bond formation in regioselectively substituted O-methylcelluloses, Carbohyd Polym, 53 (2003) 145-153.

[208] J.D. Ferry, Viscoelastic Properties of Polymers, Third Edition ed., John Wiley & Sons, New York, 1980.

[209] K. Holmberg, B. Jönsson, B. Kronberg, B. Lindman, Surfactants and Polymers in Aqueous Solution, 2nd ed., John Wiley & Sons, Chichester, 2003.

[210] M. Egermayer, M. Karlberg, L. Piculell, Gels of hydrophobically modified ethyl(hydroxyethyl) cellulose cross-linked by amylose: Effects of hydrophobe architecture, Langmuir, 20 (2004) 2208-2214.

[211] P. Zheng, L. Li, X. Hu, X. Zhao, Sol-gel transition of methylcellulose in phosphate buffer saline solutions, J Polym Sci B, 42 (2004) 1849-1860.

[212] Y. Xu, L. Li, Thermoreversible and salt-sensitive turbidity of methylcellulose in aqueous solution, Polymer, 46 (2005) 7410-7417.

[213] A. Ridell, H. Evertsson, S. Nilsson, Influence of counterion on the interaction of dodecyl sulfates and cellulose ethers, J Colloid Interf Sci, 247 (2002) 381-388.

[214] D. Ostrovskii, A.L. Kjoniksen, B. Nyström, L.M. Torell, Association and thermal gelation in aqueous mixtures of ethyl(hydroxyethyl)cellulose and ionic surfactant: FTIR and raman study, Macromolecules, 32 (1999) 1534-1540.

[215] J. Desbrières, M. Hirrien, S.B. Ross-Murphy, Thermogelation of methylcellulose: rheological considerations, Polymer, 41 (2000) 2451-2461.

[216] L. Li, P.M. Thangamathesvaran, C.Y. Yue, K.C. Tam, X. Hu, Y.C. Lam, Gel network structure of methylcellulose in water, Langmuir, 17 (2001) 8062-8068.

[217] J. Desbrières, M. Hirrien, M. Rinaudo, A calorimetric study of methylcellulose gelation, Carbohyd Polym, 37 (1998) 145-152.

[218] M. Hirrien, C. Chevillard, J. Desbrieres, M.A.V. Axelos, M. Rinaudo, Thermogelation of methylcelluloses: new evidence for understanding the gelation mechanism, Polymer, 39 (1998) 6251-6259.

[219] S.C. Joshi, Y.C. Lam, B.K. Tan, S.Q. Liu, Modeling of thermal gelation and degelation of MC and HPMC hydrogels, in: International Conference on Biomedical and Pharmaceutical Engineering 2006, 2006, pp. 545-550.

[220] K. Kobayashi, C. Huang, T.P. Lodge, Thermoreversible gelation of aqueous methylcellulose solutions, Macromolecules, 32 (1999) 7070-7077.

[221] F.E. Antunes, R.O. Brito, E.F. Marques, B. Lindman, M. Miguel, Mechanisms behind the faceting of catanionic vesicles by polycations: chain crystallization and segregation, J Phys Chem B, 111 (2007) 116-123.

[222] H.A. Barnes, J.F. Hutton, k. Walters, An Introduction to Rheology, Elsevier Science Publishers B.V., Amsterdam, 1989.

[223] P.G. De Gennes, Reptation of a polymer chain in the presence of fixed obstacles J Chem Phys, 55 (1971) 572-579.

[224] F. Tanaka, Theory of thermoreversible gelation, Macromolecules, 22 (1989) 1988-1994.

[225] C. Lind, S.D. Gates, N.M. Pedoussaut, T.I. Baiz, Novel materials through non-hydrolytic sol-gel processing: negative thermal expansion oxides and beyond, Materials, 3 (2010) 2567-2587.

[226] B. Gaweł, K. Gaweł, G. Øye, Sol-gel synthesis of non-silica monolithic materials, Materials, 3 (2010) 2815-2833.

[227] T.K. Tseng, Y.S. Lin, Y.J. Chen, H. Chu, A review of photocatalysts prepared by sol-gel method for VOCs removal, Int J Mol Sci, 11 (2010) 2336-2361.

[228] T. Cohen, J. Starosvetsky, U. Cheruti, R. Armon, Whole cell imprinting in sol-gel thin films for bacterial recognition in liquids: macromolecular fingerprinting, Int J Mol Sci, 11 (2010) 1236-1252.

[229] A. Mujahid, P.A. Lieberzeit, F.L. Dickert, Chemical sensors based on molecularly imprinted sol-gel materials, Materials, 3 (2010) 2196-2217.

[230] W. Klonowski, Representing and defining patterns by graphs: applications to sol-gel patterns and to cytoskeleton, Biosystems, 22 (1988) 1-9.

[231] J.E. Martin, D. Adolf, The sol-gel transition in chemical gels, Annu Rev Phys Chem, 42 (1991) 311-339.

[232] Y. Lee, H.J. Chung, S. Yeo, C.-H. Ahn, H. Lee, P.B. Messersmith, T.G. Park, Thermo-sensitive, injectable, and tissue adhesive sol-gel transition hyaluronic acid/pluronic composite hydrogels prepared from bio-inspired catechol-thiol reaction, Soft Matter, 6 (2010) 977-983.

[233] T. Satoshi, Y. Naoto, Y. Hitoshi, Application of thermosensitive peptide copolymer gels to removal of endocrine disruptor, in, Hindawi Publishing Corporation, 2009.

[234] N.W. Fadnavis, K. Koteshwar, An unusual reversible sol−gel transition phenomenon in organogels and its application for enzyme immobilization in gelatin membranes, Biotechnol Progr, 15 (1999) 98-104.

[235] K. Loyen, I. Iliopoulos, R. Audebert, U. Olsson, Reversible thermal gelation in polymer/surfactant systems. Control of the gelation temperature, Langmuir, 11 (1995) 1053-1056.

[236] A. Sarrazin-Cartalas, I. Iliopoulos, R. Audebert, U. Olsson, Association and thermal gelation in mixtures of hydrophobically modified polyelectrolytes and nonionic surfactants, Langmuir, 10 (1994) 1421-1426.

[237] A. Carlsson, G. Karlström, B. Lindman, Thermal gelation of nonionic cellulose ethers and ionic surfactants in water, Colloid Surface, 47 (1990) 147-165.

[238] K. Thuresson, B. Lindman, B. Nyström, Effect of hydrophobic modification of a nonionic cellulose derivative on the interaction with surfactants. Rheology, J Phys Chem B, 101 (1997) 6450-6459.

[239] G. Wang, K. Lindell, G. Olofsson, On the thermal gelling of ethyl(hydroxyethyl)cellulose and sodium dodecyl sulfate. Phase behavior and temperature scanning calorimetric response, Macromolecules, 30 (1997) 105-112.

[240] K. Lindell, B. Cabane, Structures of physical gels in the EHEC-SDS-water system, Langmuir, 14 (1998) 6361-6370.

[241] A.-L. Kjøniksen, B. Nyström, B. Lindman, Dynamic light scattering on semidilute aqueous systems of ethyl (hydroxyethyl) cellulose. Effects of temperature, surfactant concentration, and salinity, Colloid Surface A, 149 (1999) 347-354.

[242] G.T. Eom, S.Y. Oh, T.G. Park, In situ thermal gelation of water-soluble poly(N-isopropylacrylamide-co-vinylphosphonic acid), in, John Wiley & Sons, 1998.

[243] F. Zeng, X. Liu, Z. Tong, Y. Yang, S. Wu, Thermal reversible gelation during phase separation of poly(N-isopropyl acrylamide)/water solution, Sci China Ser B, 43 (2000) 428-434.

[244] F.E. Antunes, L. Gentile, L. Tavano, C.O. Rossi, Rheological characterization of the thermal gelation of poly(N-isopropylacrylamide) and poly(N-isopropylacrylamide)co-Acrylic Acid, Appl Rheol, (2009) 42064-42073.

[245] Q. Hou, P.A. De Bank, K.M. Shakesheff, Injectable scaffolds for tissue regeneration, J Mater Chem, 14 (2004) 1915-1923.

[246] H.-F. Lu, E.D. Targonsky, M.B. Wheeler, Y.-L. Cheng, Thermally induced gelable polymer networks for living cell encapsulation, Biotechnol Bioeng, 96 (2007) 146-155.

[247] I.R. Schmolka, Artificial skin I. Preparation and properties of pluronic F-127 gels for treatment of burns, J Biomed Mater Res, 6 (1972) 571-582.

[248] M.J. Cappel, J. Kreuter, Effect of nonionic surfactants on transdermal drug delivery: II. Poloxamer and poloxamine surfactants, Int J Pharm, 69 (1991) 155-167.

[249] R. Barreiro-Iglesias, C. Alvarez-Lorenzo, A. Concheiro, Poly(acrylic acid) microgels (carbopol(R) 934)/surfactant interactions in aqueous media: Part I: Nonionic surfactants, Int J Pharm, 258 (2003) 165-177.

[250] J.C. Gilbert, J. Hadgraft, A. Bye, L.G. Brookes, Drug release from Pluronic F-127 gels, Int J Pharm, 32 (1986) 223-228.

[251] S.H. Lee, J.E. Lee, W.Y. Baek, J.O. Lim, Regional delivery of vancomycin using pluronic F-127 to inhibit methicillin resistant Staphylococcus aureus (MRSA) growth in chronic otitis media in vitro and in vivo, J Control Release, 96 (2004) 1-7.

[252] J.J. Escobar-Chávez, M. López-Cervantes, A. Naïk, Y.N. Kalia, D. Quintanar-Guerrero, A. Ganem-Quintanar, Applications of thermo-reversible pluronic F-127 gels in pharmaceutical formulations, J Pharm Pharmaceut Sci, 9 (2006) 339-358.

[253] K. Derakhshandeh, M. Fashi, S. Seifoleslami, Thermosensitive Pluronic® hydrogel: prolonged injectable formulation for drug abuse, Drug Design, Development and Therapy, 4 (2010) 255–262.

[254] M. Vadnere, G. Amidon, S. Lindenbaum, J.L. Haslam, Thermodynamic studies on the gel-sol transition of some pluronic polyols, Int J Pharm, 22 (1984) 207-218.

[255] V. Lenaerts, C. Triqueneaux, M. Quartern, F. Rieg-Falson, P. Couvreur, Temperature-dependent rheological behavior of Pluronic F-127 aqueous solutions, Int J Pharm, 39 (1987) 121-127.

[256] L. Gentile, G. De Luca, F.E. Antunes, C.O. Rossi, G.A. Ranieri, Thermogelation analysis of F127-water mixtures by physical chemistry techniques, Appl Rheol, 20 (2010) 52081.52081 - 52081.52089.

[257] S.M.C. Silva, F.V. Pinto, F.E. Antunes, M.G. Miguel, J.J.S. Sousa, A.A.C.C. Pais, Aggregation and gelation in hydroxypropylmethyl cellulose aqueous solutions, J Colloid Interf Sci, 327 (2008) 333-340.

[258] C.M. Rosell, J.A. Rojas, C. Benedito de Barber, Influence of hydrocolloids on dough rheology and bread quality, Food Hydrocolloid, 15 (2001) 75-81.

[259] T. Sanz, A. Salvador, S.M. Fiszman, Innovative method for preparing a frozen, battered food without a prefrying step, Food Hydrocolloid, 18 (2004) 227-231.

[260] W. Chen-Chao, M. Tejwani, W. Roach, J. Kay, J. Yoo, H. Surprenant, D. Monkhouse, T. Pryor, Development of near zero-order release dosage forms using three-dimensional printing (3-DP™) technology, Drug Dev Ind Pharm, 32 (2006) 367-376.

[261] J. Siepmann, N.A. Peppas, Modeling of drug release from delivery systems based on hydroxypropyl methylcellulose (HPMC), Adv Drug Deliv Rev, 48 (2001) 139-157.

[262] O.E. Pérez, C.C. Sánchez, A.M.R. Pilosof, J.M. Rodríguez Patino, Kinetics of adsorption of whey proteins and hydroxypropyl-methyl-cellulose mixtures at the air-water interface, J Colloid Interf Sci, 336 (2009) 485-496.

[263] M.I.S. Veríssimo, A.A.C.C. Pais, M.T.S.R. Gomes, Following HPMC gelation with a piezoelectric quartz crystal, Carbohyd Polym, 82 (2010) 363-369.

[264] R. Bodvik, A. Dedinaite, L. Karlson, M. Bergström, P. Bäverbäck, J.S. Pedersen, K. Edwards, G. Karlsson, I. Varga, P.M. Claesson, Aggregation and network formation of aqueous methylcellulose and hydroxypropylmethylcellulose solutions, Colloid Surface A, 354 (2010) 162-171.

[265] B. Lindman, G. Karlström, Nonionic polymers and surfactants: Temperature anomalies revisited, Comptes Rendus Chimie, 12 (2009) 121-128.

[266] B. Nystroem, B. Lindman, Dynamic and Viscoelastic Properties during the Thermal Gelation Process of a Nonionic Cellulose Ether Dissolved in Water in the Presence of Ionic Surfactants, Macromolecules, 28 (1995) 967-974.

[267] B. Cabane, R. Duplessix, J Phys Chem-US, 43 (1982) 1529.

[268] F.E. Antunes, E.F. Marques, M.G. Miguel, B. Lindman, Polymer-vesicle association, Adv Colloid Interfac, 147-148 (2009) 18-35.

[269] J. François, J. Dayantis, J. Sabbadin, Hydrodynamical behaviour of the poly(ethylene oxide)-sodium dodecylsulphate complex, Eur Polym J, 21 (1985) 165–174.

[270] L. Lee, Curr Opin Colloid Interface Sci, 4 (1999) 205.

[271] H. Lange, Interaction between sodium alkylsulfates and polyvinylpyrrolidone in aqueous solutions, Kolloid Z Z Polym, 243 (1971) 101-109.

[272] E.D. Goddard, K.P. Ananthapadmanabhan, Interactions of surfactants with polymers and proteins CRC Press, Boca Raton, 1993.

[273] R. Barreiro-Iglesias, C. Alvarez-Lorenzo, A. Concheiro, Poly(acrylic acid) microgels (carbopol(R) 934)/surfactant interactions in aqueous media: Part II: Ionic surfactants, Int J Pharm, 258 (2003) 179-191.

[274] R.S. Dias, A.A.C.C. Pais, M.G. Miguel, B. Lindman, DNA and surfactants in bulk and at interfaces, Colloid Surface A, 250 (2004) 115-131.

[275] V.J. Sovilj, L.B. Petrovic, Influence of hydroxypropylmethyl cellulose-sodium dodecylsulfate interaction on the solution conductivity and viscosity and emulsion stability, Carbohyd Polym, 64 (2006) 41-49.

[276] A. Hammarström, L.O. Sundelöf, NMR study of polymer surfactant interaction in the system HPMC/SDS/water, Colloid Polym Sci, 271 (1993) 1129-1133.

[277] A.C.F. Ribeiro, A.J.M. Valente, E.F.G. Azevedo, A.M. Amado, A.M. Amorim da Costa, M.L. Ramos, H.D. Burrows, Interactions of vanadates with carbohydrates in aqueous solutions, J Mol Struct, 703 (2004) 93–101.

[278] J. Barthel, F. Feuerlein, R. Neuder, R. Wachter, Calibration of conductance cells at various temperatures, J Solution Chem, 9 (1980) 209-219.

[279] N. Cunningham, Making Use Of Models: The Cross Model, in, 2010.

[280] N. Kamenka, I. Burgaud, R. Zana, B. Lindman, Electrical conductivity, self-diffusion, and fluorescence probe investigations of the interaction between sodium dodecyl sulfate and ethyl(hydroxyethyl)cellulose, J Phys Chem-US, 98 (1994) 6785-6789.

[281] R. Zana, W. Binana-Limbele, N. Kamenka, B. Lindman, Ethyl(hydroxyethyl)cellulose-cationic surfactant interactions: electrical conductivity, self-diffusion and time-resolved fluorescence quenching investigations, J Phys Chem-US, 96 (1992) 5461-5465.

[282] A.C.F. Ribeiro, V.M.M. Lobo, A.J.M. Valente, E.F.G. Azevedo, M.da G. Miguel, H.D. Burrows, Transport properties of alkyltrimethylammonium bromide surfactants in aqueous solutions, Colloid Polym Sci, 283 (2004) 277-283.

[283] E.D. Goddard, G.C. Benson, Conductivity of aqueous solutions of some paraffin chain salts, Can J Chem, 35 (1957) 986-991.

[284] A.J.M. Valente, H.D. Burrows, S.M.A. Cruz, R.F.P. Pereira, A.C.F. Ribeiro, V.M.M. Lobo, Aggregation and micellization of sodium dodecyl sulfate in the presence of Ce(III) at different temperatures: A conductometric study, J Colloid Interf Sci, 323 (2008) 141-145.

[285] D.F. Evans, H. Wennerstrom, The colloidal domain: where physics, chemistry, biology, and technology meet, 2nd Edition ed., VCH Verlagsgesellschaft mbH, 1999.

[286] A. Chatterjee, S.P. Moulik, S.K. Sanyal, B.K. Mishra, P.M. Puri, Thermodynamics of micelle formation of ionic surfactants: A critical assessment for sodium dodecyl sulfate, cetyl pyridinium chloride and dioctyl sulfosuccinate (Na salt) by microcalorimetric, conductometric, and tensiometric measurements, J Phys Chem B, 105 (2001) 12823-12831.

[287] D. Zanette, Â.A. Ruzza, S.J. Froehner, E. Minatti, Polymer-surfactant interactions demonstrated by a kinetic probe: degree of ionization, Colloid Surface A, 108 (1996) 91-100.

[288] R. Zana, Aqueous surfactant-alcohol systems: A review, Adv Colloid Interfac, 57 (1995) 1-64.

[289] M. Prasad, R. Palepu, S. Moulik, Interaction between sodium dodecyl sulfate (SDS) and polyvinylpyrrolidone (PVP) investigated with forward and reverse component addition protocols employing tensiometric, conductometric, microcalorimetric, electrokinetic, and DLS techniques, Colloid Polym Sci, 284 (2006) 871-878.

[290] R.F.P. Pereira, A.J.M. Valente, H.D. Burrows, Thermodynamic analysis of the interaction between trivalent metal ions and sodium dodecyl sulfate: An electrical conductance study, J Mol Liq, 156 (2010) 109-114.

[291] B. Lindman, G. Karlström, L. Stigsson, On the mechanism of dissolution of cellulose, J Mol Liq, 156 (2010) 76-81.

[292] G.M.M. Medeiros, S.M.B. Costa, Premicellar aggregates in a mixed system of a surfactant (SDS) and polymer (EHEC), Colloid Surface A, 119 (1996) 141-148.

[293] S. Nilsson, Interactions between water-soluble cellulose derivatives and surfactants. 1. The HPMC/SDS/water system, Macromolecules, 28 (1995) 7837-7844.

[294] L.-J. Chen, S.-Y. Lin, C.-C. Huang, Effect of hydrophobic chain length of surfactants on enthalpy−entropy compensation of micellization, J Phys Chem B, 102 (1998) 4350-4356.

[295] J.C. Phillips, Enthalpy/entropy and volume/entropy activation ratios and solute-solvent interactions, J Phys Chem-US, 89 (1985) 3060-3066.

[296] R.F.P. Pereira, A.J.M. Valente, H.D. Burrows, M.L. Ramos, A.C.F. Ribeiro, V.M.M. Lobo, Flocculation and micellization of sodium dodecyl sulfate solutions in the presence of aluminium nitrate: effect of concentration and temperature, Acta Chim Slov, 56 (2009) 45-52.

[297] A.A. Samii, G. Karlstroem, B. Lindman, Phase behavior of a nonionic cellulose ether in nonaqueous solution, Langmuir, 7 (1991) 653-657.

[298] E. Hoff, B. Nyström, B. Lindman, Polymer−surfactant interactions in dilute mixtures of a nonionic cellulose derivative and an anionic surfactant, Langmuir, 17 (2001) 28-34.

[299] M.F. Torres, A.J. Müller, M.A. Szidarovszky, A.E. Sáez, Shear and extensional rheology of solutions of mixtures of poly(ethylene oxide) and anionic surfactants in ionic environments, J Colloid Interf Sci, 326 (2008) 254-260.

[300] B. Nyström, A.-L. Kjøniksen, B. Lindman, Effects of temperature, surfactant, and salt on the rheological behavior in semidilute aqueous systems of a nonionic cellulose ether, Langmuir, 12 (1996) 3233-3240.

[301] A.-L. Kjøniksen, B. Nyström, B. Lindman, Effects of temperature, surfactant concentration, and salinity on the dynamics of dilute solutions of a nonionic cellulose derivative, Langmuir, 14 (1998) 5039-5045.

[302] B. Nyström, B. Lindman, Dynamic and viscoelastic properties during the thermal gelation process of a nonionic cellulose ether dissolved in water in the presence of ionic surfactants, Macromolecules, 28 (1995) 967-974.

[303] A.-L. Kjøniksen, B. Nyström, B. Lindman, Dynamic viscoelasticity of gelling and nongelling aqueous mixtures of ethyl(hydroxyethyl)cellulose and an ionic surfactant, Macromolecules, 31 (1998) 1852-1858.

[304] G.A. Simon, H.I. Maibach, The pig as an experimental animal model of percutaneous permeation in man: Qualitative and quantitative observations – An overview, Skin Pharmacol Appl, 13 (2000) 229-234.

[305] W. Meyer, R. Schwarz, K. Neurand, The skin of domestic mammals as a model for the human skin, with special reference to the domestic pig, Current Problems in Dermatology, 7 (1978) 39-52.

[306] C.S. Asbill, B.B. Michniak, Percutaneous penetration enhancers: local versus transdermal activity, Pharm Sci Technol To, 3 (2000) 36-41.

[307] M. Bach, B.C. Lippold, Percutaneous penetration enhancement and its quantification, Eur J Pharm Biopharm, 46 (1998) 1-13.

[308] P.K. Wotton, B. Møllgaard, J. Hadgraft, A. Hoelgaard, Vehicle effect on topical drug delivery. III. Effect of azone on the cutaneous permeation of metronidazole and propylene glycol, Int J Pharm, 24 (1985) 19-26.

[309] I. Effendy, H.I. Maibach, Surfactants and experimental irritant contact dermatitis, Contact Dermatitis, 33 (1995) 217-225.

[310] H. Schott, Surfactant systems: Their chemistry, pharmacy and biology. By D. Attwood and A. T. Florence. Chapman & Hall, London EC4P 4EE, United Kingdom. 1983. 794 pp, J Pharm Sci, 74 (1985) 1140-1141.

[311] D. Shukla, V.K. Tyagi, Gemini surfactants: A review, J Oleo Sci, 55 (2006) 381-190.

[312] E.L. Tan, J.-C. Lid, Y.W. Chien, Effect of cationic surfactants on the transdermal permeation of ionized indomethacin, Drug Dev Ind Pharm, 19 (1993) 685-699.

[313] R. Babu, S. Mandip, K. Narayanasamy, Structure-activity relationship of chemical penetration enhancers, in: Percutaneous Penetration Enhancers, Second Edition, Informa Healthcare, 2005, pp. 17-33.

[314] P. Ashton, K.A. Walters, K.R. Brain, J. Hadgraft, Surfactant effects in percutaneous absorption I. Effects on the transdermal flux of methyl nicotinate, Int J Pharm, 87 (1992) 261-264.

[315] S. Kitagawa, M. Kasamaki, I. A., Effects of n-alkyltrimethylammonium on skin permeation of benzoic acid through excised guinea pig dorsal skin, Chem Pharm Bull, 48 (2000) 1698—1701.

[316] A. López, F. Llinares, C. Cortell, M. Herráez, Comparative enhancer effects of Span®20 with Tween®20 and Azone® on the in vitro percutaneous penetration of compounds with different lipophilicities, Int J Pharm, 202 (2000) 133-140.

[317] F.M. Menger, C.A. Littau, Gemini-surfactants: synthesis and properties, J Am Chem Soc, 113 (1991) 1451-1452.

[318] F.M. Menger, J.S. Keiper, Gemini surfactants, Angew Chem Int Edit, 39 (2000) 1906-1920.

[319] A. Laschewsky, K. Lunkenheimer, R.H. Rakotoaly, L. Wattebled, Spacer effects in dimeric cationic surfactants, Colloid Polym Sci, 283 (2005) 469-479.

[320] R. Zana, Dimeric (gemini) surfactants: Effect of the spacer group on the association behavior in aqueous solution, J Colloid Interf Sci, 248 (2002) 203-220.

[321] J.A.S. Almeida, E.F. Marques, A.S. Jurado, A.A.C.C. Pais, The effect of cationic gemini surfactants upon lipid membranes. An experimental and molecular dynamics simulation study, Phys Chem Chem Phys, 12 (2010) 14462-14476.

[322] S.M.C. Silva, L. Hu, J.J.S. Sousa, A.A.C.C. Pais, B.B. Michniak-Kohn, A combination of nonionic surfactants and iontophoresis to enhance the transdermal drug delivery of ondansetron HCl and diltiazem HCl, Eur J Pharm Biopharm, 80 (2012) 663-673.

[323] J.E. Harrison, P.W. Groundwater, K.R. Brain, J. Hadgraft, Azone® induced fluidity in human stratum corneum. A fourier transform infrared spectroscopy investigation using the perdeuterated analogue, J Control Release, 41 (1996) 283-290.

[324] I.T. Degim, A. Uslu, J. Hadgraft, T. Atay, C. Akay, S. Cevheroglu, The effects of Azone and capsaicin on the permeation of naproxen through human skin, Int J Pharm, 179 (1999) 21-25.

[325] W.J. Lambert, W.I. Higuchi, K. Knutson, S.L. Krill, Dose-dependent enhancement effects of azone on skin permeability, Pharm Res, 6 (1989) 798-803.

[326] S. Hou, G. Flynn, Enhancement of hydrocortisone permeation of human and hairless mouse skin by 1-dodecylazacycloheptan-2-one, J Invest Dermatol, 93 (1989) 774-779.

[327] K. Sugibayashi, K. Hosoya, Y. Morimoto, W. Higuchi, Effect of the absorption enhancer, Azone, on the transport of 5-fluorouracil across hairless rat skin, J Pharm Pharmacol, 37 (1985) 578-580.

[328] P. Agrawala, W. Ritschel, Influence of 1-dodecylhexahydro-2H-azepin-2-one (Azone) on the in vitro permeation of verapamil hydrochloride across rat, hairless mouse, and human cadaver skin., J Pharm Sci, 77 (1988) 776-778.

[329] W. Cheng, T. Murphy, M. Smith, W. Cooksley, J. Halliday, P. LW, Dose-dependent pharmacokinetics of caffeine in humans: relevance as a test of quantitative liver function., Clin Pharmacol Ther, 47 (1990) 516-524.

[330] M. Arnaud, Metabolism of caffeine and other components of coffee, in: G. S (Ed.) Caffeine Coffee and Health, Raven Press, New York, 1993, pp. 43-96.

[331] L. Matthieu, L. Meuleman, E. Van Hecke, A. Blondeel, B. Dezfoulian, L. Constandt, A. Goossens, Contact and photocontact allergy to ketoprofen. The Belgian experience, Contact Dermatitis, 50 (2004) 238-241.

[332] V. Devleeschouwer, R. Roelandts, M. Garmyn, A. Goossens, Allergic and photoallergic contact dermatitis from ketoprofen: results of (photo) patch testing and follow-up of 42 patients*, Contact Dermatitis, 58 (2008) 159-166.

[333] M. Hindsén, E. Zimerson, M. Bruze, Photoallergic contact dermatitis from ketoprofen in southern Sweden, Contact Dermatitis, 54 (2006) 150-157.

[334] R.L. Diaz, J. Gardeazabal, P. Manrique, J.A. Ratón, I. Urrutia, J.M. Rodríguez-Sasiain, C. Aguirre, Greater allergenicity of topical ketoprofen in contact dermatitis confirmed by use, Contact Dermatitis, 54 (2006) 239-243.

[335] F.M. Menger, C.A. Littau, Gemini surfactants: a new class of self-assembling molecules, J Am Chem Soc, 115 (1993) 10083-10090.

[336] F.M. Menger, B.N.A. Mbadugha, Gemini surfactants with a disaccharide spacer, J Am Chem Soc, 123 (2001) 875-885.

[337] E. Alami, G. Beinert, P. Marie, R. Zana, Alkanediyl-.alpha.,.omega.-bis(dimethylalkylammonium bromide) surfactants. 3. Behavior at the air-water interface, Langmuir, 9 (1993) 1465-1467.

[338] M. Hoppert, Microscopic techniques in biotechnology, in: Microscopic techniques in biotechnology, Wiley-VCH, Veinheim, 2003, pp. 114.

[339] R. Ellis, Ellis Hematoxylin and Eosin (H&E) Staining Protocol, in, 2010.

[340] B. Arechabala, C. Coiffard, P. Rivalland, L.J.M. Coiffard, Y.D. Roeck-Holtzhauer, Comparison of cytotoxicity of various surfactants tested on normal human fibroblast cultures using the neutral red test, MTT assay and LDH release, J Appl Toxicol, 19 (1999) 163-165.

[341] H.C. Eun, J.H. Chung, S.Y. Jung, K.H. Cho, K.H. Kim, A comparative study of the cytotoxicity of skin irritants on cultured human oral and skin keratinocytes, Brit J Dermatol, 130 (1994) 24-28.

[342] H.C. Korting, S. Schindler, A. Hartinger, M. Kerscher, T. Angerpointner, H.I. Maibach, MTT-assay and neutral red release (NRR)-assay: Relative role in the prediction of the irritancy potential of surfactants, Life Sci, 55 (1994) 533-540.

[343] Y. Song, C. Xiao, R. Mendelsohn, T. Zheng, L. Strekowski, B. Michniak, Investigation of iminosulfuranes as novel transdermal penetration enhancers: Enhancement activity and cytotoxicity, Pharm Res, 22 (2005) 1918-1925.

[344] R. Zana, Dimeric and oligomeric surfactants. Behavior at interfaces and in aqueous solution: a review, Adv Colloid Interfac, 97 (2002) 205-253.

[345] J.A.S. Almeida, H. Faneca, R.A. Carvalho, E.F. Marques, A.A.C.C. Pais, Dicationic alkylammonium bromide gemini surfactants. Membrane perturbation and skin irritation, PLoS ONE, 6 (2011) e26965.

[346] H.D. Burrows, M.J. Tapia, C.L. Silva, A.A.C.C. Pais, S.M. Fonseca, J. Pina, J. Seixas de Melo, Y. Wang, E.F. Marques, M. Knaapila, A.P. Monkman, V.M. Garamus, S. Pradhan, U. Scherf, Interplay of electrostatic and hydrophobic effects with binding of cationic gemini surfactants and a conjugated polyanion: experimental and molecular modeling studies, The Journal of Physical Chemistry B, 111 (2007) 4401-4410.

[347] M. Klein, D. Shaw, S. Barese, G. Chapo, C. Cuono, A reliable and cost-effective in vitro assay of skin viability for skin banks and burn centers, J Burn Care Rehabil, 17 (1996) 565-570.

[348] T. Watanabe, T. Hasegawa, H. Takahashi, T. Ishibashi, H. Itagaki, K. Sugibayashi, Utility of MTT assay in three-dimensional cultured human skin model as an alternative for draize skin irritation test: approach using diffusion law of irritant in skin and toxicokinetics-toxicodynamics correlation, Pharm Res, 19 (2002) 669-675.

[349] N. Morikawa, T. Kitagawa, K. Tomihata, Assessment of the in vitro skin irritation of chemicals using the Vitrolife-Skin™ human skin model, in: Proc. 6th World Congress on Alternatives & Animal Use in the Life Sciences, AATEX Tokyo, Japan, 2007, pp. 417-423.

[350] V.R. Sinha, M.P. Kaur, Permeation enhancers for transdermal drug delivery, Drug Dev Ind Pharm, 26 (2000) 1131-1140.

[351] K. Moser, K. Kriwet, A. Naik, Y.N. Kalia, R.H. Guy, Passive skin penetration enhancement and its quantification in vitro, Eur J Pharm Biopharm, 52 (2001) 103-112.

[352] M. Bergh, Allergenic oxidation products, Acta Derm-Venereol, 79 (1999) 5 - 26.

[353] M. Artusi, S. Nicoli, P. Colombo, R. Bettini, A. Sacchi, P. Santi, Effect of chemical enhancers and iontophoresis on thiocolchicoside permeation across rabbit and human skin in vitro, J Pharm Sci, 93 (2004) 2431-2438.

[354] F. Bounoure, M. Lahiani Skiba, M. Besnard, P. Arnaud, E. Mallet, M. Skiba, Effect of iontophoresis and penetration enhancers on transdermal absorption of metopimazine, J Dermatol Sci, 52 (2008) 170-177.

[355] Y.N. Kalia, R.H. Guy, Interaction between penetration enhancers and iontophoresis: effect on human skin impedance in vivo, J Control Release, 44 (1997) 33-42.

[356] S.S. Vaghani, M. Gurjar, S. Singh, S. Sureja, S. Koradia, N.P. Jivani, M.M. Patel, Effect of iontophoresis and permeation enhancers on the permeation of an acyclovir gel, Current Drug Delivery, 7 (2010) 329-333.

[357] A. Faruk, G. Singh, M.P.S. Ishar, In vitro passive and iontophoretically assisted transport of salbutamol sulphate through hairless mice skin, Int J Pharm Sci Nanotechnol, 3 (2010) 811-818.

[358] P. Sebastiani, S. Nicoli, P. Santi, Effect of lactic acid and iontophoresis on drug permeation across rabbit ear skin, Int J Pharm, 292 (2005) 119-126.

[359] Martindale: The Complete Drug Reference, in: S. Sweetman (Ed.), The Pharmaceutical Press, 2006.

[360] H.S. Gwak, I.S. Oh, I.K. Chun, Transdermal delivery of ondansetron hydrochloride: effects of vehicles and penetration enhancers, Drug Dev Ind Pharm, 30 (2004) 187-194.

[361] H.S. Gwak, I.S. Oh, I.K. Chun, In vitro percutaneous absorption of ondansetron hydrochloride from pressure-sensitive adhesive matrices through hairless mouse skin, Arch Pharm Res, 26 (2003) 644-648.

[362] P. Ding, H. Xu, G. Wei, J. Zheng, Microdialysis sampling coupled to HPLC for transdermal delivery study of ondansetron hydrochloride in rats, Biomed Chromatogr, 14 (2000) 141-143.

[363] E. Limpongsa, K. Umprayn, Preparation and evaluation of diltiazem hydrochloride diffusion-controlled transdermal delivery system, AAPS PharmSciTech, 9 (2008) 464-470.

[364] R. Gupta, B. Mukherjee, Development and in vitro evaluation of diltiazem hydrochloride transdermal patches based on povidone–ethylcellulose matrices, Drug Dev Ind Pharm, 29 (2003) 1-7.

[365] H.A. Ahad, K.K. Reddy, I.B. Md, H.K. C, C.S. Kumar, Formulation and permeation studies of diltiazem hydrochloride-ficus bengalensis fruit mucilage transdermal patches, J Pharm Res, 3 (2010) 928-932.

[366] N.B. Patel, R.N. Sonpal, S. Mohan, S. Selvaraj, Formulation and evaluation of iontophoretic transdermal delivery of diltiazem hydrochloride, Int J Res Pharm Sci, 1 (2010) 338-344.

[367] A.F. El-Kattan, C.S. Asbill, B.B. Michniak, The effect of terpene enhancer lipophilicity on the percutaneous permeation of hydrocortisone formulated in HPMC gel systems, Int J Pharm, 198 (2000) 179-189.